Field-based phenotyping for the effects of high night-time temperature stress in wheat and maize

by

Nathan T. Hein

B.Sc., United States Naval Academy, 2010
B.Sc., Oregon State University, 2018

AN ABSTRACT OF A DISSERTATION

submitted in partial fulfillment of the requirements for the degree

DOCTOR OF PHILOSOPHY

Department of Agronomy
College of Agriculture

KANSAS STATE UNIVERSITY
Manhattan, Kansas

2022

Abstract

Abiotic stresses can differentially alter a plant's physiology, phenology, yield and quality when coincided with different growth and developmental stages in crops. Along with varying responses due to the time of imposition, the type of abiotic stress (e.g., drought, nutrient, heat, or cold) and the duration of exposure can have differential level of impact. Under a changing climate, increasing temperatures are shown to result in significantly negative impact on crop yield and grain quality. While high day-time temperature stress has been thoroughly researched during the vegetative, reproductive, and grain-filling stages of major crops including wheat (*Triticum aestivum* L.) and maize (*Zea mays* L.), the effects of high night-time temperature stress are much less known. The grain-filling period in winter wheat and maize occurs during the summer and hence is hypothesized to be the most susceptible phase to high night-time temperature stress in Kansas under future warming scenarios.

As such, this dissertation aims to explore the agronomic and physiological responses, and changes in grain quality and micronutrient composition on exposure to high night-time temperature stress during the grain-filling period of two major cereals grown under field conditions. To address the above objective, the first North American field-based high throughput phenotyping infrastructure for high night-time temperature stress had to be developed. This dissertation will detail the process of developing a small field-based prototype tent system (Chapter 2), the expansion of this methodology into the large field-based infrastructure (Chapter 3), and, finally, the alteration of this methodology to facilitate the phenotyping of large stature crops (Chapter 5).

The field-based experiments were successful in applying a dynamic and equally distributed 3.2 °C and 3.8 °C high night-time temperature stress in the prototype tents and large

field-based infrastructure, respectively. This application of high night-time temperature stress significantly affected the phenology of wheat by advancing the onset of senescence by about 3 days, averaged across 12 different genotypes. The rate of senescence was not affected in maize as the strong stay-green traits in modern hybrids allowed the seeds to reach physiological maturity before the onset of senescence. Agronomically, winter wheat was significantly affected through a reduction in grain yield in both the prototype and large field-based infrastructure (20% and 14%, respectively) as well as a reduction in 200 kernel weight (7% and 5%, respectively). Similarly, high night-time temperature stress on maize resulted in 14% reduction in total yield and an 8% reduction in 200 kernel weight, averaged across 12 commercial hybrids. Seed quality and micronutrient composition was significantly modified due to the application of stress with significant alterations observed in starch, protein, and nutrient content in both winter wheat and maize (Chapter 4 and 5, respectively). Using a susceptible and tolerant maize hybrid, differentially expressed genes governing starch metabolism were analyzed to understand the genomic basis of high night-time temperature resilience for starch synthesis.

The evidence for a future climate which is prone to a higher level of variability has been confirmed through extensive climate-based modelling approaches. These predictions paired with the results of our current studies on high night-time temperature stress impacts, provides evidence for warming nights to have a significant negative effect on yield and quality in cereals. This dissertation is a compilation of the first-steps into phenotyping for high night-time stress impacts under field conditions which could be the basis for developing crop varieties/hybrids that can thrive under future uncertain climate.

Field-based phenotyping for the effects of high night-time temperature stress in wheat and maize

by

Nathan T. Hein

B.Sc., United States Naval Academy, 2010
B.Sc., Oregon State University, 2018

A DISSERTATION

submitted in partial fulfillment of the requirements for the degree

DOCTOR OF PHILOSOPHY

Department of Agronomy
College of Agriculture

KANSAS STATE UNIVERSITY
Manhattan, Kansas

2022

Approved by:

Co-Major Professor
Dr. Allan Fritz

Approved by:

Co-Major Professor
Dr. S.V. Krishna Jagadish

Copyright

Abstract

Abiotic stresses can differentially alter a plant's physiology, phenology, yield and quality when coincided with different growth and developmental stages in crops. Along with varying responses due to the time of imposition, the type of abiotic stress (e.g., drought, nutrient, heat, or cold) and the duration of exposure can have differential level of impact. Under a changing climate, increasing temperatures are shown to result in significantly negative impact on crop yield and grain quality. While high day-time temperature stress has been thoroughly researched during the vegetative, reproductive, and grain-filling stages of major crops including wheat (*Triticum aestivum* L.) and maize (*Zea mays* L.), the effects of high night-time temperature stress are much less known. The grain-filling period in winter wheat and maize occurs during the summer and hence is hypothesized to be the most susceptible phase to high night-time temperature stress in Kansas under future warming scenarios.

As such, this dissertation aims to explore the agronomic and physiological responses, and changes in grain quality and micronutrient composition on exposure to high night-time temperature stress during the grain-filling period of two major cereals grown under field conditions. To address the above objective, the first North American field-based high throughput phenotyping infrastructure for high night-time temperature stress had to be developed. This dissertation will detail the process of developing a small field-based prototype tent system (Chapter 2), the expansion of this methodology into the large field-based infrastructure (Chapter 3), and, finally, the alteration of this methodology to facilitate the phenotyping of large stature crops (Chapter 5).

The field-based experiments were successful in applying a dynamic and equally distributed 3.2 °C and 3.8 °C high night-time temperature stress in the prototype tents and large

field-based infrastructure, respectively. This application of high night-time temperature stress significantly affected the phenology of wheat by advancing the onset of senescence by about 3 days, averaged across 12 different genotypes. The rate of senescence was not affected in maize as the strong stay-green traits in modern hybrids allowed the seeds to reach physiological maturity before the onset of senescence. Agronomically, winter wheat was significantly affected through a reduction in grain yield in both the prototype and large field-based infrastructure (20% and 14%, respectively) as well as a reduction in 200 kernel weight (7% and 5%, respectively). Similarly, high night-time temperature stress on maize resulted in 14% reduction in total yield and an 8% reduction in 200 kernel weight, averaged across 12 commercial hybrids. Seed quality and micronutrient composition was significantly modified due to the application of stress with significant alterations observed in starch, protein, and nutrient content in both winter wheat and maize (Chapter 4 and 5, respectively). Using a susceptible and tolerant maize hybrid, differentially expressed genes governing starch metabolism were analyzed to understand the genomic basis of high night-time temperature resilience for starch synthesis.

The evidence for a future climate which is prone to a higher level of variability has been confirmed through extensive climate-based modelling approaches. These predictions paired with the results of our current studies on high night-time temperature stress impacts, provides evidence for warming nights to have a significant negative effect on yield and quality in cereals. This dissertation is a compilation of the first-steps into phenotyping for high night-time stress impacts under field conditions which could be the basis for developing crop varieties/hybrids that can thrive under future uncertain climate.

Table of Contents

List of Figures

List of Tables

Acknowledgements

I would like to thank my co-major advisors, Dr. S.V. Krishna Jagadish and Dr. Allan Fritz, as well as the other members of my committee, Dr. Ignacio Ciampitti and Dr. Jesse Tack, for their continued support over the years in completing my dissertation. I would also like to express my gratitude to my Graduate Program Director, Dr. Gerard Kluitenberg, for allowing me the use of his equipment and recommending me for participation in multiple multidisciplinary and multi-institutional collaborations. I would also like to thank other current and former faculty members, inside and outside of Agronomy, who have made a significant impact in my studies; Drs. Asabedo, Goodin, Min, Patrignani, Prasad, Rajashekar, Roozeboom, Schapaugh, and Wang. I would like to thank the farm team at the Kansas State University North Research Farm, specifically Dustan Ridder, Mark Leuthold, and Garry Harter, for their help in moving the small and large field-based systems as well as help with maintaining multiple different pieces of infrastructure for the implementation of abiotic stress. As well as Dr. Argelia Lorence from Arkansas State University and Mr. Wency Larazo for trusting me to develop the field-based phenotyping system and helping me develop as a scientist. I would also like to thank the many members of the Crop Ecophysiology Lab who have come and gone but all have helped me along the way. These members include, in no particular order, Drs. Bheemanahalli, Impa, Šebela, Vennapusa, Pokharel, Chiluwal, Fu, Peiris, Kumar, and Tiwari as well as Mr. Bustamante, Mr. Ostmeyer, Mr. Cook, Mr. Ross, and Mr. Hobbs. I would also like to thank my fellow graduate students who have made a significant impact on me and my studies during my time at Kansas State University to include Mr. Evers, Mr. Baral, Dr. Carver, Dr. Clinesmith, Dr. Yuanyuan Wang, Mr. Chaoxin Wang, and Mr. Wagner.

Dedication

This dissertation is dedicated to my loving and supportive family. It is with eternal thanks that I dedicate this to my forever patient and loving wife, Ashley, and to my children, Marlie Ann and Decker Keaton, who could always put a smile on my face no matter how long the days became. Without all of you, I would not be where I am today. I look forward to whatever may come for us in the future but know that I always have and always will love you.

- Your Husband and Dad

Chapter 1 - Bottlenecks and opportunities in field-based high-throughput phenotyping for drought, high day- and night-time temperature stress

Abstract

Flowering and grain-filling stages are highly sensitive to heat and drought stress exposure, leading to significant loss in crop yields. Therefore, phenotyping to enhance resiliency to these abiotic stresses is critical for sustaining genetic gains in crop improvement programs. However, traditional methods for screening traits related to these stresses is slow, laborious, and often expensive. Remote sensing provides opportunities to introduce low-cost, high-throughput phenotyping methods, to capture large genetic variation to facilitate enhancement of stress resiliency in crops.

This review focuses on the current status of phenotyping for high night-time temperature stress and four key physiological traits/processes that are critical in understanding crops responses to drought and daytime heat stress during reproductive and grain-filling periods. Specifically, these traits include: i) time-of-day of flowering, to escape these stresses during flowering, ii) optimizing photosynthetic efficiency, iii) storage and translocation of water-soluble carbohydrates, and iv) yield and yield components to provide in-season yield estimates. An overview of current advances in remote sensing in capturing these responses, limitations with existing technology and future direction of research to develop high-throughput phenotyping approaches for these traits and identifying high night-time temperature stress resiliency are discussed. In future, phenotyping these complex traits will require sensor advancement, high-

Hein, N.T., Ciampitti, I.A., Jagadish, S.V.K., 2021. Bottlenecks and opportunities in field-based high-throughput phenotyping for heat and drought stress. Journal of Experimental Botany 72, 5102-5116. https://www.doi.org/10.1093/jxb/erab021

quality imagery combined with machine learning tools, and importantly efforts in transdisciplinary science to foster integration across disciplines.

Hein, N.T., Ciampitti, I.A., Jagadish, S.V.K., 2021. Bottlenecks and opportunities in field-based high-throughput phenotyping for heat and drought stress. Journal of Experimental Botany 72, 5102-5116. https://www.doi.org/10.1093/jxb/erab021

Introduction

Advancements in quantifying abiotic stress impact on the productivity of field crops have become more important than ever in order to breed for heat and drought stress resiliency, or to understand the ability of a plant to maintain yield under abiotic stresses. An overall increase in agriculture production by roughly 49%, as compared to 2012, is necessary by 2050 in order to meet the global food demand (Food and Agriculture Organization [FAO], 2017; 2019). Yields in major crops such as maize (*Zea mays* L.), rice (*Oryza sativa* L.), and wheat (*Triticum aestivum* L.) have been plateauing since 1990 with an average annual increase of about 1% (FAO, 2017). This increase is significantly lower than the target needed to meet the demand. This global food crisis comes at a time when climate variability is exerting a major negative impact on crop productivity.

The Intergovernmental Panel on Climate Change (IPCC) has predicted that heat waves will occur at a more frequent rate, with increases in both duration and intensity in the future (IPCC, 2014). The increase in global mean temperature and the expected instability in precipitation creates a major risk to global food security. Gourdji *et al.* (2013) has predicted that by 2030, 31% of maize, 16% of rice, and 11% of wheat growing areas will record over five reproductive days with temperatures above their respective critical threshold in any given year. This increase in temperature coinciding with sensitive developmental stages, such as flowering, will have detrimental impacts on yield (Jagadish, 2020). Empirically, high daytime temperature (HDT) stress during the booting and flowering stages in rice reduced yield by as much as 28.5% depending on the timing and duration of heat stress (Aghamolki *et al.*, 2013). Similarly, a significant reduction in winter wheat yield was recorded with HDT stress coinciding with heading and lasting for 15 days, even though a stress period of five days was sufficient to induce

yield loss (Balla *et al.*, 2019). In addition, it is predicted that with every degree centigrade increase in mean temperature, the global wheat production will be reduced by 6% (Asseng *et al.*, 2015).

The global night-time minimum temperatures are increasing at a faster rate than the global day-time temperatures since the late 20th century (Easterling *et al.*, 1997; Vose, *et al.*, 2005; Wang, *et al.*, 2017). This unequal warming of the earth can cause major effects to several physiological and biochemical processes, including carbohydrate translocation, dark respiration, and cellular membrane repair, are modulated by temperature and occur at night (Bahuguna *et al.*, 2017; Mohammed and Tarpley, 2009b; Loka and Oosterhuis, 2010; Sadok and Jagadish, 2020). Along with causing unbalance in many physiological and biochemical processes at night, reduced photosynthesis can occur and, along with increased night respiration, is one of the ubiquitous responses to high night-time temperature (HNT) stress in production crops (Loka and Oosterhuis, 2010; Prasad and Djanaguiraman, 2011; Frantz *et al.*, 2004; Peraudeau et al., 2015a; Impa *et al.*, 2019). A reduction in photosynthesis paired with an increase in night respiration results in an altered carbon balance which causes a lower availability for carbon for growth or grain-filling (Cheng *et al.*, 2010; Impa *et al.*, 2019). HNT increased night respiration and carbon loss was significantly higher during post-flowering compared to pre-flowering stage in rice (Bahuguna *et al.*, 2017). However, the effects of increased night respiration on yield were not found during vegetative stages (Kanno *et al.*, 2009; Glaubitz *et al.*, 2014; Peradeau *et al.*, 2015b).

Drought reduced yield in roughly 75% of all globally harvested areas of maize, rice, wheat, and soybeans (*Glycine max* L.) between 1983 and 2009 (Kim *et al.*, 2019). The IPCC has also predicted a shift in the water cycle where the higher latitudes will receive increased precipitation while the mid-latitudes and those areas already prone to drought will encounter a

more substantial decrease in water supply (IPCC, 2014). Daryanto *et al.* (2016) synthesized 144 studies between 1980 and 2015 and reported an average yield reduction of roughly 21% for wheat and 39% for maize due to drought. Zhang *et al.* (2018), using a meta-analysis approach including over 110 independent studies, recorded a 28% and 25% yield reduction due to drought in wheat and rice, respectively, with the largest reduction associated with stress during grain filling. Similarly, Sehgal *et al.* (2018) reported that the most critical growth stages with significant reductions in yield due to drought and/or heat stress were the reproductive and grain-filling stages. Hence, a better understanding of plant's responses to both heat and drought stresses during reproductive and grain-filling stages is crucial to provide new opportunities for breeding programs to enhance the rate of success in developing stress-tolerant genotypes.

Remote sensing tools allow for data collection on much larger studies encompassing a wide genetic diversity in order to phenotype for abiotic stress resiliency. Remote sensing has been utilized for a variety of purposes such as measuring canopy height (Varela *et al.*, 2017; Thompson *et al.*, 2018; Thompson *et al.*, 2020; Zhou *et al.*, 2020), biomass (Neumann *et al.*, 2015; Padilla-Chacón *et al.*, 2019), canopy temperature (Romano *et al.*, 2011; Pauli *et al.*, 2016; Graß *et al.*, 2020), leaf area (Neilson *et al.*, 2015; Zhang *et al.*, 2019), and predicting yield (Rischbeck *et al.*, 2016; Becker and Schmidhalter, 2017; El-Hendawy *et al.*, 2017; Zhou *et al.*, 2020). Through the use of specialized vegetation indices (VIs) or spectral bands alone, remote sensing can quickly and efficiently collect data on different traits simultaneously, non-destructively, and with a high temporal frequency. In addition, remote sensing presents the opportunity of correlating an index with the trait of interest, without being confounded by a differential time-stamp, unlike manual measurements (Janse and Deshmukh, 2017; Xue and Su, 2017).

In order to effectively utilize remote sensing tools for the diagnosis of drought, HDT, and HNT stress impacts on crops, the data obtained should help in understanding complex physiological processes that determine yield, at a scale that cannot be achieved by manual methods. Recently, there have been attempts to review advances in sensor technology and estimation of agronomic traits such as plant height, biomass or greenness (Araus *et al.*, 2018; Chawade *et al.*, 2019). Hence, to avoid duplication, this review utilizes the progress achieved in the realm of sensor technology and focus on quantifying key physiological traits/processes that are critical in understanding crops resilience to drought and HDT stress during the reproductive and grain-filling period, while also providing an overview of the progression for remote sensing capabilities for phenotyping for HNT stress, which is still in its infancy. The specific traits for phenotyping for drought and HDT stress include phenotyping for i) time-of-day of flowering (TOF), as a means to escape heat stress during flowering, ii) photosynthetic efficiency, as a function of stay-green versus senescence, iii) water-soluble carbohydrates translocation and contribution to yield under stress, and iv) yield components i.e., grain number and kernel size determination to provide in-season (and before harvest) yield estimates. These traits define major physiological aspects related to HDT and drought stress resiliency in crops and are complex, labor-intensive, time-consuming, and change dynamically over time to be effectively captured through traditional methods. Opportunities exist with each trait and in HNT phenotyping to increase the throughput and accuracy of trait and resiliency determination via remote sensing. This review is timely and aims to identify ways to utilize advances in remote sensing, and to strengthen efforts towards developing HDT, HNT and drought tolerant crops for the future. Finally, the review identifies limitations and bottlenecks in remote sensing methods and provides recommendations for future research in order to overcome these limitations.

Time-of-day of flowering (TOF) – A route to escape HDT stress

Adapting to abiotic stress has been acquired naturally in crops over a long period of time through evolution, but are not equipped to deal with significant intra- and inter-annual variability encountered under current and predicted future climate. Traits that induce heat stress resilience can be classified into three categories: tolerance, avoidance, and escape. Tolerance is defined by the ability of the plants to continue operating their physiological processes under stressful conditions (Khan *et al.*, 2014). Traits that define avoidance allow normal processes to continue by creating a more favorable microclimate. An excellent example for heat stress avoidance is transpirational cooling, wherein canopy temperature is decreased to optimal levels even under severe ambient hotter environments (Lin *et al.*, 2017). This trait, however, is highly beneficial under sufficient water supply (Julia and Dingkuhn, 2013) but not under combined drought and heat stresses, as the competition to conserve water to survive drought is prioritized (Lin *et al.*, 2017). Escape on the other hand, provides the opportunity for sensitive physiological processes to occur during favorable times of the season (macro-escape) or during the day (micro-escape).

Shortening crop growth duration in order to complete their life cycle, to prevent exposure to severe hot and dry summers would be an example for a macro-escape (Stone, 2001; Barnabás *et al.*, 2008), while adjusting their sensitive flowering time to cooler hours is an example for micro-escape (Sheehy *et al.*, 2005; Jagadish, 2020). Heat stress during flowering leads to significant yield reductions in a large variety of crops and the inclusion (naturally or through genetic improvement) of an early morning flowering trait has been shown to significantly reduce spikelet sterility and yield losses in rice (Ishimaru *et al.*, 2010; Hirabayashi *et al.*, 2015; Bheemanahalli *et al.*, 2017) and sorghum (Chiluwal *et al.*, 2020). Although crops

can employ these three phenomena independently or in combination, this section focuses on advancing methods to phenotype for TOF as an effective means to minimize heat and drought stress damage in crops (Jung and Müller, 2009; Jagadish *et al.*, 2015b). The TOF is manually phenotyped, which is tedious, prone to human error, confounded by spatio-temporal variability of measurements, and can only be measured on a limited number of genotypes (Ishimaru *et al.*, 2010; Aiqing *et al.*, 2018; Chiluwal *et al.*, 2020; Pokharel *et al.*, 2020) (Figure 1 - 1A). Traditionally, researchers have identified the flowering pattern in crops by counting the number of opened flowers at specific time increments, but this can lead to confounding results as any physical stimuli can alter the flowering patterns (Kobayasi *et al.*, 2010).

Steps toward optimizing this methodology to reduce temporal variability with manual measurements and to overcome physical stimuli induced by human touch have been proposed. For rice, Kobayasi *et al.* (2010) utilized digital cameras to determine the flower opening time. This allowed for more frequent measurements (10 minute intervals), created a physical representation of the inflorescence at the specified time point so it could be evaluated, repeatedly if necessary, at a later date. This approach also enhanced accuracy by utilizing a tripod and a timer to initiate the data collection. Significant steps have been made in the last few years, which have allowed to increase the number of genotypes phenotyped and reduced the variability in measurements. The first step forward came via utilizing fixed field-based phenotyping systems such as the Field Scanalyzer phenotyping platform. The unit contains multiple sensors including high resolution digital cameras which, when combined with machine learning, can positively identify flowering in wheat (Sadeghi-Tehran *et al.*, 2017). This methodology has an accuracy ranging from 76 to 92% and its imprecisions are linked to the size and color of the anthers as they can vary amongst genotypes (Sadeghi-Tehran *et al.*, 2017) (Table 1-1). A significantly

higher challenge in determining the flowering opening time was observed in *Setaria viridis*, wherein the flower opening was predominant during the night, in all three tested accessions (Desai *et al.*, 2018). A Raspberry Pi system equipped with infrared imaging allowed the authors to correlate the flower opening time of the night with the movement in floral bristles, coinciding with extrusion of anthers (Desai *et al.*, 2018) (Table 1-1). The ability to capture the night-time flower opening is important to quantify the trait in some wild species known to majorly flower during night (rice; Sheehy *et al.*, 2007) or for capturing late evening flowering as seen in wheat (Aiqing *et al.*, 2018).

A mobile methodology has been developed by utilizing a high-clearance field-based high-throughput mobile phenotyping platform outfitted with multiple high resolution digital cameras which collected geo-referenced images with the help of built-in RTK GPS system (Barker *et al.*, 2016; Wang *et al.*, 2019). Utilizing deep learning tools, this methodology is able to correctly identify plant phenology and growth stages and the system was utilized to identify flowering dates, which were associated with plot-based breeder's score (Wang *et al.*, 2019) (Table 1-1). The system, however, was not employed to identify TOF due to lack of high temporal measurements on a single day. The success of the system in identifying heading and flowering dates indicates that the system is sensitive enough to be modified to capture images at a high temporal setting to explore the flowering pattern in different crops.

The success of utilizing both fixed field-based phenotyping systems and ground-based mobile phenotyping platforms indicates that aerial high-throughput phenotyping for capturing TOF in crops is achievable. Unmanned aerial vehicles (UAVs) are capable of carrying extremely high resolution RGB digital cameras and as cameras have gotten smaller, this has allowed even smaller UAVs to carry them (Colomina and Molina, 2014) (Figure 1-1B). Low altitude flights

will allow capturing extremely high-resolution images of the canopy in order to quantify the TOF. Two examples for the TOF phenomenon are presented wherein sorghum and rice genotypes vary with the time and the proportion of flowers that open at different times of the day (Figure 1-1C, D). The extremely short window (minutes after dawn) in sorghum and a much longer flowering window (hours after dawn) provides the diversity in the scale of operation in crops with TOF, and the efficiency and accuracy required to capture the genetic diversity for this trait. The difference in color between the green leaf background with a contrasting yellow by the anthers provides the opportunity to establish a phenotyping approach that can employ an area- and color-based detection method to define the temporal magnitude of flowering (Figure 1-1C, D). Employing this method will allow for screening a large number of genotypes, at high spatio-temporal frequency, with increased effectiveness, thereby facilitating integration of this trait into abiotic stress breeding programs.

Photosynthetic Efficiency – capturing stay-green versus senescence dynamics

Photosynthesis is the main driver for achieving maximum yield potential in crops under normal and stressed conditions. Attainable maximum yield can be determined by analyzing the amount of light captured, the ability of the plant to convert this energy into biomass, and the proportion of biomass partitioned to grain (Long *et al.*, 2006). The variables of the amount of light captured and the percent biomass partitioned to grain has been optimized through plant breeding, which includes improved plant canopy architecture for maximum light interception and increasing the partitioning capabilities by dwarfing stems and the number of seeds and size (Zhu *et al.*, 2010). Thus, increasing yields to meet the future global demand will rely on the further improvement of photosynthetic efficiency or crops ability to convert captured light energy into biomass.

Possible developments to improve photosynthetic efficiency for heat and drought stress resiliency include, introducing the C4 photosynthetic pathway into C3 plants, improving Rubisco kinetic properties, and increased photoprotection to reduce high levels of reactive oxygen species (ROS) (Gowik and Westhoff, 2011; Murchie and Niyogi, 2011; Whitney *et al.*, 2011). Heat and drought stress can increase the oxygenation reaction of Rubisco, which can result in a direct loss of up to 30% of fixed carbon (Raines, 2011). This degradation of fixed C is extremely influential on potential yield when drought or heat stress occur during flowering or grain filling. In addition, the early onset of senescence due to abiotic stresses is characterized by accelerated chlorophyll degradation and severely reduced photosynthetic efficiency (Hörtensteiner and Feller, 2002; Woo *et al.*, 2018). These negative effects can be reduced through functional stay-green phenotypes, by extending the activity of the photosynthetic machinery (Thomas and Ougham, 2014). Functional stay-green phenotypes are shown to have a positive effect on either yield, heat or drought stress tolerance in sorghum (*Sorghum bicolor* L.) (Borrell *et al.*, 2014), wheat (Spano *et al.*, 2003; Pinto *et al.*, 2016), barley (*Hordeum vulgare* L.) (Seiler *et al.*, 2014; Gous *et al.*, 2015), maize (Cairns *et al.*, 2012), and rice (Fu *et al.*, 2011).

Traditional measurements of photosynthetic efficiency are laborious, destructive and fail to detect the subtle changes that occur at the inception of senescence (Šebela *et al.*, 2020). Sequential biomass harvests have been proposed to capture the photosynthetic efficiency for the entire growing season (Zhu *et al.*, 2010), which is highly cumbersome to achieve with large breeding populations. A major milestone in addressing the above limitation was reached through the creation of the laser induced fluorescence transient (LIFT) method for remotely measuring this plant trait (Raesch *et al.*, 2014) (Table 1-1). The LIFT technique uses a laser at 665 nm to excite the leaves, and the fluorescent emission at 690 nm by the plant is collected by a reflective

telescope and processed (Kolber *et al.*, 2005; Pieruschka *et al.*, 2012). Advancements have been made in the mobility of this system, to allow it to be utilized in conjunction with highly precise global positioning systems in a field setting. The system, however, is still quite bulky and requires a large cart or all-terrain vehicle for its operation (Muller *et al.*, 2018). Another limitation to the system is that it measures an area larger than the targeted leaf and multiple layers of the canopy, which can confound conclusions (Raesch *et al.*, 2014).

A study using hyperspectral imaging on evergreen tree leaves exposed to a simulated short term drought stress, revealed a reduction in photosynthetic efficiency well before chlorophyll degradation was initiated. The use of longwave red-edge band vegetation indices such as red edge NDVI (NDRE740) and red edge chlorophyll index (CI740) had high correlation with photosynthetic efficiency (R^2 = 0.88 and 0.72 for stressed and non-stressed leaves, respectively) (Peng *et al.*, 2017) (Table 1-1). The photochemical reflectance index (PRI) has also been shown to have significant correlation with photosynthetic efficiency in flowering plant species in control, drought, and warming scenarios (R^2 = 0.78-0.85) (Zhang *et al.*, 2017) (Table 1-1).

The chlorophyll fluorescence, which is shown to quantify photosynthetic efficiency, has been used to measure the effective quantum yield (QY) of photosystem II in order to determine the exact change point at which senescence begins in leaves and floral tissue (Šebela *et al.*, 2015, 2020). Chlorophyll fluorescence measured through QY provides information on the overall efficiency of photochemical reactions in PSII under light-adapted state (Genty *et al.*, 1989), and has been effectively utilized to phenotype a rice diversity panel exposed to water-deficit stress (Šebela *et al.*, 2019) Therefore, using QY as a case study trait, the transition from leaf (handheld) to the plot level using UAVs and the desired phenotype for stress prone environments with

source-sink related stay green and senescence pattern is pictorially presented (Figure 1-2). The UAV platforms provides the opportunity to move beyond point based leaf or inflorescence-based photosynthetic parameter measurements (Šebela *et al.*, 2015, 2020; Figure 1-2A) to whole plant (Figure 1-2B) or canopy-based estimations (Figure 1-2C), to capture genetic diversity for extending source-sink photosynthetic efficiency. Developing varieties that can trigger senescence in the lower half of the plant/plot while retaining active photosynthetic machinery in the top half or third is a desirable phenotype for heat and drought stress prone environments (Jagadish *et al.*, 2015a). This ideotype concept proposed can be realized using advances in the sensor-based technology to help capture the differential onset and rate of senescence at different positions along the plant/plot in large diversity panels or mapping populations (Figure 1-2C). This approach makes it feasible to breed for varieties optimized with functional stay green vs senescence, sustain assimilate production and transport to sustain productivity under heat and drought prone environments.

Translocation of water-soluble carbohydrates (WSC)

The end result of photosynthesis is the production of monosaccharides such as glucose and fructose, which form the foundation blocks for storage carbohydrates (polysaccharides) such as starch. Sugars including glucose and fructans, synthesized in leaves, are transported to the stem and leaf sheaths and stored as water-soluble carbohydrates (WSC) (also known as non-structural carbohydrates [NSC]) (Schnyder, 1993; Gebbing, 2003; Ehdaie *et al.*, 2006; Fernandez *et al.*, 2020). Subsequently after storage, the accrued WSC in the stem and leaf sheaths are remobilized to the sink tissue during grain-filling (Scofield *et al.*, 2009), with the efficiency of translocation influenced by the genetic diversity in sink strength (Schnyder, 1993; Li *et al.*, 2017).

Studies have shown that as much as 0.68 to 0.78 g of yield can be produced for each 1 g of WSC stored in wheat (Kiniry, 1993). Increased rate of reallocation due to terminal drought has been stated to contribute up to 50% of yield in traditional- and as much as 70% in elite-cultivars (van Herwaarden *et al.*, 1998). Similar responses have been reported with heat (Schittenhelm *et al.*, 2020) and other biotic stresses (Sadras *et al.*, 2020). To minimize damage from stresses, newer phenotyping methods for high WSC storage and translocation is recommended in crops (Blum, 1998, Asseng and van Herwaarden, 2003; Wang *et al.*, 2016; Schittenhelm *et al.*, 2020). Studies exploring genotypic variation for WSC levels have been mainly focused on barley (Gay *et al.*, 1999), wheat (van Herwaarden *et al.*, 2003; Ruuska *et al.*, 2006; Dreccer *et al.*, 2009; Ovenden *et al.*, 2017), rice (Xiong *et al.*, 2014; Wang *et al.*, 2016; 2017; Moura *et al.*, 2017), and a few on maize (Wu *et al.*, 2019; Fernandez *et al.*, 2020).

Traditional methodology for quantifying WSC levels is destructive, time-consuming, expensive, and restricts the number of genotypes or samples that can be realistically processed. The lab-based methods for the extraction of WSC utilizes wet chemistry in different approaches. The original method was developed in 1954, by utilizing anthrone, and is still used to this day for ground-truthing or for generating benchmarks (Yemm and Willis, 1954; Giri, 2019). To increase throughput, near-infrared reflectance spectroscopy (NIRS) is being utilized alongside traditional wet chemistry methods. This medium-throughput methodology begins by determining the WSC levels in a subset of samples via wet chemistry and then are correlated with NIRS reflectance spectra. This methodology has been utilized on different crops including wheat (Rebetzke *et al.*, 2008; Wang *et al.*, 2011; Giri, 2019), rice (Wang *et al.*, 2016), and maize (Campo *et al.*, 2013).

The first step towards a true high-throughput phenotyping method for stem WSC levels was attempted on four recombinant inbred wheat lines utilizing a hyperspectral radiometer

(Dreccer *et al.*, 2014). The radiometer, with a sampling range from 350-2500 nm, was mounted onto a 4-wheel drive motorbike at 1.35 m above the soil. The remotely sensed WSC levels were then confirmed in the laboratory utilizing the anthrone method, presenting a significantly strong relationship ($R^2 = 0.90$) averaged across two years (Dreccer *et al.*, 2014) (Table 1-1). It was not until 2017 when hyperspectral imaging was used again to evaluate the concentration of WSC. A study involving estimation of sucrose content in maize leaves had success in utilizing hyperspectral imaging of the adaxial surface of a leaf with an illuminated leaf clip contact probe and partial least squares regression (PLSR) models (Yendrek *et al.*, 2017) (Table 1-1). While not as successful as Dreccer *et al.* (2014), the PLSR model was still able to predict sucrose content within the leaf with an R^2 value of 0.62. Garriga *et al.* (2017) utilized the same hyperspectral radiometer model as Dreccer *et al.* (2014) to predict WSC levels in a large variety trial, including 384 cultivars and advanced lines of spring wheat in both well-watered and water-stressed environments. The radiometer was placed at a 45-degree angle and swept over the plot three times and, utilizing multivariate regression models, the study was able to predict stem WSC levels with R^2 of 0.56 (Garriga *et al.*, 2017) (Table 1-1). It is unclear whether the difference in coefficients of determinations between Dreccer *et al.* (2014) and Garriga *et al.* (2017) was due to the angle at which the reflectance was obtained or other confounding factors, but these procedures need to be further standardized to accurately reflect the ground-truth observational data.

The next step forward in quantifying WSC levels *via* a high-throughput methodology is by implementing machine learning. This methodology has not been implemented with a row crop; however, it was recently tested with perennial ryegrass. The authors used a hyperspectral radiometer as well as a light shield in order to capture the spectra under stable light conditions

from 960 different plants, comprised of 50 experimental perennial ryegrass varieties (Smith *et al.*, 2020). The light shield was manually placed on each plant and artificial light within the shield was used as the light source. Comparatively, the cubist model resulted in an R^2 value of 0.49 while the PLSR model was only able to obtain an R^2 of 0.19 (Smith *et al.*, 2020). Although promising, the methodology may not be practical and too laborious to implement on trials that involve diversity panels or mapping populations in order to make it applicable to breeding programs. With limited research into the feasibility of utilizing hyperspectral imaging and machine learning for rapid, accurate measurements, the methodology cannot be discredited nor confirmed as the path forward which will lead to an accurate high-throughput evaluation.

Estimating yield and key yield related parameters

The economic yield of a crop is defined as the biological yield multiplied by the harvest index (HI) of dry matter or the product of grain number and grain weight (Osaki *et al.*, 1994). The ability to accurately predict yield in both stressed and non-stressed environments is an endeavor that is being continued for decades. Yield prediction is a complicated undertaking due to the dynamic environmental changes that fluctuate on a large temporal scale, from daily to yearly, and on a large geographical area, from locally to regionally, resulting in large variations in attainable crop yields. This is particularly true for heat and drought prone environments, which are shown to lead to lower seed numbers when stress coincides with flowering (Jagadish *et al.*, 2010; Bheemanahalli *et al.*, 2019; Chiluwal *et al.*, 2020; Prasad *et al.*, 2017) or loss in seed weight with stress during grain-filling (Bergkamp *et al.*, 2018; Lawas *et al.*, 2019).

Yield forecasts for regional, national and international cropping systems involve highly intricate and complicated systems utilizing an enormous amount of data and multiple regression

models or machine learning (Jeong *et al.*, 2016; Iizumi *et al.*, 2018; Han *et al.*, 2020; Schwalbert *et al.*, 2020). Advances are being made in order to estimate yield within the season in order to aid in making important management decisions in nominal, heat stress, or drought stress environments. Hence, to predict yield more reliably and accurately, particularly under abiotic stress prone environments, approaches to remotely determine the number of heads in a plot and the number of seeds on the head is required.

The first step to gaining the ability to predict yield is acquiring the capacity to accurately identify heads or panicles of crops. This area of remote sensing has garnered increased interest and utilizes different strategies employing machine and deep learning tools to ascertain accurate counts. One such experiment in 2017 attempted to identify rice panicles by applying a Convolutional Neural Network (CNN) classification and entropy rate super-pixel optimization to 684 images of pot-grown rice (Xiong *et al.*, 2017). This method outperformed three previously identified methods with an F-measure indicator, which takes in account for precision and recall, of 0.77 while the previous methodologies could only reach 0.44 (Xiong *et al.*, 2017) (Table 1-1).

The CNNs have also been utilized to detect and count the number of wheat spikes within a plot. This was achieved by employing a ground-based steel cart, with a central overhead rail equipped with high resolution cameras capable of being mounted at differing angles in relation to the crop of interest (Hasan *et al.*, 2018). The Faster R-CNN model using 305 training images at different growth stages was able to attain on average a 93% accuracy on the 30 test images after training (Ren *et al.*, 2017; Hasan *et al.*, 2018) (Table 1-1). Similarly, another study using the same approach was equally accurate during early stages after heading but was more robust during later stages when the leaves turned senescent and contrasted with greener wheat spikes (Madec *et al.*, 2019). The model achieved high relationship ($R^2 = 0.91$) when the resolution of

the image was 0.26 mm but reduced (R^2 = 0.33) when the image resolution was increased 0.78 mm, indicating the need for high resolution imagery for accurate spike detection (Madec *et al.*, 2019) (Table 1-1).

These advances in agricultural object identification are impressive, given how small wheat spikes are compared to other crops. Sorghum has had ample more research into accurate models for extracting and counting heads. Even though sorghum has much larger sized head than wheat spikes, research faces the same challenges while utilizing UAVs to obtain imagery: changing light conditions over the duration of a flight, complex and intricate backgrounds, and genotypic variations in head color, size, or shape and overlapping heads (Guo *et al.*, 2018) (Table 1-1). The same authors employed a pixel-based segmentation approach to train a digital terrain surface model (DTSM) which is supervised machine learning based on the decision tree, resulting in a F-measure of 0.92 and 0.89 on 52 images and 40 plots, respectively. The research group was then able to establish a deep learning framework with minimum supervision using CNN for head sorghum detection achieved R^2 of 0.88 with the training set comprising of only 40 randomly selected images (Ghosal *et al.*, 2019) (Table 1-1). In their most recent study, CNN models with image segmentation accurately estimated the number of sorghum heads (R^2 = 0.90) and characterized the shape and size of individual heads (Lin and Guo, 2020) (Table 1-1). This advancement could be key to estimating yield in sorghum, but seed number and weight are additional traits to be determined for effective yield prediction.

Research into using remote sensing to quantify seed number and grain weight of a plant in a field environment is quite limited. There has been success in controlled environments in which a 3D reconstruction of rice showed that seed number for the panicle had a significant ($p < 0.05$) positive correlation with the voxel count of the reconstruction throughout the grain-filling

period (r = 0.61 to 0.70) (Sandhu *et al.*, 2019). This same experiment also found significant ($p < 0.05$) positive correlation (r = 0.48 to 0.74) between voxel count and seed weight which increased approaching maturity. This method of obtaining the estimated seed number and weight works well in the laboratory setting but will be challenging to adopt under field conditions.

This challenge has been approached using a simpler method in order to allow for the methodology and the tool developed to be utilized by both researchers and farmers alike. This method follows an allometric determination method by taking RGB images with a digital camera of over 1000 sorghum heads. The head volume is determined by using the head length and diameter (measured using a ruler) and assuming the head is cylindrical and comparing this volume to grain number per head resulted in a strong relationship (R^2 of 0.68 and 0.58) for commercial hybrids and inbreds, respectively (Ciampitti *et al.*, 2014) (Figure 1-3A). This approach has been extended to estimate final yield using variables such as row spacing and estimate seed number per pound (Ciampitti *et al.*, 2015) (Figure 1-3B). The progress achieved using this approach integrated with machine learning tools is currently under development (Figure 1-3C).

Alternatively, current high-throughput estimations of yield are derived through the analysis of vegetation indices. While this method can provide relatively accurate prediction of yield, it is a secondary measure of yield and the reliability of the prediction only increases near maturity and could vary based on environmental changes (Galli *et al.*, 2020). In the near future, the primary measurement based on remote sensing that is being developed (Figure 1-3C), can be scalable to identify grain number on large populations in sorghum under field conditions, and also determine the seed loss in the head due to heat and drought stress.

Sensor-based approaches to rapidly phenotype for HNT response

As the impacts of HNT increases, it becomes ever more imperative to be able to phenotype for these effects on large populations including diversity panels, and mapping populations with higher efficiency and accuracy. The ability to phenotype for the effects of a HNT stress, however, has been mostly limited to day-time remote sensing across scales. Developments and advancements in ground-based systems, unmanned aerial systems, and satellite-based phenotyping methods have greatly increased the amount of qualitative and quantitative data that can be retrieved from a plant, field, or region without resorting to destructive methods (Tattaris *et al.*, 2016). Leaf senescence can be quantified using different vegetative indices, including Normalized Difference Vegetation Index (NDVI), Normalized Difference Red Edge Index (NDREI), Green Normalized Difference Vegetation Index (GNDVI) and Plant Senescence Reflectance Index (PSRI). At the plant level, the use of NDVI to obtain the rate of senescence in leaves is achieved through handheld sensors (Lopes and Reynolds, 2012; Christopher *et al.*, 2016; Montazeaud *et al.*, 2016).

Intricate mobile field platforms and high throughput unmanned aerial systems used to obtain RGB (red, green, blue), multispectral, and hyperspectral data allows for capturing different vegetative indices for a comprehensive depiction of the rate of senescence (Deery *et al.*, 2014; Hassan *et al.*, 2018; Makanza *et al.*, 2018). These aerial or field-based platforms can help record the rate of senescence at whole plant or plot level at high temporal frequency, which can be extended to evaluate large diversity panels or populations in a shorter period of time. Recently, a high-resolution imaging platform for rice has been developed for dynamic imaging of panicles under controlled environment conditions (Sandhu *et al.*, 2019). This platform can enable researchers to not only capture proxies for grain yield parameters but also follow the

differences in rate of panicle senescence under optimal and HNT conditions. A similar approach is also likely to work for wheat spikes, as demonstrated recently using a hand-held fluorometer (Šebela *et al.*, 2020).

As a result of post-flowering HNT exposure, cereals such as rice and wheat accumulate significantly lower amount of biomass (Bahuguna *et al.*, 2017; Impa *et al.*, 2019). The changes in above ground biomass due to HNT stress can be quantified efficiently and accurately through the use of LiDAR (Light Detection and Ranging) measurements integrated with mobile field platform (Jimenez-Berni *et al.*, 2018). In addition to LiDAR measurements, RGB and hyperspectral imaging can be used to estimate biomass and when integrated with machine learning algorithms achieves a higher accuracy than possible through basic analysis (Yue *et al.*, 2017; Lu *et al.*, 2019a). Recently, Coast *et al.* (2019), predicted leaf dark respiration based on leaf hyperspectral reflectance in wheat, which can be further developed and employed to measure carbon loss under HNT stress. In addition to above ground biomass, various reflectance spectra have been associated with grain yield (Geipel *et al.*, 2016; Liu *et al.*, 2019; Prey *et al.*, 2020), grain protein content (Geipel *et al.*, 2016), nitrogen concentration (Li *et al.*, 2010; Geipel *et al.*, 2016), plant nitrogen accumulation (Lu *et al.*, 2019b), dark respiration (Coast *et al.*, 2019), and the leaf chlorophyll content (Baret, *et al.*, 2007 Haboudane *et al.*, 2008; Cui *et al.*, 2019), which can be further explored to quantify a range of parameters affected by HNT.

Limitations and future research directions

Keeping in line with the scope of the review, we have indicated limitations and provided recommendations of utilizing advances in sensor technology to develop high throughput

phenotyping approaches to capture physiological aspects that will help enhance heat and drought stress resilience in crops.

Time-of-day of flowering

Achieving multiple flights at short temporal frequency to record TOF can be a limiting factor for many research programs. Hence, it is recommended to optimize flights that captures a large proportion of the variation on a flowering day to make the approach of using UAVs for capturing TOF feasible. In addition, the distance between the aerial sensor platform and the flowering field (after accounting for differences in plant height) needs to be optimized for different crops to ensure high quality images, for detecting genotypic differences. Algorithms will need to be developed and standardized to capture differences in color and area of foliage, and anthers and potentially accounting for soil surface in crops where the canopy does not close completely.

Photosynthetic efficiency

Designing ideotypes to maintain improved productivity under heat and drought stress and moving beyond stay-green versus senescence concepts, implemented at the plant level and small plots to phenotype diversity panels on large area has been the major bottleneck. Progress achieved in sensor technology provides the vehicle to capture temporal (flowering till maturity) changes in stay green versus senescence patterns that will allow for capturing the diversity required to incorporate into breeding programs. Experiments involving large diversity panels will need to be designed innovatively to be able to capture the gradient of changes in stay green and senescence both within and between genotypes.

Tracking water soluble carbohydrates translocation to grains

Limited progress has been achieved in employing sensor-based technology to capture the storage and translocation of WSC in plants, because of the dynamic changes, both spatially (leaf, stem

and grain) and temporally (within and between days during grain filling). This is further complicated with the stage, duration and intensity of stress, which warrants the need to capture the dynamics but still establish a practically feasible approach. Taking sensor based carbon balance in different plant parts in the morning and evening throughout the grain-filling period could help establish solid benchmarks. Using these established benchmarks, environment specific temporal intervals (in days) can be defined at which images needs to be taken that is both practical and captures >90% of changes between flowering till physiological maturity. That said, the community would still need to improve the accuracy of capturing the changes in WSC in plant parts, building on the progress achieved by Dreccer *et al.* (2014) and Garriga *et al.* (2017).

Estimating grain number and weight under stress

Heat and drought stress during flowering and post-flowering stages induces non-uniform seed-set (gaps) within panicles and heads, which deviates from the normal fully filled panicles that the system (Fig 1-3A, B) has been optimized to estimate. Having a mosaic of loss in seeds within panicles due to stress will challenge the approach developed. This would require extensive training before it can be employed or used effectively to estimate the seed loss under stress. Currently, the integration of machine learning tools into the approach could help but would still require a large sample size with different proportion of loss in seed numbers in panicles/heads, before the technology can be standardized. Unlike loss in seed numbers reduction in seed weight within panicles and different genotypes due to heat and drought stress presents a lesser challenge and can be captured using the current model.

Sensor-based approaches to rapidly phenotype for HNT response

While the advancements in utilizing the reflectance spectra for the measurement of the plant's daytime response to HNT are significant, the methods mentioned previously are inadequate and inappropriate for direct measurement of the plant's response during the night, when HNT is imposed, due to the lack of light. Infrared imaging can help fill this gap in developing adequate sensing methods during night-time and gain information on transpiration, leaf water potential, or stomatal conductance through the canopy temperature or indices such as the Crop Water Stress Index (White *et al.*, 2012). Thermal sensors have been effectively used to determine the canopy temperature differences during the day (Costa *et al.*, 2013; Sagan *et al.*, 2019), developing similar methodologies to quantify and explore plant responses to HNT would be an interesting research direction. Conversely an automated, track-based system coupled with an active sensor which provides its own illumination on the area of interest could easily be integrated with the recent advancements in field-based infrastructure for phenotyping for HNT stress. Although it would be imperative to obtain a source of illumination which would not alter the plant's overnight conditions.

Conclusions

The review provides an overview of current advances and future directions related to key physiological processes and remote sensing phenotyping related to HDT, HNT, and drought stress resilience during reproductive and grain-filling period. In order to take advantage of naturally occurring trait variation to increase heat and drought stress resiliency in crop varieties, collaborative science is imperative and inevitable. Tools in machine and deep learning in relation to agriculture are becoming fundamentally critical for evaluation of these hard to quantify and

time-sensitive traits. In order to make progress at the rate which is required by global demand and climate change, traditional and hand-measurements must be evolved in order to accurately, quickly, and reliably obtain more scalable measurements with high-resolution. The five key areas highlighted, the limitations and future research directions provide the next steps to establish high-throughput phenotyping platforms for field-based estimations and for incorporating these traits into global abiotic stress breeding programs.

References

Aghamolki, M.T.K., Yusop, M.K., Oad, F.C., Zakikhani, H., Jaafar, H.Z., Kharida, S., Musa, M.H., 2013. Heat stress effects on yield parameters of selected rice cultivars at reproductive growth stages. Journal of Food Agriculture and Environment 12, 741-746.

Aiqing, S., Somayanda, I., Sebastian, S.V., Singh, K., Gil, K., Prasad, P.V.V., Jagadish, S.V.K., 2018. Heat stress during flowering affects time of day of flowering, seed set, and grain quality in spring wheat. Crop Science 58, 380-392. https://www.doi.org/10.2135/cropsci2017.04.0221

Araus, J.L., Kefauver, S.C., Zaman-Allah, M., Olsen, M.S., Cairns, J.E., 2018. Translating high-throughput phenotyping into genetic gain. Trends in Plant Science 23, 451-466. https://www.doi.org/10.1016/j.tplants.2018.02.001

Asseng, S., van Herwaarden, A.F., 2003. Analysis of the benefits to wheat yield from assimilates stored prior to grain filling in a range of environments. Plant and Soil 256, 217-229. https://www.doi.org/10.1023/A:1026231904221

Asseng, S., Ewert, F., Martre, P., *et al.*, 2015. Rising temperatures reduce global wheat production. Nature Climate Change 5, 143-147. https://www.doi.org/10.1038/nclimate2470

Bahuguna, R.N., Solis, C.A., Shi, W., Jagadish, S.V.K., 2017. Post-flowering night respiration and altered sink activity account for high night temperature-induced grain yield and quality loss in rice (Oryza sativa L.). Physiologia Plantarum 159, 59-73. https://www.doi.org/10.1111/ppl.12485

Balla, K., Karsai, I., Bónis, P., Kiss, T., Berki, Z., Horváth, A., Mayer, M., Bencze, S., Veisz, O., 2019. Heat stress responses in a large set of winter wheat cultivars (*Triticum aestivum* L.)

depend on the timing and duration of stress. PLoS ONE 14, e0222639. https://www.doi.org/10.1371/journal.pone.0222639

Baret, F., Houlès, V., Guérif, M., 2007. Quantification of plant stress using remote sensing observations and crop models: the case of nitrogen management. Journal of Experimental Botany 58, 869-880. https://www.doi.org/10.1093/jxb/erl231

Barker III, J., Zhang, N., Sharon, J., Steeves, R., Wang, X., Wei, Y., Poland, J., 2016. Development of a field-based high-throughput mobile phenotyping platform. Computers and Electronics in Agriculture 122, 74-85. https://www.doi.org/10.1016/j.compag.2016.01.017

Barnabás, B., Jäger, K., Fehér, A., 2008. The effect of drought and heat stress on reproductive processes in cereals. Plant Cell and Environment 31, 11-38. https://www.doi.org/10.1111/j.1365-3040.2007.01727.x

Becker, E., Schmidhalter, U., 2017. Evaluation of yield and drought using active and passive spectral sensing systems at the reproductive stage in wheat. Frontiers in Plant Science 8, 379. https://www.doi.org/10.3389/fpls.2017.00379

Bergkamp, B., Impa, S.M., Asebedo, A.R., Fritz, A.K., Jagadish, S.V.K., 2018. Prominent winter wheat varieties response to post-flowering heat stress under controlled chambers and field based heat tents. Field Crops Research 222, 143-152. https://www.doi.org/10.1016/j.fcr.2018.03.009

Bheemanahalli, R., Sathishraj, R., Manoharan, M., Sumanth, H.N., Muthurajan, R., Ishimaru, T., Jagadish, S.V.K., 2017. Is early morning flowering an effective trait to minimize heat stress damage during flowering in rice?. Field Crops Research 203, 238-242. https://www.doi.org/10.1016/j.fcr.2016.11.011

Bheemanahalli, R., Sunoj, V.S.J., Saripalli, G., Prasad, P.V.V., Balyan, H.S., Gupta, P.K., Grant, N., Gill, K.S., Jagadish, S.V.K., 2019. Quantifying the impact of heat stress on pollen germination, seed set, and grain filling in spring wheat. Crop Science 59, 684-696. https://www.doi.org/10.2135/cropsci2018.05.0292

Blum, A., 1998. Improving wheat grain filling under stress by stem reserve mobilization. Euphytica 100, 77-83. https://www.doi.org/10.1023/A:1018303922482

Borrell, A.K., Oosterom, E.J.V., Mullet, J.E., George-Jaeggli, B., Jordan, D.R., Klein, P.E., Hammer, GL., 2014. Stay-green alleles individually enhance grain yield in sorghum under drought by modifying canopy development and water uptake patterns. New Phytologist 203, 817-830. https://www.doi.org/10.1111/nph.12869

Cairns, J.E., Sanchez, C., Vargas, M., Ordoñez, R., Araus, J.L., 2012. Dissecting maize productivity: ideotypes associated with grain yield under drought stress and well-watered conditions. Journal of Integrative Plant Biology 54, 1007-1020. https://www.doi.org/10.111/j.1744-7909.2012.01156.x

Campo, L., Monteagudo, A.B., Salleres, B., Castro, P., Moreno-Gonzalez, J., 2013. NIRS determination of non-structural carbohydrates, water soluble carbohydrates and other nutritive quality traits in whole plant maize with wide range variability. Spanish Journal of Agricultural Research 11, 463-471. https://www.doi.org/10.5424/sjar/2013112-3316

Chawade, A., Ham, J.V., Blomquist, H., Bagge, O., Alexandersson, E., Ortiz, R., 2019. High-throughput field-phenotyping tools for plant breeding and precision agriculture. Agronomy 9, 258. https://www.doi.org/10.3390/agronomy9050258

Cheng, W., Sakai, H., Yagi, K., Hasegawa, T., 2010. Combined effects of elevated CO2 and high night temperature on carbon assimilation, nitrogen absorption, and the allocations of C

and N by rice (Oryza sativa L.). Agricultural and Forest Meteorology 150(9), 1174-1181. https://www.doi.org/10.1016/j.agrformet.2010.05.001

Chiluwal, A., Bheemanahalli, R., Kanaganahalli, V., Boyle, D., Perumal, R., Pokharel, M., Oumarou, H., Jagadish, S.V.K., 2020. Deterioration of ovary plays a key role in heat stress-induced spikelet sterility in sorghum. Plant Cell and Environment 43, 448-462. https://www.doi.org/10.1111/pce.13673

Christopher, J.T., Christopher, M.J., Borrell, A.K., Fletcher, S., Chenu, K., 2016. Stay-green traits to improve wheat adaptation in well-watered and water-limited environments. Journal of Experimental Botany 67, 5159-5172. https://www.doi.org/10.1093/jxb/erw276

Ciampitti, I.A., Balboa, G.R., Prasad, P.V.V., 2014. Development of a new tool for estimating sorghum yields at the farm-scale. ASA, CSSA and SSSA International Annual Meeting (2014). Poster Number: 342.

Ciampitti, I.A., Azevedo, A.J., Balboa, G.R., Bossio, N., 2015. Sorghumyield app, a new tool for predicting sorghum yields: validation and calibration. ASA, CSSA, and SSSA International Annual Meeting (2015). Poster Number: 501.

Coast, O., Shah, S., Ivakov, A., *et al.*, 2019. Predicting dark respiration rates of wheat leaves from hyperspectral reflectance. Plant Cell and Environment 42, 2133-2150. https://www.doi.org/10.1111/pce.13544

Colomina, I., Molina, P., 2014. Unmanned aerial systems for photogrammetry and remote sensing: a review. ISPRS Journal of Photogrammetry and Remote Sensing 92, 79-97. https://www.doi.org/10.1016/j.isprsjprs.2014.02.013

Costa, J.M., Grant, O.M., Chaves, M.M., 2013. Thermography to explore plant-environment interactions. Journal of Experimental Botany 64, 3937-3949. https://www.doi.org/10.1093/jxb/ert029

Cui, B., Zhao, Q., Huang, W., Song, X., Ye, H., Zhou, X., 2019. A new integrated vegetation index for the estimation of winter wheat leaf chlorophyll content. Remote Sensing 11, 974. https://www.doi.org/10.3390/rs11080974

Daryanto, S., Wang, L., Jacinthe, P.A., 2016. Global synthesis of drought effects on maize and wheat production. PLOS ONE, e0156362. https://www.doi.org/10.1371/journal.pone.0156362

Deery, D., Jimenez-Berni, J., Jones, H., Sirault, X., Furbank, R., 2014. Proximal remote sensing buggies and potential application for field-based phenotyping. Agronomy 4, 349-379. https://www.doi.org/10.3390/agronomy4030349

Desai, J.S., Slabaugh, E., Liebelt, D.J., Fredenberg, J.D., Gray, B.N., Jagadish, S.V.K., Wilkins, O., Doherty, C.J., 2018. Neural net classification combined with movement analysis to evaluate *Setaria viridis* as model system for time of day of anther appearance. Frontiers in Plant Science 9, 1585. https://www.doi.org/10.3389/fpls.2018.01585

Dreccer, M.F., van Herwaarden, A.F., Chapman, S.C., 2009. Grain number and grain weight in wheat lines contrasting for stem water soluble carbohydrate concentration. Field Crops Research 112, 43-54. https://www.doi.org/10.1016/j.fcr.2009.02.006

Dreccer, M.F., Barnes, L.R., Meder, R., 2014. Quantitative dynamics of stem water soluble carbohydrates in wheat can be monitored in the field using hyperspectral reflectance. Field Crops Research 159, 70-80. https://www.doi.org/10.1016/j.fcr.2014.01.001

Easterling, D.R., Horton, B., Jones, P.D., *et al.*, 1997. Maximum and minimum temperature trends for the globe. Science 277, 364-367. https://www.doi.org/10.1126/science.277.5324.364

Ehdaie, B., Alloush, A., Madore, M.A., Waines, J.G., 2006. Genotypic variation for stem reserves and mobilization in wheat: II. postanthesis changes in internode water-soluble carbohydrates. Crop Science 46, 2093-2103. https://www.doi.org/10.2135/cropsci2006.01.0013

El-Hendawy, S., Hassan, W.M., Al-Suhaibani, N.A., Schmidhalter, U., 2017. Spectral assessment of drought tolerance indices and grain yield in advanced spring wheat lines grown under full and limited water irrigation. Agricultural Water Management 182, 1-12. https://www.doi.org/10.1016/j.agwat.2016.12.003

Fernandez, J.A., Messina, C.D., Rotundo, J., Ciampitti, I.A., 2020. Integrating nitrogen and water-soluble carbohydrates dynamics in maize: a comparison between hybrids from different decades. Crop Science 61, 1360-1373. https://www.doi.org/10.1002/csc2.20338

Food and Agriculture Organization of the United Nations. FAO Stat: Annual Population [Internet]. 2019 Available from: http://www.fao.org/faostat/en/#data/OA

Food and Agriculture Organization of the United Nations. The future of food and agriculture: Trends and challenges [Internet]. 2017 Available from: http://www.fao.org/3/a-i6583e.pdf

Frantz, J.M., Cometti, N.N., Bugbee, B., 2004. Night temperature has a minimal effect on respiration and growth in rapidly growing plants. Annals of Botany 94, 155-166. https://www.doi.org/10.1093/aob/mch122

Fu, J., Yan, Y., Kim, M.Y., Lee, S.H., Lee, B.W., 2011. Population-specific quantitative trait loci mapping for functional stay-green trait in rice (*Oryza sativa* L.). Genome 54, 235-243. https://www.doi.org/10.1139/g10-113

Galli, G., Horne, D.W., Collins, S.D., Jung, J., Chang, A., Fritsche-Neto, R., Rooney, W.L., 2020. Optimization of UAS-based high-throughput phenotyping to estimate plant health and grain yield in sorghum. The Plant Phenome Journal 3, e20010. https://www.doi.org/10.1002/ppj2.20010

Garriga, M., Romero-Bravo, S., Estrada, F., Escobar, A., Matus, I., del Pozo, A., Astudillo, C.A., Lobos, G.A., 2017. Assessing wheat traits by spectral reflectance: do we really need to focus on predicted trait-values or directly identify the elite genotypes group?. Frontiers in Plant Science 8, 280. https://www.doi.org/10.3389/fpls.2017.00280

Gay, A.P., Spink, J.H., Foulkes, M.J., 1999. Preliminary assessment of the potential for variety typing in winter barley: stem water soluble carbohydrate measurements. Project Report no. 186. Home-Grown Cereals Authority.

Gebbing, T., 2003. The enclosed and exposed part of the peduncle of wheat (*Triticum aestivum*) – spatial separation of fructan storage. New Phytologist 159, 245-252. https://www.doi.org/10.1046/j.1469-8137.2003.00799.x

Geipel, J., Link, J., Wirwahn, J., Clauepein, W., 2016. A programmable aerial multispectral camera system for in-season crop biomass and nitrogen content estimation. Agriculture 6, 4. https://www.doi.org/10.3390/agriculture6010004

Genty, B., Briantais, J.M., Baker, N.R., 1989. The relationship between the quantum yield of photosynthetic electron transport and quenching of chlorophyll fluorescence. Biochimica

et Biophysica Acta (BBA) – General Subjects 990, 87-92. https://www.doi.org/10.1016/S0304-4165(89)80016-9

Ghosal, S., Zheng, B., Chapman, S.C., *et al.*, 2019. A weakly supervised deep learning framework for sorghum head detection and counting. Plant Phenomics 2019, 1525874. https://www.doi.org/10.34133/2019/1525874

Giri, A., 2019. Wheat improvement for heat and drought stress tolerance. Ph.D. Dissertation, Kansas State University http://hdl.handle.net/2097/39551 Accessed September 2020.

Glaubitz, U., Li, X., Kohl, K.I., van Dongen, J.T., Hincha, D.K., Zuther, E., 2014. Differential physiological responses of different rice (Oryza sativa) cultivars to elevated night temperature during vegetative growth. Functional Plant Biology 41, 437-448. https://www.doi.org/10.1071/fp13132

Gourdji, S.M., Sibley, A.M., Lobell, D.B., 2013. Global crop exposure to critical high temperatures in the reproductive period: historical trends and future projections. Environmental Research Letters 8, 024041. https://www.doi.org/10.1088/1748-9326/8/2/024041

Gous, P.W., Hickey, L., Christopher, J., Franckowiak, J., Fox, G.P., 2015. Discovery of QTL for stay-green and heat-stress in barley (*Hordeum vulgare*) grown under simulated abiotic stress conditions. Euphytica 207, 305-317. https://www.doi.org/10.1007/s10681-015-1542-9

Gowik, U., Westhoff, P., 2011. The Path from C3 to C4 Photosynthesis. Plant Physiology 155, 56-63. https://www.doi.org/10.1104/pp.110.165308

Graß, R., Böttcher, U., Lilienthal, H., Wild, P., Kage, H., 2020. Is canopy temperature suitable for high throughput field phenotyping of drought resistance of winter rye in temperate

climate?. European Journal of Agronomy 120, 126104. https://www.doi.org/10.1016/j.eja.2020.126104

Guo, W., Zheng, B., Potgieter, A.B., *et al.*, 2018. Aerial imagery analysis – quantifying appearance and number of sorghum heads for application in breeding and agronomy. Frontiers in Plant Science 9, 1544. https://www.doi.org/10.3389/fpls.2018.01544

Haboudane, D., Tremblay, N., Miller, J.R., Vigneault, P., 2008. Remote estimation of crop chlorophyll content using spectral indices derived from hyperspectral data. IEEE Transactions on Geoscience and Remote Sensing 46, 423-437. https://www.doi.org/10.1109/TGRS.2007.904836

Han, J., Zhang, Z., Cao, J., Luo, Y., Zhang, L., Li, Z., Zhang, J., 2020. Prediction of winter wheat yield based on multi-source data and machine learning in China. Remote Sensing 12, 236. https://www.doi.org/10.3390/rs12020236

Hasan, M.M, Chopin, J.P., Laga, H., Miklavcic, S., 2018. Detection and analysis of wheat spikes using convolutional neural networks. Plant Methods 14, 100. https://www.doi.org/10.1186/s13007-018-0366-8

Hassan, M.A., Yang, M., Rasheed, A., Jin, X., Xia, X., Xiao, Y., He, Z., 2018. Time-series multispectral indices from unmanned aerial vehicle imagery reveal senescence rate in bread wheat. Remote Sensing, 10 809. https://www.doi.org/10.3390/rs10060809

Hirabayashi, H., Sasaki, K., Kambe, T., *et al.*, 2014. qEMF3, a novel QTL for the early-morning flowering trait from wild rice, *Oryza officinalis*, to mitigate heat stress damage at flowering in rice, *O. sativa*. Journal of Experimental Botany 66, 1227-1236. https://www.doi.org/10.1093/jxb/eru474

Hörtensteiner, S., Feller, U., 2002. Nitrogen metabolism and remobilization during senescence. Journal of Experimental Botany 53, 927-937. https://www.doi.org/10.1093/jexbot/53.370.927

Iizume, T., Shin, Y., Kim, W., Kim, M., Choi, J., 2018. Global crop yield forecasting using seasonal climate information from a multi-model ensemble. Climate Services 11, 13-23. https://www.doi.org/10.1016/j.cliser.2018.06.003

Impa, S.M., Sunoj, V.S.J., Krassovskaya, I., Bheemanahalli, R., Obata, T., Jagadish, S.V.K., 2019. Carbon balance and source-sink metabolic changes in winter wheat exposed to high night-time temperature. Plant Cell and Environment 42, 1233-1246. https://www.doi.org/10.1111/pce.13488

Intergovernmental Panel on Climate Change. Climate change 2014: synthesis report [Internet]. 2014 [cited 2020 Apr 25]. Available from: https://www.ipcc.ch/site/assets/uploads/2018/05/SYR_AR5_FINAL_full_wcover.pdf

Ishimaru, T., Hirabayashi, H., Ida, M., Takai, T., San-Oh, Y.A., Yoshinaga, S., Ando, I., Ogawa, T., Kondo, M., 2010. A genetic resource for early-morning flowering trait of wild rice *Oryza officinalis* to mitigate high temperature-induced spikelet sterility at anthesis. Annals of Botany 106, 515-520. https://www.doi.org/10.1093/aob/mcq124

Jagadish, S.V.K., Muthurajan, R., Oane, R., Wheeler, T.R., Heuer, S., Bennett, J., Craufurd, P.Q., 2010. Physiological and proteomic approaches to address heat tolerance during anthesis in rice (*Oryza sativa* L.). Journal of Experimental Botany 61, 143-156. https://www.doi.org/10.1093/jxb/Ferp289

Jagadish, S.V.K., Kishor, P.B.K., Bahuguna, R.N., von Wirén, N., Sreenivasulu, N., 2015a. Staying alive or going to die during terminal senescence – an enigma surrounding yield

stability. Frontiers in Plant Science 6, 1070. https://www.doi.org/10.3389/fpls.2015.01070

Jagadish, S.V.K., Murty, M.V.R., Quick, W.P., 2015b. Rice responses to rising temperatures – challenges, perspectives and future directions. Plant, Cell and Environment 38, 1686-1698. https://www.doi.org/10.1111/pce.12430

Jagadish, S.V.K., 2020. Heat stress during flowering in cereals – effects and adaptation strategies. New Phytologist 226, 1567-1572. https://www.doi.org/10.1111/nph.16429

Janse, P.V., Deshmukh, R.R., 2017. Hyperspectral remote sensing for agriculture: a review. International Journal of Computer Applications 172, 30-34. https://www.ijcaonline.org/archives/volume172/number7/janse-2017-ijca-915185.pdf

Jeong, J.H., Resop, J.P., Mueller, N.D., *et al.*, 2016. Random forests for global and regional crop yield predictions. PLoS ONE 11, e0156571. https://www.doi.org/10.1371/journal.pone.0156571

Jimenez-Berni, J.A., Deery, D.M., Rozas-Larraonda, P., Condon, A.G., Rebetzke, G.J., James, R.A., Bovill, M.D., Furbank, R.T., Sirault, X.R.R., 2018. High throughput determination of plant height, ground cover, and above-ground biomass in wheat with LiDAR. Frontiers in Plant Science 9, 237. https://www.doi.org/10.3389/fpls.2018.00237

Julia, C., Dingkuhn, M., 2013. Predicting temperature induced sterility of rice spikelets requires simulation of crop-generated microclimate. European Journal of Agronomy 49, 50-60. https://www.doi.org/10.1016/j.eja.2013.03.006

Jung, C., Müller, A., 2009. Flowering time control and application in plant breeding. Trends in Plant Science 14, 563-573. https://www.doi.org/10.1016/j.tplants.2009.07.005

Kanno, K., Mae, T., Makino, A., 2009. High night temperature stimulates photosynthesis, biomass, production and growth during the vegetative stage of rice plants. Soil Science and Plant Nutrition 55, 124-131. https://www.doi.org/10.1111/j.1747-0765.2008.00343.x

Khan, P.S.S.V., Nagamallaiah, G.V., Rao, M.D., Sergeant, K., Hausman, J.F., 2014. Abiotic stress tolerance in plants: insights from proteomics. In: Ahmad P, Rasool S, eds. Emerging technologies and management of crop stress tolerance. Academic Press doi: 10.1016/B978-0-12-800875-1.00002-8 https://www.doi.org/10.1016/B978-0-12-800875-1.00002-8

Kim, W., Iizumi, T., Nishimori, M., 2019. Global patterns of crop production losses associated with droughts from 1983 to 2009. Journal of Applied Meteorology and Climatology 58, 1233-1244. https://www.doi.org/10.1175/JAMC-D-18-0174.1

Kiniry, J.R., 1993. Nonstructural carbohydrate utilization by wheat shaded during grain growth. Agronomy Journal 85, 844-849. https://www.doi.org/10.2134/agronj1993.00021962008500040013x

Kobayasi, K., Matsui, T., Yoshimoto, M., Hasegawa, T., 2010. Effects of temperature, solar radiation, and vapor-pressure deficit on flower opening time in rice. Plant Production Science 13, 21-28. https://www.doi.org/10.1626/pps.13.21

Kolber, Z., Klimov, D., Ananyev, G., Rascher, U., Berry, J., Osmond, B., 2005. Measuring photosynthetic parameters at a distance: laser induced fluorescence transient (LIFT) method for remote measurements of photosynthesis in terrestrial vegetation. Photosynthesis Research 84, 121-129. https://www.doi.org/10.1007/s11120-005-5092-1

Lawas, L.M.F., Shi, W., Yoshimoto, M., Hasegawa, T., Hincha, D.K., Zuther, E., Jagadish, S.V.K., 2018. Combined drought and heat stress impact during flowering and grain

filling in contrasting rice cultivars grown under field conditions. Field Crops Research 229, 66-77. https://www.doi.org/10.1016/j.fcr.2018.09.009

Li, F., Miao, Y., Hennig, S.D., Gnyp, M.L., Chen, X., Jia, L., Bareth, G., 2010. Evaluating hyperspectral vegetation indices for estimating nitrogen concentration of winter wheat at different growth stages. Precision Agriculture 11, 335-357. https://doi.org/10.1007/s11119-010-9165-6

Li, G., Pan, J., Cui, K., Yuan, M., Hu, Q., Wang, W., Mohapatra, P.K., Nie, L., Huang, J., Peng, S., 2017. Limitation of unloading in the developing grains is a possible cause responsible for low stem non-structural carbohydrate translocation and poor grain yield formation in rice through verification of recombinant inbred lines. Frontiers in Plant Science 8, 1369. https://www.doi.org/10.3389/fpls.2017.01369

Lin, H., Chen, Y., Zhang, H., Fu, P., Fan, Z., 2017. Stronger cooling effects of transpiration and leaf physical traits of plants from a hot dry habitat than from a hot wet habitat. Functional Ecology 31, 2202-2211. https://www.doi.org/10.1111/1365-2435.12923

Lin, Z., Guo, W., 2020. Sorghum panicle detection and counting using unmanned aerial system images and deep learning. Frontiers in Plant Science 11, 534853. https://www.doi.org/10.3389/fpls.2020.534853

Liu, C., Pinto, F., Cossani, C.M., Sukumaran, S., Reynolds, M.P., 2019. Spectral reflectance indices as proxies for yield potential and heat stress tolerance in spring wheat: heritability estimates and marker-trait associations. Frontiers of Agricultural Science and Engineering 6, 296-308. https://www.doi.org/10.15302/J-FASE-2019269

Loka, D.A., Oosterhuis, D.M., 2010. Effect of high night temperatures on cotton respiration, ATP levels and carbohydrate content. Environmental and Experimental Botany 68, 258-263. https://www.doi.org/10.1016/j.envexpbot.2010.01.006

Long, S.P., Zhu, X., Naidu, S.L., Ort, D.R., 2006. Can improvement in photosynthesis increase crop yields?. Plant, Cell and Environment 29, 315-330. https://www.doi.org/10.1111/j.1365-3040.2005.01493.x

Lopes, M.S., Reynolds, M.P., 2012. Stay-green in spring wheat can be determined by spectral reflectance measurements (normalized difference vegetation index) independently from phenology. Journal of Experimental Botany 63, 3789-3798. https://www.doi.org/10.1093/jxb/ers071

Lu, N., Han, Z., Li, D., Cao, Q., Yao, X., Tian, Y., Zhu, Y., Weixing, C., Cheng, T., 2019a. Improved estimation of aboveground biomass in wheat from RGB imagery and point cloud data acquired with a low-cost unmanned aerial vehicle system. Plant Methods 15, 17. https://www.doi.org/10.1186/s13007-019-0402-3

Lu, N., Wang, W., Zhang, Q., Li, D., Yao, X., Tian, Y., Zhu, Y., Cao, W., Baret, F., Liu, S., Cheng, T., 2019b. Estimation of nitrogen nutrition status in winter wheat from unmanned aerial vehicle based multi-angular multispectral imagery. Frontiers in Plant Science 10, 1601. https://www.doi.org/10.3389/fpls.2019.01601

Madec, S., Jin, X., Lu, H., De Solan, B., Liu, S., Duyme, F., Heritier, E., Baret, F., 2019. Ear density estimation from high resolution RGB imagery using deep learning technique. Agricultural and Forest Meteorology 264, 225-234. https://www.doi.org/10.1016/j.agrformet.2018.10.013

Makanza, R., Zaman-Allah, M., Cairns, J.E., Magorokosho, C., Tarekegne, A., Olsen, M., Prasanna, B.M., 2018. High-throughput phenotyping of canopy cover and senescence in maize field trials using aerial digital canopy imaging. Remote Sensing 10, 330. https://www.doi.org/10.3390/rs10020330

Mohammed, A.R., Tarpley, L., 2009. Impact of high nighttime temperature on respiration, membrane stability, antioxidant capacity and yield of rice plants. Crop Science 49, 313-322. https://www.doi.org/10.2135/cropsci2008.03.0161

Montazeaud, G., Karatogma, H., Özturk, I., Roumet, P., Ecarnot, M., Crossa, J., Ozer, E., Ozdemir, F., Lopes, M.S., 2016. Predicting wheat maturity and stay-green parameters by modeling spectral reflectance measurements and their contribution to grain yield under rainfed conditions. Field Crops Research 196, 191-198. https://www.doi.org/10.1016/j.fcr.2016.06.021

Moura, D.S., Brito, G.G., Campos, A.D., Moraes, I., Porto, F., Teixeira, S., Fagundes, P., Andres, A., Schreiber, F., Deuner, S., 2017. Non-structural carbohydrates accumulation in contrasting rice genotypes subjected to high night temperatures. Journal of Agricultural Science 9, 12. https://www.doi.org/10.5539/jas.v9n12p302

Muller, O., Keller, B., Zimmermann, L., *et al.*, 2018. Field phenotyping and an example of proximal sensing of photosynthesis under elevated CO_2. Proceedings of the 14th International Conference on Precision Agriculture doi: 10.1109/IGARSS.2018.8517301 https://www.doi.org/10.1109/IGARSS.2018.8517301

Murchi, E.H., Niyogi, K.K., 2011. Manipulation of photoprotection to improve plant photosynthesis. Plant Physiology 155, 86-92. https://www.doi.org/10.1104/pp.110.168831

Neilson, E.H., Blomstedt, C.K., Berger, B., Møller, B.L., 2015. Utilization of a high-throughput shoot imaging system to examine the dynamic phenotypic responses of a C_4 cereal crop plant to nitrogen and water deficiency over time. Journal of Experimental Botany 66, 1817-1832. https://www.doi.org/10.1093/jxb/eru526

Neumann, K., Klukas, C., Friedel, S., Rischbeck, P., Chen, D., Entzian, A., Stein, N., Graner, A., Kilian, B., 2015. Dissecting spatiotemporal biomass accumulation in barley under different water regimes using high-throughput image analysis. Plant, Cell and Environment 38, 1980-1996. https://www.doi.org/10.1111/pce.12516

Osaki, M., Matsumoto, M., Shinano, T., Tadano, T., 1994. Parameters determining yield of field crops in relation to the amount of nitrogen absorbed. Soil Science and Plant Nutrition 40, 19-28. https://www.doi.org/10.1080/00380768.1994.10414274

Ovenden, B., Milgate, A., Lisle, C., Wade, L.J., Rebetzke, G.J., Holland, J.B., 2017. Selection for water-soluble carbohydrate accumulation and investigation of genetic x environment interactions in an elite wheat breeding population. Theoretical and Applied Genetics 130, 2445-2461. https://www.doi.org/10.1007/s00122-017-2969-2

Padilla-Chacón, D., Valdivia, C.B.P., Garcia-Esteva, A., Cayetano-Marcial, M.I., Shibata, J.K., 2019. Phenotypic variation and biomass partitioning during post-flowering in two common bean cultivars (*Phaseolus vulgaris* L.) under water restriction. South African Journal of Botany 121, 98-104. https://www.doi.org/10.1016/j.sajb.2018.10.031

Pauli, D., Andrade-Sanchez, P., Carmo-Silva, A.E., *et al.*, 2016. Field-based high-throughput plant phenotyping reveals the temporal patterns of quantitative trait loci associated with stress-responsive traits in cotton. G3: Genes, Genomes, Genetics 6, 865-879. https://www.doi.org/10.1534/g3.115.023515

Peng, Y., Zeng, A., Zhu, T., Fang, S., Gong, Y., Tao, Y., Zhou, Y., Liu, K., 2017. Using remotely sensed spectral reflectance to indicate leaf photosynthetic efficiency derived from active fluorescence measurements. Journal of Applied Remote Sensing 11, 026034. https://www.doi.org/10.1117/1.JRS.11.026034

Peraudeau, S., Lafarge, T., Roques, S., Quinones, C.O., Celment-Vidal, P.B., Rie, J.V., Jagadish, S.V.K., Dingkuhn, M., 2015a. Effect of carbohydrates and night temperature on night respiration in rice. Journal of Experimental Botany 66 3931-3944. https://www.doi.org/10.1093/jxb/erv193

Peraudeau, S., Roques, S., Quinones, C.O., Fabre, D., Rie, J.V., Ouwerkerk, P.B.F., Jagadish, S.V.K., Dingkuhn, M., Lafarge, T., 2015b. Increase in night temperature in rice enhances respiration rate without significant impact on biomass accumulation. Field Crops Research 171, 67-78. https://www.doi.org/10.1016/j.fcr.2014.11.004

Pieruschka, R., Klimov, D., Berry, J.A., Osmond, C.B., Rascher, U., Kolber, Z.S., 2012. Remote chlorophyll fluorescence measurements with the laser-induced fluorescence transient approach. Methods in Molecular Biology 918, 51-59. https://www.doi.org/10.1007/978-1-61779-995-2_5

Pinto, R.S., Lopes, M.S., Collins, N.C., Reynolds, M.P., 2016. Modelling and genetic dissection of staygreen under heat stress. Theoretical and Applied Genetics 129, 2055-2074. https://www.doi.org/10.1007/s00122-016-2757-4

Pokharel, M., Chiluwal, A., Stamm, M., Min, D., Rhodes, D., Jagadish, S.V.K., 2020. High night-time temperature during flowering and pod filling affects flower opening, yield and seed fatty acid composition in canola. Journal of Agronomy and Crop Science 00, 1-18. https://www.doi.org/10.1111/jac.12408

Prasad, P.V.V., Bheemanahalli, R., Jagadish, S.V.K., 2017. Field crops and the fear of heat stress – opportunities, challenges, and future directions. Field Crops Research 200, 114-121. https://www.doi.org/10.1016/j.fcr.2016.09.024

Prasad, P.V.V., Djanaguiraman, M., 2011. High night temperature decreases leaf photosynthesis and pollen function in grain sorghum. Functional Plant Biology 38, 993-1003. https://www.doi.org/10.1071/fp11035

Prey, L., Hu, Y., Schmidhalter, U., 2020. High-throughput field phenotyping traits of grain yield formation and nitrogen use efficiency: optimizing the selection of vegetation indices and growth stages. Frontiers in Plant Science 10, 1672. https://www.doi.org/10.3389/fpls.2019.01672

Raesch, A.R., Muller, O., Pieruschka, R., Rascher, U., 2014. Field observations with laser-induced fluorescence transient (LIFT) method in barley and sugar beet. Agriculture 4, 159-169. https://www.doi.org/10.3390/agriculture4020159

Raines, C.A., 2011. Increasing photosynthetic carbon assimilation in C3 plants to improve crop yield: current and future strategies. Plant Physiology 155, 36-42. https://www.doi.org/10.1104/pp.110.168559

Rebetzke, G.J., van Herwaarden, A.F., Jenkins, C., Weiss, M., Lewis, D., Ruuska, S., Tabe, L., Fettell, N.A., Richards, R.A., 2008. Quantitative trait loci for water-soluble carbohydrates and associations with agronomic traits in wheat. Australian Journal of Agricultural Research 59, 891-905. https://www.doi.org/10.1071/AR08067

Ren, S., He, K., Girshick, R., Sun, J., 2017. Faster R-CNN: towards real-time object detection with region proposal networks. IEEE Transaction on Pattern Analysis and Machine Intelligence 39, 1137-1149. https://www.doi.org/10.1109/tpami.2016.2577031

Rischbeck, P., Elsayed, S., Mistele, B., Barmeier, G., Heil, K., Schmidhalter, U., 2016. Data fusion of spectral, thermal and canopy height parameters for improved yield prediction of drought stressed spring barley. European Journal of Agronomy 78, 44-59. https://www.doi.org/10.1016/j.eja.2016.04.013

Romano, G., Zia, S., Spreer, W., Sanchez, C., Cairns, J., Araus, J.L., Müller, J., 2011. Use of thermography for high throughput phenotyping of tropical maize adaption in water stress. Computer and Electronics in Agriculture 79, 67-74. https://www.doi.org/10.1016/j.compag.2011.08.011

Ruuska, S.A., Rebetzke, G.J., van Herwaarden, A.F., Richards, R.A., Fettell, N.A., Tabe, L., Jenkins, C.L.D., 2006. Genotypic variation in water-soluble carbohydrate accumulation in wheat. Functional Plant Biology 33, 799-809. https://www.doi.org/10.1071/fp06062

Sadeghi-Tehran, P., Sabermanesh, K., Virlet, N., Hawkesford, M.J., 2017. Automated method to determine two critical growth stages of wheat: heading and flowering. Frontiers in Plant Science 8, 252. https://www.doi.org/10.3389/fpls.2017.00252

Sadok, W., Jagadish, S.V.K., 2020. The hidden costs of nighttime warming on yields. Trends in Plant Science 25(7), 644-651. https://www.doi.org/10.1016/j.tplants.2020.02.003

Sadras, V.O., Fereres, E., Borrás, L., Garzo, E., Moreno, A., Araus, J.L., Fereres, A., 2020. Aphid resistance: an overlooked ecological dimension of nonstructural carbohydrates in cereals. Frontiers in Plant Science 11, 937. https://www.doi.org/10.3389/fpls.2020.00937

Sagan, V., Maimaitijiang, M., Sidike, P., *et al.*, 2019. UAV-Based high resolution thermal imaging for vegetation monitoring, and plant phenotyping using ICI8640 P, FLIR Vue Pro R 640, and thermo MAP cameras. Remote Sensing 11(3), 330. https://www.doi.org/10.3390/rs11030330

Sandhu, J., Zhu, F., Paul, P., Gao, T., Dhatt, B., Ge, Y., Staswick, P., Yu, H., Walia, H., 2019. PI-Plat: a high-resolution image-based 3D reconstruction method to estimate growth dynamics of rice inflorescence traits. Plant Methods 15, 162. https://www.doi.org/10.1186/s13007-019-0545-2

Schittenhelm, S., Langkamp-Wedde, T., Kraft, M., Kottmann, L., Matschiner, K., 2020. Effect of two-week heat stress during grain filling on stem reserves, senescence, and grain yield of European winter wheat cultivars. Journal of Agronomy and Crop Sciences 206, 722-733. https://www.doi.org/10.1111/jac.12410

Schnyder, H., 1993. The role of carbohydrate storage and redistribution in the source-sink relations of wheat and barley during grain filling – a review. New Phytologist 123, 233-245. https://www.jstor.org/stable/2557991

Schwalbert, R., Amado, T., Nieto, L., Corassa, G., Rice, C., Peralta, N., Schauberger, B., Gornott, C., Ciampitti, I., 2020. Mid-season county-level corn yield forecast for US corn belt integrating satellite imagery and weather variables. Crop Science 60, 739-750. https://www.doi.org/10.1002/csc2.20053

Scofield, G.N., Ruuska, S.A., Aoki, N., Lewis, D.C., Tabe, L.M., Jenkins, C.L.D., 2009. Starch storage in the stems of wheat plants: localization and temporal changes. Annals of Botany 103, 859-868. https://www.doi.org/10.1093/aob/mcp010

Šebela, D., Quiñones, C., Olejníčková, J., Jagadish, S.V.K., 2015. Temporal chlorophyll fluorescence signals to track changes in optical properties of maturing rice panicles exposed to high night temperature. Field Crops Research 177, 75-85. https://www.doi.org/10.1016/j.fcr.2015.02.025

Šebela, D., Bheemanahalli, R., Tamilselvan, A., Kadam, N.N., Jagadish, S.V.K., 2019. Genetic dissection of photochemical efficiency under water-deficit stress in rice. Plant Physiology Reports 24, 238-339. https://www.doi.org/10.1007/s40502-019-00467-7

Šebela, D., Bergkamp, B., Somayanda, I.M., Fritz, A.K., Jagadish, S.V.K., 2020. Impact of post-flowering heat stress in winter wheat tracked through optical signals. Agronomy Journal https://www.doi.org/10.1002/agj2.20360

Seiler, C., Harshavardhan, V.T., Reddy, P.S., *et al.*, 2014. Abscisic acid flux alterations result in differential abscisic acid signaling in responses and impact assimilation efficiency in barley under terminal drought stress. Plant Physiology 164, 1677-1696. https://www.doi.org/10.1104/pp.113.229062

Sehgal, A., Sita, K., Siddique, K.H.M., Kumar, R., Bhogireddy, S., Varshney, R.K., HanumanthaRao, B., Nair, R.M., Prasad, P.V.V., Nayyar, H., 2018. Drought or/and heat-stress effects on seed filling in food crops: impacts on functional biochemistry, seed yields, and nutritional quality. Frontiers in Plant Sciences 9, 1705. https://www.doi.org/10.3389/fpls.2018.01705

Shearman, V.J., Sylvester-Bradley, R., Scott, R.K., Foulkes, M.J., 2005. Physiological processes associated with wheat yield progress in the UK. Crop Physiology & Metabolism 45, 175-185.

Sheehy, J., Elmido, A., Centeno, G., Pablico, P., 2005. Searching for new plants for climate change. Journal of Agricultural Meteorology 60, 463-468. https://www.doi.org/10.2480/agrmet.463

Sheehy, J.E., Mabilangan, A.E., Dionora, M.J.A., Pablico, P.P., 2007. Time of day of flowering in wild species of the genus *Oryza*. International Rice Research Notes 32, 12-13. https://www.doi.org/10.3860/irrn.v32i1.1082

Smith, C., Karunaratne, S., Badenhorst, P., Cogan, N., Spangenberg, G., Smith, K., 2020. Machine learning algorithms to predict forage nutritive value of in situ perennial ryegrass plants using hyperspectral canopy reflectance data. Remote Sensing 12, 928. https://www.doi.org/10.3390/rs12060928

Spano, G., Di Fonzo, N., Perrotta, C., Platani, C., Ronga, G., Lawlor, D.W., Napier, J.A., Shewry, P.R., 2003. Physiological characterizations of 'stay green' mutants in durum wheat. Journal of Experimental Botany 54, 1415-1420. https://www.doi.org/10.1093/jxb/erg150

Stone, P., 2001. The effects of heat stress on cereal yield and quality. In: Basra, A.S., eds. Crop responses and adaptations to temperature stress. Binghamton, NY: Food Products Press, 243-291.

Tattaris, M., Reynolds, M.P., Chapman, S.C., 2016. A direct comparison of remote sensing approaches for high-throughput phenotyping in plant breeding. Frontiers in Plant Science 7, 1131. https://www.doi.org/10.3389/fpls.2016.01131

Thomas, H., Ougham, H., 2014. The stay-green trait. Journal of Experimental Botany 65, 3889-3900. https://www.doi.org/10.1093/jxb/eru037

Thompson, A.L., Thorp, K.R., Conley, M., Andrade-Sanchez, P., Heun, J.T., Dyer, J.M., White, J.W., 2018. Deploying a proximal sensing cart to identify drought-adaptive traits in upland cotton for high-throughput phenotyping. Frontiers in Plant Science 9, 507. https://www.doi.org/10.3389/fpls.2018.00507

Thompson, C.N., Mills, C., Pabuayon, I.L.B., Ritchie, G.L., 2020. Time-based remote sensing yield estimates of cotton in water-limiting environments. Agronomy Journal 112, 975-984. https://www.doi.org/10.1002/agj2.20126

van Herwaarden, A.F., Angus, J.F., Richards, R.A., Farquhar, G.D., 1998. 'Haying-off', the negative grain yield response of dryland wheat to nitrogen fertilizer II. carbohydrate and protein dynamics. Crop and Pasture Science 49, 1083-1094. https://www.doi.org/10.1071/A97040

van Herwaarden, A., Richards, R., Angus, J., 2003. Water soluble carbohydrates and yield in wheat. In 'Proceedings of the 11th Australian Agronomy Conference'. The Australian Society of Agronomy: Geelong.

Varela, S., Assefa, Y., Prasad, P.V.V., Peralta, N.R., Griffin, T.W., Sharda, A., Ferguson, A., Ciampitti, I.A., 2017. Spatio-temporal evaluation of plant height in corn via unmanned aerial systems. Journal of Applied Remote Sensing 11, 036013. https://www.doi.org/10.1117/1.JRS.11.036013

Vose, R.S., Easterling, D.R., Gleason, B., 2005. Maximum and minimum temperature trends for the globe: An update through 2004. Geophysical Research Letters 32, 23822. https://www.doi.org/10.1029/2005GL024379

Wang, D.R., Han, R., Wolfrum, E.J., McCouch, S.R., 2017. The buffering capacity of stems: genetic architecture of nonstructural carbohydrates in cultivated Asian rice, *Oryza sativa*. New Phytologist 215, 658-671. https://www.doi.org/10.1111/nph.14614

Wang, D.R., Wolfrum, E.J., Virk, P., Ismail, A., Greenberg, A.J., McCouch, S.R., 2016. Robust phenotyping strategies for evaluation of stem non-structural carbohydrates (NSC) in rice. Journal of Experimental Botany 67, 6125-6138. https://www.doi.org/10.1093/jxb/erw375

Wang, K., Li, Y., Wang, Y., Yang, X., 2017. On the asymmetry of the urban daily air temperature cycle. Journal of Geophysical Research: Atmospheres 122, 5625-5635. https://www.doi.org/10.1002/2017JD026589

Wang, X., Xuan, H., Evers, B., Shrestha, S., Pless, R., Poland, J., 2019. High-throughput phenotyping with deep learning gives insight into the genetic architecture of flowering time in wheat. GigaScience 8, giz120. https://www.doi.org/10.1093/gigascience/giz120

Wang, Z., Liu, X., Li, R., Chang, X., Jing, R., 2011. Development of near-infrared reflectance spectroscopy models for quantitative determination of water-soluble carbohydrate content in wheat stem and glume. Analytical Letters 44, 2478-2490. https://www.doi.org/10.1080/00032719.2011.551859

White J. W., Andrade-Sanchez P. A., Gore M. A., *et al.*, 2012. Field-based phenomics for plant genetics research. Field Crops Research 133, 101-112. https://www.doi.org/10.1016/j.fcr.2012.04.003

Whitney, S.M., Houtz, R.L., Alonso, H., 2011. Advancing our understanding and capacity to engineer nature's CO_2 sequestering enzyme, rubisco. Plant Physiology 155, 27-35.

Woo HR, Masclaux-Daubresse C, Lim PO. 2018. Plant senescence: how plants know when and how to die. Journal of Experimental Botany 69, 715-718. https://www.doi.org/10.1104/pp.110.164814

Wu, Y., Zhao, B., Li, Q., *et al.*, 2019. Non-structural carbohydrates in maize with different nitrogen tolerance are affected by nitrogen addition. PLoS ONE 14, e0225753. https://www.doi.org/10.1371/journal.pone.0225753

Xiong, D., Yu, T., Ling, X., Fahad, S., Peng, S., Li, Y., Huang, J., 2014. Sufficient leaf transpiration and nonstructural carbohydrates are beneficial for high-temperature

tolerance in three rice (*Oryza sativa*) cultivars and two nitrogen treatments. Functional Plant Biology 42, 347-356. https://www.doi.org/10.1071/fp14166

Xiong, X., Duan, L., Liu, L., Tu, H., Yang, P., Wu, D., Chen, G., Xiong, L., Yang, W., Liu, Q., 2017. Panicle-SEG: a robust image segmentation method for rice panicles in the field based on deep learning and superpixel optimization. Plant Methods 13, 104. https://www.doi.org/10.1186/s13007-017-0254-7

Xue, J., Su, B., 2017. Significant remote sensing vegetation indices: a review of developments and applications. Journal of Sensors, 1353691. https://www.doi.org/10.1155/2017/1353691

Yemm, E.W., Willis, A.J., 1954. The estimation of carbohydrates in plant extracts by anthrone. Biochemical Journal 57, 508-514. https://www.doi.org/10.1042/bj0570508

Yendrek, C.R., Tomaz, T., Montes, C.M., Cao, Y., Morse, A.M., Brown, P.J., McIntyre, L.M., Leakey, A.D.B., Ainsworth, E.A., 2017. High-throughput phenotyping of maize leaf physiological and biochemical traits using hyperspectral reflectance. Plant Physiology 173, 614-626. https://www.doi.org/10.1104/pp.16.01447

Yue, J., Yang, G., Li, C., Li, Z., Wang, Y., Feng, H., Xu, B., 2017. Estimation of winter wheat above-ground biomass using unmanned aerial vehicle-based snapshot hyperspectral sensor and crop height improved models. Remote Sensing 9, 708. https://www.doi.org/10.3390/rs9070708

Zhang, C., Filella, I., Liu, D., Ogaya, R., Llusiá, J., Asensio, D., Peñuelas, J., 2017. Photochemical reflectance index (PRI) for detecting responses of diurnal and seasonal photosynthetic activity to experimental drought and warming in a Mediterranean shrubland. Remote Sensing 9, 1189. https://www.doi.org/10.3390/rs9111189

Zhang, C., Pumphrey, M.O., Zhou, J., Zhang, Q., Sankaran, S., 2019. Development of an automated high-throughput phenotyping system for wheat evaluation in a controlled environment. Transactions of the ASABE 62, 61-74. https://www.doi.org/10.13031/trans.12856

Zhang, J., Zhang, S., Cheng, M., Jiang, H., Zhang, X., Peng, C., Lu, X., Zhang, M., Jin, J., 2018. Effect of drought on agronomic traits of rice and wheat: a meta-analysis. International Journal of Environmental Research and Public Health 15, 839. https://www..doi.org/10.3390/ijerph15050839

Zhou, J., Zhou, J., Ye, H., Ali, M.L., Nguyen, H.T., Chen, P., 2020. Classification of soybean leaf wilting due to drought stress using UAV-based imagery. Computers and Electronics in Agriculture 175, 105576. https://www.doi.org/10.1016/j.compag.2020.105576

Zhu, X., Long, S.P., Ort, D.R., 2010. Improving photosynthetic efficiency for greater yield. Annual Review of Plant Biology 61, 235-261. https://www.doi.org/10.1146/annurev-arplant-042809-112206

Figures

Figure 1-1 Quantifying time-of-day of flowering (TOF) in crops.

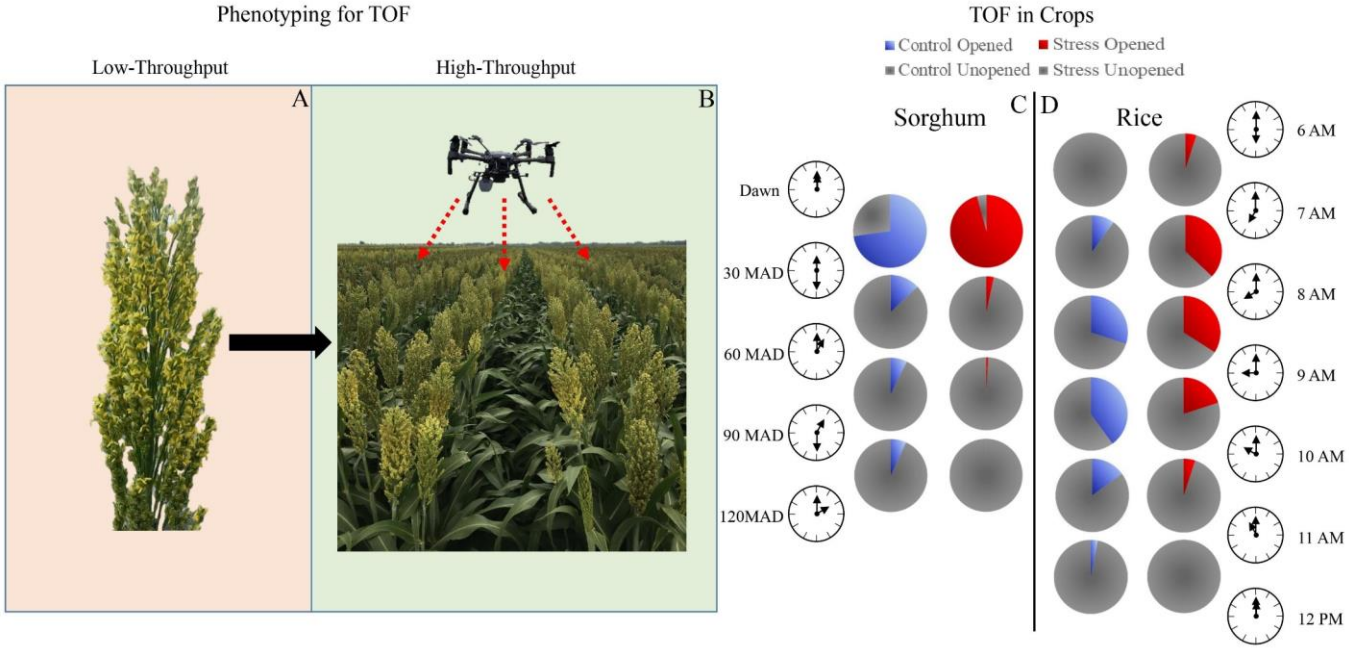

Figure shows potential transition of methodologies in recording TOF in crops and provides cases studies related to TOF in sorghum and rice. Traditional low-throughput measurement via manual counts (A) which is labor intensive, induces temporal variability, and is subject to human error to use of low-altitude UAVs and high-resolution imagery to easily acquire high-temporal and accurate data to record TOF (B). Natural alteration of flowering time in sorghum (C; Chiluwal et al., 2020) and the change in flower opening time in rice due to the genetic incorporation of early morning flowering trait (see far right pie charts) from wild rice into popular variety (D; Ishimaru et al., 2010).

Figure 1-2 Optimizing stay-green and senescence dynamics

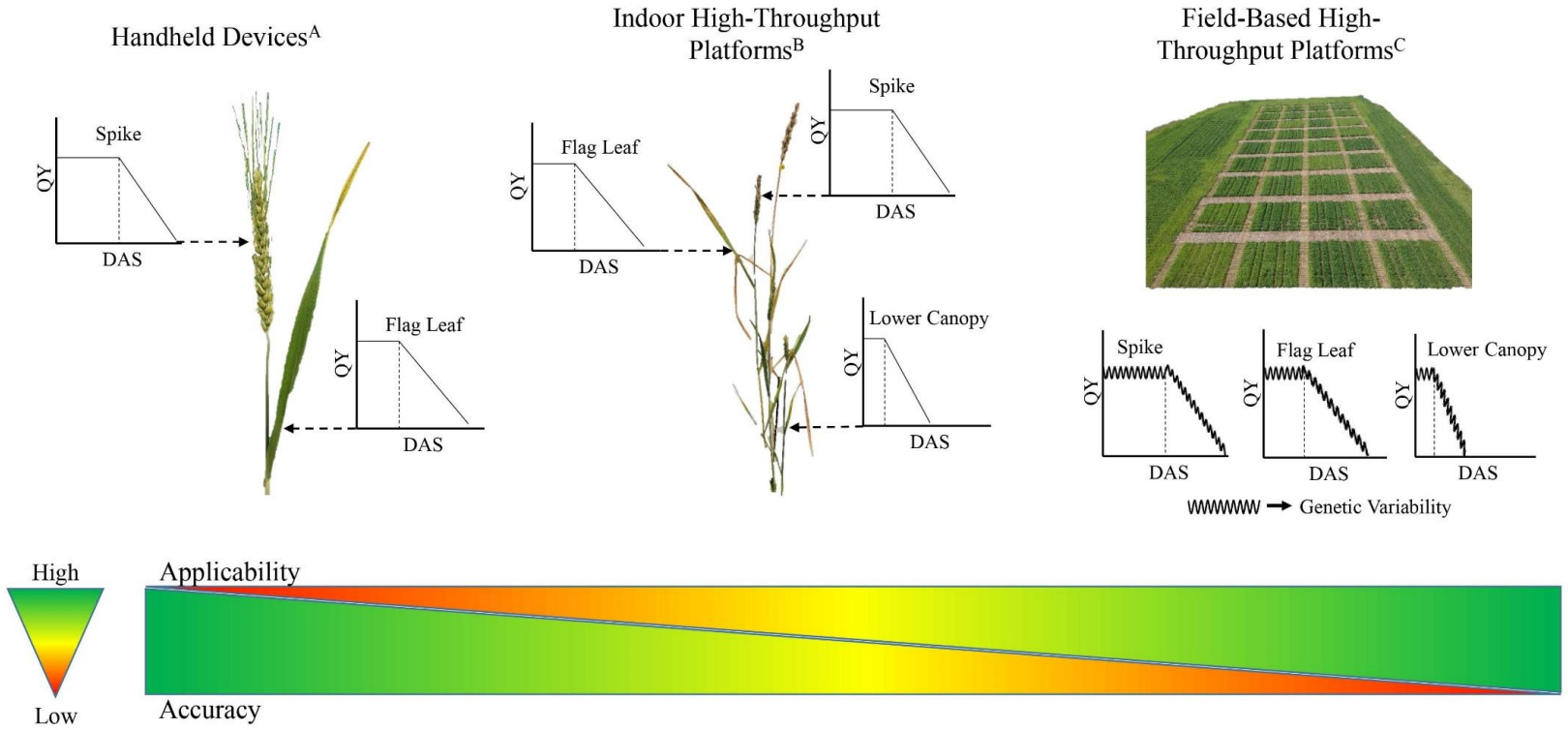

Handheld, indoor high-throughput, and field-based high-throughput techniques for quantifying photosynthetic efficiency is presented using effective quantum yield of photosystem II (QY) as a case study. Handheld devices (A), though sensitive enough to detect subtle changes such as initiation of senescence, are highly laborious, provide data either at a leaf or spike level, and challenging to be deployed on large scale phenotyping. Indoor high-throughput platforms (B) having similar or higher sensing capability can easily acquire trait information on the whole plant automatically without human interventions. Field-based high-throughput platforms (C) have the capability of gathering reflectance data on a large number of genotypes with extreme sensitivity and low-temporal variation.

Figure 1-3 Estimation of yield and yield related parameters

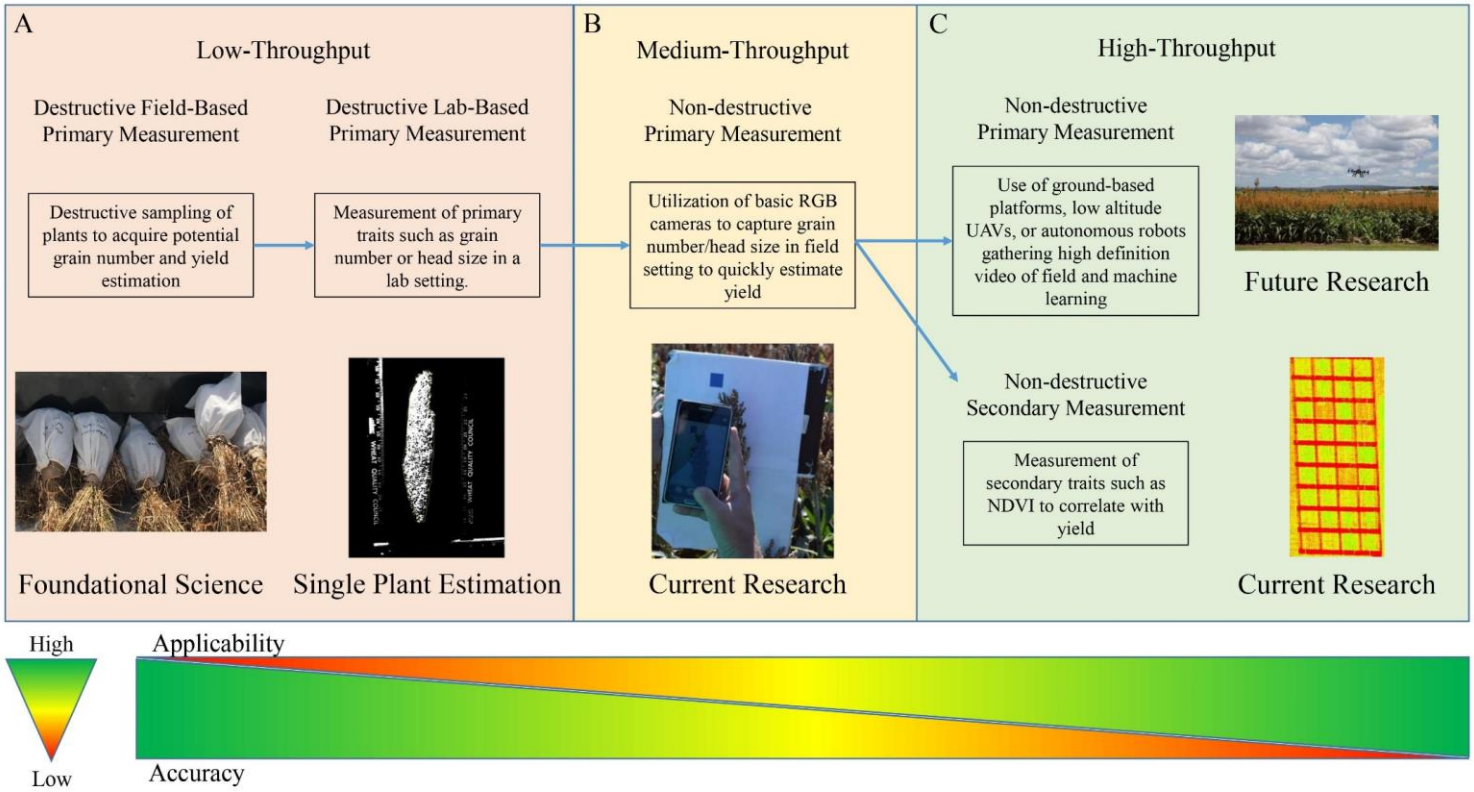

Figure illustrates the progression from destructive field-based primary measurements in order to obtain an estimation of yield to new high-throughput measurements to estimate yield through both primary and secondary measurements. The methods of gathering information for yield estimation are ordered from least applicable but highly accurate to most applicable but less accurate or from low-throughput to high-throughput and include destructive sampling and lab-based primary measurements (A), field-based primary measurements (B) and current investigation on developing high-throughput non-destructive primary and secondary measurements (C).

Tables

Table 1-1 Overview of research advances for phenotyping target traits

Trait	Reference	Crop	Throughput	Location	Platform	Sensor	Sensor Measured Trait	Observed Agronomic Trait
Time-of-day of flowering	Sadeghi-Tehran *et al.*, 2017	Wheat	High	Field	Field Scanalyzer	RGB Digital Camera	Flower Opening Time (FOT)	FOT
	Desai *et al.*, 2018	*Setaria viridis*	Medium	Lab	Fixed Mount	RGB Digital Camera (Daytime)	FOT	FOT
						Infrared Camera (Nighttime)	FOT	FOT
	Wang *et al.*, 2019	Wheat	High	Field	Tractor Mount	RGB Digital Camera	Percent Heading	Percent Heading
Photosynthetic efficiency	Raesch *et al.*, 2014	Barley and Sugar Beet	Medium	Field	Fixed Mount	LIFT System	Chl a	Daily Average Fluorescence Values
	Peng *et al.*, 2016	Aspen and Cherry Tree	Medium	Field/Lab	Hand-Held	Hyperspectral Radiometer	$NDRE_{740}$	Photosynthetic Efficiency
						SPAD Meter	Chlorophyll Index	Photosynthetic Efficiency
	Zhang *et al.*, 2017	Evergreen Shrub	Medium	Field	Hand-Held	Field Spectroradiometer	PRI	Photosynthetic Efficiency

Translocation of WSC	Dreccer *et al.*, 2014	Wheat	High	Field	Tractor Mount	Hyperspectral Radiometer	Spectral Region (350 - 1290 nm)	WSC Amount
	Yendrek *et al.*, 2017	Maize	Medium	Field	Hand-Held	Hyperspectral Radiometer	Reflectance Spectra	Sucrose Content
	Garriga *et al.*, 2014	Wheat	Medium	Field	Fixed Mount	Hyperspectral Radiometer	Spectral Region (350 - 2500 nm)	WSC Concentration
Estimating yield and yield parameters	Xiong *et al.*, 2017	Rice	Medium	Field	Fixed Mount	RGB Digital Camera	Panicle Count	Panicle Count
	Hasan *et al.*, 2018	Wheat	Medium	Field	Tractor Mount	RGB Digital Camera	Spike Count	Spike Count
	Madec *et al.*, 2019	Wheat	Medium	Field	Hand-Held	RGB Digital Camera	Ear Count	Ear Density
	Guo *et al.*, 2018	Sorghum	High	Field	UAV-Based	RGB Digital Camera	Head Count	Head Count
	Ghosal *et al.*, 2019	Sorghum	High	Field	UAV-Based	RGB Digital Camera	Head Count	Head Count
	Lin and Guo, 2020	Sorghum	High	Field	UAV-Based	RGB Digital Camera	Head Count	Head Count

Chapter 2 - Integrating field-based heat tents and cyber-physical system technology to phenotype high night-time temperature impact on winter wheat

Abstract

Many agronomic traits have been bred into modern wheat varieties, but wheat (*Triticum aestivum L.*) continues to be vulnerable to heat stress, with high night-time temperature (HNT) stress shown to have large negative impact on yield and quality. Global mean temperature during the day is consistently warming with the minimum night temperature increasing at a much quicker pace. Currently, there is no system or method that allows crop scientists to impose HNT stress at key developmental stages on wheat or crops in general under field conditions, involving diverse genotypes and maintaining a dynamic temperature differential within the tents compared to the outside.

Through implementation of a side roll up and a top ventilation system, heaters, and a custom cyber-physical system using a Raspberry Pi, the heat tents were able to consistently maintain an elevated temperature through the night to differentiate heat stress impact on different genotypes. When the tents were placed in their day-time setting they were able to maintain ambient day-time temperature without having to be removed and replaced on the plots. Data averaged from multiple sensors over three consecutive weeks resulted in a consistent but small temperature difference of 0.25^{o}C within the tents, indicating even distribution of heat. While targeting a temperature differential of 4 °C, the tents were able to maintain an average differential of 3.2 °C consistently throughout the night-time heat stress period, compared to the

Hein, N.T., Wagner, D., Bheemanahalli, R., Šebela, D., Bustamante, C., Chiluwal, A., Neilsen, M.L., Jagadish, S.V.K., 2019. Integrating field-based heat tents and cyber-physical system technology to phenotype high night-time temperature impact on winter wheat. Plant Methods 15, 41. https://www.doi.org/10.1186/s13007-019-0424-x

outside ambient conditions. The impact of HNT stress was confirmed through a statistically significant yield reduction in eleven of the twelve genotypes tested. The average yield under HNT stress was reduced by 20.3% compared to the controls, with the highest reduction being 41.4% and a lowest reduction of 6.9%. Recommendations for fine-tuning the system are provided.

This methodology is easily accessible and can be widely utilized due to its flexibility and ease of construction. This system can be modified and improved based on some of the recommendations and has the potential to be used across other crops or plants as it is not reliant on access to any hardwired utilities. The method tested will help the crop community to quantify the impact of HNT stress, identify novel donors that induce tolerance to HNT and help the breeders develop crop varieties that are resilient to changing climate.

Hein, N.T., Wagner, D., Bheemanahalli, R., Šebela, D., Bustamante, C., Chiluwal, A., Neilsen, M.L., Jagadish, S.V.K., 2019. Integrating field-based heat tents and cyber-physical system technology to phenotype high night-time temperature impact on winter wheat. Plant Methods 15, 41. https://www.doi.org/10.1186/s13007-019-0424-x

Introduction

Winter wheat (*Triticum aestivum L.*), with centuries of genetic improvement, has acquired a suite of favorable traits essential for adaptation to a wide range of environmental conditions. Some of the key developments in wheat breeding and domestication includes larger grain size and a phenotype without seed shattering (Eckardt, 2010). Further improvements benefitting from technological advances over the last century by introducing high yielding varieties, fertilizer, pesticides, and modern equipment, have resulted in translating wheat into one of the major staple cereals of the world. Over the last six decades (1961 and 2016) the overall production of wheat has increased by over 500 million tonnes with only a 15.9 million ha increase in harvested area (Food and Agriculture Organization of the United Nations [FAO], 2018a). Improved genetic and management interventions have transformed the average wheat yield from 1.09 t ha^{-1} in 1961 to 3.41 t ha^{-1} in 2016 (FAO, 2018a). In spite of the dramatic increase in overall wheat production, the rate of increase in production is unable to meet the current or the predicted global demand for the future (FAO, 2018b). Even though the annual per capita consumption of wheat is expected to drop by about one percent, the overall annual consumption of wheat is predicted to increase by almost 90 Mt between 2014 and 2024, as a result of increasing population and demand from the biofuel industry (OECD-FAO, 2015).

The two main components determining wheat yield potential are the number of grains per meter square and the average weight of each grain (Slafer, 2005). Many genetic, environmental, and field management decisions can alter physiological processes that determine grain number and weight and eventually grain yield. Some of these factors include nutrient availability, temperature, water and solar radiation, fertilizer, and genotype (Golba *et al.*, 2018). Among the environmental factors, high temperatures during flowering and grain filling have shown to

induce significant loss in grain numbers and weight (Yang *et al.*, 2017; Bergkamp *et al.*, 2018). Although the overall average temperature has warmed across the globe, recent analysis has shown that the daily minimum temperature (occurring during the night) is increasing at a faster rate than the daily maximum temperature (Easterling *et al.*, 1997; Houghton *et al.*, 2001). Hence, it is important and timely to understand the impact of high night-time temperature (HNT) on crops in general and in the sensitive field crops including winter wheat.

During 1979 and 2003, the annual mean maximum temperature increased by 0.35 °C and the annual mean minimum temperature increased by 1.13 °C at the International Rice Research Institute experimental farm, Philippines. As a result, the rice yield decreased by 10% for every 1°C temperature increase in mean minimum temperature during the dry season (Peng *et al.*, 2004). The same study found that the increase in mean maximum temperature did not have the same effect on yield as the mean minimum temperature (Peng *et al.*, 2004). Recent studies on the effects of HNT stress on different field grown crops has, until now used (i) field-based tents with a static system (Shi *et al.*, 2013, 2016; 2017; Bahuguna *et al.*, 2017) or (ii) much smaller tents with a cyber-physical system that captures single genotype responses to HNT stress and has to be physically placed and removed daily (Garcia *et al.*, 2015). The impact of HNT and the physiological route through which yield and quality losses occur has been documented in rice using field-based heat tents (Shi *et al.*, 2013, 2016, 2017; Chaturvedi *et al.*, 2017). Although the existing field tents at IRRI, Philippines, can potentially include moderate number of genotypes, the HNT treatment imposition is static at a predetermined target temperature while the outside temperature can vary quite dynamically. A cyber-physical system is a computer system that incorporates electrical engineering and computer science to bridge the digital and physical worlds through the use of embedded technology (Department of Homeland Security, 2016).

Through the use of software and sensors, the cyber-physical system is able to interact with and react to their environment. The only field experiment involving wheat**,** HNT, and a cyber-physical system used 3 m x 1.3 m x 1.3 m structures that were manually placed on plots of a single variety of wheat called Baguette 13 for 12 hours every night from the third detectable stem node to 10 days post-flowering. This experiment recorded a 7% reduction in grain yield along with a reduction in biomass and grain number (Garcia *et al.*, 2015).

Phenotyping facilities such as rain-out shelters for quantifying drought stress responses (Zhan *et al.*, 2015; Hoober *et al.*, 20180 and the use of naturally occurring hotter summer conditions have been extensively used to study the impact of high day-time temperature (HDT) stress across crops (Tack *et al.*, 2015, 2017; Bheemanahalli *et al.*, 2016). However, there doesn't exist a large field-based phenotyping system that can capture larger genetic diversity for HNT responses at critical growth and developmental stages and at the same time induce a dynamic HNT treatment closely following the outside ambient temperature. Hence, our major objective was to develop and test a robust field-based cyber-physical system by modifying a currently available HDT stress heat tent. The overall aim was to impose a HNT stress of 4 ℃ automatically following the dynamic changes in the open field i.e., outside the structures and simultaneously capturing genetic diversity for HNT stress impact on physiological parameters and grain yield. While the system and methodology developed is tested on winter wheat, there is potential that this technology is scalable and can be extended to crops or plants of interest to the scientific community, although this is yet to be evaluated.

Materials and Methods

Heat Tent

The heat tents that were used for this specific project were built and used in previous studies to quantify HDT effects on wheat and sorghum (Prasad *et al.*, 2015; Sunoj *et al.*, 2017; Bergkamp *et al.*, 2018). Each tent was built using a steel frame for the base and heavy piping to create the sidewalls and apex. The heat tents were constructed in the Gothic style with vertical framing every 1.2 m along the sidewall. The heat tents are 7.2 m long, 5.4 m wide, and 3.0 m tall at the apex. Lock channel and wiggle wire was installed around the available edges of the frame to enclose the tent. The heat tents were enclosed using polyethylene film (6 mil Sun Master® Pull and Cut Greenhouse Film) with 92% light transmission according to the manufacturer. New plastic was installed on all the tents before the start of the experiment. The main components in converting the HDT tents into HNT included the top vent, side roll vents, heating system, and a cyber-physical thermostat controller system operated by a Raspberry Pi.

Top Vent

In order to maintain ambient conditions throughout the day within the tents, the top vent (Figure 2-1.1) was kept functional from the HDT set up. In previous experiments, the top vent was used to prevent excess heating above a set temperature by opening the vent when the desired temperature target was met. However, in the HNT set up, the top vent was opened throughout the day to maintain temperature within the tent closer to ambient conditions to prevent confounding our HNT research by imposing HDT stress. The vent was forced closed during the night to impose and maintain a consistent level of elevated temperature compared to the outside ambient temperature.

A secondary frame was built that was 0.6 m wide and 7.2 m long from the same material as the structure of the heat tent. The frame was placed at the top of the apex with the bottom hinged to the tent structure. This setup allowed the vent to open up and away from the apex allowing as much heat as possible to escape through the vent (Figure 2-1A). Two linear actuator motors (Venture Manufacturing) were attached to the vent framework (Figure 2-1.1). When powered, these motors would open and close the vent framework *via* the hinges that connect the vent to the main structure. The power for these linear actuators was provided by a 12v VRLA battery that was connected to a solar panel attached to the front apex of the roof. The solar panel charged the 12v battery during the day, allowing the battery to be charged and used throughout the experiment. The battery power was run through a thermostat controller (Dayton Temperature Control 4LZ95A) (Figure 2-2.1). During the day the thermostat was set to 0 °C to ensure the vent stayed open throughout the day and at night at 44 °C to keep the vent closed throughout the night.

Side Roll Vents

The purpose of the side roll vents was to allow for maximum air flow through the wheat canopy during the day. Combined with the top vent, the side roll up vents on both sides of the tent allowed ambient air to flow through the tent and forced hot air to be expelled through the top vent. Pressure treated 2” x 6” (5.1 cm x 15.24 cm) wooden boards were installed along the very bottom of the side walls with screws that were rated to attach wood to metal (Everbilt #14 2-3/4 in. Phillips Flat-Head Self-Drilling Screw). The boards used were 3.04 m in length, which required multiple boards to cover the length of the side walls. The boards were attached to each other using deck screws to ensure stability (Deckmate #9 x 3 in. Star Flat-Head Wood Deck

Screws). These wooden boards were then run across the side wall at 1.5 m above the base and secured in the same fashion (Figure 2-1.3).

The horizontal lock channel and wiggle wire was installed on the upper third of the outside face of the top row of wooden boards with metal to wood screws (Teks #12 1 in. Hex-Head Self-Drilling Screws). The vertical lock channel along the end walls was then installed down along the frame, so the end wall plastic could be secured all the way to the ground. It was at this point during the set up that the new plastic was applied on all the tents. The side walls were done first with enough plastic hanging down from the top row of wooden boards to reach the ground. The plastic was secured along the vertical lock channel on the side walls from the top to the bottom row of wooden boards and then left loose below that.

Eye screws (Everbilt #206 x 1-3/8 in. Zinc-Plated Steel Screw Eye) were installed on both the top and bottom row of boards at either end and then alternating between the top and the bottom set of boards to form a zigzag pattern (Figure 2-1.3). The top row of eye screws were placed through the hanging plastic while the bottom row of eye screws did not go through the plastic so that the plastic could be rolled up.

To create the metal bar that the extra plastic would be rolled up on resulting in the side roll vents, three pieces of 3.5 cm x 3.2 m 17-gauge galvanized piping were combined using Teks #12 1 in. Hex-Head Self-Drilling Screws. Two of the pieces were used in full while the third was cut to 1.52 m in length allowing an extra 0.3 m of piping on either end of the heat tent. In total, for each side wall a 7.92 m length of piping was used. Each pole had a tapered end and a full end. The tapered ends of the poles were inserted into the full ends and then screwed together with the Tek screws. The screws were then wrapped in duct tape to ensure the screw heads would not rip the plastic.

A handle was added to one end of the roll up bar to rotate the bar to facilitate the rolling up and lowering of the side walls (Figure 2-1.2). The 3.5 cm x 3.2 m 17-gauge galvanized piping was cut into two 0.3 m lengths and then attached to the end using an aluminum gate ell. Two pieces of piping and two aluminum gate ells were used to create the handle for each roll up, on either side of the tent. The 7.92 m long pipe was then laid along the side walls of the heat tent on top of the excess plastic that was draped on the ground. The plastic was evenly wrapped around the pole in a clockwise manner and duct taped every 1 m to attach the pipe firmly with the plastic.

A piece of polypropylene rope was attached to the top eye screws on the wooden boards on the end with the handle and a loop made on the other end so that it could be attached to a screw on the interior of the tent to hold the roll up when the side walls were open. The handle was then rotated in a clockwise rotation to roll the plastic up to the top row of the wooden boards and then secured with the loop that was previously put in place. The same polypropylene rope was then run from the top eye screw on one end of the top wooden board to a similar screw on the bottom wooden board and then pulled through the eye screws in the zig zag pattern that was made previously. Once the rope had reached the far end, it was run through both the top and bottom eye screws, pulled tight, and secured. This rope was necessary to keep the roll up flush against the heat tent during the rolling process, and also prevented billowing when the side walls were rolled down (Figure 2-1.3). The end walls then had their polyethylene film applied over the top of the sidewall plastic so as to seal the ends of the heat tents (Appendix A Figure - 1)

Heating System

Before any decisions could be made on the size and type of heating system, the amount of heat that was necessary to raise the tent to the targeted temperature was calculated by using the

formula $Q = \frac{\Delta T * A}{R}$. The amount of heat (Q), British Thermal Unit per hour (BTU h^{-1}), required to attain the target temperature differential (ΔT in °F) was figured using the surface area of the heat tent (A in ft^2) and the capacity of the covering of the heat tent to resist heat flow (R in inch-pound). Some manufacturers or materials may not provide an R value but rather a heat loss value (U) which is equal to 1/R. The heat tents had a surface area of 1,100 square feet and an R value of 0.87. The target maximum temperature difference inside the tent from the outside ambient temperature during the night was 4 °C or 7.2 °F. Using these values in the above formula, the minimum heat required to raise temperature inside the tent by 4 °C was 9,103 BTU h^{-1} or 2,667 Watts (1 BTU = 0.293 watts).

The Thermosphere Ceiling-Mount Garage Heater was installed in the tent hanging from a horizontal structural pipe two thirds of the distance from the apex (Figure 2-2.4). The capacity of this unit was 5,000 Watts, 17,065 BTU h^{-1}, 240 V (model number PH-950). In addition to the heater, a single box fan (Lasko Ltd.) was hung in the opposite end of the tents to ensure air within the tent was circulated throughout the night (Figure 2-2.2). These fans drew 75 watts each and ran off of an 110v circuit, with the power provided by the generator (Appendix A Figure - 2).

This experiment had three independent heat tents running overnight powered with a Caterpillar XQ35 Generator which provided 27kW of power consistently using 8.8 liters of diesel per hour. The diesel was stored in a 3785-liter tank with an electrical pump that was battery operated and used to refill the generator (Appendix A Figure - 2). The generator was wired to the heaters using Southwire 8/2 AWG UF-B Underground Feeder Cable with Ground and Southwire 10/2 AWG UF-B Underground Feeder Cable with Ground depending on the

length of run between the generator and the heater. The box fans were provided power with HDX 16/3 Indoor/Outdoor Extension Cords.

Although the calculations were accurate for the amount of heat needed to raise the temperature of a typical greenhouse, the modifications made to the heat tent structure affected its ability to retain heat. Hence, an additional source of heat was necessary to maintain the target differential. A Sunrite™ by Mr. Heater® 15,000 BTU Tank Top Portable Propane Heater (Figure 2-2.3) was added to achieve the target temperature. The propane heater provided 10,000 BTU h^{-1} on low, 12,000 BTU h^{-1} on medium, and 15,000 BTU h^{-1} on the high setting. The propane heater was set to its medium setting which provided a radiant heat source but was not equipped with a forced air component and can potentially pose a fire hazard on the ground level. Hence, the propane tank and heater were placed on a stand built with cinderblocks to raise it above the height of the wheat and placed directly below the path of the air blown by the box fans. The propane tank top heater increased the interior temperature towards the target temperature via radiant heating and air movement by the fan while the final target differential of $4^{o}C$ was achieved and regulated by the electric heater by turning on and off as needed.

A low-level fire hazard did exist with the use of a diesel generator and propane tank top heater. However, the diesel generator itself did not create a fire risk unless a complete component failure occurred. The generator was self-contained on a trailer and had adequate insulation and protective measures to minimize risk. On the other hand, the fire hazard posed by the propane tank can be completely eliminated by increasing the wattage of the original electric heater and eliminate the need for a propane tank top heater.

Another aspect related to utilizing a propane tank top heater is the possibility of CO_2 build up within the tent and its effects on the plants. Direct estimation of CO_2 concentration using

at least two sensors within each tent would have been an ideal approach to ensure that there were no unintended effects of elevated CO_2 on the plants. Higher levels of CO_2 would warrant the addition of more ventilation to allow for fresh air to enter the tents and a ducted ventilation tube for the gasses produced during the combustion of propane. However, no additional ventilation was required for the heat tents as they were not airtight and allowed for ample ventilation. The top vent did not seal when closed and the side roll ups were taped shut on the end walls but were not sealed along the side walls. This inherent ventilation in the design allowed for a continuous flow of fresh air and created the necessity for an extra heat source. This is evident with the increase in BTUs required to raise the interior temperature by 4^{o}C compared to the exterior. In a completely sealed environment with the same volume as the heat tent, it would only take 8,854.4 BTUs to achieve the target temperature and overcome conductive heat loss. However, our system used over 29,000 BTUs which correlates to over 20,000 BTUs being needed to overcome perimeter heat loss and air infiltration heat loss. At that rate of heating, the tent had to complete an air exchange every 1.32 minutes. While CO_2 was not directly measured, the combination of frequent air exchanges i.e., the top vent not being sealed which allowed for the warm CO_2 to escape, and the side roll vents not being sealed which allowed the CO_2 to escape when cooled would have prevented any excess CO_2 accumulating within the tent and compounding the effects of the HNT stress.

Temperature Controller System

Overall Description/Functionality

A cyber-physical system is a physical mechanism controlled by computer-based algorithms in real time. This cyber-physical system was designed to monitor the temperature from the outside environment and regulate temperature within the tent. When the temperature inside the tent was

not warmer than the outside by 4°C, the system turned the heater on to help increase or maintain the indoor temperature differential. Otherwise, the heater was turned off and the temperature was continued to be monitored.

Design Philosophy

This system was designed around a simple, plug-and-play philosophy using a Raspberry Pi, a low-cost, high-performance computer system developed by the Raspberry Pi Foundation (Raspberry Pi Foundation, 2012). When the system received power, it booted up and began monitoring the outside and inside temperatures. If the system failed to start, which only occurred twice during the HNT stress period, then the faults were isolated into two categories: Raspberry Pi failures and sensor failures. The Raspberry Pi failures were manually tested by checking for sufficient power source (5V, 2.1A) and verifying the integrity of the microSD card. Sensor failures were detected by checking the power, electrical ground, and data connections to the Raspberry Pi. The system's simplicity was exhibited in both hardware and software. The system could be separated into its material components rather simply; the Raspberry Pi, solid-state relay, sensors, and 240V relay could be isolated by disconnecting at most five wires and could be improved and modified easily without affecting the other components. Software could be modified very rapidly through the Python script (Appendix A Document - 1 Python Script) and uploaded to the Raspberry Pi within minutes by modifying the microSD card.

Hardware Components and Connections

The thermostat system consisted of several hardware components: a Raspberry Pi, solid-state relay, 24VAC adapter, 240V relay, and two DS18B20 temperature sensors. Additionally, the system was placed within a plastic housing for water- and dust-proofing (Figure 2-3). The Raspberry Pi was connected to the solid-state relay by three wires: 5V power, electrical ground,

and a signal wire (Figure 2-4). A high bit on the signal wire forced the relay to complete the connection to the heater. The following pin assignments were based on the physical numbering scheme on the Raspberry Pi Model 3B:

- The 5V connection was routed to pin 2.
- The ground connection was routed to pin 9.
- The signal connection was routed to pin 11.

The solid-state relay was connected to the 240V relay and 24VAC adapter. This relay caused the other relay to engage and helped complete the circuit to the heater, as the single relay itself could not support the heater's electrical load. Two ports from the solid-state relay were used: common and normally open (NO), which were chosen for safety because the heater circuit would not normally be electrically active. The common lead was connected to one lead of the 24VAC adapter, and the NO lead was connected directly to the 24VAC lead of the 240V relay. In this manner, the solid-state relay completed a circuit between the 24VAC adapter and the 240V relay.

The 24VAC adapter was connected to power *via* the generator cables. The adapter provided power to the 240V relay and heater circuit. An unpolarized electrical plug was attached to the input terminals. Electrical wire (14-gauge) was connected to each terminal of the plug and then connected to the generator lines; the ground lead was connected to the generator ground, and the power lead was connected to the black 120V line of the generator. The 240V relay had four connections: two inputs and two outputs to the heater. One input has been described above and was directly connected to the NO lead of the solid-state relay. The common input terminal was connected directly to the other terminal of the 24VAC adapter. The common output terminal was wired to one of the generator's 120V lines, and the NO terminal was connected to the

corresponding line on the heater. The neutral and second 120V lines were connected directly from the generator to the heater; the relay switched a single 120V line to complete the circuit.

The two DS18B20 temperature sensors were wired in parallel and shared the same three pin connections (Figure 2-4). A 4.7kΩ pull-up resistor was connected between the power and data lines and prevented a floating wire state and a wire short (Sparkfun Electronics, 2018). The following pin assignments were similar to the solid-state relay:

- The 3.3V connection was routed to pin 1.
- The ground connection was split and routed to pins 6 and 39.
- The data connection was routed to pin 7.

Software Description

The software was written in a Python script, version 2.7 (Python Software Foundation, 2019) (Appendix A Document - 1 Python Script). This allowed for rapid prototyping and quick implementation of the sensor readings. When the Raspberry Pi was booted, the software first polled the system bus for the sensors and added them to a list, which allowed for more sensors to be connected to the system. Next, the signal pin of the solid-state relay was set-up *via* software for toggling: otherwise, the pin would either be on or off. Then, the data log file was opened and a blank line was appended to delimit the start of a new session of logging. This log file was in comma separated value format for easy importing to Microsoft Excel or any other spreadsheet program.

After the setup was completed, the software entered its main loop. First, it attempted to read the sensors that are connected to it using manufacturer code (Monk and Fried, 2013). If the software detected an invalid sensor reading, the error was displayed once the interface was initialized. If the sensor readings were valid, the differential of the indoor and outdoor

temperatures was measured and the heater was either turned on or off depending on the value; a value below 4 ^{o}C caused the heater to be turned on and being above 4 ^{o}C turned the heater off. Then, the interface was created and updated to the new indoor and outdoor temperatures, as well as the status of the heater (Appendix A Figure - 3). If an error occurred with the sensors in the previous steps, then the heater displayed the word “SENSOR” and the connections from the Pi to each sensor was manually verified.

If the elapsed time reached the logging interval, then the current time, indoor and outdoor temperatures, and the heater’s status were recorded to file. If the amount of time elapsed had not reached the interval, a nested loop was executed. The system would go into a sleep mode for half a second and the process was repeated until the target interval had reached. Once the interval had been reached and the status was recorded, the next loop iteration would commence.

Crop Cultivation

A field experiment was conducted at the Agronomy research farm at Manhattan (39°11′N, 96°35′W), Kansas. In this experiment, five prominent varieties of Kansas (Everest, Larry, SY-Monument, WB 4458, and WB-Cedar) and five breeding lines (Jagger X060724, KS070736 K-1, KS070729 K-26, KS070717 M-1, and P1 X060725) and two exotic genotypes (Tascosa and Tx86A5606) known for differential heat stress response during grain filling (Bergkamp, *et al.*, 2018; Impa *et al.*, 2019), were used to study the impact of post-flowering HNT stress under field condition. Wheat genotypes were planted using a tractor and research plot grain drill with global positioning system (GPS) guidance system on 17th October 2018. Each replicate plot per genotype comprised of six rows with each row being four-meter long (6 rows occupied 1.15 m, with each row placed 0.19 m apart). The plots were top dressed with 45 kg N ha^{-1} (Urea ammonium nitrate solution) on 17th February 2018. Both the control and the stress plots were

irrigated throughout the experiment, even during the HNT stress period, either through rainfall or manually once every week to avoid confounded by water-deficit stress. Days to complete flowering across the twelve genotypes was not more than five days. HNT treatment was imposed during grain filling using the custom designed heat tents. Twelve winter wheat genotypes were successfully exposed to an average night-time differential of +3.2 °C (interior; inside heat tents) during the grain filling (10 d after 50% flowering to physiological maturity), compared to ambient night-time temperature (exterior; outside heat tents).

Biological data collection

Chlorophyll Fluorescence Measurement

Five representative plants for each genotype per replicate were randomly selected and tagged at flowering for measuring flag leaf and the main spike chlorophyll fluorescence (Chl-F) in both interior and exterior conditions. Chl-F data was recorded between 1000 and 1300 h by using a portable hand-held fluorometer (FluorPen FP 100, Photon System Instruments, Ltd., Brno, Czech Republic), which gives the effective quantum yield of PSII (QY). Saturating light [intensity approximately 3,000 µmol (photons) m^{-2} s^{-1}] and measuring light [intensity approximately 0.09 µmol (photons) m^{-2} s^{-1}] were used to measure both maximal fluorescence yield (FM`) and actual fluorescence yield (Ft) of light adapted samples, respectively. Subsequently, the effective quantum yield of PSII (QY) was calculated using the formula $QY = (FM` - Ft)/FM` = \Delta F/FM`$ [31]. Electron transport rate (ETR) which indicated the capacity of overall photosynthesis was calculated by using the formula as described previously (Genty *et al.*, 1989).

$$ETR = QY\ x\ PAR\ x\ 0.84\ x\ 0.5$$

Where QY is the effective quantum yield of PSII, PAR is actual photosynthetic active radiation (µmol (photons) m^{-2} s^{-1}), 0.84 is an approximate level of light being absorbed by the leaf, and 0.5

is the ratio of PSII to PSI reaction centers. Three measurements were taken along the middle of the flag leaf blade and spikes on each replicate plant and averaged.

Grain Yield

At physiological maturity (Zadoks growth scale 9-ripening; not dented by thumbnail), replicates of one-meter row length from four central rows was manually cut in each plot to minimize border effects. Spikes were separated from the stem and dried for 96 h at 40°C and spikes were threshed using an LD 180 Laboratory thresher (Wintersteiger, Ried im Innkreis, Austria) and grain yield was recorded. The seeds were then counted in an automated seed counter (Key-Mat Inc., St. Charles Il, USA) to obtain seed number and the total sample yield was divided by the seed number and multiplied by 200 to obtain 200 kernel weight.

Statistical analysis

The experiment was conducted in a split-plot randomized complete block design with temperature as the main plot factor and genotype as the sub-plot factor. Replicated observations for each trait were analyzed for means and standard errors. ANOVA was performed using GenStat (Genstat, 2019).

Results and Discussion

To induce heat stress using the components described above, the process of converting the structures from its day-time setting to its night-time setting began at 7:15 PM every night. A single side wall from each tent was lowered and sealed using duct tape. Alternatively, this could also be accomplished by running a strip of Velcro along the end wall and adhering it to the sidewall plastic. Following the sidewall roll down, the top vent was closed to seal the roof. After all the tents had a single sidewall down and the overhead vents lowered and sealed, the portable

power packs were plugged into the Pis to start the systems, to initiate the temperature monitoring programs. Then the generator was turned on to supply power to each tent. The Pi system was considered operational if the electric heater was running with the red indicator light. The additional propane heater was turned on after all the other parts of the system were fully operational. As a final step the second side wall was lowered and sealed to fully enclose the tent for the night (Figure 2-5B).

At 5:45 AM every morning, the generator was shut down, so that no electricity was flowing through the system. The sidewalls were unsealed from the end walls, rolled up, and secured at the top with polypropylene rope, the propane heater was shut down, the top vent opened (Figure 2-5A), and the battery from the Pi system was removed to shut it down for the day. The batteries were removed every day but only recharged every other day off site from the experiment. The propane tanks were refilled after three consecutive nights of HNT stress.

The system was monitored through a combination of sensors in the interior of the tent and the exterior. One HOBO UX 100-011 temperature/relative humidity data loggers (Onset Computer Corp., Bourne, MA) with a sensitivity of 0.2°C was placed in a central location on the experimental plot to log the ambient air temperature and humidity. Similarly, two HOBO sensors were placed within each tent to log both day-time and night-time temperature and humidity. The Pi temperature sensing and controller system was also equipped with one sensor inside the tent and the other sensor placed outside each tent having an accuracy of 0.5 °C. In total, each tent was equipped with three sensors. The two main goals of this field set up was to induce a HNT stress with a pre-decided target differential supported by the Pi's programming, and to ensure an even distribution of the heat throughout the night to minimize a temperature gradient or irregular

warming patterns within the tent. In addition, the aim during the day-time was to ensure temperatures within the tent were close to the outside ambient temperature.

Distribution of Heat

To ensure that the tent was not experiencing a gradient in temperature within the tent, two different HOBO sensors were placed within the wheat plots on opposite sides of the tents directly above the canopy to measure the temperature throughout the night and day at 15-minute interval. The distribution of heat was enabled through the box fan that operated from one end and the electric heater that ran on the opposite side. The electric heater with an inbuilt forced air system complemented the box fan on the other end to distribute the heat evenly throughout the tent.

The difference between the two HOBO sensors within the tent was on average 0.75 °C (Figure 2-6A). The HOBO sensors at the start of the treatment recorded a large differential of 2.5 °C on average due to the heating system turning on to bring the tent up to its target differential temperature and possibly due to one of the sensors placed in the path of the heater's air flow. Once the tents reached the target temperature (roughly around 9 PM) the difference between the two HOBO temperature loggers leveled out and were within the range of 0.5 and 0.75 °C. In addition, the distribution of heat was also confirmed by comparing the average of two HOBO temperature readings with the interior Pi system sensor. Overall average difference between the HOBO sensors and the Pi sensors was -0.25 °C, with the Pi system sensors reading 0.25 °C warmer than the HOBOs (Figure 2-6B). A consistent but small temperature difference was recorded within the tent indicating even distribution of heat.

Temperature Differential

The second goal of the heat tent system was to maintain a set temperature differential between the interior of the heat tent and the exterior. The tents were programmed to maintain a temperature differential of 4 ^{o}C throughout the night. Comparing the Pi systems sensors, the tents were able to maintain an average differential of 3.2 °C consistently throughout the heat stress period (Figure 2-6C). The figure shows that the temperature at 8:00 PM were almost equal at the time the tents were sealed and the heating system was turned on. An hour after the start, the temperature reached a stable differential and then followed the exterior temperature throughout the night, while still maintaining the differential.

This effect can also be seen in Figure 2-6D which is a comparison between the temperature recorded from HOBO sensors placed within and outside the heat tent. The elevated interior temperature follows the exterior temperature through the night and in the morning both outside and the inside tent temperatures return to the same level, after the tents are opened. The HOBO sensors also measured an average of 3.2 °C temperature differential throughout the experiment, providing additional independent validation of the system's successful imposition of HNT stress.

Ambient Day Time Temperature and Relative Humidity

The main concern during the day for the heat tent infrastructure was its ability to regulate the air temperature inside the tent, so that the wheat inside the tent is exposed to similar conditions as outside the tent. The readings from both HOBO data loggers inside each tent were averaged and on comparing to the exterior HOBO indicated 0.8 °C warmer temperature within the tent during the day.

The interior temperature of the tents warmed quicker in the morning than the exterior temperature (Figure 2-7A). This rise in temperature compared to the ambient temperature can be credited to the greenhouse effect from the plastic on the heat tents and the typical lack of air movement in the morning hours. With low air movement there is less pressure differential between the inside and outside of the top vent, resulting in much slower circulation of air out of the tent. This effect caused the interior temperature of the tents to reach a maximum of 2.54 °C higher than the exterior by 7:40 AM, with both becoming equal by 12:05 PM after which the average exterior temperature was higher than the interior temperature. The temperatures stayed almost equal from noon until 6:30 PM. After 6:30 PM the temperature differential between the inside of the tents compared to the exterior rose until the heat stress began. The rise in temperature in the later hours of the day can be attributed to the tent retaining the day's heat longer due to its covering versus the open exterior.

On average, the tent's relative humidity was 15.6% higher than the ambient average (Figure 2-7B). The difference between the interior and exterior peaked after the imposition of the HNT stress at 6:00 AM and then reduced throughout the morning until noon. After noon, there was a consistently higher level of humidity inside the tent until 6:00 PM in which the difference receded until the stress imposition began again. It is also apparent through the data that the relative humidity differential between the interior and the exterior was the greatest during the HNT stress period when the tent was sealed. Using the relative humidity and air temperature data from inside and outside of the heat tents, the vapor pressure difference (VPD) was calculated through both the stress and non-stress periods. The VPD was highest during the day when the temperature was at its warmest and the relative humidity at the lowest (Figure 2-7C). To account

for any variation in evaporation and transpiration due to the changes in RH and VPD within the tents, the plots were irrigated weekly from flowering until harvest.

Physiological and Yield Response to HNT

A significant ($P<0.001$) decline in the electron transport rate (ETR) of the flag leaves was observed after seven days of treatment imposition (Figure 2-8A). Among the tested genotypes, KS070717 M-1 and Larry recorded the lowest percent reduction (<1%) in flag leaf ETR under heat stress compared to control, whereas Tascosa (14.3%) followed by KS 070729 K-26 (13%) recorded the highest reduction in flag leaf ETR (Figure 2-8A). Similarly, a significant ($P<0.001$) treatment impact was recorded for main spike ETR, ranging from 5.7% (KS 070729 K-26) to 19.4% (KS070717 M-1) with HNT compared to control, with an average reduction of 14.3% (Figure 2-8B). Significant ($P<0.001$) effect of temperature and genotype were observed with grain yield but with no treatment and genotype interaction (Figure 2-8C). Eleven genotypes (except WB 4458) out of the twelve responded to heat stress treatment by reducing their grain yield, with an average reduction of 20.3%, ranging between 6.9% in P1 X060725 and 41.4% in KS070717 M-1 (Figure 2-8C). Under HNT stress exposure during grain-filling (Figure 2-8C), WB 4458 had the highest grain yield (394.2 g m^2) followed by SY-Monument (352.5 g m^2), whereas the lowest grain yield was recorded in KS070717 M-1 (202.4 g m^2). All 12 genotypes responded to the HNT stress with a reduction in 200 kernel weight with the greatest reduction occurring in Tascosa (11%) and the smallest reduction occurring in WB-4458 (1%). The average reduction in 200 kernel weight for all 12 genotypes was 6.66%.

System Improvements

By further improving, the system can be adequately scaled up for phenotyping larger genetic diversity and the gap between the target average temperature differential (4 °C) and the achieved (3.2 °C) can be narrowed through minor improvements to the system.

1. Adding more temperature sensors will help obtain an average temperature from multiple points within the tent which will lead to improved heating accuracy. The total number of sensors that can be attached to an individual Pi is 117 which allows ample capacity for a single Raspberry Pi to handle a much larger and extensive setup (Monk and Fried, 2012). Additional sensors that sense relative humidity, CO_2 and light intensity will track microclimatic parameters within the tent and facilitate in maintaining target experimental conditions.
2. Adding another fan can improve uniformity in distribution of heat within the tent. This will help the extra sensors accurately determine the temperature within the tent and improve the system's capabilities when designing a larger experiment.
3. Higher precision sensors - The sensors that were used within the system connected to the Pi had an accuracy of 0.5 °C. Sensors with higher accuracy will result in less variable temperature readings and when averaged with the additional sensors throughout the tent a much more precise reading of the temperature can be attained.
4. Increasing the recording frequency in the Pi system. This will help by turning the heater on and off as frequently as necessary. The changes made to the tents to help maintain ambient air temperature during the day adds to the heat loss during night. The longer amount of time between readings from the Pi system results in a larger swing in temperature while the heater

is off. With more frequent readings, the heater would be able to modulate the temperature more efficiently.

5. Heater that receives input air from the exterior via venting - This will help mitigate the increased relative humidity and possible buildup of CO_2 within the tent. This would allow fresh air with an ambient level of relative humidity and CO_2 to enter the system and be circulated throughout the tent instead of the same air from within the tent being drawn into the heater and then dispersed.

Conclusions

A robust field-based system with the use of roll up and down side ventilation, top ventilation, a heating system, and a cyber-physical system using a Raspberry Pi was constructed that was able to effectively impose HNT stress while automatically following the dynamic changes of the outside environment. The top and side ventilation also allowed the system to maintain near ambient temperatures throughout the day without having to physically remove the tent from the field, while still being able to seal them overnight providing a HNT stress exposure on multiple wheat genotypes in a field setting. The system and the methodology followed indicated that crop agronomic and physiological responses to HNT can be effectively captured under realistic field conditions to help ongoing breeding efforts aimed at improving crops adaptation to changing climates. This system can be altered, improved based on some of the above recommendations. Although the methodology has only been tested on wheat, since it is not reliant on access to any hardwired utilities and is reliable, simple, and cost-effective, this system can be used to phenotype other crops or plants for HNT responses.

References

Bahuguna, R., Solis, C., Shi, W., Jagadish, S.V.K., 2017. Post-flowering night respiration and altered sink activity account for high night temperature induced grain yield and quality loss in rice (*Oryza sativa* L.). Physiologia Plantarum 159, 59-73. https://www.doi.org/10.1111/ppl.12485

Bergkamp, B., Impa, S.M., Asebedo, A.R., Fritz, A.K., Jagadish, S.V.K., 2018. Prominent winter wheat varieties response to post-flowering heat stress under controlled chambers and field-based heat tents. Field Crops Research 222, 143-152. https://www.doi.org/10.1016/j.fcr.2018.03.009

Bheemanahlli, R., Sathishraj, R., Tack, J., Nalley, L.L., Muthurajan, R., Jagadish, S.V.K., 2016. Temperature thresholds for spikelet sterility and associated warming impacts for sub-tropical rice. Agricultural and Forest Meteorology 221, 122-130. https://doi.org/10.1016/j.agrformet.2016.02.003

Chaturvedi, A., Bahuguna, R., Shah, D., Jagadish, S.V.K., 2017. High temperature stress during flowering and grain filling offsets beneficial impact of elevated CO_2 on assimilate portioning and sink strength in rice. Scientific Reports 7, 8227. https://www.doi.org/10.1038/s41598-017-07464-6

Department of Homeland Security, 2016. Cyber Physical Systems Security. Accessed 04 February 2019. https://www.dhs.gov/science-and-technology/csd-cpssec

Easterling, D.R., Horton, B., Jones, P.D., *et al.*, 1997. Maximum and minimum temperature trends for the globe. Science 277, 364-367. https://www.doi.org/10.1126/science.277.5324.364

Eckardt, N.A., 2010. Evolution of domesticated bread wheat. Plant Cell 22, 993. https://www..doi.org/10.1105/Ftpc.110.220410

Food and Agriculture Organization of the United Nations, 2018a. FAOStat: Crops and Livestock Products. Accessed 19 June 2018. https://www.fao.org/faostat/en/#data/QC

Food and Agriculture Organization of the United Nations, 2018b. FAOStat: Annual Population. Accessed 19 June 2018. https://www.fao.org/faostat/en/#data/OA

Garcia, G., Dreccer, M.F., Miralles, D.J., Serrago, R.A., 2015. High night temperatures during grain number determination reduce wheat and barley grain yield: a field study. Global Change Biology 21, 4153-4164. https://www.doi.org/10.111/gcb.13009

Genstat. VSNi. Accessed 02 February 2019. https://www.vsni.co.uk/software/genstat

Genty, B., Briantais, J.M., Baker, N.R., 1989. The relationship between the quantum yield of photosynthetic electron transport and quenching of chlorophyll fluorescence. Biochimica et Biophysica Acta (BBA) – General Subjects 990, 87-92. https://www.doi.org/10.1016/S0304-4165(89)80016-9

Golba, J., Studnicki, M., Gozdowski, D., Madry, W., Rozbicki, J., 2018. Influence of genotype, crop management, and environment on winter wheat grain yield determination based on components of yield. Crop Science 58, 660-669. https://www.doi.org/10.2135/cropsci2017.07.0425

Hoober, D., Wilcox, K., Young, K., 2018. Experimental droughts with rainout shelters: a methodological review. Ecosphere 9, e02088. https://www.doi.org/10.1002/ecs2.2088

Houghton, J.T., Ding, Y., Griggs, D.J., Nouger, M., Van der Linden, P.J., Xiaosu, D., eds., 2001. Climate Change 2001: The scientific Basis. Cambridge: Cambridge University Press, 944.

Impa, S.M., Sunoj, V.S.J., Krassovskaya, I., Bheemanahalli, R., Obata, T., Jagadish, S.V.K., 2018. Carbon balance and source-sink metabolic changes in winter wheat exposed to high night-time temperature. Plant, Cell & Environment 42, 1233-1246. https://www.doi.org/10.1111/pce.13488

Monk, S., Fried, L., 2012. Adafruit's raspberry pi lesson 4: GPIO setup. Accessed 01 February 2019. https://learn.adafruit.com/adafruits-raspberry-pi-lesson-4-gpio-setup/configuring-i2c

Monk, S., Fried, L., 2013. Adafruit's raspberry pi lesson 11: temperature sensing. Accessed 10 July 2018. https://learn.adafruit.com/adafruits-raspberry-pi-lesson-11-ds18b20-temperature-sensing/

Peng, S., Huang, J., Sheehy, J.E., Laza, R.C., Visperas, R.M., Zhong, X., Centeno, G.S., Khush, G.S., Cassman, K.G., 2004. Proceedings of the National Academy of Sciences of the United States of America 101, 9971-9975. https://www.doi.org/10.1073/pnas.0403720101

Prasad, P.V.V., Djanaguiraman, M., Perumal, R., Ciampitti, I.A., 2015. Impact of high temperature stress on floret fertility and individual grain weight of grain sorghum: sensitive stages and thresholds for temperature and duration. Frontiers in Plant Science 6,820. https://www.doi.org/10.3389/fpls.2015.00820

Python Software Foundation, 2019. Python language reference. Accessed 04 February 2019. https://www.python.org

Raspberry Pi Foundation, 2012. Raspberry pi foundation – about us. Accessed 04 February 2019. https://www.raspberrypi.org/about/

Slafer, G.A., 2005. Physiology of determination of major wheat yield components. In: Buck, H.T., Nisi, J.E., Salomon, N., eds. Wheat production in stress environments. Dordrecht: Spring, 557-565. https://www.doi.org/10.1007/1-4020-5497-1_68

Shi, W., Muthurajan, R., Rahman, H., Selvam, J., Peng, S., Zou, Y., Jagadish, S.V.K., 2012. Source-sink dynamics and proteomic reprogramming under elevated night temperature and their impact on rice yield and grain quality. New Phytologist 197, 825-837. https://www.doi.org/10.1111/nph.12088

Shi, W., Yin, X., Struik, P., Xie, F., Schmidt, R., Jagadish, S.V.K., 2016. Grain yield and quality responses of tropical hybrid rice to high night-time temperature. Field Crops Research 190, 18-25. https://www.doi.org/10.1016/j.fcr.2015.10.006

Shi, W., Yin, X., Struik, P.C., Solis, C., Xie, F., Schmidt, R.C., Huang, M., Zou, Y., Ye, C., Jagadish, S.V.K., 2017. High day- and night-time temperatures affect grain growth dynamics in contrasting rice genotypes. Journal of Experimental Botany 68, 5233-5245. https://www.doi.org/10.1093/jxb/erx344

Sparkfun Electronics, 2018. Pull-up resistors. Accessed 09 July 2018. https:///learn.sparkfun.com/tutorials/pull-up-resistors

Sunoj, V.S.J., Somayanda, I.M., Chiluwal, A., Perumal, R., Prasad, P.V.V., Jagadish, S.V.K., 2017. Resilience of pollen and post-flowering response in diverse sorghum genotypes exposed to heat stress under field conditions. Crop Science 57, 1658-1669. https://www.doi.org/10.2135/cropsci2016.08.0706

Tack, J., Barkley, A., Nalley, L.L., 2015. Effect of warming temperatures on US wheat yields. Proceedings of the National Academy of Sciences of the United States of America 112, 6931-6936. https://www.doi.org/10.1073/pnas.1415181112

Tack, J., Lingenfelser, J., Jagadish, S.V.K., 2017. Disaggregating sorghum yield reductions under warming scenarios exposes narrow genetic diversity in US breeding programs. Proceedings of the National Academy of Sciences of the United States of America 114, 9296-9301. https://www.doi.org/10.1073/pnas.1706383114

Yang, X., Tian, Z, Sun, L., Chen, B., Tubiello, F.N., Xu, Y., 2017. The impacts of increased heat stress events on wheat yield under climate change in China, Climate Change 140, 605-620. https://www.doi.org/10.1007/s10584-016-1866-z

Zhan, A., Schneider, H., Lynch, J.P., 2015. Reduced lateral root branching density improves drought tolerance in maize. Plant Physiology 168, 1603-1615. https://www.doi.org/10.1104/pp.15.00187

Figures

Figure 2-1 Prototype vent system layout

A: HNT heat tent during daytime 1: Venture Manufacturing 12 Volt Linear Actuator used to open Top Vent. 2: Handle used to manually operate Side Roll Up Ventilation. 3: Side rolled up with polypropylene rope securing it against the tent.

Figure 2-2 Prototype heating system layout

A: Layout of heating system within the Tent. 1: Dayton Thermostat Controller used to raise and lower the top vent. 2: Lasko 20 inch Box Fan. 3: Hobo temperature/relative humidity sensor and propane tank with the Sunrite™ by Mr. Heater® 15,000 BTU tank top portable propane heater. 4: Thermosphere 5000-Watt Ceiling-Mount garage heater. 5: Thermostat Controller System built using a Raspberry Pi.

Figure 2-3 Waterproof enclosure for Raspberry Pi and electric system

The system was contained within a plastic box that latched closed (left) to protect the underlying circuitry and opened (right) to allow access to the system. Inside each enclosure was a battery pack, USB to microUSB cable to supply power, one Raspberry Pi computer with touchscreen display, a ribbon cable to extend connections to the computer, and a blue solid-state relay. A hole was drilled in the side of the enclosure to facilitate electrical connections to the heater circuit; this hole was filled with caulk for water protection.

Figure 2-4 System Wiring Diagram

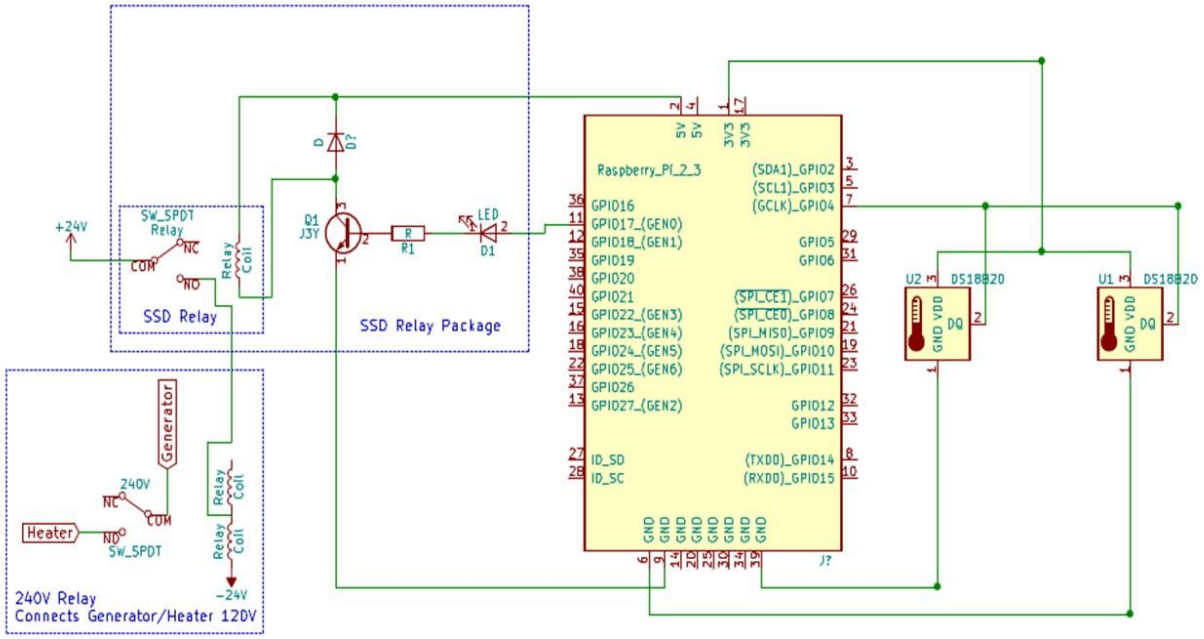

Figure 2-5 Prototype day setting vs night setting

A: Heat Tent in day-time setting with top vent and side wall vents opened up. B: Heat Tent during night-time when heat stress was imposed with the top vent and side wall vents closed.

Figure 2-6 Temperature comparison between sensors

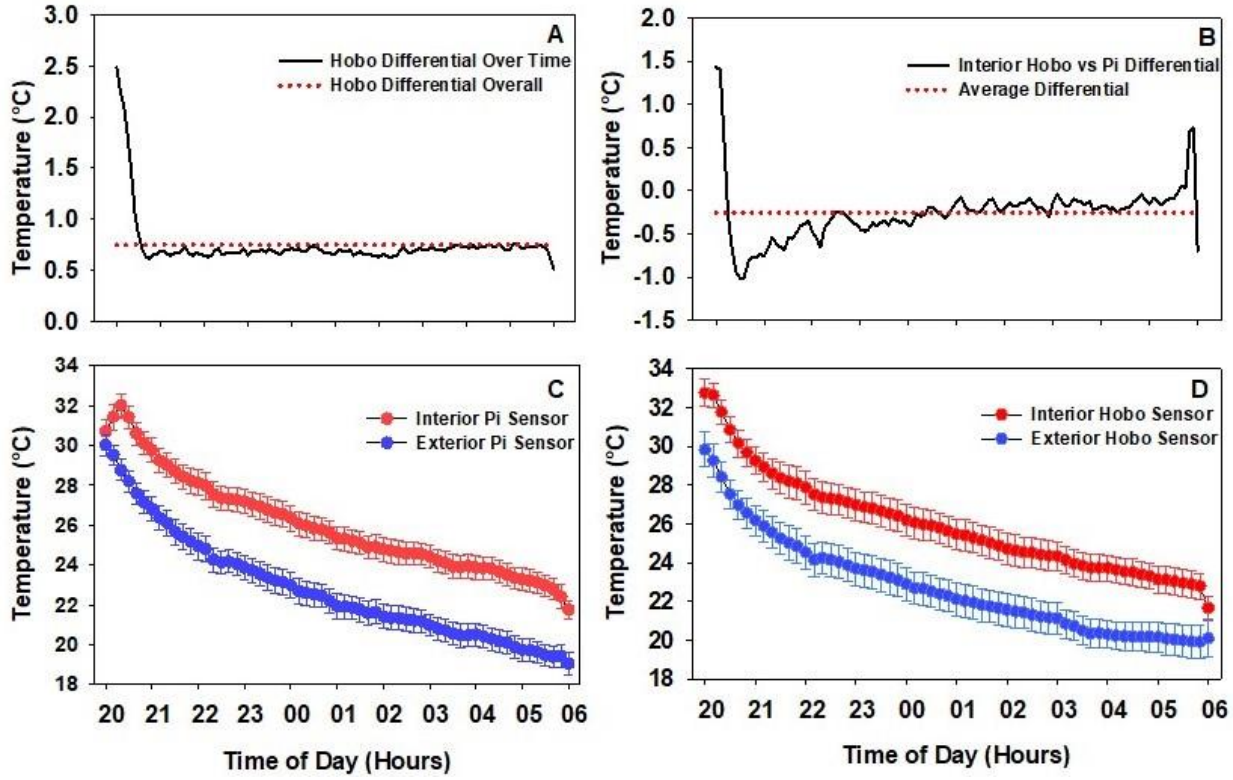

A: HOBO vs HOBO HNT differential within the same tent B: Interior HOBO vs Interior Pi temperature differential C: Interior Pi vs Exterior Pi temperature during HNT stress D: Interior HOBO vs Exterior HOBO temperature during HNT stress

Figure 2-7 Ambient temperature and relative humidity comparison

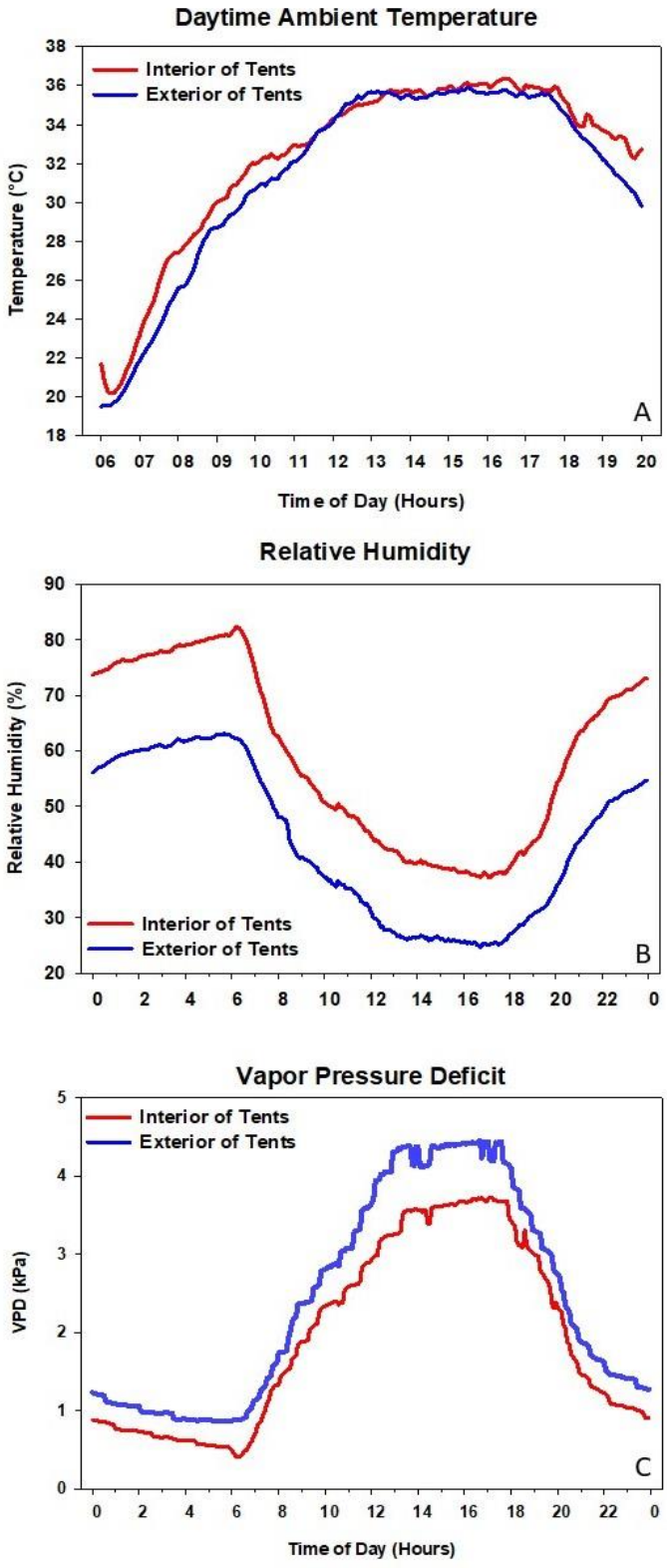

A: Day-time ambient temperature comparison between the interior HOBOs and the exterior HOBO. B: The average relative humidity of the interior of the tent HOBOs compared to the exterior HOBO. C: Comparison of the Vapor Pressure Deficit between the interior and exterior of the heat tents.

Figure 2-8 Physiological and yield response to HNT

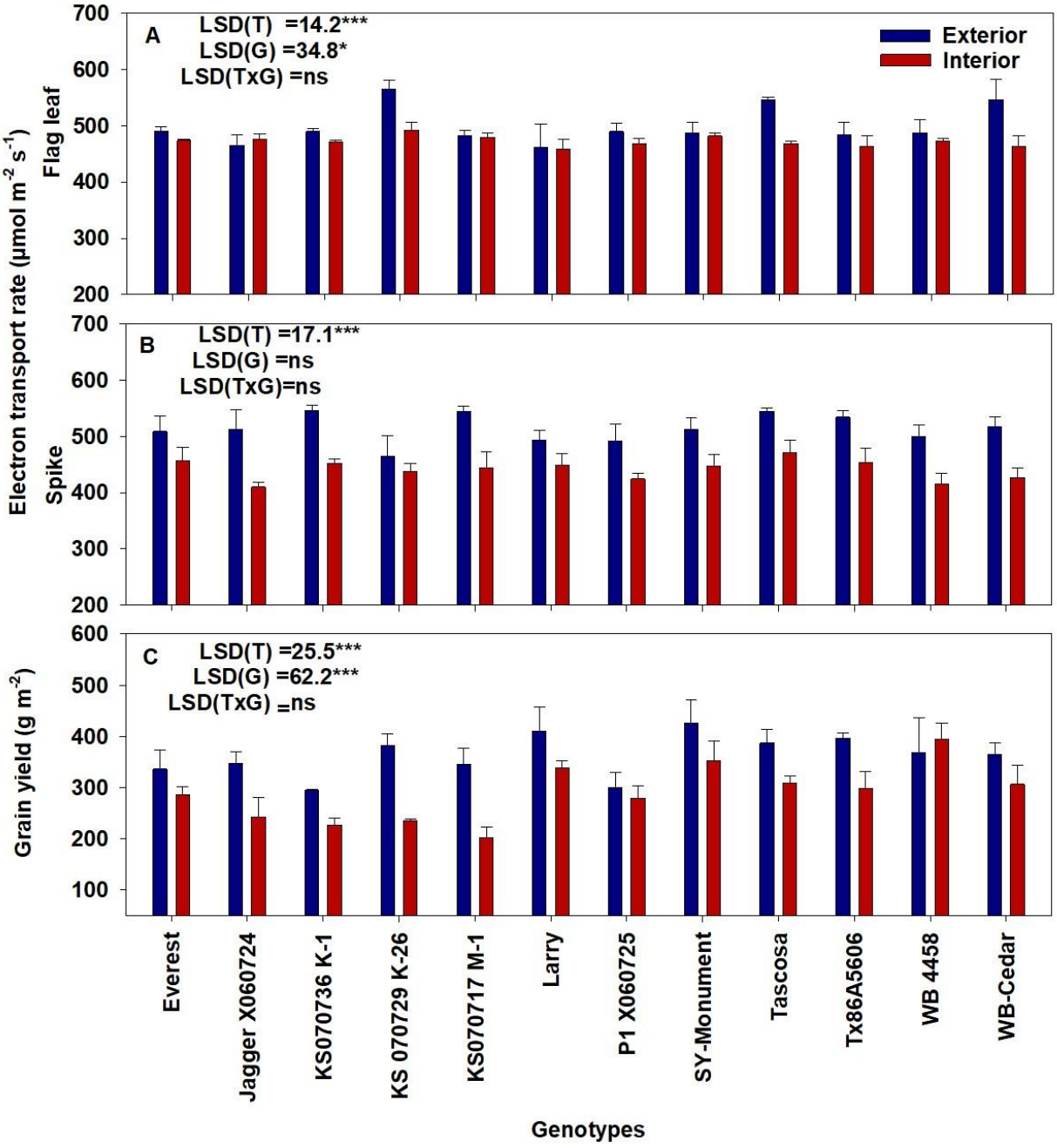

Flag leaf (A) and spike (B) electron transport rate recorded 7 d after treatment imposition and grain yield (C) of twelve winter wheat genotypes under exterior (control) and interior (HNT treatment) conditions. Analysis of variance with least significant difference (LSD) is presented

for each trait. T- treatment, G- Genotype, ns- Non-significant. *P <0.05; ***P <0.001. Bars indicate mean ± standard error (n = 3).

Chapter 3 - Improved cyber-physical system captured post-flowering high night temperature impact on yield and quality of field grown wheat

Abstract

Winter wheat (*Triticum aestivum* L.) is essential to maintain food security for a large proportion of the world's population. With increased risk from abiotic stresses due to climate variability, it is imperative to understand and minimize the negative impact of these stressors, including high night temperature (HNT). Both globally and at regional scales, a differential rate of increase in day and night temperature is observed, wherein night temperatures are increasing at a higher pace and the trend is projected to continue into the future. Previous studies using controlled environment facilities and small field-based removable chambers have shown that post-anthesis HNT stress can induce a significant reduction in grain yield including wheat. A prototype was previously developed by utilizing field-based tents allowing for simultaneous phenotyping of popular winter wheat varieties from US Midwest and advanced breeding lines. Hence, the objectives of the study were to (i) design and build a new field-based infrastructure and test and validate the uniformity of HNT stress application on a scaled-up version of the prototype (ii) improve and develop a more sophisticated cyber-physical system to sense and impose post-anthesis HNT stress uniformly through physiological maturity within the scaled-up tents; and (iii) determine the impact of HNT stress during grain filling on the agronomic and grain quality parameters including starch and protein concentration.

Hein, N.T., Bheemanahalli, R., Wagner, D., Vennapusa, A., Bustamante, C., Ostmeyer, T., Pokharel, M., Chiluwal, A., Fu, J., Srikanthan, D.S., Neilsen, M.L., Jagadish, S.V.K., 2020. Improved cyber-physical system captured post-flowering high night temperature impact on yield and quality of field grown wheat. Scientific Reports 10, 22213. https://www.doi.org/10.1038/s41598-020-79179-0

The system imposed a consistent post-anthesis HNT stress of +3.8 °C till maturity and maintained uniform distribution of stress which was confirmed by (i) 0.23 °C temperature differential between an array of sensors within the tents and (ii) statistically similar performance of a common check replicated multiple times in each tent. On average, a reduction in grain-filling duration by 3.33 days, kernel weight by 1.25% per °C, grain number by 2.36% per °C and yield by 3.58% per °C increase in night temperature was documented. HNT stress induced a significant reduction in starch concentration indicating disturbed carbon balance.

The pilot field-based facility integrated with a robust cyber-physical system provides a timely breakthrough for evaluating HNT stress impact on large diversity panels to enhance HNT stress tolerance across field crops. The flexibility of the cyber-physical system and movement capabilities of the field-based infrastructure allows this methodology to be adaptable to different crops.

Hein, N.T., Bheemanahalli, R., Wagner, D., Vennapusa, A., Bustamante, C., Ostmeyer, T., Pokharel, M., Chiluwal, A., Fu, J., Srikanthan, D.S., Neilsen, M.L., Jagadish, S.V.K., 2020. Improved cyber-physical system captured post-flowering high night temperature impact on yield and quality of field grown wheat. Scientific Reports 10, 22213. https://www.doi.org/10.1038/s41598-020-79179-0

Introduction

Winter wheat (*Triticum aestivum* L.) is an important staple cereal and a major source of calories for a large proportion of the world's population. Wheat production has increased over the last two decades and currently competes with rice (*Oryza sativa*) to be the second most produced cereal in the world, after maize (*Zea mays*) (FAO, 2019a). Despite the progress made, by 2028 worldwide production of wheat is expected to increase by 1.01%, while the demand is projected to increase at 1.13% due to a substantial increase in world population (FAO, 2019b, OECD/FAO, 2019). Along with the inherent need to increase production for a growing population, the changing climate also threatens the future yield potential of food crops including wheat. The Intergovernmental Panel on Climate Change (IPCC) (IPCC, 2014) has concluded that the mean surface temperature of the Earth will continue to rise this century and that heat waves will continue to occur more frequently, with more intensity and with each event lasting for longer duration. This increase in global mean surface temperature is being driven by an increase in the average daily minimum temperature, which is rising at a quicker rate than the average daily maximum temperature (Easterling *et al.*, 1997; Alexander *et al.*, 2006; Sillman *et al.*, 2013; Davy *et al.*, 2017). Studies related to high night temperature (HNT) stress on different crops have increased recently (between 2010 and 2020) with many of these focused on rice (Mohammed and Tarpley, 2009; Nagarajan *et al.*, 2010; Shi *et al.*, 2012, 2016; Bahuguna *et al.*, 2017; Chaturvedi *et al.*, 2017; Coast *et al.*, 2019). A comprehensive study conducted at the International Rice Research Institute in the Philippines showed that the mean maximum temperature between 1979 and 2003 rose by 0.35 °C while the annual mean minimum temperature rose by 1.13 °C. This study revealed that grain yield in rice was reduced by 10% for every 1 °C increase in average seasonal minimum temperature (Peng *et al.*, 2004). Other studies

have also shown detrimental effects of HNT stress in different crops including sorghum (Prasad and Djanguiraman, 2011), cotton (Loka and Oosterhuis, 2010, 2016; Echer *et al.*, 2014), soybean (Djanaguiraman *et al.*, 2013), corn (Cantarero *et al.*, 1999) and wheat (Impa *et al.*, 2019, 2020).

Studies on HNT stress in winter wheat have been mainly accomplished by using controlled environment growth chambers (Prasad *et al.*, 2008; Narayanan *et al.*, 2015; Impa *et al.*, 2019, 2020) or small chambers under field conditions (Lizana and Calderini, 2013; Garcia *et al.*, 2015, 2016). These facilities would have inherent difficulty in capturing large genetic diversity to HNT stress and chambers in particular would be challenged by differences in light, wind speed and humidity compared to field conditions, resulting in altered microclimate. Until 2019, there did not exist a large mobile field-based infrastructure with the ability to impose controlled HNT stress on crops. In response to this need, a field-based prototype was constructed which facilitated successful imposition of HNT stress throughout the grain-filling period in winter wheat (Hein *et al.*, 2019). A stable HNT stress of +3.2 ^{o}C throughout the grain-filling period resulted in a 5% reduction in yield (averaged across 12 cultivars) per ^{o}C increase in night temperature, supporting findings from Garcia *et al.* (2016) (Hein *et al.*, 2019). Finding solutions by utilizing diversity panels or mapping populations to address the negative impact and minimize the damage caused by HNT requires effective upscaling of the prototype presented in Hein et al. (Hein *et al.*, 2019). Necessary components which required upscaling to provide the ability to impose stress on large diversity panels or mapping populations include the heat tent structure and heating system along with a brand new cyber-physical system (Table 3-1). In addition, grain size, in particular grain width, was demonstrated to be a key trait that translated to lower yield and poor grain quality i.e. increased protein and lipids at the cost of starch under HNT stress (Impa *et al.*, 2020; Sadok and Jagadish, 2020). This information on grain protein and starch

imbalance has been captured under controlled environment growth chambers, but whether the same results can be extended to field grown wheat is not known Impa *et al.*, 2020). Hence, the objectives of the study were to (i) design and build a new field-based infrastructure and test and validate the uniformity of HNT stress application on a scaled-up version of the prototype presented in Hein *et al.* (2019); (ii) improve and develop a more sophisticated cyber-physical system to sense and impose post-anthesis HNT stress uniformly till physiological maturity, within the scaled-up tents; and (iii) determine the impact of HNT stress during grain filling on the agronomic and grain quality parameters including starch and protein concentration.

Materials and Methods

Field infrastructure

The custom designed and movable heat tents are 9.1 m wide, 14.6 m long and 4.4 m tall (Four Season Tools, Kansas City, MO, USA; Table 3-1, Figure 3-1; Appendix B Figure - 1). The structures had 1.9 m tall sidewalls that were joined with a vertical truss every 1.8 m along the length of the building. The combination of taller sidewall piping with the roof trusses allowed for a 2.4 m working height below the bottom chord of the roof trusses. The buildings were designed to study the impact of HNT stress on a wide variety of row crops including corn and sorghum which was not possible in the previous iteration of the system (Table 3-1). Each heat tent was built on top of 15.2 m long skids with integrated ski tips on the ends allowing the tent to be moved in either direction utilizing a tractor. The end walls were built with retractable studs to be removed during movement which gives the heat tent the ability to be placed over the crop during the target developmental stage/s, otherwise allowing the crop to grow in normal field conditions.

Due to its movement capabilities, the structure was braced throughout to prevent bending or misshaping.

The tents were enclosed with a 6 mm polyethylene plastic with a 92% light transmission according to the manufacturer (Berry Global Plastics, Evansville, IN, USA). A motorized roll-up system (Advancing Alternatives, Lancaster, PA, USA) on all the sidewalls, endwalls and roofs were installed to allow the heat tents to be as open as possible throughout the day as to not impose a high day temperature stress, similar to the principle published in rice (Shi *et al.*, 2012; Baguguna *et al.*, 2017). This system utilized 24 VDC motors with guide bars that, when initiated, automatically rolled the plastic up to the day setting and allowed for a more open and truly ambient daytime condition when compared to Hein *et al.* (2019) (Table 3-1, Figure 3-1).

To increase the temperature within the tents designated for elevated stress, a heating system was designed to operate automatically overnight. A Modine HDB100 Hot Dawg propane heater (Ferguson Plumbing and Heating, Manhattan, KS, USA) was installed in each stress tent utilizing square steel and steel rods between the end wall and first vertical truss (Figure 3-1). This unit has an 82% efficiency rating and outputs 82,000 BTU/hour at 781 FPM. The heater was augmented with a duct transition to allow the attachment of convection tubing. The tubing itself was 45.7 cm in diameter and 13.7 m in length (Figure 3-1; Appendix B Figure - 1). The convection tubing was punctured every 1.2 m with round openings with a diameter of 5.7 cm at 3 o'clock and 9 o'clock to force the heated air to escape parallel with the field. The heaters were supplied with propane via individual 1829.7 L tanks (Propane Central, Clay Center, KS, USA). Two 30.5 cm horizontal air flow fans (J&D Manufacturing, Eau Claire, WI, USA) with an air flow rate of 1,020 CFM were hung from the bottom chord of the trusses in opposite corners to evenly circulate the heated air (Figure 3-1; Appendix B Figure - 1). The larger heating system

with convection tubing and dual circulation fans allowed for a single heater to completely and equally impose stress while, along with the addition of the combustion exhaust, created a safer and more controlled environment than previously capable in Hein *et al.* (2019) (Table 3-1).

The control tents were outfitted with a very similar set up without the implementation of heat. To imitate the same sensation of air movement on the plants as in the stress tents, a 45.7 cm power tube fan (Coolair, Jacksonville, FL, USA) was installed and convection tubing ran with the same hole set up as the stress tents. The same horizontal air flow fans were also installed to circulate the air throughout each of the three control tents.

To operate the tents, a Caterpillar XQ30 electric generator (Foley Power Solutions, Topeka, KS, USA) was placed centrally located in the field. The generator output 30 KW/38 KVA. A 3785.4 liter diesel tank (Capital City Oil, Topeka, KS, USA) was positioned very near to the generator and was outfitted with a battery operated 12-volt DC pump with an output of 75.7 liters per minute, hose and nozzle for refueling the generator, similar to Hein *et al.* (2019). Two 50 amp spider boxes were wired to the generator with 30.5 m twist-lock cords to allow distribution of electricity to all tents. Electricity was then distributed to each tent using various lengths and gauges of extension cords depending on the size of load and length of run.

Temperature Controller System

Overall description/functionality

The thermostat controller system was newly designed to monitor the temperature within each tent, average the temperature sensor array readings and wirelessly transmit the temperature from the control tents to their corresponding stress tents for comparing the control and stress environments. When the temperature within a stress tent was less than 4 °C warmer than the corresponding control tent, the system engaged the propane heater to increase the interior

temperature of the stress tent. If the stress tent was 4 °C or more above the control tent, the heater was not engaged and the temperatures continued to be monitored. This improved functionality as well as having the capability to be equipped with multiple different sensor types to gather data on different environmental variables simultaneously resulted in a much more robust and stable system (Table 3-1).

The thermostat controller system consisted of a Raspberry Pi (Raspberry Pi Foundation, Cambridge, UK), six MCP9808 temperature sensors (Adafruit, New York City, NY, USA) and one DS3231 Real-Time Clock (RTC) module (Adafruit) for each tent. In addition, stress tents contained a four-channel Solid State Relay (Keyes KY-019 Relay Module, Songle Relay, Yuyao City, Zhejiang, China) for controlling the heater (Appendix B Figure – 2, 3, 4) and one MH-Z19 carbon dioxide sensor (Zhengzhou Winsen Electronics Technology Co., Ltd., China) for monitoring carbon dioxide levels. An electrical junction box was used to water- and dust-proof the Raspberry Pi, RTC and the Solid State Relay (Appendix B Figure – 2). Each individual temperature sensor and the CO_2 level within the tent was read every minute and logged into a CSV file with accurate timestamps from the RTC module. The overall system health was logged to file for troubleshooting and verification purposes. A systematic view of the overall spread of the temperature sensors within the tents, the integration of wireless flow of information on temperature between control and heat tents is illustrated in Fig 3-2.

Design philosophy

Autonomy, versatility, ease of use and robustness were factored into the system design. When the system was powered on, the controller automatically initialized itself and began reading temperature sensors and logging data to the file automatically. The code base allows users to define their own implementations for interacting with different types of sensors i.e., different

heaters can be used with few changes to the code (Appendix B Document -1). Users can interact with the system using simple Linux commands to verify that everything is operating correctly and to retrieve the log files. The system does not crash when a sensor fails to read, it instead attempts to reboot after a set number of consecutive read errors and, after a maximum number of reboots, remains online to continue the experiment.

Software failures were typically resolved by rebooting the Raspberry Pi. If the temperature sensors were detected on the I2C bus but were not read, the baud rate was reduced further, this allowed more time for the signals to propagate down the leads to be read by the Pi. If none of the sensors were being read, then each individual sensor connected to the system was manually inspected for short circuited pins, any found were removed from the system and replaced with new components and tested after installation. For more detailed description and explanation of the temperature control system hardware, components and codebase, as well as a detailed list of components and their sources for the entire field-based infrastructure system see Appendix B Document - 1, Appendix B Figure - 2, 3 and 4, and Appendix B Table - 1 and 2 for Tent and Raspberry Pi Components.

Operation of the tents and stress imposition

The HNT stress was imposed at night from 8:00 PM till 6:00 AM beginning after all genotypes reached 50% anthesis and continued till physiological maturity. The experimental process began at 6:30 PM with rolling down the roofs of the stress tents and then the side and end walls. After the stress tents were closed, the control tents roofs were closed and the side and end walls were lowered to 20 cm above the baseboard to allow ambient air to circulate through the tent (Figure 3-1; Appendix B Figure - 1). By 7:00 PM the generator was activated and all control tents were

provided power immediately to initialize their systems. After the cyber-physical systems were running in the control tents, the stress tents were turned on consecutively to allow for monitoring the initiation of the propane heaters. The stress tents were deemed operational by physically viewing the operation of the propane heaters and the entire cyber-physical system was judged operational through wireless analysis of the Raspberry Pi. The system then achieved the indicated differential temperature in the heat tents by 8:00 PM to start the overnight stress period.

The system began to be shut down at 6:00 AM by first wirelessly collecting the data from the Raspberry Pis and then consecutively removing the power from the Raspberry Pis within the stress tents. Without electricity, the call for heat from the cyber-physical system would cease and the heaters would go through their shutdown procedure. Once all heaters had processed through their shutdown procedure, the generator was turned off which removed power from the entire system. The propane was then turned off both within the heater and on the tank for safety redundancy. The roofs, endwalls and sidewalls were raised to their daytime ambient setting on all tents concurrently with the system shutdown procedure.

Each tent was monitored with multiple sets of sensors to allow the capture of temperature, relative humidity and carbon dioxide. The Raspberry Pi system itself utilized six temperature sensors, spread across the tent, with a sensitivity of ±0.25°C which monitored the tents throughout the night while the system was running and recorded data every minute (Figure 3-2). This new and expanded sensor array not only gathered a more accurate representation of current temperature levels within the tents, but also allowed for post-analysis of the uniformity of heat distribution through individual sensor recordings (Table 3-1). The Raspberry Pi system in the stress tents also recorded carbon dioxide levels with one MH-Z19 carbon dioxide sensor, with a sensitivity of ±50 ppm (+ 5% reading value), randomly placed within the tent 25 cm

above canopy level. Each tent was also equipped with two HOBO UX 100-011 temperature/relative humidity data loggers (Onset Computer Corp., Bourne, MA, USA) to record relative humidity with an accuracy of ±2.5%, recorded once every 15 minutes. Finally, the heat tents were outfitted with two HOBO UA 002-64 Pendent data loggers (Onset Computer Corp., Bourne, MA, USA) which recorded temperature at a sensitivity of ±0.53°C and light intensity. These data loggers recorded data at 15-minute intervals throughout the course of the experiment (Figure 3-2).

Crop cultivation

The tents and connected cyber-physical systems were tested in a field-based experiment at the Kansas State University, Agronomy North Farm in Manhattan, Kansas (39°12'47.3"N 96°35'35.0"W). This experiment utilized the same set of genotypes tested in the prototype (Hein *et al.*, 2019), which were included as a subset within the larger diversity panel (n =320; aimed at Genome Wide Association Studies [GWAS]). The selection included five wheat varieties extensively grown in Kansas (Everest, Larry, SY-Monument, WB-4458 and WB-Cedar), five common breeding lines from the Kansas wheat breeding program (Jagger X060724, KS 070736 K-1, KS 070729 K-26, KS 070717 M-1 and P1 X060725) and two exotic varieties (Tascosa and Tx86A5606) which have been previously shown to have differential responses to heat stress (Bergkamp *et al.*, 2018; Impa *et al.*, 2019; Hein *et al.*, 2019). As a part of the larger study, each heat and control tent had eight blocks accommodating all 320 accessions for GWAS analysis, with 40 rows each per block. Each genotype was planted in a single row in each of the three control and heat stress replications with the exception of Everest. This widely used wheat variety in Kansas was used as a check-line to evaluate equal distribution of the heat stress within and

between the tents. Each of the eight blocks in all six tents contained a row of Everest, resulting in eight rows of Everest per tent, distributed randomly across blocks.

The space within the tents was measured and marked at 8.2 x 10.7 m. Each tent contained eight blocks containing 40 rows with each row measuring 1.2 m and spaced 19.1 cm apart and with 0.5 m alley between blocks. The rows were trenched to a depth of 3.8 cm using a tool with eight equally spaced prongs to ensure exact and equal depth and spacing throughout the blocks and tents. The trenches were hand planted at 88 seeds per row or 383 seeds/m^2 or at a rate of 4.45 million seeds per hectare. The seeds were treated before planting with a mixture of 50% Cruiser Maxx Vibrance Cereals (Sedaxane, Difenoconazole, Mefenoxam, Thiamethoxam), 43.75% water and 6.25% Cruiser 5FS (Thiamethoxam) at a rate of 0.33 mL/50 g of seeds and the plots were hand planted on October 23, 2018. Prior to planting 47.07 kg N ha^{-1} (urea ammonium nitrate solution) was applied to the field. On 25th March 2019, 0.88 L ha^{-1} of MCPA herbicide (2-methyl-4-chlorophenoxyacetic acid) and 2.19 cL ha^{-1} of Finesse Cereal and Fallow herbicide (Chlorsulfuron, Metsulfuron Methyl) were applied followed by 57.16 kg N ha^{-1} (urea ammonium nitrate solution) on 26th March, 2019. On 14th May 2019, 0.49 L ha^{-1} of Approach Prima fungicide (Picoxystrobin Methyl, Cyproconazole) was applied to the plots to manage Fusarium Head Blight and the custom built tents were pulled over the plots on 15th May, 2019.

The stress period for the experiment began on May 26th, 2019 as all 12 genotypes had reached 50% anthesis by May 24th, 2019 and continued throughout the grain-filling period till physiological maturity. Hence, the flowering phenology between the 12 genotypes was very narrow i.e., just 2 days and so had no confounding effect on the results. The plots were irrigated with 1325 liters of water per tent or 15.1 L m^{-2} on 12th June, 2019 and on 18th June, 2019 to avoid water-limited stress. The plots were irrigated minimally due to an unusually wet spring at the

experimental site. The total precipitation for the month of May at the experimental site was 29.1 cm, which is 17.8 cm above the normal precipitation amount. June had a nearly average precipitation totaling to 11.83 cm which was only 1.09 cm below the normal (National Weather Service).

Agronomic observations

Yield and yield components

For grain yield and yield components, a 0.5 m central strip of each genotype, including the eight rows of Everest check-lines in each tent, was hand harvested at physiological maturity (Feekes 11.4). Maturity was determined by daily evaluation of a sample seed set and whether a thumbnail could dent the seed. Spikes were immediately removed from the biomass and dried at 40 °C for 96 hours. The biomass was dried separately at 60 °C for 168 hours. Spike weight was taken and then the spikes were threshed using an LD 180 Laboratory Thresher (Wintersteiger, Ried im Innkreis, Austria) and grain yield and yield components were recorded. To ascertain any possible impact of Fusarium Head Blight, yield and yield components were also calculated by utilizing the average seed weight of non-infected seeds for each sample. After threshing, the seeds from each sample were manually separated into infected and non-infected categories and the non-infected seeds were then counted and weighed. The non-infected seed sample count and weight was then used to calculate average single seed weight for the non-infected seeds. This average single seed weight was then used to obtain total sample seed weight by multiplying average single seed weight of non-infected seed by the total number of seeds in the harvested sample (including both infected and non-infected seeds). The extrapolated data was highly correlated with the non-categorized whole-sample results with the differential (HNT as a percentage of control) R-Squared values of 0.92, 0.96 and 0.93 for 200 kernel weight, grain yield per m^2 and

harvest index, respectively (Appendix B Figure - 5G, H and I, respectively). Based on the above finding, the non-categorized whole-sample data for yield and yield components were used for analysis of grain yield per m^2, 200 kernel weight and harvest index (grain yield / total above ground plant weight including grain yield). The dried biomass weight was recorded for calculating harvest index.

Grain Protein and Starch Concentration

For quantification of grain protein and starch, samples from all twelve genotypes were evaluated utilizing wet chemistry. Grain samples were ground in an 8000M SPEX Mixer/Mill grinder (SPEX Industries Inc., Metuchen, NJ, USA). A portion of the ground sample was sent to the Kansas State Soil Testing Lab (Manhattan, KS, USA), which used a LECO TruSpec CN combustion analyzer to obtain nitrogen concentration on a percent weight basis. This nitrogen concentration was then multiplied by 5.7 to calculate the grain protein concentration (Breese, 1931). The remaining portion of ground sample was tested for starch concentration utilizing a total starch hexokinase kit (K-THSK, Megazyme, Wicklow, Ireland) as detailed in Impa *et al.* (2019).

HNT effect on emergence and seedling vigor

To test HNT effect on the next generation emergence and seedling vigor, harvested seeds were used to quantify these parameters in controlled environment growth chambers. Each plastic tray had six rows with each row having eight individual cells. Each individual cell measured 5.1 cm in diameter and depth. Seeds from all 12 genotypes and both HNT and control were planted randomly in rows, with a single seed in each cell. Each genotype was replicated thrice (i.e. 3 rows = 24 seeds per genotype and treatment). The cells were filled with three parts Vermiculite #3 (Hummert International, Topeka, Kansas, USA) and one part Perlite Hort Grade Coarse

(Hummert International, Topeka, Kansas, USA). The soil was dampened with water prior to planting and the seeds were planted at 1.3 cm depth. The trays placed on flat holder trays were moved to a controlled environment growth chamber set at 28/15 °C (actual 28.4/15.3 °C; day/night) with a four hour transition period between day and night and with a photoperiod of 16/8 (light/dark). The flat trays allowed for 1 cm depth of standing water at the bottom ensuring ample water availability throughout (Impa *et al.*, 2020). Seedling emergence counts were recorded daily at 4:00 PM and used to calculate total emergence percentage and emergence index (Moghimi *et al.*, 2019). Seedlings were uprooted 14 days after planting, washed and oven dried to record the total seedling biomass as a measure of seedling vigor.

Statistical analysis

The experiment was a split-plot randomized complete block design. Temperature was the main plot factor and the sub-plot factor was the genotype. Replicated observations for each trait were analyzed for means and standard error and ANOVA was performed using R v.3.6.1 (R Core Team, 2017).

Results

Environmental results

Implementation and distribution of HNT stress

Through the use of horizontal air flow fans and convection tubing in each tent, a uniform distribution of heat was achieved (Figure 3-3A). On average, the system measured a 0.6 °C differential between the six temperature sensors within the stress tents (Appendix B Table - 3). The HOBO UA 002-64 Pendent data loggers were also used to validate uniform heat distribution

in control and stress tents. The HOBO Pendent loggers measured an average of 0.2 °C temperature difference at any given time within the control and stress tents (Figure 3-3A).

The varieties within the stress tents were exposed to an elevated HNT conditions which averaged +3.8 °C, as measured by the Raspberry Pi sensor array, compared to the average night-time temperature of the control tents (Figure 3-3B). The overall average temperature during the stress period, in the stress tents was 22.1 °C while it was 18.4 °C in the control tents (Appendix B Table - 3). The temperature within the stress tents and the control tents began to diverge from 6 PM as the closing of the stress tents was initiated (Figure 3-3B), reaching +2.8 °C and +3.5 °C by 7 and 8 PM, respectively. The average differential continued to rise and maintained at ~3.8 °C from 10 PM till returning to ambient conditions, as the experiment was turned off and tents were opened at 6 AM.

Effective day time ambient temperature

Between 7 AM and 6 PM, the control and heat tents were on average 0.4 °C warmer than the ambient conditions as measured by the HOBO UA 002-64 Pendent data loggers (Fig 3-3B). The tents had the largest differential away from ambient in the early morning immediately after the HNT stress was released, which were 2.4 °C warmer than ambient. This was reduced to 1.9 °C by 8 AM and the difference was only 0.4 °C at 9 AM. Between 10 AM and 1 PM the tents temperature average was cooler than the ambient conditions and after 1 PM they stayed within 1 °C of ambient conditions till 6 PM when steps to cover the tents were initiated (Figure 3-3B).

Relative humidity, vapor pressure deficit and carbon dioxide

During the non-stress period the stress tents relative humidity (RH) was on average 2.3% higher than the control tents (Figure 3-3C). From 10 AM to 6 PM the difference in RH between the two sets of tents ranged between 0.2 and 4%. During this period, the control tents had a slightly

higher RH than the stress tents for the majority of this period, with an average of 52.6% and 52.0% respectively. The vapor pressure deficit (VPD) within the tents during the non-stress period ranged from 0 kPa to 0.5 kPa but the overall average difference was only 0.1 kPa (Figure 3-3C). During the stress period, the stress tents RH ranged from 11% to 19% higher than the control tents (Figure 3-3C), with 0.01 kPa lower VPD in the stress tents compared to the control tents. The overall average CO_2 concentration within the stress tents was 538 ppm but ranged from 457 ppm when the tents were first closed to 565 ppm while the CO_2 concentration within the control tents was 544 ppm and ranged from 480 ppm to 576 ppm (Appendix B Table - 3).

Agronomic responses to HNT stress

Everest check lines

The results from each Everest check line were grouped based on their position within the tent (blocks one through four and blocks five through eight) and ANOVA was performed to evaluate the differences within each tent based on grain yield (g/m^2), 200 kernel weight (g) and harvest index. At a 95% confidence interval, there were no significant differences between the two different groupings within each of the tents for all three traits (Appendix B Table - 4). This further reinforced the conclusion of a highly consistent and uniform distribution of heat stress within each of the heat tents, supporting the findings presented in Figure 3.

Across the tents, there was no significant difference between the control tents for both 200 kernel weight and harvest index (Figure 3-4A, C). However, with grain yield, both control tents 1 and 2 did not differ significantly, but control tent 3 recorded a significantly higher grain yield compared to control tents 1 and 2 (Figure 3-4B). This can be attributed to the placement of control tent 3 towards the southern end of the plot, which was possibly influenced by the inputs from the previous sorghum crop. This was also reflected in the heat stress tent 3, which was

paired with control tent 3 (Figure 3-4B) (Appendix B Figure - 6). Based on the design of the system wherein one control tent was paired with one stress tent, comparing findings between the pairs is appropriate while determining the effectiveness of the HNT stress (Appendix B Figure - 6). Comparing 200 kernel weight and harvest index between the respective control and heat tents, recorded a statistically significant difference (Figure 3-4A, C). Although there was a significant difference between two tent pairs for grain yield, overall, the HNT resulted in a significant reduction in 200 kernel weight, grain yield and harvest index compared to control (Figure 3-4).

Grain-filling duration

Recording the start of flowering and physiological maturity for all lines across both treatments allowed for the determination of the grain-filling duration. HNT stress had a significant effect with treatment, genotype and their interaction on grain-filling duration (Figure 3-5A; Table 3-2). Exposure to HNT stress reduced grain-filling duration in 10 of the 12 genotypes (except KS 070736 K-1 and Jagger X060724), with eight of the 10 recording a significant reduction (Figure 3-5A). Averaged across the genotypes, grain-filling duration was reduced by 3.33 days or 7.7% or 2.0% per °C. The largest reduction of 5.5 days was recorded in the genotype Tascosa, while the least affected variety was KS 070736 K-1 wherein the grain-filling duration increased by over a day (Figure 3-5A).

200 Kernel weight and grain yield

The effect of HNT stress on 200 kernel weight was significant at the treatment, genotype and their interaction levels (Figure 3-5B; Table 3-2). HNT stress reduced the overall 200 kernel weight of the tested genotypes by an average of 4.8% or 1.3% per °C. Of the 12 genotypes, 10 recorded a reduction in 200 kernel weight. The largest reduction in 200 kernel weight was

observed in KS 070717 M-1 followed by P1 X060725 and WB-4458 and, conversely, a substantial increase was recorded in Jagger X060724.

All 12 varieties tested had a lower grain yield with HNT exposure compared to control conditions. P1 X060725 recorded the largest reduction in grain yield with a 30.4% or 189.29 g/m^2 reduction as compared to control conditions. The variety with the lowest reduction was TX86A5606 and the reduction in grain yield averaged 13.6% or 68.60 g/m^2 or 3.6% per °C across all 12 genotypes. Treatment and genotype had a significant impact but not their interaction (Figure 3-5C; Table 3-2). Everest, KS 070717 M-1 and P1 X060725 recorded a significant reduction in grain yield.

Comparing the grain-filling duration and yield changes due to HNT stress can help elucidate genotypic variations in response to stress. WB-Cedar and Tascosa had two of the largest reductions in grain-filling duration (-16.8% and -14.5%, respectively), however they also reported two of the lowest reductions in yield at -3.9% and -4.7%, respectively (Figure 3-5). Alternatively, KS 070717 K-1 and Jagger X060724 had increased grain-filling durations (3.1% and 0.8%, respectively), and responded with substantial reductions in yield of -13.8% and -12.5%, respectively. This comparison shows that, even though the grain-filling period was reduced, WB-Cedar and Tascosa were able to overcome this reduction and yielded close to non-stress conditions. While KS 070717 K-1 and Jagger X060724 were able to maintain their grain-filling duration but not grain yield under stress. This indicated that there could be other physiological processes that lead to yield reduction under HNT, besides reduced grain-filling duration.

Seed number, aboveground biomass and harvest index (HI)

Seed number was significantly affected by the treatment and genotype but not their interaction (Table 3-2; Appendix B Figure - 7A). The average reduction in seed number was 9.0% or 2.4% per °C with the highest reduction found in P1 X060725 followed by Jagger X060724 while WB-Cedar had a marked increase in seed number. Eleven of the 12 genotypes had lower seed number, while the reductions in P1 X060725 and Jagger X060724 were significant.

Aboveground biomass varied significantly with genotype but not with treatment and their interaction (Table 3-2). The two genotypes with the largest reduction were P1 X060725 and Tascosa. On average, the 12 genotypes recorded a 5% or 1.4% per °C reduction in the biomass. Tx86A5606 has the largest increase in aboveground biomass (Appendix B Figure - 7B). HNT stress had a significant effect on HI with treatment and genotype but not with their interaction (Table 3-2; Appendix B Figure - 7C). While eight genotypes recorded a reduction in HI, the only genotype that was significantly reduced was P1 X060725 (Appendix B Figure - 7C).

Starch and protein concentration

The HNT stress effect on grain starch concentration was statistically significant at the treatment and the genotype level but not their interaction (Table 3-2). Eleven of the 12 genotypes had reduced starch concentration, with just KS 070736 K-1 not affected negatively (Table 3-3). The largest reduction was in KS 070717 M-1 with the starch concentration reducing from 56.1% under control conditions to 37.2% with stress. The only other genotype to record a significant reduction in starch concentration was Tascosa. On average, the reduction in starch concentration among the 12 genotypes was 15.3% (Table 3-3). The average protein concentration of the 12 genotypes increased by 2.9% with SY-Monument having the largest increase. Of the 12 genotypes only three recorded lower protein concentration, and not varying significantly with treatment, genotype and treatment interaction (Table 3-3).

Seedling emergence and vigor

Both emergence index and emergence percentage did not vary significantly in the controlled environment growth chamber experiment, in seeds obtained from HNT experiment in the field. On average, the emergence index was increased by 5.6% and the total emergence percentage was reduced by 5.3%. Total seedling biomass was significantly affected by the HNT treatment, with an average reduction of 6.94% or 3.9 g recorded across the genotypes. Among the genotypes, Jagger X060724 and P1 X060725 recorded a significant reduction in seedling biomass (Appendix B Table - 5).

Discussion

Scalability and effectiveness in imposing HNT stress on a large scale

The major challenge faced with scaling up the HNT stress imposing prototype system to a custom-built large-scale field-based infrastructure was a significantly updated cyber-physical system which could successfully impose and measure a predetermined temperature differential (Hein *et al.*, 2019). In addition, this had to be achieved without significantly altering the environmental conditions within the tents during the day compared to the outside temperature and implement HNT stress uniformly throughout the tent for the entire duration of the grain-filling period. The improvised system achieved an average stress of +3.8 °C, an improvement over the prototype, which was able to achieve +3.2 °C differential (Hein *et al.*, 2019), with a target of +4.0 °C in both cases. This increase of 3.8 °C is similar to the results obtained in other field-based HNT experiments utilizing much smaller enclosures, wherein a single genotype was tested (Garcia *et al.*, 2015, 2016). Hence, the presented system demonstrates for the first time the

possibility of imposing HNT stress consistently on a large scale with higher precision than the previous prototype or other small scale enclosures.

Unlike Hein *et al.* (2019), the improved system included a full-fledged ventilation to exhaust the off-gasses from the combustion of propane, similar to many greenhouse structures used for horticultural purposes (Sanford, 2011). Despite this, a higher CO_2 concentration in both control and stress tents (Appendix B Table - 3) reflected an increase in night respiration, altering the carbon balance with the control tents also naturally reaching the threshold temperature of 20 °C for HNT stress on wheat (Garcia *et al.*, 2016). A similar phenomenon was demonstrated in wheat grown under controlled environment conditions, wherein HNT resulted in increased carbon loss due to high night respiration, leading to lower grain yield (Impa *et al.*, 2019, 2020). A similar response has been captured in rice grown in chambers and field conditions (Shi *et al.*, 2012; Bahuguna *et al.*, 2017). Although the study was unable to estimate the impact of HNT on night respiration on individual accessions, the tent-scale increase in CO_2 concentration provides justification for loss of carbon under HNT affecting yield and quality in field grown wheat (Figure 3-5; Table 3-3). However, a larger increase in CO_2 levels with HNT could not be captured due to the structural settings of the tents that facilitated air exchange from outside the tents, although minimal, to maintain comparable RH with the control tents.

Another challenge with the upscaled experimental design was not only to impose stress on a much larger area but also to ensure that the HNT stress was applied uniformly on a single row layout. This was demonstrated using actual temperature sensor array from the cyber-physical system which measured an average difference of 0.6 °C between the six sensors spread randomly throughout the tent. This was further validated independently from two HOBO pendent loggers which measured an average difference of 0.2 °C, across tents for the entire stress

period. Further, the imposition of temperature stress *per se* may not completely justify the uniformity of the system unless a similar measure is observed at the plant level. The uniformity in stress imposition was demonstrated in the statistical similarity in yield and yield components in the check line, Everest, which was planted randomly in each of the eight blocks in all six tents (Fig 4; Appendix B Table - 4). In summary, a combination of +3.8 °C average heat stress with a very small average differential between 0.2 and 0.6 °C between sensors within a tent, a non-significant variation with yield and its components in a common check line confirms that the design was able to successfully impose HNT stress both consistently and uniformly throughout the grain-filling duration. In addition, the sophistication added to the physical components, revised algorithms and improvements to the cyber-physical system allowed the methodology to be successfully scaled up to impose HNT stress on a large diversity panel.

Comparative response of HNT across chambers and field based facilities

HNT beyond 20 °C starting from booting until maturity had a significant impact on grain filling-duration in wheat grown under chamber conditions (Garcia *et al.*, 2016). The response to HNT across scales was consistent, wherein the grain-filling duration was reduced by 3 days in chambers at 20 °C and the current field study at 22 °C (Garcia *et al.*, 2016) (Fig 3-5, 3-6). The reduction in grain-filling duration caused by early senescence in winter wheat due to HNT stress is one of the main factors responsible for lower 200 kernel weight. Reduced grain-filling duration on exposure to HNT lowers the active photosynthetic area and duration affecting the overall assimilate accumulation and supply to the developing grains, inducing yield and quality losses (Impa *et al.*, 2019, 2020) (Figure 3-5; Table 3-3).

HNT exposure in the current study, on average, reduced the 200 kernel weight by 4.8% or 1.3% per °C, which was more consistent with other field-based experiments as compared to results from controlled environment chamber studies (Garcia *et al.*, 2016; Hein *et al.*, 2019) (Figure 3-6). Grain number was reduced on average by 9.0% or 2.4% per °C in the current study with post-flowering HNT exposure. HNT stress exposed from flowering till maturity induced a higher reduction in seed number under controlled environment study (Impa *et al.*, 2020). A higher reduction in grain number was attributed to the impact of HNT on the later developing tillers, with the sensitive reproductive organ development i.e., gametogenesis coinciding with the stress period (Impa *et al.*, 2020; Aiqing *et al.*, 2018; Bergkamp *et al.*, 2018). Similarly, a longer duration of HNT stress starting from booting till maturity would have impacted the later developing tillers more significantly, leading to a much higher reduction in grain numbers (Prasad *et al.*, 2008). The combination of reduced grain-filling duration (2.0% per °C), 200 kernel weight (1.3% per °C) and grain number (2.4% per °C) caused a significant yield reduction of 3.6% per °C of HNT stress (Figure 3-6). Recent field experiments recorded a 3.4% and 6.3% per °C reduction in grain yield under post-flowering HNT stress (Garcia *et al.*, 2016; Hein *et al.*, 2019), while growth chamber experiments reduced grain yield by 3.5% and 5% per °C (Impa *et al.*, 2020; Prasad *et al.*, 2008) (Figure 3-6). Overall, the impact of HNT across scales was consistent with yield and its components and the deviations seen in some cases can be attributed to the range in genetic diversity in the respective study and the intensity and duration in night temperatures.

The reduction in grain yield in this experiment was lower than previously reported with 3.2 °C higher night temperature (Hein *et al.*, 2019), which can be attributed to the inter-annual ambient night temperature variations. This is apparent when comparing this study to Hein *et al.*

(2019), which had a slightly lower heat stress increase (+3.2 °C vs +3.8 °C) but saw a much larger reduction in yield per degree Celsius (6.3% vs 3.6%). This is due to the ambient conditions during the experimental period being warmer in Hein et al. compared to the current experiment (Hein *et al.*, 2019). The average temperature of stress induced in Hein et al. was 26 °C while the average temperature in the current study was 22 °C which accounts for the differing degrees of impact induced by HNT stress (Hein *et al.*, 2019).

Elevated night temperatures negatively affect grain quality by altering the major constituents of the grain. The major impact observed in this experiment was HNT stress induced reduction in total starch concentration (Table 3-3), which is in line with a recent growth chamber study (Impa *et al.*, 2020). A significant reduction in grain starch due to HNT allowed for additional protein and lipid accumulation in two contrasting genotypes. This study found a significant increase in protein concentration in KS 070717 M-1 but did not observe a similar increase in the tolerant SY-Monument (Impa *et al.*, 2020). A similar striking response with protein concentration was not observed in our study but the response in starch reduction between the susceptible KS 070717 M-1 and the tolerant SY Monument was in agreement with Impa *et al.* (2020). Though starch and protein deposition in grains is initiated at the same time, starch deposition is completed around 45 days after flowering. Protein deposition, however, reaches its peak at around 20 days after flowering and hence is not equally affected due to shortened grain-filling duration (Herzog and Stamp, 1983; Emes *et al.*, 2003). Findings from the current field study possibly captures this phenomenon more accurately due to the rapid rate of terminal senescence compared to significantly slower senescence rate under well-watered conditions maintained till maturity under chamber conditions (Impa *et al.*, 2020). In summary, it can be

hypothesized that a significant loss in grain starch due to HNT under field conditions may not always result in increase in grain protein.

Conclusions

The methodology first proposed in Hein *et al.* (2019) was successfully upscaled through significant upgrades in the heat tent structure, heating system, and a fully redesigned cyber-physical system. The large mobile field-based infrastructure was successful in imposing HNT stress uniformly within the tent and consistently throughout the grain filling-duration (Table 3-1). These comparable results in both agronomic and quality parameters from growth chambers, small field-based enclosures and large field-based experiments reveal consistent effects of HNT in a variety of testing environments. Having demonstrated the agreement of findings across controlled environments and field conditions, provides new avenues to use high throughput phenotyping indices identified under chamber conditions (Coast *et al.*, 2019). Extending chamber based indices will facilitate effective utilization of advances in phenotyping to large scale field infrastructure involving diversity panels and mapping populations. In addition, the confidence provided with these comparative assessments across scales strengthen our ability to take relevant decisions on contrasting genotypes, traits, physiological and molecular markers for enhancing HNT tolerance in wheat and other field crops.

References

Alexander, L.V., Zhang, X., Peterson, T.C., *et al.*, 2006. Global observed changes in daily climate extremes of temperature and precipitation. Journal of Geophysical Research Atmospheres 111, D05109. https://www.doi.org/10.1029/2005JD006290

Aiqing, S., Somayanda, I., Sebastian, S.V., Singh, K., Gill, K., Prasad, P.V.V., Jagadish, S.V.K., 2018. Heat stress during flowering affects time of day of flowering, seed set, and grain quality in spring wheat. Crop Science 58, 380-392. https://www.doi.org/10.2135/cropsci2017.04.0221

Bahuguna, R.N., Solis, C.A., Shi, W., Jagadish, S.V.K., 2016. Post-flowering night respiration and altered sink activity account for high night temperature-induced grain yield and quality loss in rice (*Oryza sativa* L.). Physiologia Plantarum 159, 59-73. https://www.doi.org/10.1111/ppl.12485

Bergkamp, B., Impa, S.M., Asebedo, A.R., Fritz, A.K., Jagadish, S.V.K., 2018. Prominent winter wheat varieties response to post-flowering heat stress under controlled chambers and field based heat tents. Field Crops Research 222, 143-152. https://www.doi.org/10.1016/j.fcr.2018.03.009

Breese, J.D., 1931. Factors for converting percentages of nitrogen in foods and feeds into percentages of proteins. Washington, D.C.: U.S. Department of Agriculture. https://www.ars.usda.gov/ARSUserFiles/80400525/Data/Classics/cir183.pdf

Cantarero, M.G., Cirilo, A.G., Andrade, F.H., 1999. Night temperature at silking affects set in maize. Crop Science 39, 703-710. https://www.doi.org/10.2135/cropsci1999.0011183X003900020017x

Chaturvedi, A.K., Bahuguna, R.N., Shah, D., Pal, M., Jagadish, S.V.K., 2017. High temperature stress during flowering and grain filling offsets beneficial impact of elevated CO_2 on assimilate partitioning and sink-strength in rice. Scientific Reports 7, 8227. https://www.doi.org/10.1038/s41598-017-07464-6

Coast, O., Šebela, D., Quiñones, C., Jagadish, S.V.K., 2019. Systematic determination of the reproductive growth stage most sensitive to high night temperatures stress in rice (*Oryza sativa* L.) Crop Science 60, 391-403. https://www.doi.org/10.1002/csc2.20086

Davy, R., Esau, I., Chernokulsky, A., Outten, S., Zilitinkevich, S., 2017. Diurnal asymmetry to the observed global warming. International Journal of Climatology 37, 79-93. https://www.doi.org/10.1002/joc.4688

Djanaguiraman, M., Prasad, P.V.V., Schapaugh, W.T., 2013. High day- or nighttime temperature alters leaf assimilation, reproductive success, and phosphatidic acid of pollen grain in soyben [*Glycine max* (L.) Merr.]. Crop Science 53, 1594-1604. https://www.doi.org/10.2135/cropsci2012.07.0441

Easterling, D.R., Horton, B., Jones, P.D., *et al.*, 1997. Maximum and minimum temperature trends for the globe. Science 277, 364-367. https://www.doi.org/10.1126/science.277.5324.364

Echer, F.R., Oosterhuis, D.M., Loka, D.A., Rosolem, C.A., 2014. High night temperatures during the floral bud stage increase the abscission of reproductive structures in cotton. Journal of Agronomy and Crop Sciences 200, 191-198. https://www.doi.org/10.1111/jac.12056

Emes, M.J., Bowsher, C.G., Hedley, C., Burrell, M.M., Scrase-Field, E.S.F., Tetlow, I.J., 2003. Starch synthesis and carbon partitioning in developing endosperm. Journal of Experimental Botany 54, 569-575. https://www.doi.org/10.1093/jxb/erg089

Food and Agriculture Organization of the United Nations, 2018a. FAOStat: Crops and Livestock Products. Accessed 19 June 2018. https://www.fao.org/faostat/en/#data/QC

Food and Agriculture Organization of the United Nations, 2018b. FAOStat: Annual Population. Accessed 19 June 2018. https://www.fao.org/faostat/en/#data/OA

García, G., Dreccer, M.F., Miralles, D.J., Serrago, R.A., 2015. High night temperatures during grain number determination reduce wheat and barley grain yield: a field study. Global Change Biology 21, 4153-4164. https://www.doi.org/10.1111/gcb.13009

García, G., Serrago, R.A., Dreccer, F., Miralles, D.J., 2016. Post-anthesis warm nights reduce grain weight in field-grown wheat and barley. Field Crops Research 195, 50-59. https://www.doi.org/10.1016/j.fcr.2016.06.002

Hein, N.T., Wagner, D., Bheemanahalli, R., Šebela, D., Bustamante, C., Chiluwal, A., Neilsen, M.L., Jagadish, S.V.K., 2019. Integrating field-based heat tents and cyber-physical system technology to phenotype high night-time temperature impact on winter wheat. Plant Methods 15, 41. https://www.doi.org/10.1186/s13007-019-0424-x

Herzog, H., Stamp, P., 1983. Dry matter and nitrogen accumulation in grains at different ear position in ‘gigas’, semidwarf, and normal spring wheats. Euphytica 32, 511-520. https://www.doi.org/10.1007/BF00021463

Impa, S.M., Sunoj, V.S.J., Krassovskaya, I., Bheemanahalli, R., Obata, T., Jagadish, S.V.K., 2019. Carbon balance and source-sink metabolic changes in winter wheat exposed to

high night-time temperature. Plant, Cell & Environment 42, 1233-1246. https://www.doi.org/10.1111/pce.13488

Impa, S.M., Vennapusa, A.R., Bheemanahalli, R., Šebela, D., Boyle, D., Walia, H., Jagadish, S.V.K., 2020. High night temperature induced changes in grain starch metabolism alters starch, protein, and lipid accumulation in winter wheat. Plant, Cell & Environment 43, 431-447. https://www.doi.org/10.1111/pce.13671

Intergovernmental Panel on Climate Change, 2014. Climate change 2014: synthesis report. https://www.ipcc.ch/site/assets/uploads/2018/05/SYR_AR5_FINAL_full_wcover.pdf

Lizana, X.C., Calderini, D.F., 2013. Yield and grain quality of wheat in response to increased temperatures at key periods for grain number and grain weight determination: considerations for the climatic change scenarios of Chile. The Journal of Agricultural Science 151, 209-221. https://www.doi.org/10.1017/S0021859612000639

Loka, D.A., Oosterhuis, D.M., 2010. Effect of high night temperatures on cotton respiration, ATP levels and carbohydrate content. Environmental and Experimental Botany 68, 258-263. https://www.doi.org/10.1016/j.envexpbot.2010.01.006

Loka, D.A., Oosterhuis, D.M., 2016. Increased night temperatures during cotton's early reproductive stage affect leaf physiology and flower bud carbohydrate content decreasing flower bud retention. Journal of Agronomy and Crop Science 202, 518-529. https://www.doi.org/10.1111/jac.12170

Moghimi, N., Desai, J.S., Bheemanahalli, R., Impa, S.M., Vennapusa, A.R., Šebela, D., Perumal, R., Doherty, C., Jagadish, S.V.K., 2019. New candidate loci and marker genes on chromosome 7 for improved chilling tolerance in sorghum. Journal of Experimental Botany 70, 3357-3371. https://www.doi.org/10.1093/jxb/erz143

Mohammed, A.R., Tarpley, L., 2009. High nighttime temperatures affect rice productivity through altered pollen germination and spikelet fertility. Agricultural and Forest Meteorology 149, 999-1008. https://www.doi.org/10.1016/j.agrformet.2008.12.003

Nagarajan, S., Jagadish, S.V.K., Prasad, A.S.H., Thomar, A.K., Anand, A., Pal, M., Agarwal, P.K., 2010. Agriculture, Ecosystems & Environment 138, 274-281. https://www.doi.org/10.1016/j.agee.2010.05.012

Narayanan, S., Prasad, P.V.V., Fritz, A.K., Boyle, D.L., Gill, B.S., 2015. Impact of high night-time and high daytime temperature stress on winter wheat. Journal of Agronomy and Crop Science 201, 206-218. https://www.doi.org/10.1111/jac.12101

National Weather Service, Climate: NOWData. Accessed 19 June 2018. https://w2.weather.gov/climate/index.php?wfo=top

OECD/FAO, 2019. The OECD-FAO agricultural outlook 2019-2028. Paris: OECD Publishing https://www.oecd.org/agriculture/oecd-fao-agricultural-outlook-2019/

Peng, S., Huang, J., Sheehy, J.E., Laza, R.C., Visperas, R.M., Zhong, X., Centeno, G.S., Khush, G.S., Cassman, K.G., 2004. Rice yields decline with higher night temperature from global warming. Proceedings of the National Academy of Sciences 101, 9971-9975. https://www.doi.org/10.1073/pnas.0403720101

Prasad, P.V.V., Pisipati, S.R., Ristic, Z., Bukovnik, U., Fritz, A.K., 2008. Impact of nighttime temperature on physiology and growth of spring wheat. Crop Science 48, 2372-2380. https://www.doi.org/10.2135/cropsci2007.12.0717

Prasad, P.V.V., Djanaguiraman, M., 2011. High night temperature decreases leaf photosynthesis and pollen function in grain sorghum. Functional Plant Biology 38, 993-1003. https://www.doi.org/10.1071/fp11035

R Core Team, 2017. R Foundation for Statistical Computing. https://www.R-project.org/

Sadok, W., Jagadish, S.V.K., 2020. The hidden costs of nighttime warming on yields. Trends in Plant Science 25, 644-651. https://www.doi.org/10.1016/j.tplants.2020.02.003

Sanford, S., 2011. Greenhouse unit heaters: types, placement, and efficiency (A3907-02). University of Wisconsin-Madison. https://cdn.shopify.com/s/files/1/0145/8808/4272/files/A3907-02.pdf

Shi, W., Muthurajan, R., Rahman, H., Selvam, J., Peng, S., Zou, Y., Jagadish, S.V.K., 2013. Source-sink dynamics and proteomic reprogramming under elevated night temperature and their impact on rice yield and grain quality. New Phytologist 197, 825-837. https://www.doi.org/10.1111/nph.12088

Shi, W., Yin, X., Struik, P.C., Xie, F., Schmidt, R.C., Jagadish, S.V.K., 2016. Grain yield and quality responses of tropical hybrid rice to high night-time temperature. Field Crops Research 190, 18-25. https://www.doi.org/10.1016/j.fcr.2015.10.006

Sillman, J., Kharin, V.V., Zhang, X., Zwiers, F.W., Bronaugh, D., 2013. Climate extremes indices in the CMIP5 multimodel ensemble: part 1. Journal of Geophysical Research Atmospheres 118, 1716-1733. https://www.doi.org/10.1002/jgrd.50203

Figures

Figure 3-1 An overview of field and tent layout.

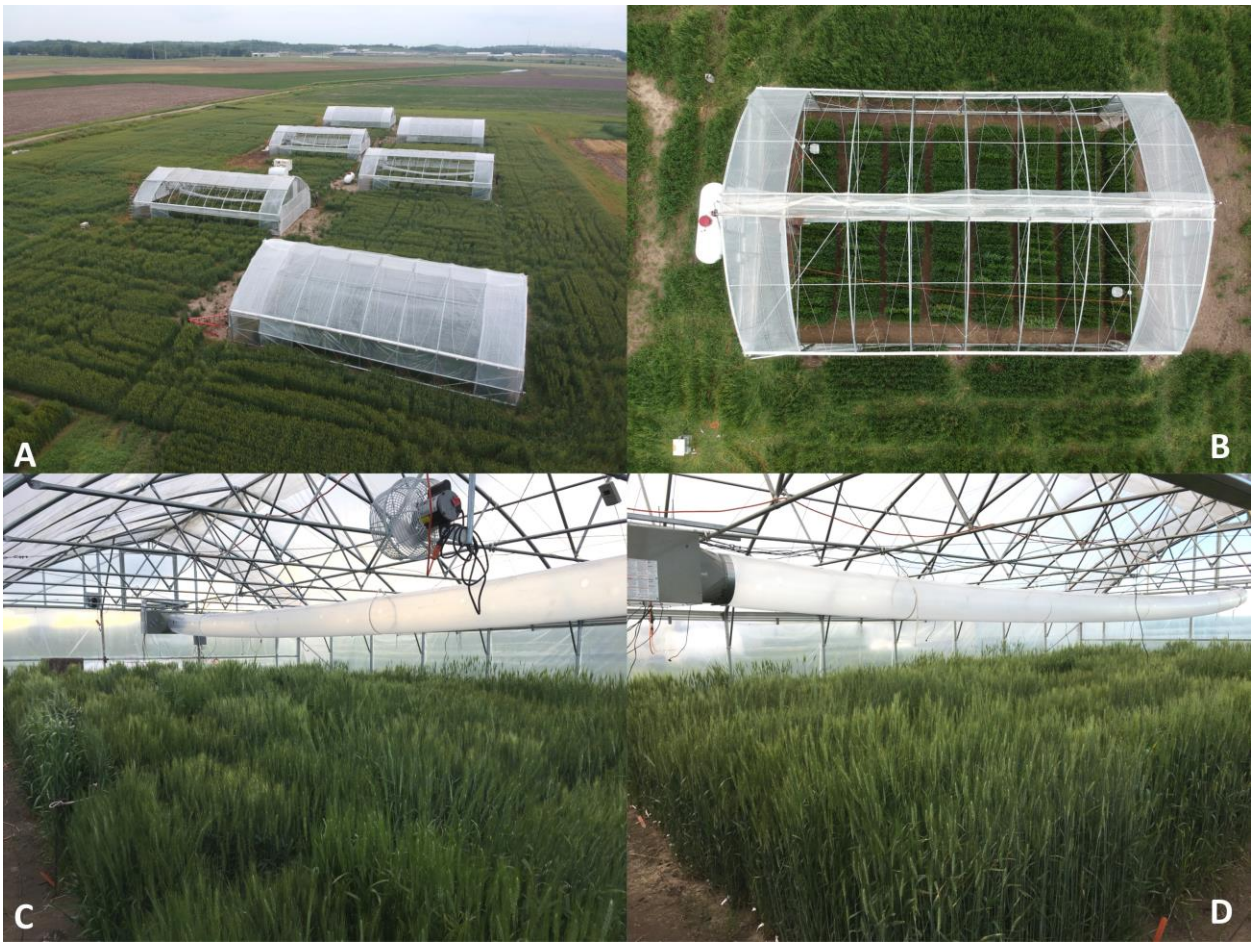

(A). An over-head view of all six tents with the three control tents (two in the farthest background and one in the closest foreground) in their night setting with the roof closed and the sidewall lowered and three stress tents (centrally located) in their day setting. (B). Overhead view of a stress tent with a propane tank on the far left and the roof opened to its daytime setting. Eight blocks of 40 individual rows shown along with circulation fans in the upper-left and bottom-right portion of the interior of the tent. (C). Interior view of a stress tent looking towards the heater with the circulation fan in the foreground and propane heater in the background. The convection tubing extended from the propane heater throughout the entire tent to distribute the

heated air uniformly. (D). Interior view of a stress tent looking from the heater towards the opposite side of the tent. The convection tubing is seen all the way extended to the endwall and the roof and sidewalls lowered in their night setting. An additional figure indicating each component within and outside the tents is presented in Appendix B Figure - 1.

Figure 3-2 Diagrammatic presentation of a paired control tent with a stress tent.

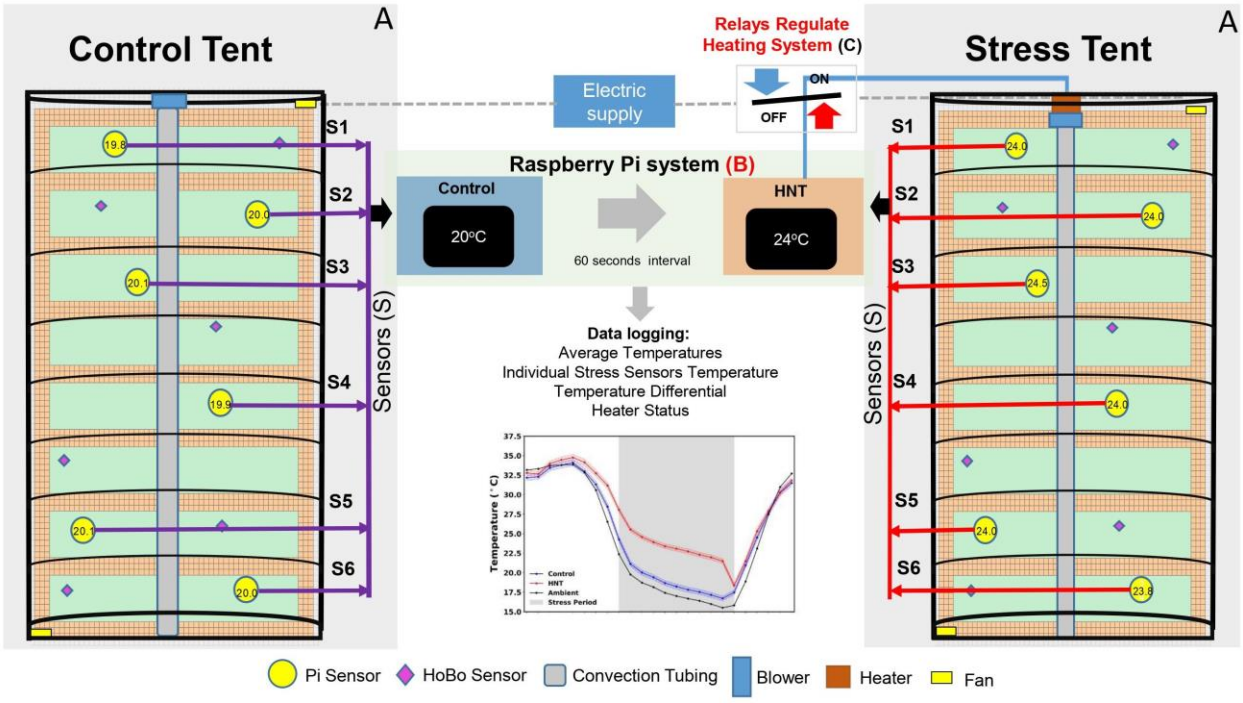

(A). A detailed interior view of the stress and control tent; see Appendix B Figure - 1. (B). A detailed explanation of Raspberry Pi System and its wiring is presented in Appendix B Figure -. 2, 3 and 4, Appendix B Document - 1 System Details and Code and Appendix B Table - 2. (C). An overview of the relay system and their wiring can be found in Appendix B Figure - 3 and 4.

Figure 3-3 Environmental conditions in control and stress tents.

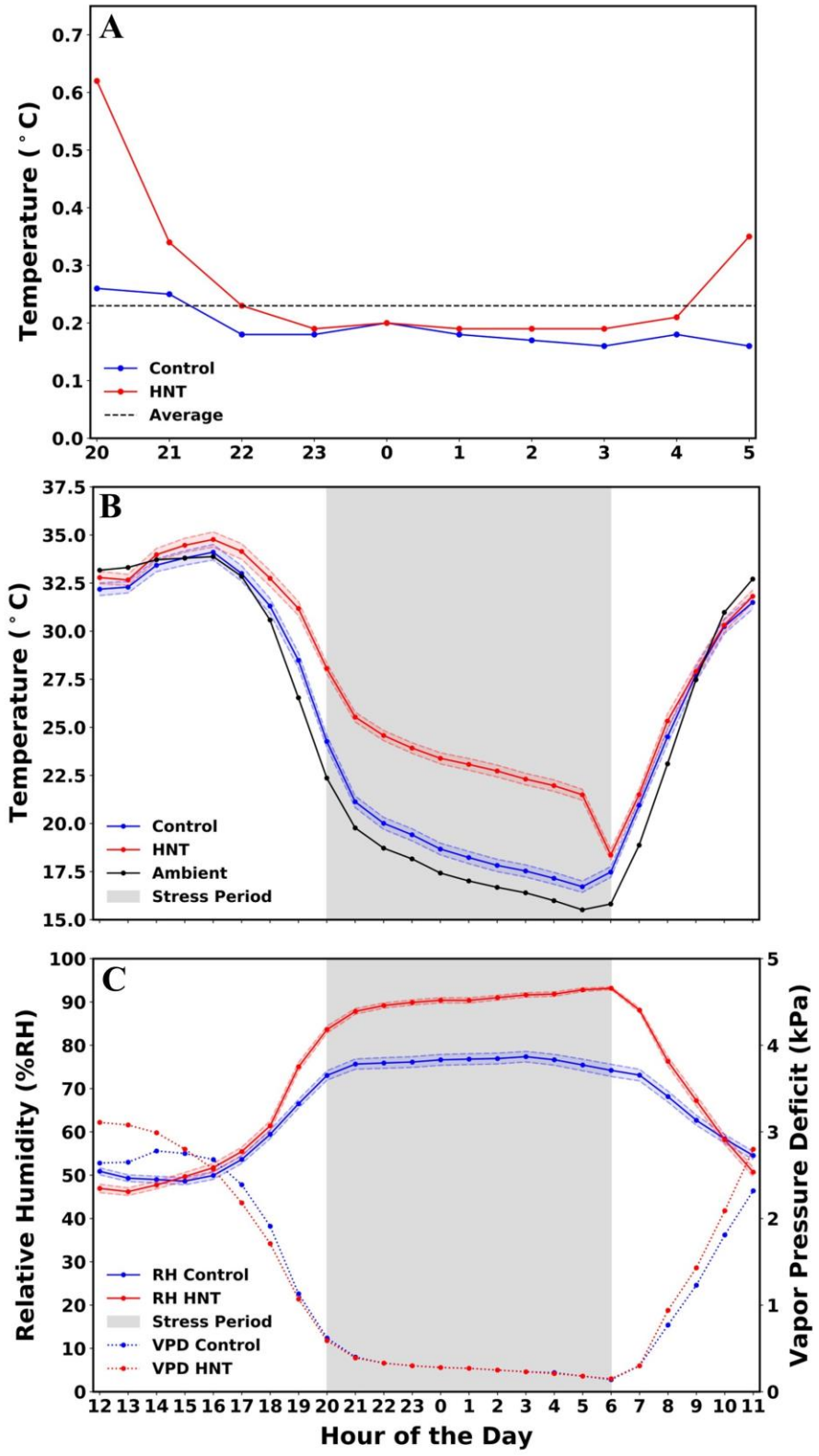

(A). Comparison of the temperature differences between the HOBO data loggers within the same tents for control, HNT and overall average. The lower the temperature on the graph represents a more uniform heat distribution as the sensors were spread randomly throughout each tent, see Figure 2. (B). A comparison of the average temperature within the stress tents, control tents and ambient conditions starting at 12:00 PM and ending at 12:00 AM over the entire duration of the experiment. (C). The control and stress tents average relative humidity and vapor pressure deficit are shown throughout the day. 95% confident intervals are represented by the shaded regions above and below the control and stress lines for temperature (B) and relative humidity (C).

Figure 3-4 Comparison of Everest check lines.

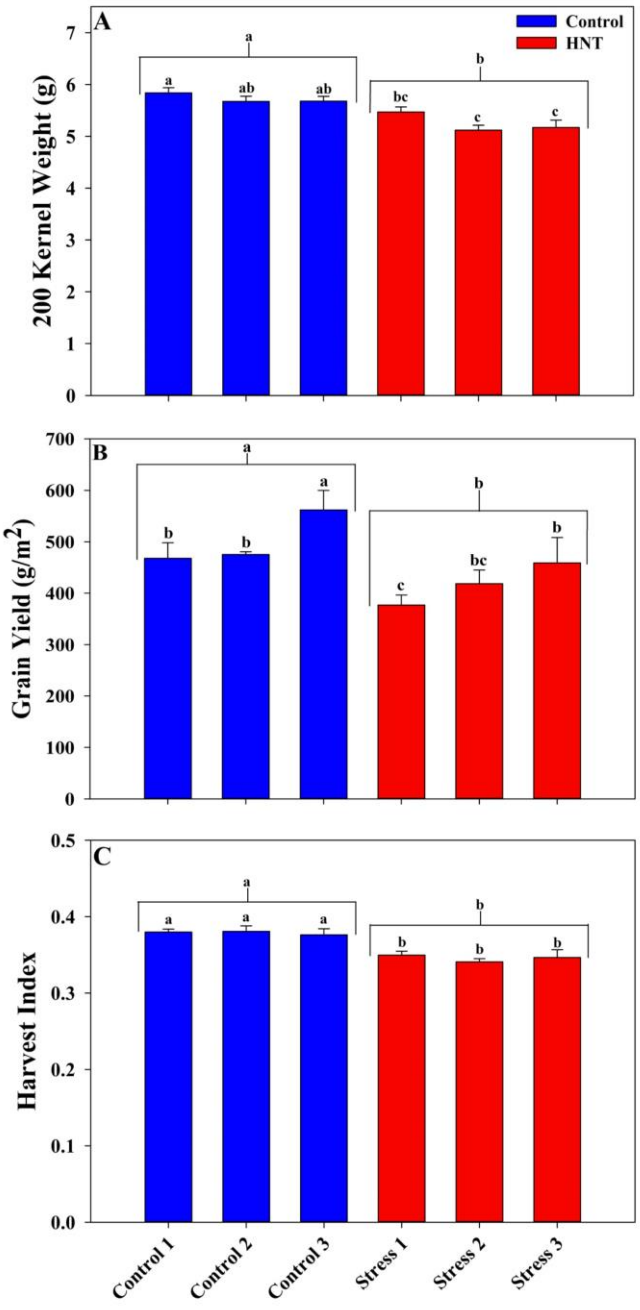

Comparison of 200 Kernel Weight (g) (A), grain yield (g/m^2) (B) and Harvest index (C) in the three control and stress tents. Each column is an average of eight rows of check line Everest and bars indicate +/-SE. Letters above the bars and the brackets indicate groups differing significantly ($p < 0.05$).

Figure 3-5 Agronomic response of wheat genotypes exposed to HNT.

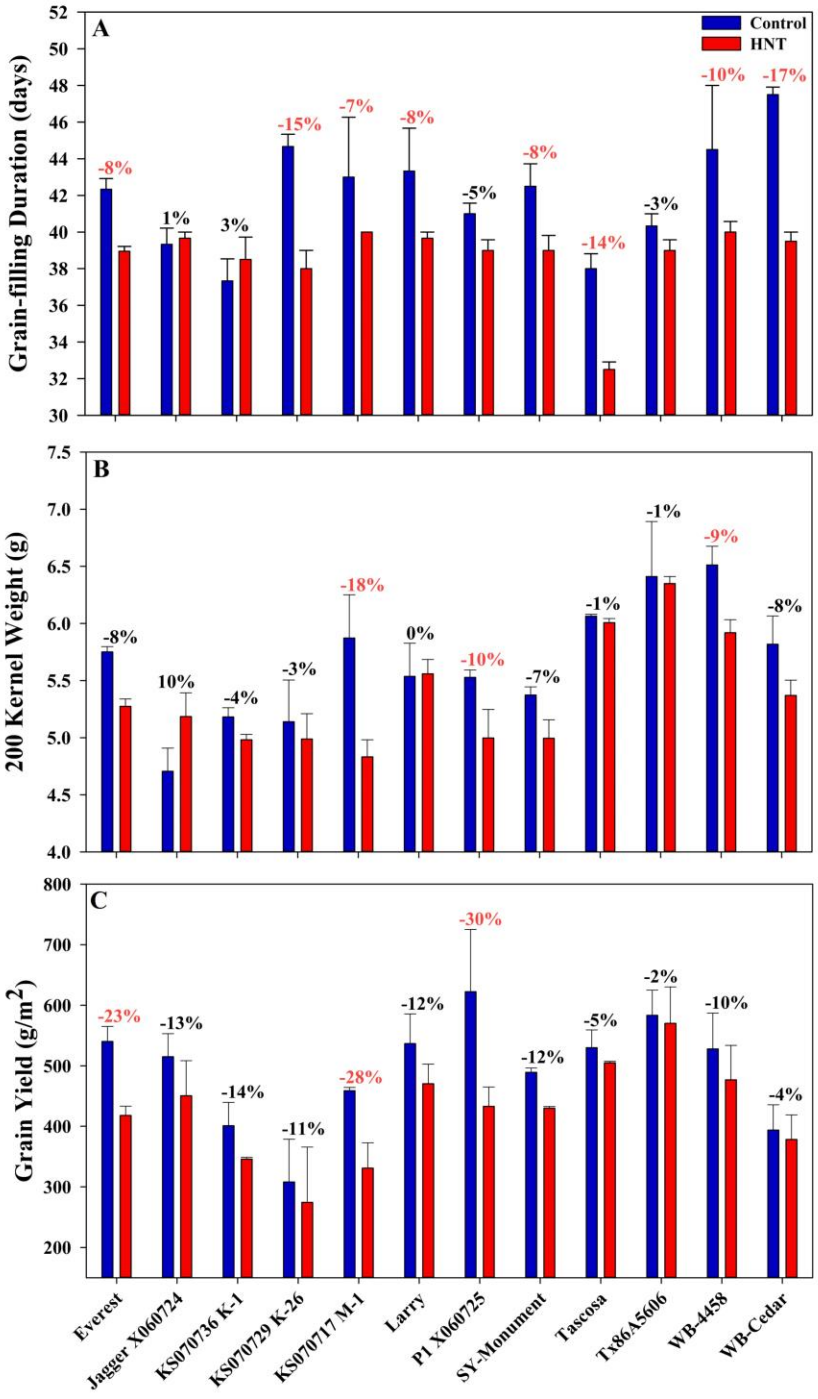

Grain-filling duration (A), 200 kernel weight (B) and grain yield (C) of 12 winter wheat genotypes exposed to HNT stress and control conditions for the entire grain-filling period. Reductions in red signify significant reduction ($p < 0.05$).

Figure 3-6 Graphical comparison of HNT stress impact on key agronomic parameters between six independent experiments in wheat.

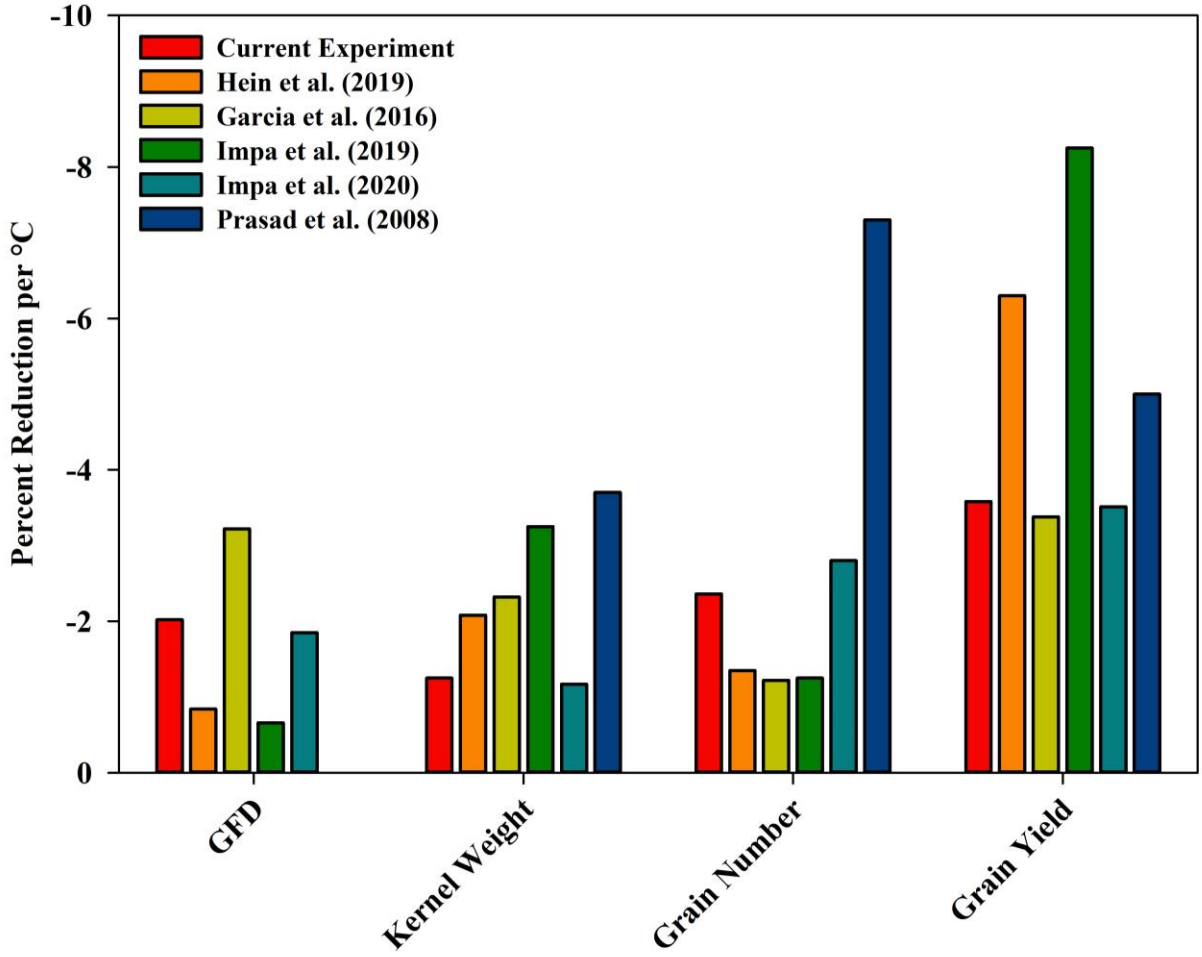

The results are presented as percent reduction per °C of heat stress and represents the average of all genotypes within the experiment. If multiple HNT stress levels were tested in a single experiment, the average reduction was calculated for each treatment level and then the results of each treatment were averaged to gain an overall experimental percent reduction. In the current experiment HNT stress was imposed post-anthesis through maturity with an average stress level of +3.8 °C and control of 18 °C. In Hein et al. [30] (field-based) HNT stress was imposed post-anthesis through maturity with an average stress level of +3.2 °C with a 22 °C control. Both Hein et al. [30] and the current study had 12 winter wheat genotypes. In Garcia et al. [28] (field-based) HNT stress was imposed post-anthesis through maturity with an average stress level of +4.15 °C

during two different years (+4.9 ℃ with a 17 ℃ control and +3.4 ℃ with a 14.3 ℃ control) with a single genotype of winter wheat. In Impa et al. [23] (controlled environment growth chamber) HNT stress imposition after heading and maintained a +8 ℃ HNT stress through maturity with a 15 ℃ control. Six genotypes were used. In Impa et al. [24] (controlled environment growth chamber) HNT stress was applied post-anthesis through maturity. The experiment had five levels of heat stress (+3, +6, +8, +10, and +12 ℃) and a 15 ℃ control and 10 different genotypes. In Prasad et al. [26] (controlled environment growth chamber) HNT stress applied at the booting stage till maturity. The experiment had three levels of heat stress (+3, +6, and +9 ℃) with a 14 ℃ control and utilized two spring wheat cultivars.

Tables

Table 3-1 Improvements in large scale field-based heat tents compared to prototype

System Component	Feature	Hein et al., 2019 Prototype Heat Tent	Large Scale Mobile Heat Tent
Heat Tent Structure	Dimensions	7.2 m x 5.4 m x 3.0 m	9.1 m x 14.6 m x 4.4 m
	Number of Genotypes	12	320
	Planting Height	Could only accommodate wheat or small row crops	Can accommodate small rows crops, sorghum, maize, pearl millet etc.
	Ventilation	Small roof vent and manual sidewall roll-ups	Roof, sidewalls, and end-walls mechanical roll-ups
	Mobility	Hand carried by 12 people	Built on skids - moved through towing with a tractor
	Number of heat tents	3 heat tents with control plots under ambient open field conditions	3 heat and 3 control tents
Heating System	Heater	Small electrical heater	Energy efficient propane heater
		Tank top propane heater	N/A
	Heat Distribution	Built in fan on heater	Additional blower fan on heater with convection tubing allowed efficient and uniform heat distribution
	Ventilation	N/A	Direct ventilation of combustion exhaust to the exterior of the tent
	Fans	Box fan above tank top propane heater	Two powerful circulation fans
Cyber-Physical System	Basic Function	Line voltage disruption	Operated multiple relays to act as thermostat
	Sensor System	Single sensor indoors and outdoors	Six sensor temperature arrays
	Communication	N/A	Wireless communication between control and stress at 1 minute interval
	Additional Sensor Capabilities	N/A	CO_2, relative humidity, and rain sensors

Heat Distribution Analysis	N/A	Capable of mapping heat distribution and uniformity across the entire tent
Control Environment	Ambient conditions not accounting for tent structure	Ambient conditions but within a tent to isolate unaccounted external variables

Improvements in large scale field-based heat tents and cyber-physical system compared to the prototype presented in Hein et al., (2019), for phenotyping impact of high night-time temperature stress.

Table 3-2 Probability values of effects of temperature (T), genotype (G) and T x G interaction on biomass, grain yield and quality traits.

Traits	Variables			Main effect of temperature (mean)	
	T	G	T x G	Control	HNT
Grain filling duration (d)	0.004	<0.001	0.031	42.0[a]	38.9[b]
200 kernel weight (g)	<0.001	<0.001	0.012	5.7[a]	5.3[b]
Grain yield (g m^{-2})	0.002	<0.001	0.729	512.8[a]	424.9[b]
Seed number (m^{-2})	0.012	<0.001	0.874	18112.6[a]	15879.8[b]
Biomass (g m^{-2})	0.11	<0.001	0.649	607.7[a]	570.0[a]
Harvest index	0.013	<0.001	0.122	0.38[a]	0.35[b]
Starch concentration (%)	<0.001	<0.001	0.6149	59.0[a]	50.0[b]
Protein concentration (%)	0.431	<0.001	0.932	14.1[a]	14.5[a]

Means were separated using Tukey's honest significant difference (HSD) test at $p = 0.05$ and are indicated by superscripts.

Table 3-3 Starch and protein concentration (%) of mature seeds in 12 field-grown winter wheat genotypes exposed to HNT and control environments during grain filling.

	Starch Concentration (%)			Protein Concentration (%)		
Genotype	Control	HNT	% Difference	Control	HNT	% Difference
Everest	59.80	46.87	-21.62	14.92	15.69	5.22
Jagger X060724	59.27	48.17	-18.73	14.55	14.57	0.13
KS 070736 K-1	48.82	51.80	6.12	14.27	14.73	3.20
KS 070729 K-26	54.33	44.34	-18.40	13.74	14.42	4.98
KS 070717 M-1	56.07	37.20	-33.67	15.68	15.56	-0.73
Larry	49.27	45.31	-8.04	14.46	14.25	-1.45
P1 X060725	48.36	39.99	-17.32	14.36	14.99	4.37
SY-Monument	63.23	59.40	-6.06	13.13	14.02	6.80
Tascosa	67.77	51.15	-24.52	12.98	13.28	2.34
Tx86A5606	59.66	51.02	-14.47	12.64	13.21	4.51
WB 4458	63.49	59.98	-5.52	13.36	14.27	6.83
WB-Cedar	78.29	64.66	-17.41	14.95	14.92	-0.25
Overall Average	59.03[a]	49.99[b]	-15.31	14.09[a]	14.49[a]	2.89

Means were separated using Tukey's honest significant difference (HSD) test at $p = 0.05$ and are indicated by superscripts.

Chapter 4 - Grain micronutrient composition and yield components in field-grown wheat are negatively impacted by high night-time temperature

Abstract

Wheat (*Triticum aestivum* L.) is highly vulnerable to heat stress during sensitive growth and developmental stages, including grain-filling. The impact of high daytime heat stress on wheat yield and quality losses has been extensively investigated, while information related to high night-time temperature (HNT) is limited. The major objective was to ascertain the changes in wheat grain macro- and micro-nutrient composition and yield-related parameters on exposure to HNT during grain-filling. Twelve diverse genotypes were grown in field-based custom-built heat tents that allowed natural light and temperature conditions during the day and imposed stress overnight. The field-tents imposed a 3.2 °C higher night-time temperature compared to ambient conditions throughout the grain-filling period. HNT stress reduced 200 grain weight by 1.9%, grain yield by 3.1%, seed starch content by 2.5%, and seed protein content by 3.6% per °C increase in HNT.

HNT had significant negative effect on grain macro- and micro-nutrient content. However, starch and protein concentrations were differentially correlated with grain nutrients, with starch negatively correlated with many of the micronutrients under control and HNT. This negative correlation highlights the imperative balance of seed micronutrient composition that needs to be maintained as efforts are intensified to enhance grain yield under favorable and warming environments.

Hein, N.T., Impa, S.M., Wagner, D., Bheemanahalli, R., Kumar, R., Tiwari, M., Prasad, P.V.V., Tilley, M., Wu, X., Neilsen, M., Jagadish, S.V.K., 2021. Grain micronutrient composition and yield components in field-grown wheat are negatively impacted by high night-time temperature. Cereal Chemistry 99, 615-624. https://www.doi.org/10.1002/cche.10523

Introduction

Wheat (*Triticum aestivum L.*) productivity has increased since the Green Revolution during the 1960s and has become a major staple crop supporting about 35% of the world population (IDRC, 2010). Wheat and wheat products, on average, supply nearly 550 kcal capita^{-1} day^{-1} which accounts for ≈20% of the average daily caloric intake (Alexandratos & Bruinsma, 2012; FAO, 2018). The average caloric intake is projected to reach 3000 kcal capita^{-1} day^{-1} and the world population to increase by over 2 billion by 2050 compared to 2018 (Alexandratos & Bruinsma, 2012; FAO, 2021). This increase in population and average daily caloric intake coupled with a projected expansion of the biofuel industry creates a scenario wherein demand for wheat is projected to steadily increase through 2050 (International Food Policy Research Institute, 2013).

To accomplish this increase in production, factors that affect yield, including nutrient and water, solar radiation, fertilizer, genotype, and temperature responses, need to be optimized (Golba *et al.*, 2018). While water availability can be augmented with supplemental irrigation and management practices can help maximize the benefits of fertilizer with appropriate genotype selection, addressing adverse impacts of temperature extremes are challenging. Heat events can be highly detrimental to yield when they coincide with vulnerable developmental stages such as panicle initiation, gametogenesis, flowering, and grain-filling (Prasad *et al.*, 2015; Wu *et al.*, 2016, 2017). Specifically, high day-time temperature stress during panicle initiation, gametogenesis and flowering in wheat can drastically affect grain number while the same during grain-filling can significantly reduce grain weight (Bergkamp *et al.*, 2018; Balla *et al*., 2019).

Several analyses have revealed that the average minimum temperature (night-time low temperature) is increasing at a faster rate than the average maximum temperature (day-time high temperature) in different geographies around the world (Easterling *et al*., 1997; Houghton *et al*.,

2001; Vose *et al.*, 2005; Davy *et al.*, 2017). High night-time temperature (HNT) stress has been shown to be detrimental to yield in many different crops including rice (*Oryza sativa* L.) (Shi *et al*., 2016; Bahuguna *et al.*, 2017; Bheemanahalli *et al.*, 2021), barley (*Hordeum vulgare* L.) (Garcia *et al.*, 2015, 2016), soybean (*Glycine max* L.) (Taiyu *et al.*, 2020), and cotton (*Gossypium arboreum* L.) (Loka and Oosterhuis, 2010).

Based on the quantification of the negative impact of HNT on field-grown rice by Peng *et al.* (2004), efforts to determine impact of HNT on wheat were initiated using controlled environment growth chambers (Prasad *et al.*, 2008; Narayanan *et al.*, 2015). Explorations then moved to field-based experiments using smaller and readily movable heat chambers (Garcia *et al*., 2015, 2016). Eventually, larger field-based facilities and methods were developed to phenotype for HNT stress impact during grain-filling in genetically diverse genotypes (Hein *et al.*, 2019, 2020; Impa *et al.*, 2021). These studies revealed sensitive growth stages when HNT begins to affect wheat, evaluated changes in grain protein, starch, and lipid accumulation, and quantified changes to carbon balance and source-sink metabolic profiles (Prasad *et al*., 2008; Narayanan *et al.*, 2016; Impa *et al*., 2019, 2020; Hein *et al.*, 2020). However, the dynamics related to grain macro- and micro-nutrient composition have not been evaluated.

Therefore, the study consisted of 12 winter wheat genotypes exposed to HNT stress throughout the grain-filling period using a custom-built field-based infrastructure to: (i) determine the changes in grain micro- and macro-nutrient composition in field-grown wheat exposed to HNT stress and (ii) ascertain the impact of HNT during grain-filling on yield-related parameters.

Materials and methods

Heat tent structure

Three heat tent structures were utilized to increase night-time temperatures throughout the grain-filling period while also maintaining the ability to allow for ambient conditions during the day. The heat tents were 7.2 m (length) x 5.4 m (width) x 3.0 m (height) in dimension. The structures were enclosed with 6 mm polyethylene greenhouse film. A top vent at the apex of the roof covering the entire length of the heat tent allowed the tent to maintain ambient temperatures during the day. Sidewall roll-up ventilation was also installed to allow maximum air-flow through the tent during the daytime. By rolling up the sidewalls and opening the vent simultaneously, ambient air could enter through the sidewalls, while hotter air was drawn out through the top vent (for additional details see Hein *et al.*, 2019).

Heating system

A heating system was installed to increase the overnight temperatures within the tents. The system consisted of a 5,000-watt electrical heater, a 15,000 BTU h^{-1} propane tank top heater on its medium setting, a single 75-watt box fan, and a Raspberry Pi system to control the electric heating unit (Appendix C Figure - 1). All electrical components were powered *via* a diesel electric generator and were hard-wired to the generator using 8/2 and 10/2 AWG UF-B cable with a ground. The Raspberry Pi system monitored the outside ambient temperature as well as the interior temperature with wired sensors. The system was programmed to increase the interior temperature by 4 °C as compared to the ambient temperature. This allowed the tent to impose a continuous and uniform heat stress while adjusting the temperature set-point in relation to the ambient temperature. The Raspberry Pi system used a solid-state relay, 24VAC adapter, and a 240V relay to turn on and off the electric heater depending on the temperatures within and

outside the tent (Appendix C Figure - 1). For a complete and detailed write-up on the heat tent and Raspberry Pi system and the different components that make up this facility, the readers are directed to Hein *et al.* (2019).

Crop management and stress treatment

The experiment was conducted at the Kansas State Agronomy North Research Farm (39°11′N, 96°35′W). The soil type is Smolan silt loam which comprises of silt loam from 0 to 15 cm and then transitions to a silty clay loam from 15 cm and 46 cm. Twelve genotypes of winter wheat were sown on October 17th, 2017 in replicate plots which were one meter long and consisted of six rows with 0.19 m spacing via a tractor and research plot grain drill. The 12 genotypes included entries with established contrasting HNT responses (Tascosa and Tx86A5606), prominent local cultivars (Everest, Larry, SY-Monument, WB 4458 and WB-Cedar), and breeding lines (Jagger X060724, KS070736 K-1, KS070729 K-26, KS070717 M-1 and P1 X060725). Details related to the significance of these genotypes can be obtained from Bergkamp *et al.* (2018) and Impa *et al*. (2019).

The plots were given a green-up nitrogen application at the rate of 45 kg N ha^{-1} (Urea ammonium nitrate solution) on February 17th, 2018 and were irrigated throughout the vegetative and flowering stages through rainfall. During stress imposition, all plots were irrigated manually as there were only three precipitation events during the grain-filling period. HNT stress imposition began 10 days after 50% flowering and continued until physiological maturity. All genotypes reached 50% flowering within four days after the initial genotype had reached 50% flowering, indicating narrow phenological differences among the tested genotypes. The experiment was conducted with three replications, with three heat tents for stress and three open-air plots for control. The average overnight minimum temperature was 19 °C with an average

daytime maximum temperature of 36 °C. Though the target stress was 4 °C, genotypes were exposed to an average increase of 3.2 °C night-time temperature compared to the ambient (Hein *et al.,* 2019). The heat tents were also able to stay within 1 ^{o}C of ambient daytime conditions throughout the stress period indicating highly comparable daytime conditions for both control and stress plots.

Observations

When the replicate plots reached physiological maturity, five individual plants were harvested from the two center rows of the plots. The spikes were separated from the stems and were dried for 96 hours at 40 °C while the stems and leaves were dried for 168 hours at 60 °C. The spikes were weighed, hand threshed, and yield per plant and yield components (200 grain weight, total spike number, spike weight and grain number per plant) were recorded. The dried biomass (shoot weight) was weighed, and this was added with the spike weight without grains to obtain total biomass. The total biomass along with grain yield, was used to calculate harvest index.

To quantify grain starch content, grain samples were ground, and concentration was measured using a total starch (AA/AMG) assay kit and the concentration was multiplied by the sample grain weight to obtain grain starch content. Whole grain samples were analyzed at the Kansas State Soil Testing Lab (Manhattan, KS, USA) in which a LECO TruSpec CN combustion analyzer obtained nitrogen concentration, and a Nitric Perchloric digest was used to measure Ca, Mg, Zn, Fe, Cu, Mn, S, K, and P concentrations. The nitrogen concentration was multiplied by 5.7 to obtain the grain protein concentration and multiplied by the sample grain weight to obtain protein content (Breese, 1931). The nutrient concentrations were then multiplied by the average grain weight of the genotype in both control and HNT treatments to obtain nutrient content per

plant. To allow for an unbiased comparison of findings across studies, the percent change of each parameter was divided by 3.2 to obtain trait response per °C increase in night temperature.

Statistical analysis

Two-way analysis of variance (ANOVA) was performed for all the measured parameters using PROC MIXED procedure in SAS software (Version 9.4, SAS Institute). The experiment was laid out in a split-plot randomized complete block design with temperature as the main plot factor and genotype as a sub-plot factor with three replications each for control and HNT treatments (3 independent field-based tents).

Results

Yield and yield components

Except for grain yield per plant, 200 grain weight and harvest index, none of the other yield-related components, including total biomass, shoot weight, spike number, spike weight and grain number per plant, were significantly affected by HNT or genotype x treatment interaction (Table 4-1).

200 Grain weight

On exposure to HNT, 200 grain weight was reduced by 1.9% per °C increase in night-time temperature, with a 6.1% overall reduction across genotypes (Figure 1, Appendix C Table - 1). 200 grain weight varied significantly for treatment, genotype, and their interaction effect (Table 4-1). KS070729 K-26 had the largest reduction (-14%) in 200 grain weight or a 4.3% reduction per °C increase in HNT (Figure 4-2A), with KS070736 K-1 being the most resilient genotype. Among the 12, only two genotypes (KS070736 K-1 [+9.1%] and WB 4458 [+0.8%]) did not record a reduction in 200 grain weight (Figure 4-2A, Appendix C Table - 1).

Grain yield per plant

HNT stress treatment had a significant effect on yield, but genotype and temperature x genotype interaction were not significant (Table 4-1). Average grain yield was reduced by 9.9% among the genotypes with a 3.1% loss per °C increase in night-time temperature (Figure 4-1, Appendix C Table - 1). Among the genotypes, Larry was highly sensitive to HNT, recording a 22% reduction in yield under HNT compared to control with a 6.8% decrease in yield per °C increase (Figure 4-2B). KS070736 K-1 was the most tolerant genotype under HNT stress and recorded an increase in yield by 12.1% under HNT compared to control (Figure 4-2B, Appendix C Table - 1).

Seed composition

Starch and protein content

The average starch content was reduced from 2.8 g plant^{-1} to 2.5 g plant^{-1} or a 2.5% reduction per °C increase in HNT, however this reduction was not significant (Figure 4-1; Appendix C Table - 2). Protein content per plant had a significant treatment and genotype effect but not with their interaction (Table 4-2). On average, the protein content per plant across the 12 genotypes was reduced by 3.6% per °C increase in HNT (Figure 4-1). All the genotypes recorded a reduction in protein content under HNT compared to control, except for KS070736 K-1, which had an increase of 11.2% (Appendix C Table - 2). WB 4458 had the largest reduction (-20.8%) in protein content under HNT compared to control.

Grain primary and secondary macronutrient content

Identical to protein content, total nitrogen was significantly affected by treatment and genotype but not their interaction. Phosphorus was not significantly affected by treatment, genotype and their interaction effect, while potassium content varied significantly only with genotype (Table 4-2).

Calcium, magnesium and sulfur are considered as secondary macronutrients for normal growth and development. Calcium content per plant varied significantly between treatments and was reduced by 12.4% under HNT compared to control (Table 4-2). This equated to a 3.9% reduction per °C increase in HNT (Figure 4-1). Magnesium content was also significantly affected by HNT and recorded a nearly 3% reduction per °C increase in night temperature. Sulfate-sulfur (SO_4-S) content was significantly affected by treatment and also genotype but not their interaction. HNT stress reduced sulfate-sulfur content by 3.8% per °C increase in HNT (Figure 4-1, Table 4-2, Appendix C Table - 2).

Grain micronutrient content

Among the micronutrients, grain Cu, Mn and Zn contents were significantly affected by treatment, with all the micronutrients recording a reduction in content under HNT compared to control (Table 4-2). On average, genotypes exhibited 11.9%, 11.6% and 10.5% reduction in grain Cu, Mn and Zn contents, respectively, under HNT compared to control (Table 4-2, Appendix C Table - 2). All the four micronutrients varied significantly among genotypes, but none had a significant treatment x genotype effect (Table 4-2).

Correlation between yield related parameters and seed nutrient concentration

In control, 200 grain weight was not significantly correlated with any of the yield or nutrient traits (Figure 4-3). However, when exposed HNT stress, 200 grain weight had a significantly positive correlation with seed total carbon, phosphorous, magnesium, sulfate-sulfur, manganese and zinc (Figure 4-3). In control conditions, total biomass had a statistically positive correlation with seed total carbon, however under HNT stress this correlation was severely reduced and was non-significant (Figure 4-3). Grain number, grain weight, and biomass were significantly

correlated amongst themselves under both the temperature treatments with a stronger correlation under HNT (Figure 4-3).

Starch concentration was negatively correlated with all grain nutrients measured under control conditions with a significant negative correlation with N, Mg, SO_4-S, Cu and Zn (Figure 4-3). Similarly, under HNT, starch exhibited a significant negative correlation with grain N, C, SO_4-S, Cu, Mn and Zn (Figure 4-3). Grain N or protein had significant positive correlation with all the measured macro and micronutrients except Fe under control. Whereas, on exposure to HNT, grain protein recorded a significant positive correlation with only Mg, SO_4-S, Cu, Mn and Zn (Figure 4-3).

Discussion

High night-time temperatures during grain-filling have a significant and direct impact on yield loss in winter wheat (Garcia *et al.*, 2016, Impa *et al.*, 2020a). This yield loss is realized through a significant reduction in grain weight, which is the major factor leading to HNT induced yield reduction when stress coincides with the grain-filling period. HNT induced reduction in grain weight has been shown to be the result of shortened grain-filling duration (Garcia *et al.*, 2016) and alterations in plant's carbon balance due to enhanced night respiration under HNT stress (Impa *et al.*, 2019).

Grain protein levels are positively associated with micronutrients

In the present study, protein concentration of wheat grains was reduced under HNT and similar results were noticed with high day temperature stress (Aiqing *et al*., 2018, Appendix C Table - 3). However, under the control environmental conditions, protein deposition in wheat grains exposed to HNT either remained unaffected or increased compared to control (Impa *et al.*, 2020).

A higher intensity of HNT stress in chambers, leading to significant reduction in starch levels, provides an additional opportunity for protein accumulation (Impa *et al.*, 2020), while a similar distinct difference was not seen under field conditions due to moderate stress levels.

Grain protein can be found in the endosperm as gluten or throughout the seed as storage proteins, which account for roughly 50% of the total protein in mature cereal grains (Kent, 1966; Shewry & Halford, 2001). The positive correlation between protein and micronutrients, especially metallic elements, can be traced to spherical storage vacuoles called globoids. Globoids in wheat contain roughly 40% phytate, 46% protein, 10% moisture, and the elements K, Mg, Ca, Zn, Fe, Cu, Mn, Na, S, and B (Madsen & Brinch-Pedersen, 2020). Phytate is the major source of phosphorous for the seed and can form complexes with metal cations to allow for the storage of critical nutrients for the seedling to utilize upon germination (Madsen & Brinch-Pedersen, 2020). This inter-connectedness between storage proteins, phytate, and elemental cations causes a positive correlation in which the seed's ability to store nutrients is significantly correlated to the protein content of the seed.

Global effects due to reduced nutritional value

This significant positive correlation between grain protein and macro/micronutrients emphasizes the importance of maintaining or improving protein content in wheat, to enhance the nutritive value of wheat even under future warmer scenarios. Cereals, such as wheat, rice and maize, provide as much as 60% of the daily caloric intake in developing countries (FAO, 2018; Ritchie and Roser, 2018). The reduction in micronutrients in a diet can result in a deficiency which can cause disturbances in mental and physical development, immune competence, as well as increasing the severity of infectious diseases (Gibson & Hotz, 2002; Black *et al.*, 2013). In order to combat micronutrient deficiencies, many cereal products are fortified with iron, zinc, or

other micronutrients, however this practice is not mandatory and there are still regions throughout the world in which this does not take place and their populations are at risk for malnutrition (Cardoso *et al.*, 2019). It is for these reasons that the negative effects due to HNT stress on the quality and micronutrient concentration of wheat will disproportionately affect the nutritional health of women, children, and those living in third-world countries where the practice of product fortification is not mandatory.

Conclusions

The imposition of a 3.2 °C HNT stress significantly reduced grain yield, 200 grain weight, and harvest index. HNT stress also reduced starch and protein content, however, starch and protein are differently correlated with grain micronutrients. While increased accumulation of starch increases individual seed weight, it is negatively correlated with grain micronutrient composition. Protein, conversely, was found to be positively correlated with grain micronutrient levels, indicating the relevance of maintaining higher protein levels as a target in wheat improvement programs. Wheat varieties with improved post flowering carbon balance (photosynthesis/respiration) accompanied with higher grain protein levels are required to meet the caloric and nutritional demand from a growing population under changing climate.

References

Alexandratos, N., & Bruinsma, J., 2012. World agriculture towards 2030/2050: the 2012 revision. ESA Working paper No. 12-03. Rome, FAO.

Bahuguna, R., Solis, C., Shi, W., Jagadish, S.V.K., 2017. Post-flowering night respiration and altered sink activity account for high night temperature-induced grain yield and quality loss in rice (Oryza sativa L.). Physiologia Plantarum 159, 59-73. https://www.doi.org/10.1111/ppl.12485

Balla, K., Karsai, I., Bónis, P., Kiss, T., Berki, Z., Horvath, A., Mayer, M., Bencze, S., 2019. Heat stress responses in a large set of winter wheat cultivars (Triticum aestivum L.) depend on the timing and duration of stress. PLOS ONE 14, e0222639. https://www.doi.org/10.1371/journal.pone.0222639

Beckles, D.M., Thitisaksakul, M., 2014. How environmental stress affects starch composition and functionality in cereal endosperm. Starch 66, 58-71. https://www.doi.org/10.1002/star.201300212

Bergkamp, B., Impa, S.M., Asebedo, A.R., Fritz, A.K., Jagadish, S.V.K., 2018. Prominent winter wheat varieties response to post flowering heat stress under controlled chambers and field-based heat tents. Field Crops Researchh 222, 143-52. https://www.doi.org/10.1016/j.fcr.2018.03.009

Black, R.E., Victora, C.G., Walker, S.P., Bhutta, Z.A., Christian, P., De Onis, M., Ezzati, M., 2013. Maternal and child undernutrition and overweight in low-income and middle-income countries. The Lancet 382, 427-451. https://www.doi.org/10.1016/S0140-6736(13)60937-X

Breese, J.D., 1931. Factors for converting percentages of nitrogen in foods and feeds into percentages of proteins. Washington, D.C., U.S. Department of Agriculture. https://www.ars.usda.gov/ARSUserFiles/80400525/Data/Classics/cir183.pdf

Cardoso, R.V.C., Fernandes, A., Gonzalez-Paramas, A.M., Barros, L., Ferreira, I.C.F.R., 2019. Flour fortification for nutritional and health improvement: A review. Food Research International 125, 108576. https://www.doi.org/10.1016/j.foodres.2019.108576

Davy, R., Esau, I., Chernokulsky, A., Outten, S., Zilitinkevich, S., 2017. Diurnal asymmetry to the observed global warming. International Journal of Climatology, 37, 79–93. https://www.doi.org/10.1002/joc.4688

Easterling, D., Horton, B., Jones, P.D., Peterson, T.C., Karl, T.R., Parker, D.E., Salinger, M.J., Razuvayev, V., Plummer, N., Jamason, P., Folland, C., 1997. Maximum and minimum temperature trends for the globe. Science 277, 364-367. https://www.doi.org/10.1126/science.277.5324.364

Food and Agriculture Organization of the United Nations, 2018. FAO Crops Database: New Food Balances. Accessed 10 May 2021. http://www.fao.org/faostat/en/#data/FBS.

Food and Agriculture Organization of the United Nations, 2021. FAO Crops Database: Annual Population. Accessed 10 May 2021. http://www.fao.org/faostat/en/#data/OA.

Garcia, G., Dreccer, M.F., Miralles, D.J., Serrago, R.A., 2015. High night temperatures during grain number determination reduce wheat and barley grain yield: a field study. Global Change Biology 21, 4153-4164. https://www.doi.org/10.1111/gcb.13009

Garcia, G.A., Serrago, R.A., Dreccer, M.F., Miralles, D.J., 2016. Post-anthesis warm nights reduce grain weight in field-grown wheat and barley grain yield: a field study. Field Crops Research 195, 50–59. https://www.doi.org/10.1016/j.fcr.2016.06.002

Gibson, R.S., Hotz, C., 2002. Dietary diversification/modification strategies to enhance micronutrient content and bioavailability of diets in developing countries. British Journal of Nutrition 85, 159-166. https://www.doi.org/10.1079/BJN2001309

Golba, J., Studnicki, M., Gozdowski, D., Madry, W., Rozbicki, J., 2018. Influence of genotype, crop management, and environment on winter wheat grain yield determination based on components of yield. Crop Science 58, 660-669. https://www.doi.org/10.2135/cropsci2017.07.0425

Hein, N.T., Wagner, D., Bheemanahalli, R., Sebela, D., Bustamante, C., Chiluwal, A., Neilsen, M.L., Jagadish, S.V.K., 2019. Integrating field-based heat tents and cyber-physical system technology to phenotype high night-time temperature impact on winter wheat. Plant Methods 15, 41. https://www.doi.org/10.1186/s13007-019-0424-x

Hein, N.T., Bheemanahalli, R., Wagner, D., Vennapusa, A., Bustamante, C., Ostmeyer, T., Pokharel, M., Chiluwal, A., Fu, J., Srikanthan, D.S., Neilsen, M.L., Jagadish, S.V.K., 2020. Improved cyber-physical system captured post-flowering high night temperature impact on yield and quality of field grown wheat. Scientific Reports 10, 22213. https://www.doi.org/10.1038/s41598-020-79179-0

Hurkman, W.J., Wood, D.F., 2011. High temperature during grain fill alters the morphology of protein and starch deposits in the starch endosperm cells of developing wheat (Triticum aestivum L.) grain. Journal of Agricultural and Food Chemistry 59, 4938-4946. https://www.doi.org/10.1021/jf102962t

Houghton, J.T., Ding, Y., Griggs, D.J., Nouger, M., Van der Linden, P.J., Xiaosu, D., 2001. Climate change 2001: The scientific basis. Cambridge: Cambridge University Press; p. 944.

IDRC: Facts & figures on food and biodiversity. 2010. International Development Research Centre. Accessed July 29, 2021. https://www.idrc.ca/en/research-in-action/facts-figures-food-and-biodiversity.

Impa, S.M., Sunoj, J., Krassovskaya, I., Bheemanahalli, R., Obata, T., Jagadish, S.V.K., 2019. Carbon balance and source-sink metabolic changes in winter wheat exposed to high night-time temperature. Plant, Cell & Environment 42, 1233-1246. https://www.doi.org/10.1111/pce.13488

Impa, S.M., Vennapusa, A.R., Bheemanahalli, R., Sebela, D., Boyle, D., Walia, H., Jagadish, S.V.K., 2020. High night temperature induced changes in grain starch metabolism alters starch, protein, and lipid accumulation in winter wheat. Plant, Cell & Environment 43, 431–447. https://www.doi.org/10.1111/pce.13671

Impa, S.M., Bheemanahalli, R., Hein, N.T., Sandhu, J., Prasad, P.V.V., Walia, H., Jagadish, S.V.K., 2021. High night temperature effects on wheat and rice: current status and way forward. Plant, Cell & Environment 44, 2049 – 2065. https://www.doi.org/10.1111/pce.14028

International Food Policy Research Institute (IFPRI), 2012. Global food policy report. 2013. Washington, D.C.: International Food Policy Research Institute. http://www.doi.org/10.2499/9780896295537

IPCC. 2019. Climate Change and Land: an IPCC special report on climate change, desertification, land degradation, sustainable land management, food security, and greenhouse gas fluxes in terrestrial ecosystems Shukla, P.R., Skea, J., Calvo Buendia, E., *et al.*, (eds.). In press.

IPCC, 2021. Summary for policymakers. In V. Masson-Delmott, P. Zhai, A. Pirani, S.L. Connors, *et al.* (eds.). Climate Change 2021: The Physical Science Basis. Contribution of working Group 1 to the Sixth Assessment Report of the Intergovernmental Panel of Climate Change. Cambridge University Press. In Press.

Jiang, L., Phillips, T., Hamm, C.A., Drozdowicz, Y.M., Rea, P.A., Maeshima, M., Rogers, S.W., Rogers, C., 2001. The protein storage vacuole: a unique compound organelle. Journal of Cell Biology 155, 991-1002. https://www.doi.org/10.1083/jcb.200107012

Keeling, P.L., Bacon, P.J., Holt, D.C., 1993. Elevated temperature reduces starch deposition in wheat endosperm by reducing the activity of soluble starch synthase. Planta 191, 342-348. https://www.doi.org/10.1007/BF00195691

Kent, N.L., 1966. Subaleurone endosperm cells of high protein content. Cereal Chemistry 43, 585-601.

Madsen, C.K., Brinch-Pedersen, H., 2020. Globoids and phytase: The mineral storage and release system in seeds. International Journal of Molecular Sciences 21, 7519. https://www.doi.org/10.3390/ijms21207519

Narayanan, S., Prasad, P.V.V., Fritz, A.K., Boyle, D.L., Gill, B.S., 2015. Impact of high night-time and high daytime temperature stress on winter wheat. Journal of Agronomy and Crop Science 201, 206-218. https://www.doi.org/10.1111/jac.12101

Narayanan, S., Tamura, P.J., Roth, M.R., Prasad, P.V., Welti, R., 2016. Wheat leaf lipids during heat stress: I. High day and night temperatures result in major lipid alterations. Plant, Cell & Environment 39, 787-803. https://www.doi.org/10.1111/pce.12649

OECD/FAO, 2018. OECD-FAO Agricultural Outlook 2018-2027. OECD Publishing, Paris/FAO, Rome. https://www.doi.org/10.1787/agr_outlook-2018-en

Peng, S., Huang, J., Sheehy, J.E., Lazza, R.C., Visperas, R.M., Zhong, X., Centeno, G.S., Khush, G.S., Cassman, K.G., 2004. Rice yields decline with higher night temperature from global warming. Proceedings of the National Academy of Sciences of the United States of America 101, 9971-75. https://www.doi.org/10.1073/pnas.0403720101

Prasad, P.V.V., Pisipati, S.R., Bukovnik, U., Fritz, A.K., 2008. Impact of nighttime temperature on physiology and growth of spring wheat. Crop Science 48, 2372–2380. https://www.doi.org/10.2135/cropsci2007.12.0717

Prasad, P., Djanaguiraman, M., Perumal, R., Ciampitti, I.A., 2015. Impact of high temperature stress on floret fertility and individual grain weight of grain sorghum: sensitive stages and thresholds for temperature and duration. Frontiers in Plant Science 6, 820. https://www.doi.org/10.3389/fpls.2015.00820

Ritchie, H., Roser, M., 2018. Diet Composition. Accessed 10 May 2021. https://www.ourworldinadata.org/diet-compositions

Shewry, P.R., Halford, N.G., 2001. Cereal seed storage proteins: structures, properties and role in grain utilization. Journal of Experimental Botany 53, 947-958. https://www.doi.org/10.1093/jexbot/53.370.947

Shi, W., Yin, X., Struik, P., Xie, F., Schmidt, R., Jagadish, S.V.K., 2016. Grain yield and quality responses of tropical hybrid rice to high night-time temperature. Field Crops Research 190, 18-25. https://www.doi.org/10.1016/j.fcr.2015.10.006

Taiyu, L., Yuki, O., Yuichi, N., Tatsuhiko, S., 2020. The influence of high night temperature on yield and physiological attributes of Soybean cv. Fukuyutaka, Plant Production Science 24, 267-278. https://www.doi.org/10.1080/1343943X.2020.1842215

Vose, R.S., Easterling, D.R., Gleason, B., 2005. Maximum and minimum temperature trends for the globe: An update through 2004. Geophysical Research Letters 32, L23822. https://www.doi.org/10.1029/2005GL024379

Wu, C., Cui, K., Wang, W., Li, Q., Fahad, S., Hu, Q., Huang, J., Nie, L., Peng, S., 2016. Heat-induced phytohormone changes are associated with disrupted early reproductive development and reduced yield in rice. Scientific Reports 6, 34978. https://www.doi.org/10.1038/srep34978

Wu, C., Cui, K., Wang, W., Li, Q., Fahad, S., Hu, Q., Huang, J., Nie, L., Mohapatra, P.K., Peng, S., 2017. Heat-induced cytokinin transportation and degradation are associated with reduced panicle cytokinin expression and fewer spikelets per panicle in rice. Frontiers in Plant Science 8, 371. https://www.doi.org/10.3389/fpls.2017.00371

Figures

Figure 4-1 Percent change in agronomic, grain quality and nutrient parameters.

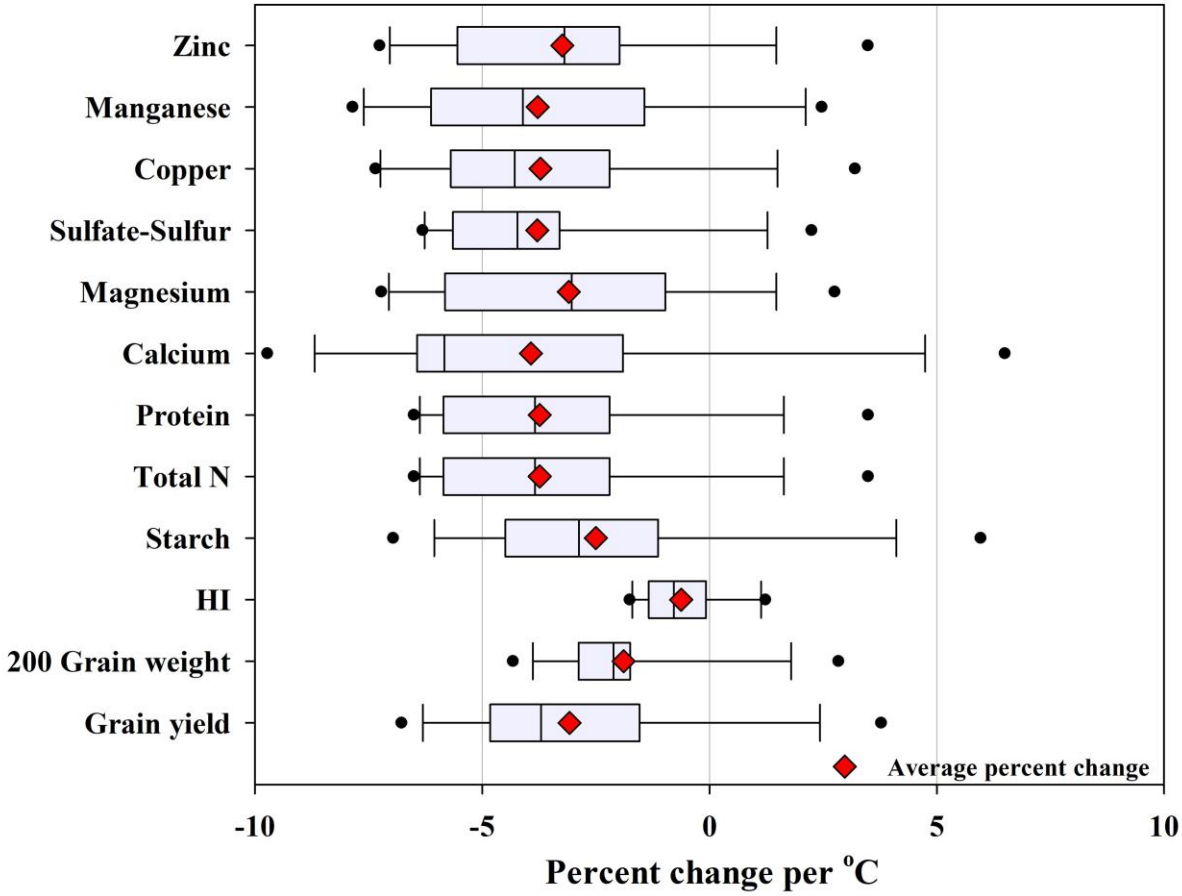

Percent change in agronomic, grain quality and nutrient parameters (grain yield, 200 grain weight, harvest index (HI), starch, total N, protein, calcium, magnesium, sulfate-sulfur, copper, manganese, and zinc) per ℃ increase in night temperature. Red diamond indicates average percent change, left edge of the box represents 25th percentile, right edge of the box represents 75th percentile, line within the box represents median, exterior lines represent the minimum (25% quartile – [interquartile range (IQR) * 1.5]) and maximum (75% quartile + [IQR * 1.5]), and black dots represent outliers. Average percentage change – indicates the change averaged across all 12 genotypes.

Figure 4-2 Response of 200 grain weight and grain yield to HNT stress

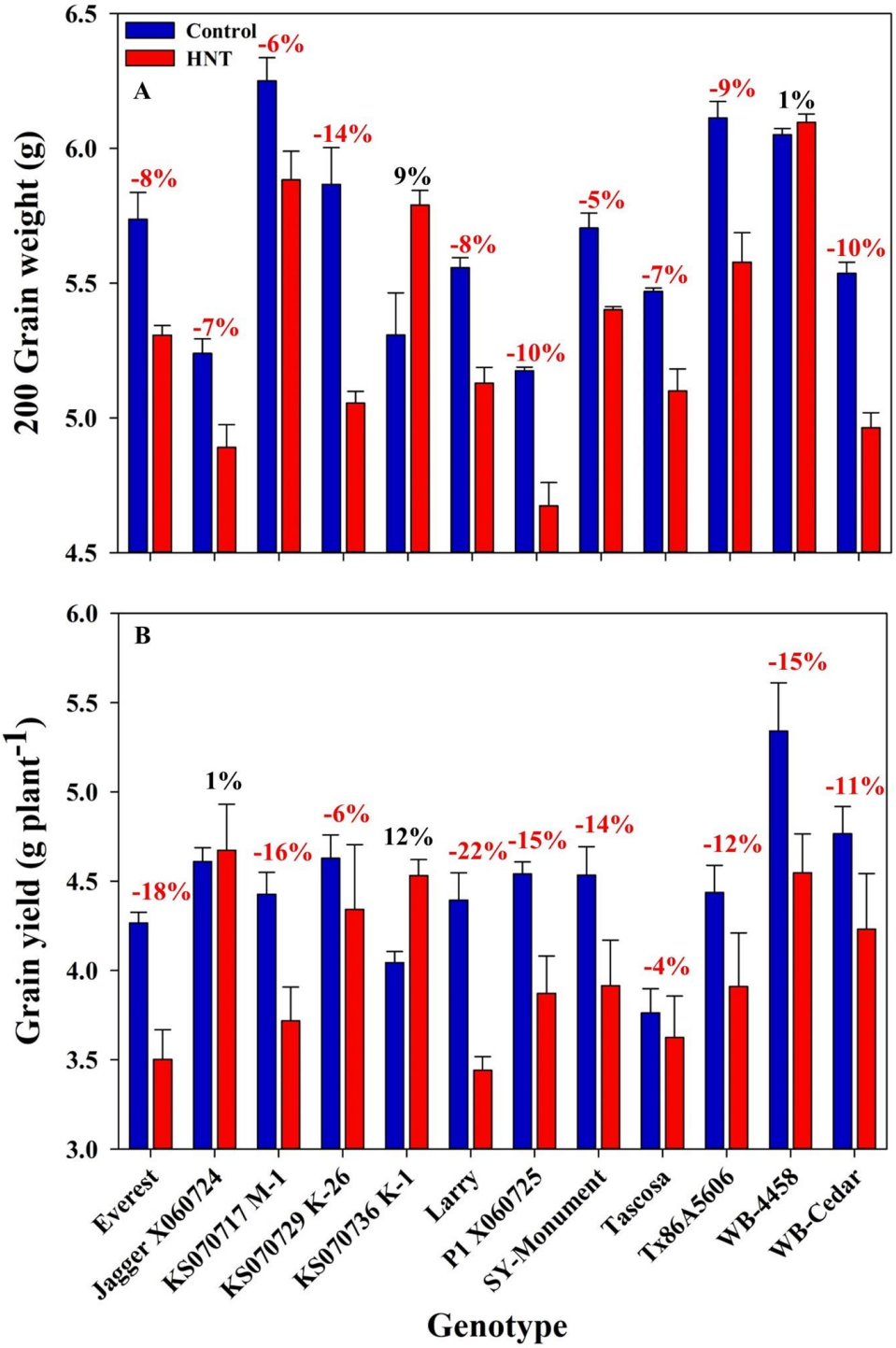

Response of 200 grain weight (A) and grain yield (B) to HNT stress. Numbers above bars indicate total percentage change as compared to control with a red and black colors indicate reduction and increase, respectively.

Figure 4-3 Heat map of correlations between yield parameters and grain quality and nutrient concentrations.

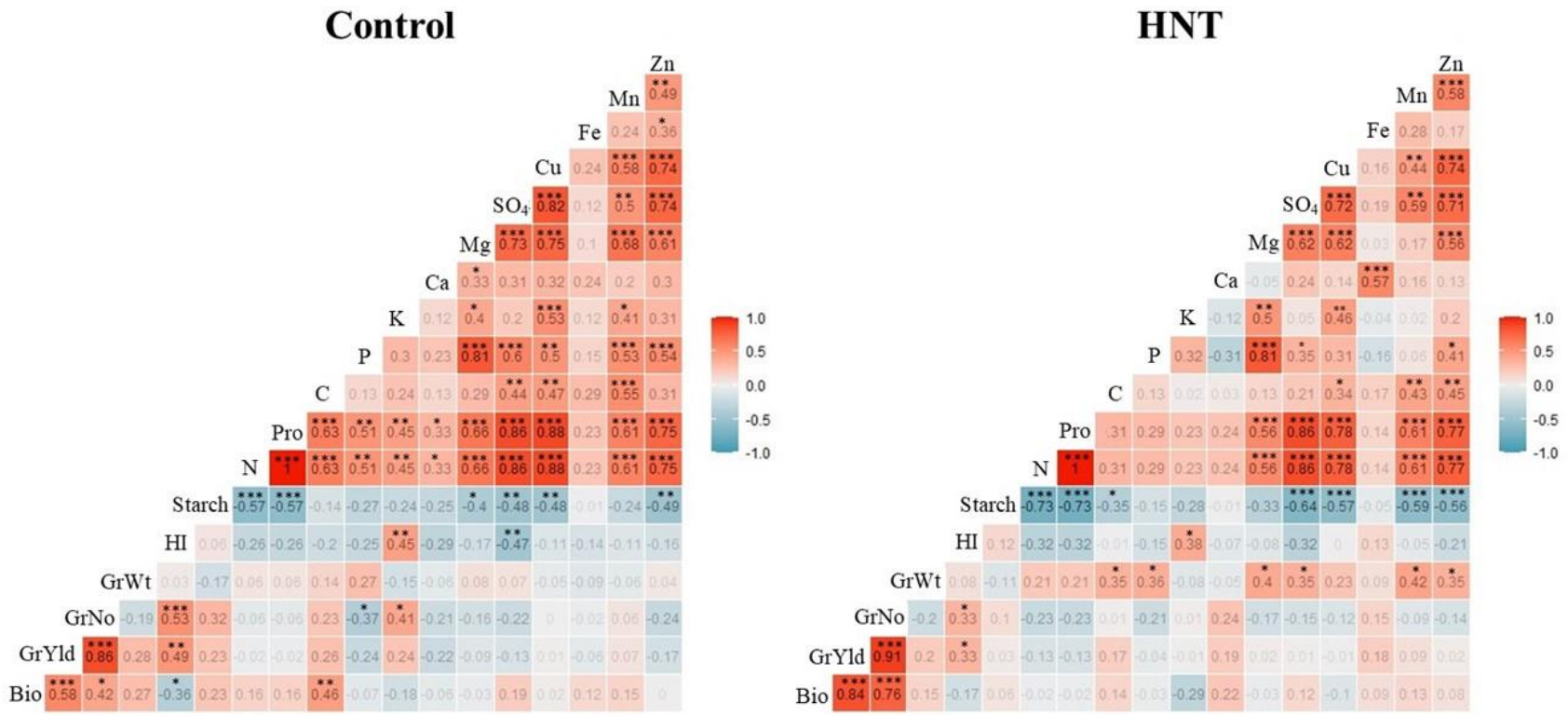

Red cells indicate positive correlation and blue cells indicate negative correlation. Darker shaded cells indicate the strength of the correlation while more transparent cells indicate a weaker correlation. Statistically significant correlations at $p < 0.05$, $p < 0.01$, and $p < 0.001$ are indicated by *, **, and ***, respectively. Bio: biomass, GrYld: grain yield, GrNo: grain number, GrWt: 200 grain weight, HI: harvest index, Pro: protein.

Tables

Table 4-1 Significance of treatment (T), genotype (G) and T x G interaction on agronomic parameters.

Trait	Variables			Mean	
	Treatment	**Genotype**	**TxG**	**Control**	**HNT**
Total biomass (g plant^{-1})	0.104	**0.019**	0.934	5.5^{a}	5.1^{a}
Shoot weight (g plant^{-1})	0.179	**0.008**	0.925	3.6^{a}	3.4^{a}
Spike number (plant^{-1})	0.329	**<0.001**	0.687	4.9^{a}	4.8^{a}
Spike weight (g plant^{-1})	0.061	0.561	0.925	6.4^{a}	5.7^{a}
Grain number (plant^{-1})	0.459	**0.047**	0.917	157.7^{a}	151.7^{a}
Grain yield (g plant^{-1})	**0.014**	0.25	0.919	**4.5^{a}**	**4.0^{b}**
200 grain weight (g)	**0.049**	**<0.001**	**0.016**	**5.7^{a}**	**5.3^{b}**
Harvest index	**0.038**	**<0.001**	0.546	**0.5^{a}**	**0.4^{b}**

Significance of treatment (T), genotype (G) and T x G interaction on total biomass, shoot weight, spike number, spike weight, grain number, grain yield, 200 grain weight, and harvest index. Means were separated using Tukey's honest significant difference (HSD) test at p = 0.05. Different letters in superscripts indicate significant difference between control and HNT. HNT – High night-time temperature.

Table 4-2 Significance of treatment (T), genotype (G), and T x G interaction on seed composition.

	Variables			Mean	
Trait	**Treatment**	**Genotype**	**TxG**	**Control**	**HNT**
Starch (g plant^{-1})	0.37	0.36	0.86	2.8^{a}	2.5^{a}
Total N (mg plant^{-1})	**0.002**	**0.002**	0.81	**121.3^{a}**	**106.8^{b}**
Protein (mg plant^{-1})	**0.002**	**0.002**	0.71	**691.7^{a}**	**608.9^{b}**
Total C (g plant^{-1})	0.07	0.22	0.92	1.9^{a}	1.7^{a}
P (mg plant^{-1})	0.07	0.25	0.89	12.6^{a}	11.6^{a}
K (mg plant^{-1})	0.35	**0.007**	0.92	14.7^{a}	14.1^{a}
Ca (mg plant^{-1})	**0.05**	0.19	0.86	**2.3^{a}**	**2.0^{b}**
Mg (mg plant^{-1})	**0.02**	0.06	0.90	**6.5^{a}**	**5.9^{b}**
SO_4-S (mg plant^{-1})	**0.003**	**0.006**	0.95	**7.3^{a}**	**6.4^{b}**
Cu (µg plant^{-1})	**0.003**	**< 0.001**	0.80	**25.0^{a}**	**22.0^{b}**
Fe (µg plant^{-1})	0.25	**0.03**	0.75	258.1^{a}	239.5^{a}
Mn (µg plant^{-1})	**0.04**	**< 0.001**	0.76	**214.2^{a}**	**188.3^{b}**
Zn (µg plant^{-1})	**0.02**	**< 0.001**	0.94	**195.8^{a}**	**175.5^{b}**

Significance of treatment (T), genotype (G), and T x G interaction on seed quality and nutritional content including starch, total nitrogen (N), protein, total carbon (C), phosphorous (P), potassium (K), calcium (Ca), magnesium (Mg), sulfate-sulfur (SO_4-S), copper (Cu), iron (Fe), manganese (Mn), and zinc (Zn). Means were separated using Tukey's honest significant difference (HSD) test at $p = 0.05$. Different letters in superscripts indicate significant difference between control and HNT.

Chapter 5 - Post-flowering high night-time temperature stress impact on physiology and starch metabolism in field-grown maize

Abstract

Due to asymmetric warming, the global average daily minimum temperatures are increasing at a quicker pace than the average daily maximum temperatures. This increased night-time warming is imposing stress on crops and is predicted to increase in severity impacting global food production. Limited research has been conducted on the physiological and genomic response of cereals to high night-time temperature (HNT) stress, with the majority of this research focused on wheat (*Triticum aestivum* L.) and rice (*Oryza sativa* L.). Recently, research into the effects of HNT stress in maize (*Zea mays* L.) has increased but is mostly restricted to controlled environment chambers or greenhouses.

This experiment focuses on elucidating the physiological and transcriptional response to HNT stress in 12 region-specific commercial hybrids using novel field-based infrastructure. As such, our experimental objectives were to (i) impose an accurate and uniformly distributed post-flowering high night-time temperature stress of +4.0 °C until physiological maturity, (ii) quantify the impact of HNT stress on physiological traits, yield, kernel weight, and rate of senescence, (iii) establish the impact on end-use quality of maize kernels formed under HNT stress through changes in grain macro- and micronutrients composition, and (iv) analyze the differential expression of genes involved in grain starch metabolism in a susceptible and resilient maize hybrid. The custom-built field-based infrastructure successfully imposed an accurate, consistent and uniformly distributed HNT stress of 3.8 °C throughout the grain-filling period. This high night-time temperature stress significantly reduced yield (-14%), kernel weight (-8%), and increased the rate of senescence in the lower canopy. Kernel macro- and micronutrient content

was significantly reduced with a reduction in all nutrients except calcium, copper, and manganese. HNT stress also caused significant changes to the differentially expressed starch metabolism related genes when comparing a resilient and susceptible hybrid. This research shows that HNT stress is an inexorable threat to the continued yield and quality performance in the majority of current maize hybrids, however the physiological and genomic basis for future resilience can be attained from specific hybrids currently in production.

Introduction

Abiotic stresses, such as high daytime and night-time temperatures (HDT and HNT, respectively), have been extensively studied in rice (*Oryza sativa* L.) and wheat (*Triticum aestivum* L.) (Boyer, 1982; Halford *et al.*, 2014; Bergkamp *et al.*, 2018; Mamrutha *et al.*, 2019; Sadok and Jagadish, 2020; Kumar *et al.*, 2021). Findings from these studies reveal significant negative impacts on the agronomic and physiological responses, leading to lower yield and poor grain quality. Further, it has been shown that HDT and HNT stresses are already having significant impact on total global yields and the negative trend is predicted to continue and intensify in the future (Peng *et al.*, 2004; Hatfield and Prueger, 2015; IPCC 2021). Along these lines, it has been predicted that 31% of maize (*Zea mays* L.), 16% of rice and 11% of wheat growing areas will record five or more days with temperatures higher than the critical thresholds during the reproductive stage (Gourdji *et al.*, 2013).

The effects on crop yield due to increases in daily mean temperature are not being solely or primarily driven by the increase in the average daily maximum as the average daily minimum is rising at a faster rate than the daily maximum temperature (Easterling *et al.*, 1997; Alexander *et al.*, 2006; Davy *et al.*, 2017). This was shown in a comprehensive climatological and agricultural study from 1979 to 2003, wherein average maximum temperature rose by only 0.35 °C while the average minimum temperature increased by 1.13 °C. This same study also showed that for every degree increase in average minimum temperature, rice recorded a 10% reduction in yield (Peng et al., 2004).

HNT stress can cause multiple disfunctions in plant physiological processes resulting in lower quality and yield in different crops including wheat (Garcia *et al.*, 2015; Hein *et al.*, 2019, 2020; Impa *et al.*, 2020), rice (Glaubitz *et al.*, 2015; Shi *et al.*, 2013, 2016; Bahuguna *et al.*,

2017), quinoa (*Chenopodium quinoa* Willd.) (Lesjak and Calderini, 2017) and cotton (*Gossypium hirsutum* L.) (Loka and Oosterhuis, 2010). The primary hypothesis for the physiological basis of these reductions is increased night respiration (Loka and Oosterhuis, 2010; Shi *et al.*, 2013; Bahuguna *et al.*, 2017). This hypothesis has been supported through studies directly measuring the respiration rate, as well as identifying increased intermediate metabolites of the tricarboxylic acid cycle (Loka and Oosterhuis, 2010; Glaubitz *et al.*, 2015; Bahuguna *et al.*, 2017; Impa *et al.*, 2019; Tombesi *et al.*, 2019). Increased night respiration has also been shown to not only reduce the amount of carbon assimilate available for translocation to the grain, but also reduces the 'stay-green' period or the duration of grain-filling resulting in significantly lower grain weight and grain size (Lesjak and Calderini, 2017; Impa *et al.*, 2019; Hein *et al.*, 2020). Along with the reduction in weight, grain quality can be severely diminished due to the limited availability of carbon assimilate and reduced nutrient translocation (Shi *et al.*, 2013, 2016; Bahuguna *et al.*, 2017; Hein *et al.*, 2020; Impa *et al.*, 2020).

Research into the effects of HNT stress on maize has only recently gained interest in the scientific community (Suwa *et al.*, 2010; Neiff *et al.*, 2016; Sunoj *et al.*, 2016; Wang *et al.*, 2019; Kettler *et al.*, 2022). However, these studies have either focused on increases in both HDT and HNT (Suwa *et al.*, 2010; Neiff *et al.*, 2016; Sunoj *et al.*, 2016) or were conducted in controlled environment chambers (Wang *et al.*, 2019). The extremely limited number of field-based studies conducted to assess the impacts of HNT stress in maize have either not been able to systematically control the overnight temperature, interfered with amount of incoming radiation during the daytime hours, or have utilized a single or few hybrids (Cantarero *et al.*, 1999; Niu, J. *et al.*, 2021; Kettler *et al.*, 2022).

For these reasons, our experiment was designed to understand the physiological responses impacting yield, seed quality, and expression pattern of genes involved in starch metabolism on exposure to HNT stress in 12 commercial hybrids utilizing the previously developed HNT field-based infrastructure (Hein *et al.*, 2020). Specific objectives were to (i) impose an accurate and uniformly distributed post-flowering high night-time temperature stress of +4.0 °C until physiological maturity, (ii) quantify the impact of HNT stress on physiological traits, yield, kernel weight, and rate of senescence, (iii) establish the impact on end-use quality of maize kernels formed under HNT stress through changes in grain macro- and micronutrients composition, and (iv) analyze the differentially expression of genes involved in grain starch metabolism in a susceptible and tolerant maize hybrid.

Materials and Methods

Crop Cultivation

The effects of HNT on maize were evaluated in 2021 at the Kansas State University Agronomy North Farm in Manhattan, Kansas (39°12’47.3” N, 96°35’35.0” W). The experiment consisted of 12 commercially available hybrids. These hybrids (H1-H12) were selected from four different companies with H1 and H2 from Company A, H3 through H6 from Company B, H7 from Company C, and H8 through H12 from Company D. Hybrid names or companies are not presented due to the hybrids being proprietary.

Each tent had an effective planting area of 7.9 x 12.5 m and this planting area was divided into 4 blocks of 2.4 x 12.5 m in size with 0.9 m between the plots. A row spacing of 76 cm allowed for 10 rows per block and a seed spacing of 15 cm within the rows allowed for 16 plants per row or a planting density of 86,000 seeds per hectare. Each block contained three

randomly assigned hybrids (3 hybrids x 4 blocks = 12 hybrids) with three rows per hybrid and a filler row. The filler row was either row 1 or 10 and alternated between each block.

Field soil tests analyzed by the Kansas State Soil Testing Lab (Manhattan KS, USA) showed an increased level of residual nitrogen within the 0 – 15 cm soil layer in the HNT plots as compared to the control plots (11.73 and 9.57 ppm NO_3-N, respectively) as well as in the 15 – 30 cm soil layer (17.12 and 16.5 ppm NO_3-N, respectively). To prevent nitrogen limitations within the experiment, a rate of 224.17 kg/ha of nitrogen was applied in the form of UAN-28 as well as 0.38 kg/ha of Explorer Herbicide (Syngenta; active ingredient: Mesotrione), 1.54 kg/ha of Brawl II (Tenkoz, Inc., active ingredient: S-metolachlor), and 2.94 kg/ha of Atrazine 4L (Drexel Chemical Company; active ingredient: Atrazine [2-chloro-4-ethylamino-6-isopropylamino-s-triazine]) prior to planting. The planting area and blocks were first measured and marked and then the rows were trenched to a depth of 3.8 cm using a custom made three-pronged rake to ensure exact distance and depth were maintained before seeds were planted on May 13, 2021.

All 12 hybrids reached 50% anthesis by July 22, 2021, with the average date of 50% anthesis occurring on July 18, 2021 and all hybrids reaching flowering within ±3.5 days of this date (Appendix D Figure - 1). The stress period began 3 days after all hybrids had reached 50% anthesis on July 25, 2021 (Appendix D Figure - 2). Shortly after flowering, 1.4 kg/ha of Prevathon Insecticide (FMC Ag US; active ingredient: Rynaxypry) was applied on July 28, 2021, and then again on August 18, 2021, at the same rate to control potential pests. The plots were irrigated six times during the plants life cycle (three times before stress and twice after) at a rate of 673 liters per tent or 6.8 liters/m^2. The stress period was concluded on September 2, 2021, after 39 days of stress when all hybrids had a developed black layer in the kernels at the bottom

of the cobs, indicating physiological maturity. Plants remained in the field until September 27, 2021 in order to reach appropriate moisture content for harvest.

Field Infrastructure

To apply an accurate and precise HNT stress, a custom-built field-based infrastructure was constructed. The field infrastructure consisted of six heat tents (3 HNT and 3 control), with each tent of size 9.1 x 14.6 m and 4.4 m tall (Four Season Tools, Kansas City MO, USA). The structures were purposefully built with increased height before the bottom chord of the roof trusses to allow for phenotyping different crops. The tents utilized 6 mm polyethylene plastic with a 92% light transmission rating to encapsulate the frame and contain the heat during the stress (Berry Global Plastics, Evansville IN, USA). In order to prevent the infrastructure from imposing an unintended high daytime temperature stress, the sidewalls, endwalls, and the roof plastic was attached to a motorized roll-up system which allowed for all walls and the roof to be raised to their peaks (open position) during the day. This capability to roll the plastic from over the plants allowed for complete ambient conditions throughout the day during the stress period and followed the principal that has been established in rice (Shi *et al.*, 2013; Bahuguna *et al.*, 2016).

To operate the system, a Caterpillar XQ30 electric generator (Foley Power Solutions, Topeka KS, USA) was wired to two 50-amp spider boxes which allowed for the distribution of electricity to all tents. The temperature within the HNT tents was increased using a HDB100 Hot Dawg Propane Heater (Ferguson Plumbing and Heating, Manhattan KS, USA) which has an 82% efficiency rating and outputs 82,000 BTU/hour at 781 FPM. Convection tubing was attached to the heater which ran the length of the tent with holes cut at the 12 o'clock position to allow heat to be distributed vertically in order to avoid direct heating on any of the plants. The

heater was supplied by a propane tank with an 1829.7 L capacity which was placed in front of each HNT tent. Along with the convection tubing, two 30.5 cm horizontal air flow fans (J&D Manufacturing, Eau Claire WI, USA) were installed in opposite corners above the canopy to improve air flow in all tents. To simulate the stimulation from the air flow on the plants in the HNT tents, a 45.7 cm power tube fan (Coolair, Jacksonville FL, USA), convection tubing, and horizonal air flow fans were installed in all three control tents.

Operation of the Tents and Stress Imposition

The stress conditions were controlled by a custom-built raspberry pi cyber-physical system which included a Raspberry Pi (Raspberry Pi Foundation, Cambridge, UK), six MCP9808 temperature sensors (Adafruit, New York City NY, USA) and one DS3231 Real-Time Clock (RTC) module (Adafruit) for each tent as well as a Keyes KY-019 Relay Module (Songle Relay, Yuyao City Zhejiang, China) within the stress tent's cyber-physical system to allow for control of the heater. The system was designed so that each of the six temperature sensors would take a reading every minute and these readings were logged with accurate timestamps from the RTC. The control tent's cyber-physical system would obtain its reading and wirelessly send the average temperature to the stress tents and the stress tent's cyber-physical system would compare the temperatures of the stress and control tents. If the stress tent was not 4 °C warmer than the control tent, the propane heater was turned on, and if the stress tent had achieved the previously set differential, the cyber-physical system would turn off the propane heater. For a more detailed explanation of the field-based infrastructure and the cyber-physical system and its components, please refer Hein *et al.* (2020).

The execution of the experiment began at 6:30 P.M. each night throughout the grain-filling period with the closing of the tents. All tents were closed simultaneously with the stress

tents being shut completely and the control tent's roofs being completely shut but the endwalls and sidewalls left 20 cm above the baseboard to allow for ambient air to circulate through the tent. The electric generator and the control tent's cyber-physical systems were turned on simultaneously by 7:00 P.M. and then the cyber-physical systems within the heat tents were turned on consecutively allowing the stress tents to reach the indicated temperature differential by 8:00 P.M. and starting the overnight stress period. The stress was concluded at 6:00 A.M. the following day by wirelessly collecting the data, consecutively shutting down the stress tents, and then simultaneously shutting down the electric generator and control cyber-physical systems. The sidewalls, endwalls, and roofs were raised concurrently with the shutdown procedures of the cyber-physical system and generator.

During the overnight period, the stress and control tents were monitored by an array of sensors. The cyber-physical system in each tent had six temperature sensors with a sensitivity of ± 0.25 °C, two HOBO UX 100-011 temperature/relative humidity data loggers (Onset Computer Corp., Bourne MA, USA) with a relative humidity sensitivity of ±2.5% and a temperature sensitivity of ±0.21 °C, and two HOBO UA 002-64 Pendent Data Loggers (Onset Computer Corp., Bourne MA, USA) which had a temperature sensitivity of ±0.53 °C. The cyber-physical system was only capable of logging during the overnight period as it required an external power source, however HOBO data loggers operated 24 hours a day at a lower measurement interval of 15 minutes throughout the entirety of the experiment. All sensors monitoring temperature were placed at cob level within the canopy to record the temperature and conditions in which the cobs developed.

Agronomic Observations

Yield and Yield Components

To record grain yield and yield components, a 1.83 m section (6 plants) from the central row of each hybrid was collected at harvest maturity with an 84 cm Bypass Lopper (Ace Hardware, Manhattan KS, USA) at ground level. Each plant was separated into leaves, stems, and cobs for additional analysis. After drying at 60 °C for 14 days, the cobs were weighed and then stripped of their husks and silks. The cobs were then measured for length from bottom to the top row of kernels on the cob and then marked at the 1/3 and 2/3 points. The cobs were then hand threshed separating the kernels into top, middle, and bottom third portions. These three groups of kernels were weighed and counted separately for each genotype, treatment and replicate. The weights and counts were added together to get total yield and kernel number, respectively. The total yield was then subtracted from the previously measured cob weight (with husks and silk) to obtain the cob biomass weight. This cob biomass weight was then added to the leaves and stem biomass weights to obtain total aboveground biomass. The yield, kernel number, and total biomass were used to obtain different secondary measurements such as yield per m^2, 200 kernel weight, and harvest index.

Stay-green/Rate of Senescence Observations

To observe and quantify the effective stay-green trait of individual hybrids, a SPAD 502 Plus Chlorophyll Meter (Spectrum Technologies, Inc., Aurora Il, USA) and the Fluorpen FP100 (Photon Systems Instruments, Drásov, Czech Republic), a portable PAM fluorometer, was used to measure chlorophyll fluorescence. Measurements with the SPAD and Fluorpen began 12 days after treatment (DAT) imposition and then repeated at 23 DAT and 30 DAT. In order to obtain individual leaf and average rate of senescence per plant, measurements were taken on the top third, sixth, and ninth leaves. To obtain overall leaf chlorophyll rating, measurements were

conducted at the base, middle, and tip of the leaves and then averaged. The results from the third, sixth, and ninth leaves were then averaged together for the overall plant stay-greenness.

Seed Quality

To quantify kernel starch, protein, macro-, and micronutrients, kernel samples from the middle section of the cob from all 12 hybrids were submitted to the Kansas State Soil Testing Lab (Manhattan KS, USA). The Soil Testing Lab used a LECO TruSpec CN combustion analyzer to obtain total nitrogen concentration. This nitrogen concentration was multiplied by 6.25 to obtain total protein concentration (Breese, 1931). The Soil Testing Lab then used a nitric perchloric digestion method to quantify C, P, K, Ca, Mg, S-SO_4, Cu, Fe, Mn, and Zn concentrations within the kernel. For kernel starch concentration, the same ground samples representing kernels from the middle third portion of the cobs were used with a total starch (K-TSHK) assay kit (Megazyme, Bray, Ireland). After the starch was extracted from the samples, a standard curve was developed using known glucose concentration solutions provided within the kit. The optical density of each starch sample was then determined and used against the glucose standard curve to determine the final concentration. The starch, protein, and nutrient concentrations were then multiplied by the total yield for the corresponding hybrid and treatment to obtain total starch, protein, and nutrient content.

Expression profile of genes involved in starch metabolism

The digital expression profile of starch metabolism enzymes listed in Impa *et al.* (2020) was performed. Briefly, RNA-seq datasets from heat stressed leaf and kernel tissues (10 days after silking) of maize cultivars Xianyu 335 (heat sensitive) and Zhengdan 958 (heat tolerant) were downloaded from National Center for Biotechnology Information (NCBI) SRA database (Niu, S. *et al.*, 2021; NCBI, 2022). NCBI's SRA toolkit was used to successfully retrieve the complete

datasets followed by splitting of reads file into two individual files representing paired end reads using reformat.sh script of BBMap tool (Bushnell *et al.*, 2017). FastP was used to quality filter the reads and trim any residual adapter sequences followed by FastQC analysis to check the final quality of reads (Chen *et al.*, 2018). The mRNA sequences of maize homolog of wheat starch metabolism enzymes listed in Impa *et al.* (2019) were downloaded from NCBI database and the fasta sequences are provided in Supplementary File 1. The genes used for analysis were amyloplastic-ADP- glucose pyrophosphorylase (large subunit; AM-AGPase LS), amyloplastic-ADP-glucose pyrophosphorylase (small subunit; AM-AGPase SS), fructose kinase I (FKI), granule bound starch synthase I and II (GBSSI and GBSSII, respectively), invertase, cytosolic invertase; isoamylase I, II, and III (ISAI, ISAII, and ISAIII), phosphoglucoisomerase (PGI), phosphoglucomutase I (PGMI), starch-branching enzyme I (SBEI), starch synthase I, II, and III (SSI, SSII, and SSIII, respectively), sucrose synthase (SUS), UDP-glucose pyrophosphorylase (UGPase), α-amylase and β-amylase. Seal.sh script from BBMap package was used to identify insilico expression of genes. The Log2 values of FPKM expression was plotted in form of a heat-map using MeV software (Howe *et al.*, 2010).

Based on the in-silico expression profile of starch metabolism enzymes, 10 genes (AGPase SS, GBSSI, GBSSII, ISAI, PGMI, SSIII, SUS, UGPase, α-amylase, and β-amylase) were selected for expression analysis in sensitive H12 and resilient H4 maize hybrids under control and HNT stress. qRT-PCR was performed to quantify the expression of genes related to starch metabolism enzymes. Two kernels taken from mid-portion of the cob were ground in liquid nitrogen and RNA was extracted using Trizol reagent protocol, followed by DNase1 treatment to remove DNA contamination. The quality of RNA was checked by running on 1% denaturing agarose gel and the quantity was estimated using a NanoDrop ND-1000

spectrophotometer (NanoDrop Technologies, Wilmington, DE, USA). 1µg RNA was used for first strand cDNA synthesis using an iScript cDNA synthesis kit (Bio-Rad Inc., Hercules CA, USA) following manufacturer's protocol. Primer3 was used to prepare the primers. The PCR primers used for expression analysis of starch associated genes are listed in Supplementary Table 1. qRT-PCR based expression profile was performed using an Applied Biosystems PowerUp SYBR Green Master Mix (Thermo Fisher Scientific, Waltham MA, USA) on CFX96-Touch^{TM} Real-Time PCR Detection System (Bio-Rad Inc., Hercules CA, USA). Actin and EF1α were used as endogenous control. The experiment was performed in three biological and three technical replicates and $2^{-\Delta\Delta CT}$ method was used to calculate the relative expression in comparison to control tissue of H12.

Statistical Analysis

The experimental design was a split-plot randomized complete block design with temperature as the main plot factor and genotype as the sub-plot factor with three replications (three independent field-based tents) each for control and HNT. The results were analyzed using two-way analysis of variance (ANOVA) using the PROC MIXED procedure in SAS software with a significance level of $p < 0.05$ (Version 9.4, SAS Institute).

Results

Environmental Results

Application of HNT Stress

The experimental design successfully and accurately applied a 3.81 °C elevated HNT stress as measured by the Raspberry Pi cyber-physical system temperature system array as compared to the control tents (Figure 5-1A). The control tents averaged an overnight temperature of 22.76 °C

while the HNT tents maintained an average of 26.58 °C throughout the grain-filling period. After the initiation of the Raspberry Pi cyber-physical system at 7 PM, the HNT temperature tents were able to obtain a 3.45 °C increase by 8 PM over the control tents. This differential continued to increase until 5 AM in which the average differential reached its maximum at 3.96 °C (Figure 5-1A). This increase in overnight temperature is confirmed by the HOBO 002-64 Pendent Data loggers which recorded the average increase by 4.09 °C between control and HNT tents was with the tents reaching a 3.15 °C difference by 8 PM and peaking at 4.30 °C at 5 AM (Figure 5-1A).

To measure the efficacy of the system in the imposition of uniformly distributed heat stress, the HOBO UX 100-011 sensors which were placed in randomly separated positions within the tent were compared. During the overnight stress period, the HOBO UX 100-011 within the HNT tents measured an average differential of 0.18 °C throughout the grain-filling period indicating an extremely uniform implementation of the HNT stress. The control tents averaged a 0.09 °C differential during the same time period (Appendix D Figure - 3).

To quantify the performance of the Raspberry Pi temperature sensor array, the standard deviation from the average was computed for the array for every individual measurement. The control tents maintained an extremely uniform overnight temperature and averaged a sensor standard deviation of 0.17 °C. The HNT tents had more variability due to higher temperature imposition, however, the sensor standard deviation only rose to 0.58 °C which is acceptable given the temperature sensors have a published sensitivity of ±0.25 °C (Ada, 2014).

Ambient Daytime Temperature Conditions

As the Raspberry Pi cyber-physical system only ran during the stress period, the HOBO UX 100-011 and HOBO 002-64 Pendent Data Loggers were used to quantify the effectiveness of achieving an ambient daytime condition within the tents. To evaluate the distribution of

temperatures within the tent during the daytime setting, the HOBO UX100-011 data was quantified, and it was found that the differential between the sensors inside the tents averaged 0.73 °C in the control tents and 0.67 °C in the HNT tents. These results indicate a homogenous daytime environment throughout both the control and stress tents.

A HOBO 002-64 Pendent Data Logger was placed in the open field in order to measure the ambient temperatures outside of the tents. When the pendent data loggers from within the tents are compared to the ambient field-based pendent data logger, the ambient pendent data logger averaged 0.62 °C warmer than the averaged measurements from within the tents. These results are plausible as the ambient data logger was placed in the field above the canopy while the experimental data loggers were placed at cob level within the canopy and would benefit from the reduction in temperature from the canopy's microclimate.

Relative Humidity and Vapor Pressure Deficit

High night-time temperature stress coincided with a decrease in relative humidity and an increase in vapor pressure deficit. During the stress period throughout grain-filling, relative humidity was on average 9.3% lower than the control tents (Figure 5-1B). At the initiation of stress, the relative humidity within both the control and stress tents was nearly identical (HNT: -0.82%). By 11 PM the HNT tents were 9.1% lower than the control tents and this differential achieved its maximum at 4 AM when the HNT tents were 12.4% lower than the control tents. Due to reduced relative humidity and increased temperature, the HNT tents had an increase in vapor pressure deficit (VPD) (Figure 5-1B). The HNT tents during the stress period had an average VPD 0.49 kPa higher than that of the control tents. At the initiation of the stress period, the VPD differential was only 0.26 kPa, however the differential between the two sets of tents was at its highest at 2 AM with a difference of 0.56 kPa.

The HNT tents during the non-stress period, on average, measured a relative humidity of 2.18% lower than the control tents. This difference was minimized at 2 PM when the relative humidity in the heat tents was only 1.2% lower than the control tents and maximized at 11 AM when the HNT tents were 3.1% lower. These minimal adjustments to relative humidity falls within the accuracy range of the sensor (±2.5%) and can be considered non-significant. The reduced relative humidity slightly altered VPD throughout the day with the HNT tents having on average, a VPD that is 0.12 kPa above the control tents. The difference between HNT and control tents reached its maximum at 12 PM with a 0.23 kPa increase in the HNT tents and was minimized at 3 PM when the HNT tents had a VPD that was 0.004 kPa below the control tents. In summary, the changes to relative humidity and vapor pressure deficit during the non-stress period were negligible.

Agronomic Results

Yield

High night-time temperature stress had a significant effect on total yield (g m^{-2}) at the treatment (T) and genotype (G) level while also recording significance ($p < 0.1$) at the TxG level (Table 5-1). H12 had the largest reduction out of the 12 hybrids with 28% or 7.35% lower yield per °C (Figure 5-2A). H4 and H10 were the only hybrids to record an increase in total yield with a 4.4% or 1.2% per °C increase. On average, post-flowering HNT stress significantly reduced the overall yield by 13.8% or a 3.64% decrease in yield per °C (Figure 5-2A; Appendix D Figure - 4).

HNT stress on the yield in different portions on the cob resulted in a significant reduction with treatment and genotype level in the bottom, middle, and top portions of the cob while the bottom and middle portions also recorded a significant reduction ($p < 0.1$) with TxG (Table 5-1). The distribution of the average yield reduction for the entire cob was quite equal when separated

by the bottom (-13.9%; -3.64% per °C), middle (-14.0%; -3.67% per °C), and top (-13.6%; -3.59% per °C) portions (Figure 5-2B; Appendix D Figure - 4). H12 recorded the largest yield reductions in the bottom and middle portions of the cob (-31.5% or -8.27% per °C and -28.0% or -7.34% per °C, respectively) while H2 had the largest reduction in yield at the top portion of the cob (-22.8% or -5.98% per °C) Along with recording the largest reductions in two of the three portions, H12 logged the second largest reduction in yield in the top portion of the cob (-22.4% or -5.87% per °C) (Figure 5-2B). Similar to total yield, H4 and H10 both increased in yield in the top portion of the cob (+14.6% or +3.84 per °C and +8.1% or +2.12% per °C, respectively). However, their responses to HNT stress differed in the bottom and middle portion of the cob with H4 recording a reduction at the bottom and an increase in the middle (-1.63% or -0.43% per °C and +3.6% or +0.94% per °C, respectively) while H10 recorded an increase at the bottom and a reduction in the middle (+8.6% or +2.26% per °C and -2.5% or -0.65% per °C, respectively) (Figure 5-2B).

200 Kernel Weight

The 200 kernel weight of all 12 hybrids tested in this experiment was reduced under HNT. The reductions caused by the imposition of stress was significant at the treatment and genotype but was not significant for their interaction (Table 5-1). H2 and H8 recorded the largest reductions in kernel weight by -12.4% and -11.6% or -3.25% and -3.04% per °C, respectively (Figure 5-3A). H4 had the lowest reduction amongst the tested hybrids with only a 3.5% reduction or 0.92% decrease in 200 kernel weight per °C. Overall, the 200 kernel weight of all hybrids was reduced by 8.2% on average or 2.14% per °C (Figure 5-3A; Appendix D Figure - 4).

When the spatial location of the kernels was considered, the bottom, middle and top portions of the cob had a significant reduction in kernel weight with treatment and genotype

(Table 5-1). However, 200-kernel weight only in the top portion of the cob had a significant reduction with TxG. On average, larger reductions occurred as the location of the kernels moved down from the top to the bottom of the cob. The bottom portion resulted in 10.3% reduction or 2.71% per °C, the middle portion had 7.5% or 2.37% per °C reduction in kernel weight, while the top portion recorded a 5.6% or 1.48% reduction in 200 kernel weight per °C (Figure 5-3B; Appendix D Figure - 4). All 12 hybrids recorded lower kernel weight in both the bottom and middle portions of the cob, while 10 out of 12 hybrids resulted in lower kernel weight in the top portion of the cob. H4 and H10 had an increase in kernel weight at the top portion of the cob with an increase of 16.6% or 4.36% per °C and 11.7% or 3.06% per °C, respectively (Figure 5-3B).

Harvest Index

HNT stress caused a significant reduction in harvest index at the treatment and genotype level but not their interaction (Table 5-1). Harvest index in all 12 hybrids was reduced due to HNT stress with an average 7.1% or 1.87% reduction per °C of harvest index (Figure 5-4). H12 incurred the largest reduction at 13.1% or 3.43% per °C while H4 had the lowest at 2.5% or 0.65% reduction per °C of harvest index (Figure 5-4).

Aboveground Biomass and Kernel Number

HNT stress did not have a significant effect on the aboveground biomass at the treatment and TxG levels, however, the effect was significant with genotype (Table 5-1). On average, the 12 hybrid's aboveground biomass increased by 1.76% or 0.46% per °C. The largest increase was achieved by H10 which resulted in a 31.7% or 8.31% per °C increase in biomass. The hybrid with the largest reduction in aboveground biomass was H3, which had an 8% reduction or 2.10% per °C. The imposition of HNT did not result in a significant change in the total kernel number

with treatment, genotype or their interaction (Table 5-1). On average, total kernel number was increased by 1.6% or 0.42% per °C with H1 having the largest increase (+16.3% or +4.28% per °C) and H12 having the largest reduction (-13.2% or -3.47% per °C).

Stay Green and Rate of Senescence

The effects of HNT temperature stress on the effectiveness of the stay-green trait and the rate of senescence was not significant at the T or TxG level for changes in chlorophyll fluorescence (Appendix D Table - 2). The measurement of chlorophyll fluorescence was significantly reduced at the G level at 12, 23, and 30 days after treatment. The SPAD chlorophyll content measurements did not show a significant reduction in the T, G, or TxG interactions at 12 and 23 days after treatment. However, it did show a significant difference at the G level at 30 days after treatment.

Quality Results

Starch and Protein Content

Starch content was significantly affected by high night-time temperature at the treatment and genotype level, but not their interaction (Table 5-2). On average, the total starch content was lowered from 113.33 g plant^{-1} to 101.67 g plant^{-1} which equates to 10.3% or 2.7% reduction per °C (Figure 5–5, Table 5-2). The hybrid with the largest reduction, H12, recorded a 21% reduction or 5.51% lower starch content per °C. Two of the hybrids, H4 and H10, increased in starch content when HNT was imposed resulting in an elevation of 2.5% and 2.9% or 0.66% or 0.75% per °C, respectively (Figure 5-5, Appendix D Table - 3).

HNT stress had a significant effect on protein content at the treatment, genotype and their interaction (Table 5-2). On average, the total protein content per plant was reduced under HNT (Table 5-2) leading to a 11.5% or 3.02% per °C loss in protein (Figure 5-6). H12 had the largest

reduction in protein content at 29.9% or 7.83% per °C. In contrast to this response, H4 and H10 recorded a 12.6% and 17.55% or 3.32% and 4.61% per °C, respectively, increase in protein content (Appendix D Table - 3).

Macro- and Micronutrient Content

HNT stress had differential effects on macronutrient content depending on the nutrient. Carbon content (g plant^{-1}) varied significantly at the treatment, genotype and TxG levels (Table 5-2). The average carbon content was reduced by 12% or 3.27% per °C from 81.79 g plant^{-1} to 71.59 g plant^{-1} (Figure 5-6). H12 recorded the largest reduction of 26.8% or 7.03% per °C. H4 and H10 were the only two hybrids which had an increase in carbon content with an increase of 6.9% and 6.3% or 1.80% and 1.66% per °C, respectively. HNT stress also significantly reduced magnesium content from 0.175 g plant^{-1} to 0.156 g plant^{-1} which equates to a 11% reduction or 2.88% per °C (Figure 5-6). This reduction in magnesium content was significant at the treatment and genotype level but not their interaction (Table 5-2). H12 had the greatest reduction in magnesium at 28% or 7.35% per °C while H10 recorded an increase of 20.9% or 5.48% per °C while H4 and H6 also recorded increases in magnesium content (Appendix D Table - 3).

Phosphorous, potassium, and sulfate-sulfur was also reduced due to HNT stress, but their reductions were only significant at the genotype level (Table 5-2). The average calcium content (g plant^{-1}) was increased due to HNT stress, but this increase was not significant (Table 5-2). Copper, iron, and zinc changes due to HNT stress were significant at the genotype level but not the treatment or TxG (Table 5-2). Manganese content increased from 0.073 g plant^{-1} to 0.075 g plant^{-1} which was significant at the genotype and TxG level but not treatment (Figure 5–6, Table 5-2).

Transcriptional analysis

In silico expression of starch metabolism enzymes

The expression pattern of starch metabolism enzymes listed in Impa *et al.* 2019 were evaluated using previously published heat stressed maize leaf and kernel transcriptome datasets in tolerant (Zhengdan 958) and sensitive (Xianyu 335) genotypes as described in M&M section. The expression analysis revealed that SUS, GBSSI, ISAI, and β-amylase has comparatively higher expression in kernel tissue compared to leaf, whereas GBSSII, SSIII and α-amylase showed the opposite with higher expression in leaf compared to kernel. On the other hand, UGPase and PGMI showed higher expression in heat stressed kernel tissue of tolerant cultivars (Appendix D Figure -5). Based on this expression pattern the above-mentioned genes with differential expression were chosen for qRT-PCR based expression analysis.

qRT-PCR based expression analysis of selected starch metabolism enzymes under heat stress in kernel tissue

The expression pattern of β-amylase, PGMI, SSIII, SUS and UGPase were low in kernel tissue under heat stress and control condition. All the genes showed higher expression under HNT in tolerant kernel tissue compared to its control, however significantly higher expression was observed for α-amylase, ISAI, GBSSI, GBSSII and SSIII. Few genes such as AGPase SS, β-amylase, GBSS2, PGMI, SUS and UGPase showed opposite expression pattern under heat stress in the tolerant and sensitive cultivars compared to respective controls.

Discussion

Physiological Mechanisms for Yield Reductions due to HNT Stress

The physiological basis for the kernel weight reduction caused by HNT stress has recently been a topic of research interest, however it was first investigated in 1979 (de Vries *et al.*, 1979). This early experiment measured the respiration of three different cereals (wheat, maize, and ryegrass [*Lolium perenne* L.]) and noted a distinct increase in respiration which was dependent on the temperature imposed under controlled environment chambers (de Vries *et al.*, 1979). The researchers did not propose this as a HNT stress and the plants were placed in 24 hours of light before immediately being placed in darkness at variable temperatures (de Vries *et al.*, 1979), hence further exploration into the subject is warranted.

In 2004, a study found that an increase in night-time temperatures had a non-significant effect on carbon gain and dry mass in young, fast-growing plant species, however, increases in night respiration of 20% to 46% per 10 °C were noted (Frantz *et al.*, 2004). Mohammed and Tarpley (2009) later investigated the effects of HNT during the booting, early grain-filling and mid-dough stages in rice and found that plants under HNT stress had a 26% increase in night respiration and the carbon loss rate was highest during the early grain-filling stage. Impa *et al.* (2019) furthered the understanding of the physiological responses to HNT stress in wheat during the reproductive stages by showing a significant reduction in days to physiological maturity, grain yield, grain number, and net CO_2 assimilation accompanied by a significantly increase in respiration. A similar study was completed during the reproductive period of maize in which it was also found that HNT exposure resulted in a reduction in grain yield induced by an altered carbon balance and increase in night respiration (Wang *et al.*, 2020).

While the foundational understanding of the physiological response to HNT stress has been established within controlled environment settings, very little has been done to test these theories in the field. One of the earliest field-based experiments into the physiological basis of HNT responses explored the effects of HNT stress beginning from panicle initiation through physiological maturity in rice (Bahuguna *et al.*, 2017). This study found a reduction in 1000 grain weight, grain yield, carbon content and an increase in grain chalkiness due to HNT induced increases in night respiration during the grain-filling phase. Most recently, a study in maize using a temperate and a subtropical hybrid imposed HNT stress from two days after silking until 16 days after silking (Kettler *et al.*, 2022). This study supports the theory of an altered carbon balance due to an increase in night respiration but also showed a significant decrease in photosynthesis and postulated a significant negative correlation between the two (Kettler *et al.*, 2022).

Our current study supports the continued research into HNT stress in cereals. Through the use of a larger number of region-specific hybrids, our findings demonstrate a reduction in yield and seed carbon content which we hypothesize was the result of increased night respiration thereby altering the plant carbon balance during the grain-filling period. It is encouraging, however, that hybrids H4 and H10 could tentatively be indicated as resilient to increased overnight temperatures given their maintenance of grain yield and starch, protein and nutrient content as compared to the control.

The increase in magnesium content can provide tolerance against heat stress (Siddiqui *et al.*, 2018). An increased concentration of magnesium empowers the plant with a better carbohydrate transport from the source to the sink i.e., from leaf to cob in this case (Cakmak and Kirkby, 2008). Heat stress imparts magnesium deficiency which results in significant

carbohydrate accumulation in leaves (Siddiqui *et al.*, 2018; Zhang *et al.*, 2020). Magnesium is a key element responsible for phloem loading of carbohydrates and even resupplying magnesium to deficient leaves to restore the phloem loading and transport from source to sink (Cakmak and Kirkby, 2008, Tränkner *et al.*, 2018). A meta-analysis performed by Hauer-Jákli *et al.* revealed that adequate Mg supply enhances net CO_2 assimilation by 140%, leading to a biomass increase of 61% compared to Mg deficient control plants (Huaer-Jákli and Tränkner, 2019). The results of this study support the hypothesis of increasing magnesium content imparting a level of tolerance to heat stress. H4 and H10, which were the only two hybrids to see an increase in yield, were two of the three hybrids which saw an increase in magnesium content (Appendix D Table - 3). The third hybrid which saw an increase had the smallest reduction in yield compared to the remaining hybrids.

While the effects of HNT stress is becoming more widely understood, there is still a distinct lack of understanding on how this stress affects kernels based on their locations on the cob. When grain yield results are recorded based on the kernel's position on the cob, there is not a significant difference between the top, middle and bottom portions in the overall average reduction. This equal distribution of reduction to grain yield along the cob occurred due to the highly variable responses amongst the hybrids. Three of the hybrids had the largest reduction in yield in the top portion, five hybrids in the middle portion, and four hybrids in the bottom portion. The two hybrids which recorded an increase in grain yield also varied in response with H4 having a reduction in the bottom but increases in the middle and top while H10 saw a reduction in the middle and increases in the bottom and top. Even though the response to HNT stress varied amongst hybrids, the top portion of the cob had the largest reduction amongst the hybrids which had an overall decrease in yield. This pattern could indicate that preservation of

yield at the top portion of the cob would be a significant step towards maintaining yield during HNT stress.

The responses in 200 kernel weight were more uniform with the bottom portion having the largest reduction followed by the middle and then the top. Only one hybrid had the largest reduction in kernel weight occur in the middle, while all other hybrids saw the greatest reduction in the bottom or top. Interestingly the most tolerant hybrids, H4 and H10, saw an increase in kernel weight in the top portions while no other hybrid saw an increase. This supports the theory that maintaining yield and kernel weight in the top portion of the cob will be an essential trait in combating HNT stress.

These differences in filling characteristics show a wide range of plant responses to elevated high night-time temperature stress. Interestingly while H4 and H10 were the only two hybrids to see increased yield and increased kernel weight in the top portion of the cob, they were also the only hybrids to record an increase in total starch, protein, and magnesium content. When these responses are considered, it is apparent that H4 and H10 were able to maintain the plant's carbon balance at a higher efficiency and synthesize more starch for the kernels as compared to the other hybrids. More research is necessary to substantiate this hypothesis and, if found plausible, to determine whether the carbon balance was maintained through an increased carbon uptake through increased photosynthetic efficiency, increased ability in translocation of nutrients and greater mobilization of water-soluble carbohydrates or an ability to maintain night respiration during increased overnight temperatures. Through more extensive studies, the apparent tolerance mechanisms from specific hybrids could be identified and integrated into a larger number of commercial hybrids and offer a level of protection to future HNT stress.

Differential transcriptional regulation of starch metabolism in maize kernels under HNT

The tolerant and sensitive hybrids starch, carbon, and biomass content under HNT. Therefore, to study the effect of heat stress and correlate the physiological response with the molecular mechanism, expression profile of genes involved in starch metabolism was performed. The expression analysis was aimed at addressing two aspects, (i) starch biosynthesis and (ii) starch degradation. ADP-glucose is the glucosyl donor for α-1,4-glucosidic chain elongation and thus participates in the synthesis of glycogen and starch in plants and bacteria (Ballicora *et al.,* 2003). SUSI, UGPase, cytosolic AGPase and SS are sequentially involved in ADP-glucose formation and thus regulate starch synthesis (Impa *et al.,* 2020). Specially, AGPase enzyme controls the rate-limiting step in starch biosynthesis and thus affects the total starch content (Kawagoe *et al.*, 2005). Starch synthesis mutants, *sugary* and *shrunken*, display reduced activities of ISAI and cytosolic AGPase enzymes, respectively. The ISAI catalyze granule synthesis at the initiation step and AGPase is responsible for subsequent enlargement of granules (Kawagoe *et al.,* 2005). Interestingly, these four enzymes showed higher expression under HNT compared to control tissue in tolerant H4 hybrid whereas in sensitive H12 hybrid the expression pattern was opposite with higher expression under control and lower during HNT (Figure 5-7).

Moving to the other molecular cues involved in starch synthesis, granule bound starch synthase, are involved in amylose synthesis as well as in building the final structure of amylopectin whereas soluble starch synthase, SSIII is involved in amylopectin synthesis (Crofts *et al.,* 2022). GBSSI expression in maize seeds increase amylose accumulation (Guo *et al.,* 2006; Keeling and Myers, 2010). Mutant and overexpression analysis in different plant species such as rice, maize, pea and potato clearly established that a positive correlation exist between SSIII and

GBSSI levels and synthesis of amylopectin and amylose, respectively (Keeling and Myers, 2010). We also found a higher expression of these starch synthesis enzymes under HNT compared to control in tolerant hybrids.

These results in conjunction indicates a higher starch synthesis in the tolerant hybrids. In addition to higher starch synthesis a starch degrading enzyme α-amylase was significantly higher in the tolerant compared to sensitive whereas surprisingly β-amylase remained almost constant. This is in contrast as studies report that β-amylase catalyzed starch degradation in leaf tissue under heat stress produce maltose which acts as thermoprotectant (Kaplan and Guy, 2004; Impa *et al.*, 2020). The higher expression of α-amylase observed in kernel tissue could be a protective mechanism which operates differently from the leaf tissue and further detailed investigation is warranted.

Conclusions

The asymmetric increase in the minimum night-time temperature and maximum daytime temperature suggests that the effects of HNT stress will become even more prevalent under future changing climate during a time in which the world's reliance on cereals continues to grow. This study has shown that with a 3.8 °C increase in overnight temperatures, maize grain yield and quality will be significantly diminished, and these reductions will be differentially realized based on the hybrid and location of the kernel on the cob. Significant reductions in 200 kernel weight and macro- and micronutrient content necessitate further research involving field-based studies with large variety panels in order to identify possible tolerant hybrids so that their tolerance mechanisms can be distributed to the commercial hybrid populations.

References

Ada, L., 2014. Adafruit MCP9808 precision I2C temperature sensor guide. Adafruit. Accessed May 06, 2021. https://learn.adafruit.com/adafruit-mcp9808-precision-i2c-temperature-sensor-guide

Alexander, L.V., Zhang, X., Peterson, T.C., *et al.*, 2006. Global observed changes in daily climate extremes of temperature and precipitation. Journal of Geophysical Research: Atmospheres 111(D5). https://www.doi.org/10.1029.2005jD006290

Alexandratos, N., Bruinsma, J., 2012. World agriculture towards 2030/2050: The 2012 Revision. ESA Working paper No. 12-03. Rome, FAO.

Asseng, S., Ewert, F., Martre, P., *et al.*, 2015. Rising temperatures reduce global wheat production. Nature Climate Change 5, 143-147. https://www.doi.org/10.1038/nclimate2470

Bahuguna, R.N., Solis, C.A., Shi, W., Jagadish, S.V.K., 2017. Post-flowering night respiration and altered sink activity account for high night temperature-induced grain yield and quality loss in rice (*Oryza sativa* L.). Physiologia Plantarum 159, 59-73. https://www.doi.org/10.1111/ppl.12485

Ballicora, M.A., Iglesias, A.A., Preiss, J., 2003. ADP-glucose pyrophosphorylase, a regulatory enzyme for bacterial glycogen synthesis. Microbiology and Molecular Biology Reviews 67, 213-225. https://www.doi.org/10.1128/MMBR.67.2.213-225.2003

Bergkamp, B., Impa, S.M., Asebedo, A.R., Fritz, A.K., Jagadish, S.V.K., 2018. Prominent winter wheat varieties response to post-flowering heat stress under controlled chambers and field based heat tents. Field Crops Research 222, 143-152. https://www.doi.org/10.1016/j.fcr.2018.03.009

Breese, J.D., 1931. Factors for converting percentages of nitrogen in foods and feeds into percentages of proteins. *United States Department of Agriculture Circular, 183*, 16-21. https://www.ars.usda.gov/ARSUserFiles/80400525/Data/Classics/cir183.pdf

Boyer, J.S., 1982. Plant productivity and environment. Science 218(4571), 443-448. https://www.doi.org/10.1126/science.218.4571.443

Bushnell, B., Rood, J., Singer, E., 2017. BBMerge – accurate paired shotgun read merging via overlap. PLoS ONE 12, e01-i85056. https://www.doi.org/10.1371/journal.pone.0185056

Cakmak, I., Kirkby, E.A., 2008. Role of magnesium in carbon partitioning and alleviating photooxidative damage. Physiologia Plantarum 133, 692-704. https://www.doi.org/10.1111/j.1399-3054-2007.01042.x

Cantarero, M.G., Cirilo, A.G., Andrade, F.H., 1999. Night temperature at silking affects kernel set in maize. Crop Science 39, 703-710. https://www.doi.org/10.2135/cropsci1999.0011183X003900020017x

Chen, S., Zhou, Y., Chen, Y., Gu, J., 2018. Fastp: an ultra-fast all-in-one FASTQ preproccessor. Bioinformatics 34, i884-i890. https://www.doi.org/10.1093/bioinformatics/bty560

Crofts, N., Domon, A, Miura, S., Hosaka, Y., Oitome, N.F., Itoh, A., Noge, K., Fujita, N., 2022. Starch synthases SSIIa and GBSSI control starch structure but do not determine starch granule morphology in the absence of SSIIIa and SSIVb. Plant Molecular Biology 108, 379-398. https://www.doi.org/10.1007/s11103-021-01197-x

Davy, R., Esau, I., Chernokulsky, A., Outten S., Zilitinkevich, S., 2016. Diurnal asymmetry to the observed global warming. International Journal of Climatology 37(1), 79-93. https://www.doi.org/10.1002/joc.4688

de Vries, F.W.T.P., Witlage, J.M., Kremer, D., 1979. Rates of respiration and of increase in structural dry matter in young wheat, ryegrass and maize plants in relation to temperature, to water stress and to their sugar content. Annals of Botany 44, 595-609. https://www.doi.org/10.1093/oxfordjournals.aob.a085772

Easterling, D.R., Hornton, B., Jones, P.D., *et al.*, 1997. Maximum and minimum trends for the globe. Science 277(5324, 364-367. https://www.doi.org/10.1126/science.277.5324.364

Frantz, J.M., Cometti, N.N., Bugbee, B., 2004. Night temperature has a minimal effect on respiration and growth in rapidly growing plants. Annals of Botany 94, 155-166. https://www.doi.org/10.1093/aob/mch122

Food and Agriculture Organization of the United Nations, 2020. FAO Global Statistical Yearbook. Accessed 04/10/22. https://www.fao.org/faostat/en/#data/FBS

García, G.A., Dreccer, M.F., Miralles, D.J., Serrago, R.A., 2015. High night temperatures during grain number determination reduce wheat and barley grain yield: a field study. Global Change Biology 21, 4153-4164. https://www/doi.org/10.1111/gcb.13009

Glaubitz, U., Erban, A., Kopka, J., Hincha, D.K., Zuther, E., 2015. High night temperature strongly impacts TCA cycle, amino acid and polyamine biosynthetic pathways in rice in a sensitivity-dependent manner. Journal of Experimental Botany 66, 6385-6397. https://www.doi.org/10.1093/jxb/erv352

Gourdji, S.M., Sibley, A.M., Lobell, D.B., 2013. Global crop exposure to critical high temperatures in the reproductive period: historical trends and future projections. Environmental Research Letters 8, 024041. https://www.doi.org/10.1088/1748-9326/8/2/024041

Guo, S., Li, J., Qiao, W., Zhang, X., 2006. Analysis of amylose accumulation during seed development in maize. Acta Genetica Sinica 33, 1014-1019. https://www.doi.org/10.1016/50379-4172(06)60137-6

Halford, N.G., Curtis, T.Y., Chen, Z., Huang, J., 2014. Effects of abiotic stress and crop management on cereal grain composition: implication for food quality and safety. J Exp Bot 66(5), 1145-1156. https://www.doi.org/10.1093/jxb/eru473

Hatfield, J.L., Prueger, J.H., 2015. Temperature extremes: effect on plant growth and development. Weather and Climate Extremes 10, 4-10. https://www.doi.org/10.1016/j.wace.2015.08.001

Hauer-Jákli, M., Tränkner, M., 2019. Critical leaf magnesium thresholds and the impact of magnesium on plant growth and photo-oxidative defense: a systematic review and meta-analysis from 70 years of research. Frontiers in Plant Science 10, 766. https://www.doi.org/10.3389/fpls.2019.00766

Hein, N.T., Wagner, D., Bheemanahalli, R., Šebela, D., Bustamante, C., Chiluwal, A., Neilsen, M.L., Jagadish, S.V.K., 2019. Integrating field-based heat tents and cyber-physical system technology to phenotype high night-time temperature impact on winter wheat. Plant Methods 15, 41. https://www.doi.org/10.1186/s13007-019-0424-x

Hein, N.T., Bheemanahalli, R., Wagner, D., et al., 2020. Improved cyber-physical system captured post-flowering high night temperature impact on yield and quality of field grown wheat. Scientific Reports 10, 22213. https://www.doi.org/10.1038/s41598-020-79179-0

Howe, E., Holton, K., Nair, S., Schlauch, D., Sinha, R., Quackenbush, J., 2010. MeV: multiexperiment viewer. In: Ochs, M., Casagrande, J., Davuluri, R., (eds.). Biomedical

informatics for cancer research. Springer, Boston, MA. https://www.doi.org/10.1007/978-1-4419-5714-6_15

Impa, S.M., Sunoj, V.S.J., Krassovskaya, I., Bheemanahalli, R., Obata, T., Jagadish, S.V.K., 2019. Carbon balance and source-sink metabolic changes in winter wheat exposed to high night-time temperature. Plant, Cell & Environment 42, 1233-1246. https://www.doi.org/10.1111/pce.13488

Impa, S.M., Vennapusa, A.R., BHeemanahalli, R., Sebela, D., Boyle, D., Walia, H., Jagadish, S.V.K., 2020. High night temperature induced changes in grain starch metabolism alters starch, protein, and lipid accumulation in winter wheat. Plant, Cell & Environment 43, 431-447. https://www.doi.org/10.1111/pce.13671

Kaplan, F., Guy, C.L., 2004. β-amylase induction and the protective role of maltose during temperature shock. Plant Physiology 135, 1674-1684. https://www.doi.org/10.1104pp.104.040808

Kawagoe, Y., Kubo, A., Satoh, H., Takaiwa, F., Nakamura, Y., 2005. Roles of isoamylase and ADP-glucose pyrophosphorylase in starch granule synthesis in rice endosperm. The Plant Journal 42, 164-174. https://www.doi.org/10.1111/j.1365-313X.2005.02367.x

Keeling, P.L., Myers, A.M., 2010. Biochemistry and genetics of starch synthesis. Annual Reviews 1, 271-303. https://www.doi.org/10.1146/annurev.food.102308.124214

Kettler, B.A., Carrera, C.S., Sonzogni, F.D.N., Trachsel, S., Andrade, F.H., Neiff, N., 2022. High night temperature during maize post-flowering increases night respiration and reduces photosynthesis, growth and kernel number. Journal of Agronomy and Crop Science, Early View. https://www.doi.org/10.1111/jac.12589

Kumar, A., Gupta, C., Thomas, J., Pereira, A., 2021. Genetic dissection of grain yield component traits under high nighttime temperature stress in a rice diversity panel. Frontiers in Plant Science 12, 712167. https://www.doi.org/10.3389/fpls.2021.712167

Lesjak, J., Calderini, D.F., 2017. Increased night temperature negatively affects grain yield, biomass and grain number in Chilean quinoa. Frontiers in Plant Science 8, 352. https://www.doi.org/10.3389/fpls.2017.00352

Loka, D.A., Oosterhuis, D.M., 2010. Effect of high night temperatures on cotton respiration, ATP levels and carbohydrate content. Environmental and Experimental Botany 68, 258-263. https://www.doi.org/10.1016/j.envexpbot.2010.01.006

Mamrutha, H.M., Singh, R., Sharma, D., Venkatesh, K., Pandey, G.C., Kumar, R., Tiwari, R., Sharma, I., 2019. Physiological and molecular basis of abiotic stress tolerance in wheat. In: Rajpal, V., Sehgal, D., Kumar, A., Raina, S. (eds.) Genetic Enhancement of Crops for Tolerance to Abiotic Stress: Mechanisms and Approaches 20, 99-124. Springer, Cham. https://www.doi.org/10.1007/978-3-319-91956-0_5

Mohammed, A.R., Tarpley, L., 2009. Impact of high nighttime temperature on respiration, membrane stability, antioxidant capacity, and yield of rice plants. Crop Science 49, 313-322. htpps://www.doi.org/10.2135/cropsci2008.03.0161

NCBI, SRA run selector. National Center for Biotechnology Information. Released Feb. 15, 2022. https://www.ncbi.nlm.nih.gov/Traces/study/?acc=SRP334391&o=acc_s%3Aa

Neiff, N., Trachsel, S., Valentinuz, O.R., Ballbi, C.N., Andrade, F.H., 2016. High temperatures around flowering in maize: effects on photosynthesis and grain yield in three genotypes. Crop Science 56, 2702-2712. https://www.doi.org/10.2135/cropsci2015.12.0755

Niu, J., Feng, J., Zhang, X., Chen, S., Shao, L., 2021. Open field simulating nocturnal warming on summer maize performance in the north China plain. Agronomy 11, 992. https://www.doi.org/10.3390/agronomy11050992

Niu, S., Du, X., Wei, D., Liu, S., Tang, Q., Bian, D., Zhang, Y., Cui, Y., Gao, Z., 2021. Heat stress after pollination reduces kernel number in maize by insufficient assimilates. Frontiers in Genetics 12, 728166. https://www.doi.org/10.3389/fgene.2021.728166

OECD/FAO, 2021. Agricultural Outlook 2021-2030. OECD Publishing, Paris. https://www.doi.org/10.1787/19428846-en

Peng, S., Huang, J., Sheehy, J.E., Laza, R.C., Visperas, R.M., Zhong, X., Centeno, G.S., Khush G.S., Cassman, K.G., 2004. Rice yields decline with higher night temperature from global warming. Proceedings of the National Academy of Sciences 101(27). https://www.doi.org/10.1073/pnas.0403720101

Sadok, W., Jagadish, S.V.K., 2021. The hidden costs of nighttime warning on yields. Trends in Plant Science 25, 644-651. https://www.doi.org/10.1016/j.tplants.2020.02.003

Shi, W., Muthurajan, R., Rahman, H., Selvam, J., Peng, S., Zou, Y., Jagadish, S.V.K., 2013. Source-sink dynamics and proteomic reprogramming under elevated night temperature and their impact on rice yield and grain quality. New Phytologist 197, 825-837. https://www.doi.org/10.1111/nph.12088

Shi, W., Yin, X., Struik, P.C., Xie, F., Schmidt, R.C., Jagadish, S.V.K., 2016. Grain yield and quality responses of tropical hybrid rice to high night-time temperature. Field Crops Research 190, 18-25. https://www.doi.org/10.1016/j.fcr.2015.10.006

Siddiqui, M.H., Slamri, S.A., Al-Khaishany, M.Y.Y., Al-Qutami, M.A., Ali, H.M., Al-Whaibi, M.H., Al-Wahibi, M.S., Alharby, H.F., 2018. Mitigation of adverse effects of heat stress

on Vicia faba by exogenous application of magnesium. Saudi Journal of Biological Sciences 25, 1393-1401. https://www.doi.org/10.1016/j.sjbs.2016.09.022

Sunoj, V.S.J., Shroyer, K.J., Jagadish, S.V.K., Prasad, P.V.V., 2016. Diurnal temperature amplitude alters physiological and growth response of maize (*Zea mays* L.) during the vegetative stage. Environmental and Experimental Botany 130, 113-121. https://www.doi.org/10.1016/j.envexpbot.2016.04.007

Tillman, D., Blazer, C., Hill, J., Befort, B.L., 2011. Global food demand and the sustainable intensification of agriculture. Proceedings of the National Academy of Science USA 108, 20260-20264. https://www.doi.org/10.1073/pnas.1116437108

Tombesi, S., Cincera, I., Frioni, T., Ughini, V., Gatti, M., Palliotti, A., Poni, S., 2019. Relationship among night temperature, carbohydrate translocation and inhibition of grapevine leaf photosynthesis. Environmental and Experimental Botany 157, 293-298. https://www.doi.org/10.1016/j.envexpbot.2018.10.023

Tränkner, M., Tavakol, E., Jákli, B., 2018. Functioning of potassium and magnesium in photosynthesis, photosynthate translocation and photoprotection. Physiologia Plantarum 163, 414-431. https://www.doi.org/10.1111/ppl.12747

van Dijk, M., Morley, T., Rau, M.L., Saghai, Y., 2021. A meta-analysis of projected global food demand and population at risk of hunger for the period 2010-2050. Nature Food 2,494-501. https://www.doi.org/10.1038/s43016-021-00322-9

Wang, Y., Tao, H., Zhang, P., Hou, X., Sheng, D., Tian, B., Wang, P., Huang, S., 2020. Reduction in seed set upon exposure to high night temperature during flowering in maize. Physiologia Plantarum 169, 73-82. https://www.doi.org/10.1111/ppl.13049

Zhang, B., Cakmak, I., Feng, J., Yu, C., Chen, X., Xie, D., Wu, L., Song, Z., Cao, J., He, Y., 2020. Magnesium deficiency reduced the yield and seed germination in wax gourd by affecting the carbohydrate translocation. Frontiers in Plant Science 11, 797. https://www.doi.org/10.3389/fpls.2020.00797

Figures

Figure 5-1 Environmental Results

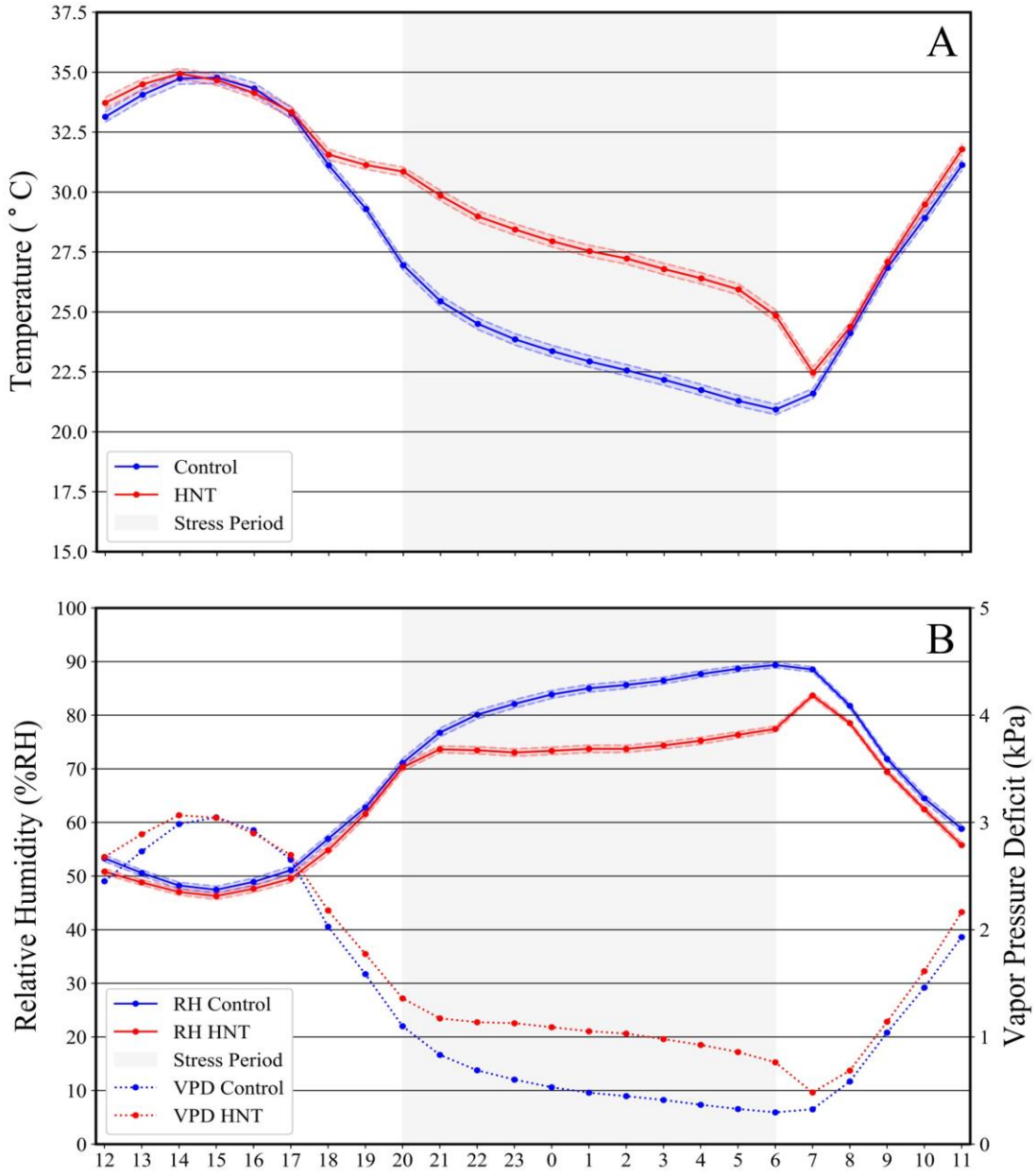

Environmental results of temperature, relative humidity, and vapor pressure deficit from stress imposition during grain-filling.

Figure 5-2 Yield results after exposure to HNT during grain-filling

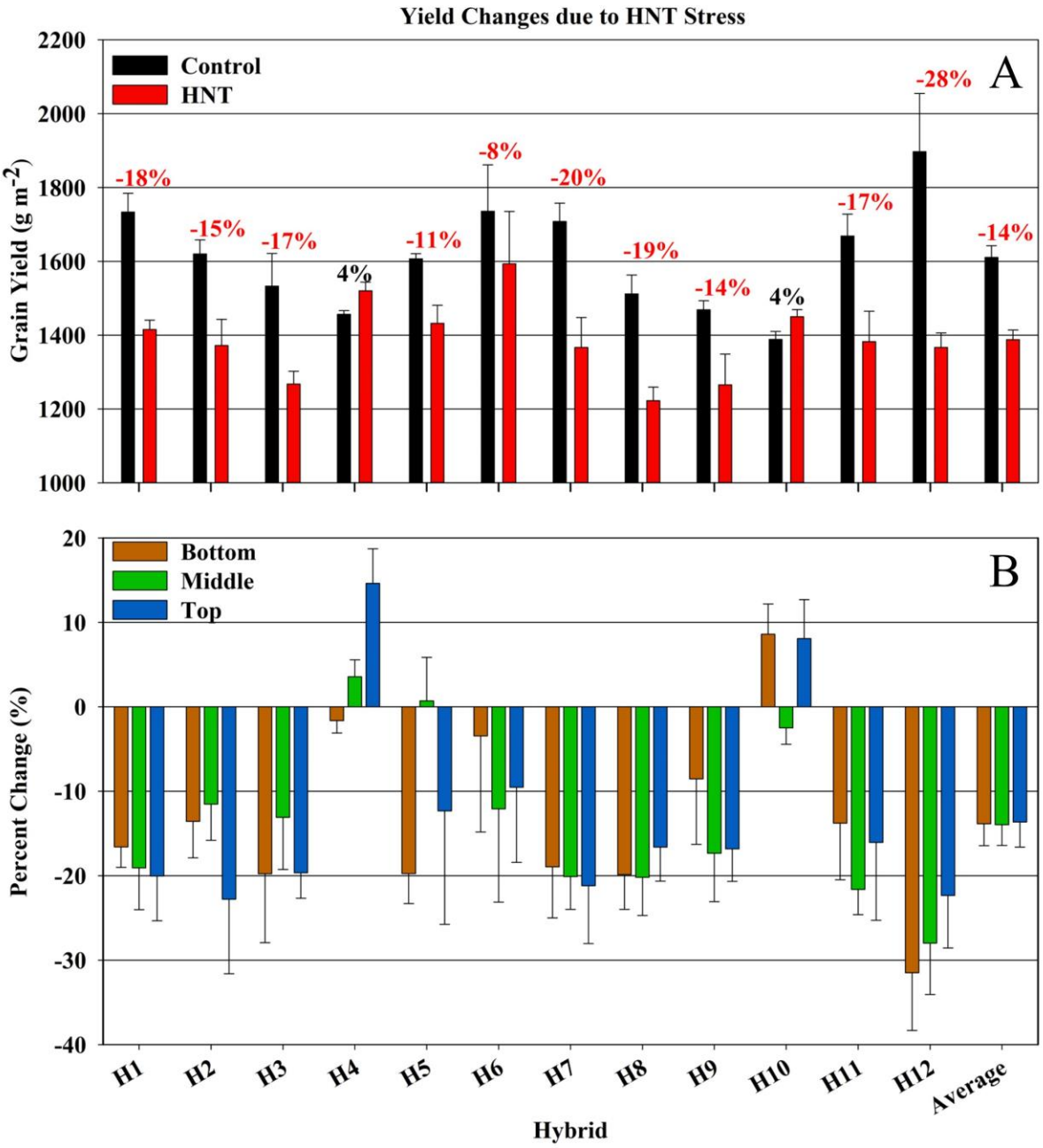

Yield Results after exposure to HNT during grain-filling. A: The resulting grain yield (g m^{-2}) for control, treatment and the percent reduction for each hybrid as well as the overall average for all 12 hybrids. B: Yield response to HNT stress showing differential responses due to location on the cob presented as percent change (%).

Figure 5-3 200 kernel weight changes due to HNT stress

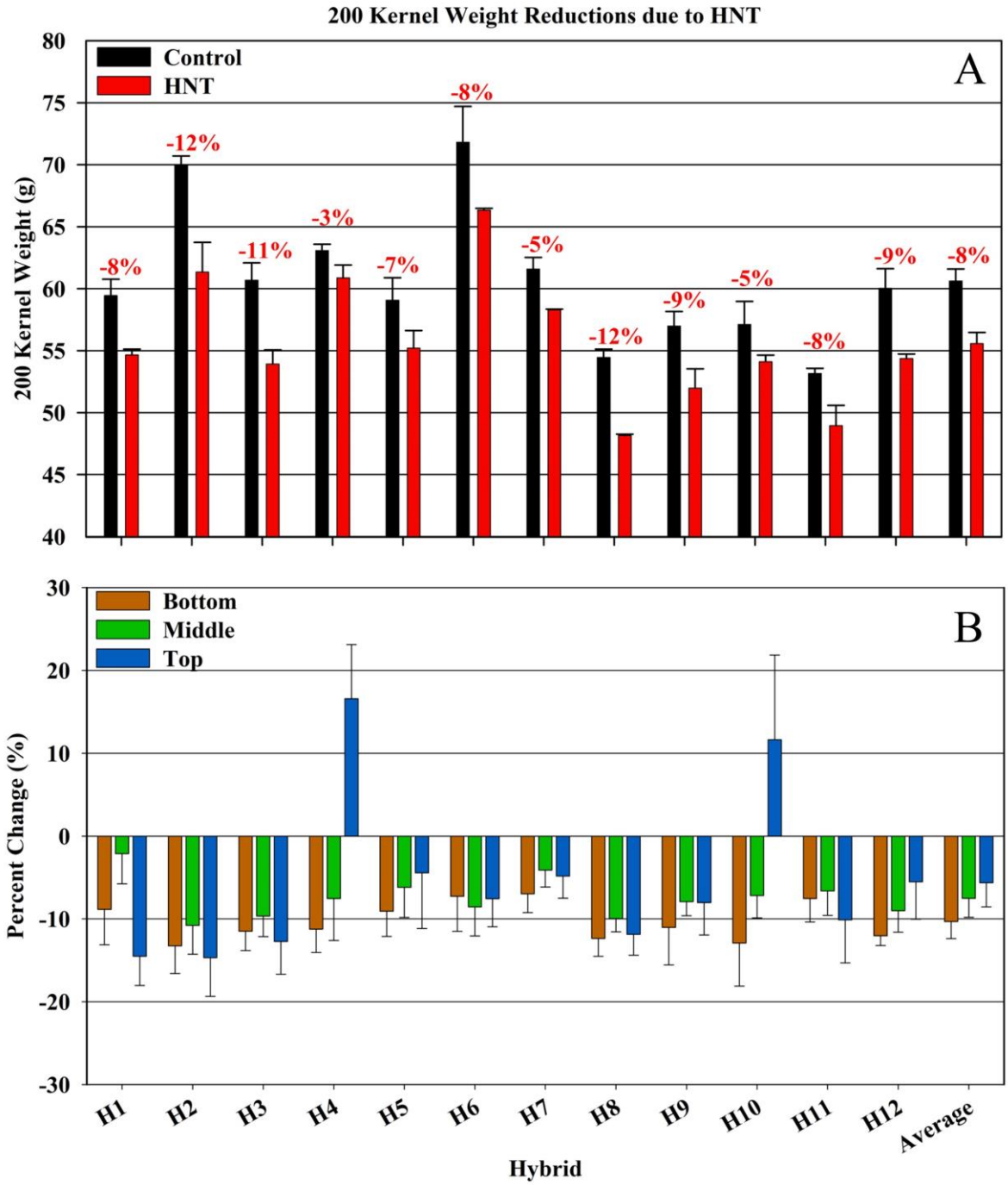

200 kernel weight changes due to HNT stress. A: The resulting 200 kernel weight (g) for control, treatment and the percent reduction for each hybrid as well as the overall average for all 12 hybrids. B: 200 kernel weight response to HNT stress showing differential responses due to location on the cob presented as percent change (%).

Figure 5-4 Harvest Index reductions due to HNT

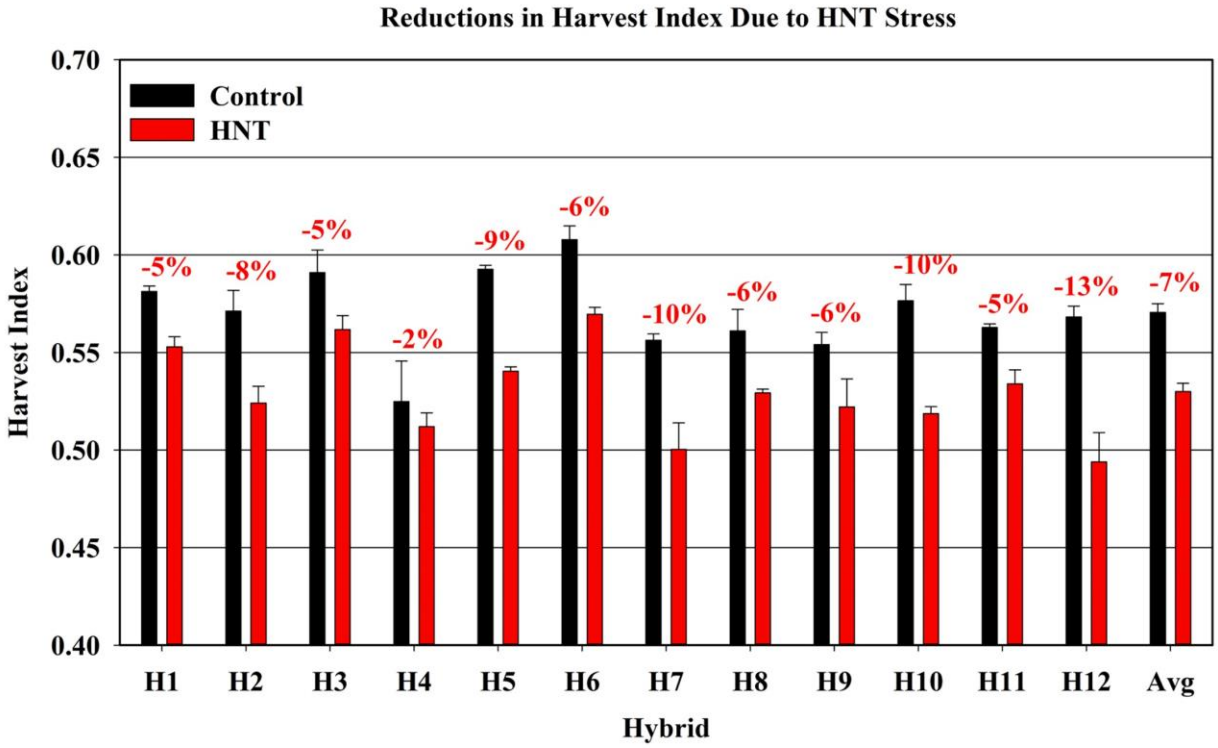

Harvest index reduction due to HNT stress displayed for the control, treatment, and percent change (%) for each hybrid as well as the overall average of all 12 hybrids.

Figure 5-5 HNT induced changes to starch content

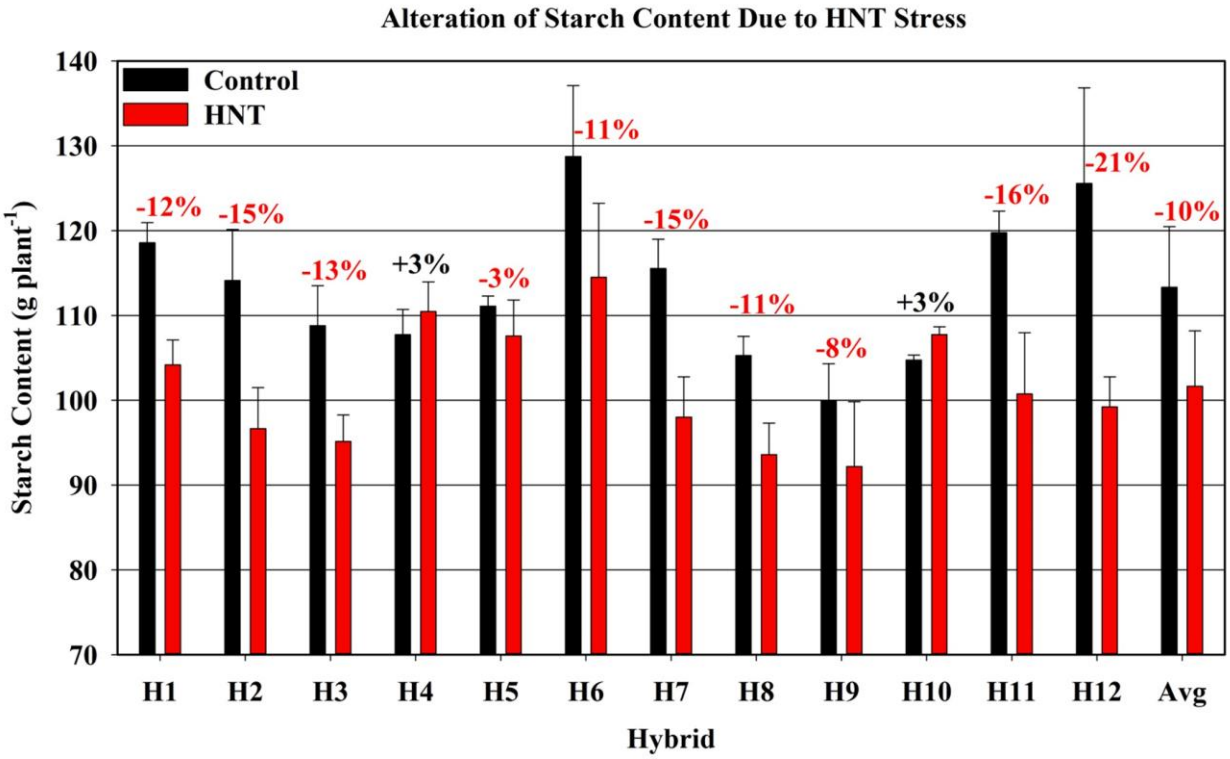

Changes in starch content (g plant^{-1}) as a result of HNT stress. Results for the control, treatment and percent change (%) for each hybrid as well as the overall average for all 12 hybrids.

Figure 5-6 Changes in yield and macro- and micronutrient content

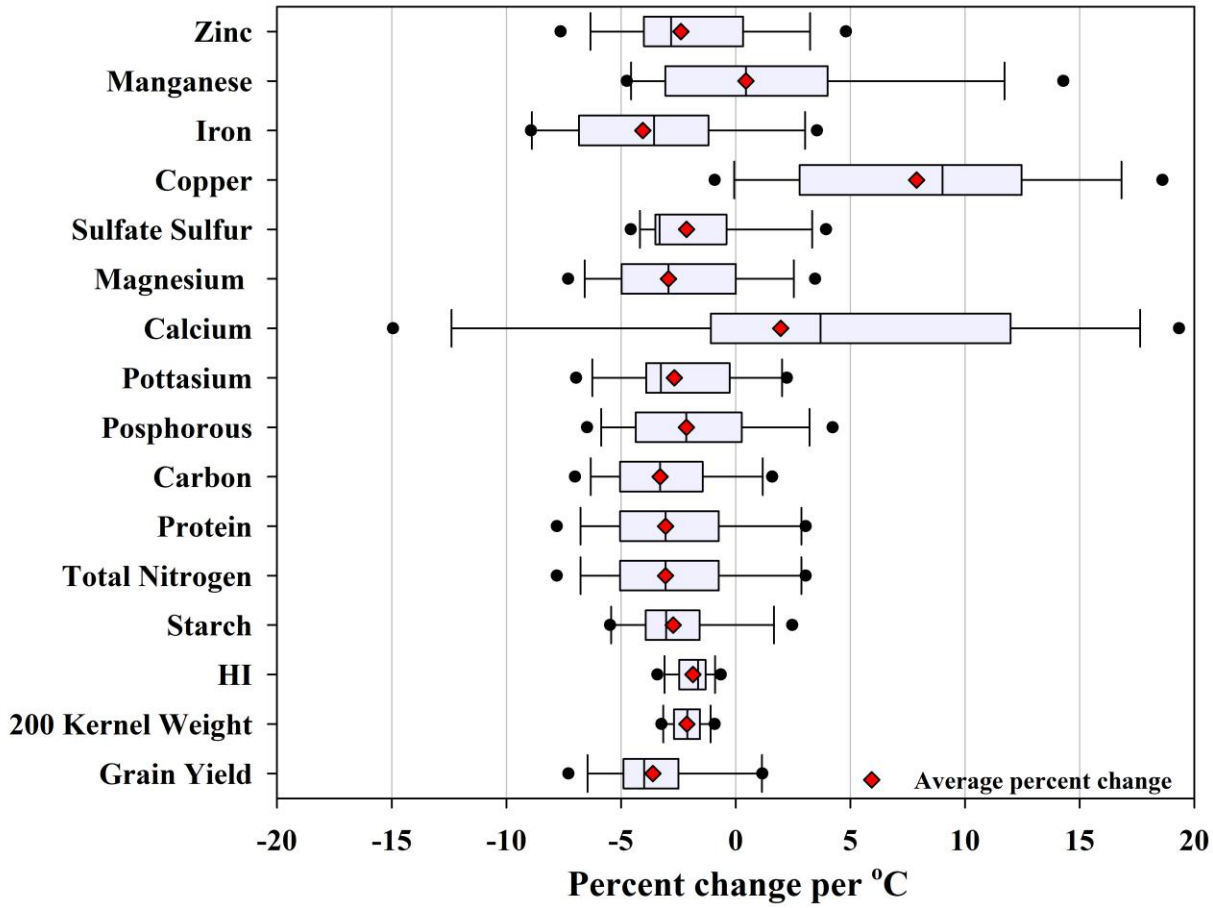

Box and whisker plot highlighting the changes in yield, kernel weight, harvest index, and seed composition to include starch, protein, and the major- and micronutrients. Red stars indicate the average percent change (%) per °C.

Figure 5-7 Relative expression of starch metabolism enzymes

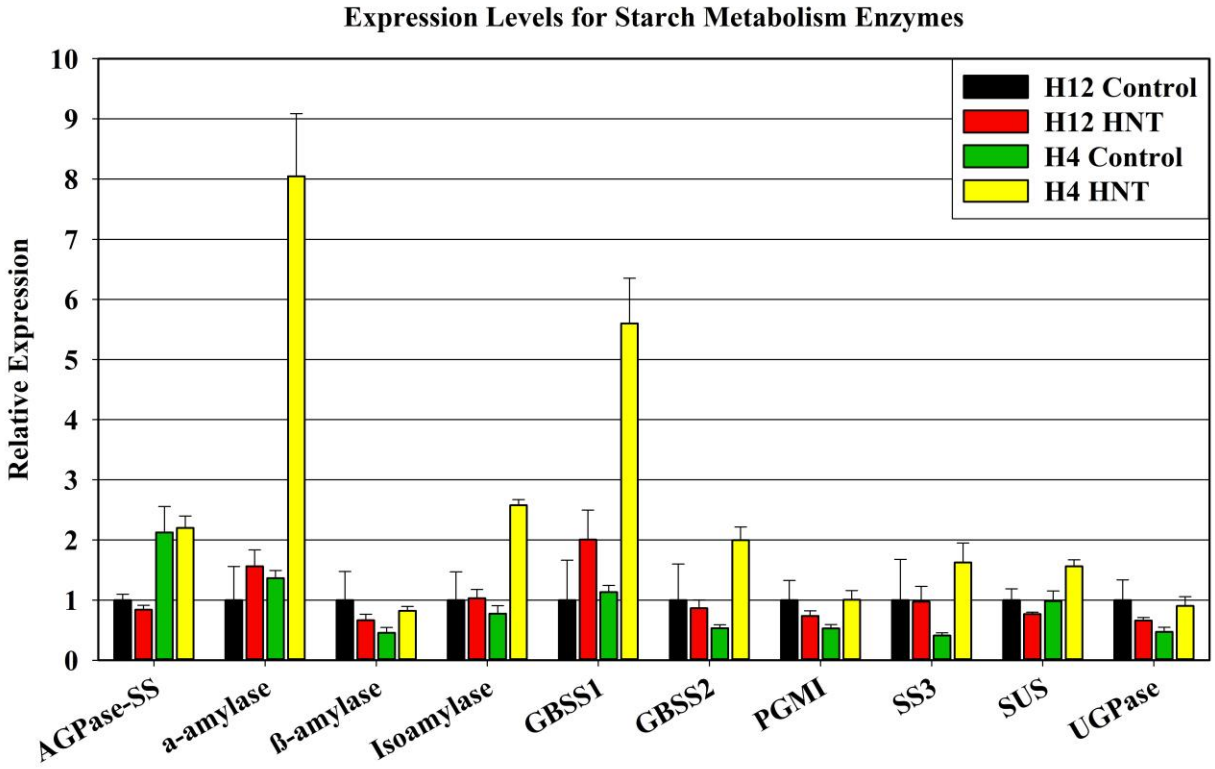

Relative expression of starch metabolism enzymes for the susceptible (H12) and resilient (H4) hybrids. All results were compared to the susceptible hybrid control treatment responses.

Tables

Table 5-1 Significance of changes in agronomic properties

	Variables		
Trait	**Treatment**	**Genotype**	**TxG**
Total Yield (g plant^{-1})	**<0.0001**	**0.010**	0.065*
200 Kernel Weight (g)	**<0.0001**	**<0.0001**	0.790
Total Kernel Number (# plant^{-1})	0.795	0.201	0.218
Shoot Biomass (g plant^{-1})	0.144	**<0.001**	0.559
Aboveground Biomass (g plant^{-1})	0.545	**0.001**	0.419
Harvest Index	**0.023**	**<0.0001**	0.197
Bottom Yield (g plant^{-1})	**<0.0001**	**0.030**	0.069*
Middle Yield (g plant^{-1})	**<0.0001**	**0.005**	0.071*
Top Yield (g plant^{-1})	**<0.0001**	**0.023**	0.145
Bottom 200 Kernel Weight (g)	**<0.0001**	**<0.0001**	0.980
Middle 200 Kernel Weight (g)	**<0.0001**	**<0.0001**	0.903
Top 200 Kernel Weight (g)	**0.004**	**<0.0001**	0.015

Significance of agronomic changes at the treatment, genotype, and TxG levels. Bold indicates significance at $p < 0.05$ and * indicates significance at $p < 0.10$.

Table 5-2 Significance of changes in nutrient content

	Variables			Mean	
Trait	**Treatment**	**Genotype**	**TxG**	**Control**	**HNT**
Starch Content (g plant^{-1})	**<0.0001**	**0.026**	0.457	**113.33^{a}**	**101.67^{b}**
Protein Content (g plant^{-1})	**<0.0001**	**0.0006**	**0.018**	**16.53^{a}**	**14.60^{b}**
Carbon Content (g plant^{-1})	**<0.0001**	**0.0089**	0.0573*	**81.79^{a}**	**71.59^{b}**
Phosphorous Content (g plant^{-1})	0.226	**0.030**	0.317	0.37	0.34
Potassium Content (g plant^{-1})	0.129	**0.0002**	0.170	0.48	0.43
Calcium Content (g plant^{-1})	0.580	0.101	0.565	0.0068	0.0074
Magnesium Content (g plant^{-1})	**0.0008**	**0.004**	0.126	**0.175^{a}**	**0.156^{b}**
Sulfate Sulfur Content (g plant^{-1})	0.311	**0.003**	0.537	0.168	0.155
Copper Content (g plant^{-1})	0.352	**0.007**	0.493	0.034	0.045
Iron Content (g plant^{-1})	0.279	**0.0009**	0.419	0.37	0.32
Manganese Content (g plant^{-1})	0.870	**<0.0001**	0.078*	0.073	0.075
Zinc Content (g plant^{-1})	0.428	**0.012**	0.539	0.39	0.36

Significance of nutrient content changes at the treatment, genotype, and TxG levels. Bold indicates significance at $p < 0.05$ and * represents significance at $p < 0.10$.

Chapter 6 - General Conclusions and Future Research Direction

High night-time temperature stress is an imminent threat to cereal grain production and quality. The daily minimum temperature is rising at a faster rate than the daily maximum temperature and will become an apparent threat to cereal production under future warming scenarios through a reduction in grain yield, kernel weight and alterations of seed composition (Peng *et al.*, 2004; Hein *et al.*, 2019, 2020; Impa *et al.*, 2019, 2020; Wang *et al.*, 2020). Previous research into the effects of high night-time temperature stress have been limited to controlled environment growth chambers (Prasad *et al.*, 2008; Narayanan *et al.*, 2008; Impa *et al.*, 2019,2020) or small chambers in field-based studies (Lizana and Calderini, 2013; Garcia *et al.*, 2015, 2016).

In response to the lack of field-based studies, this dissertation aimed to explore the agronomic and physiological responses, and changes in grain quality and micronutrient composition in wheat and maize exposed to high night-time temperature stress during the grain-filling period. This effort was first accomplished through the development of a field-based prototype system which allows for phenotyping a set of diverse genotypes that requires limited resources and overcomes the barrier for researching high night-time temperature stress under field conditions. After success in developing a low-cost field-based method, the methodology was expanded and a large field-based infrastructure was developed with the capability of phenotyping a large diversity panel and multiple different crops.

In this aim, the prototype system was able to impose a high night-time temperature stress of 3.2 °C while the large field-based infrastructure was able to maintain a high night-time temperature stress of 3.8 °C in both years of operation. The imposition of the high night-time temperature stress caused a significant reduction on the grain-filling duration (-8%) in wheat as well as reduced grain yield (wheat: -20% and -14%; maize: -14%) and 200 kernel weight (wheat:

-6% and 5%; maize: -8%) and altered seed composition through reductions in both micro- and macronutrients in wheat and maize. Along with these agronomic and physiological adjustments, differential expression of starch metabolism related enzymes was found through transcriptional analysis of a tolerant and susceptible maize hybrid. The tolerant hybrid was found to have an increased expression of all genes tested but had a significant increase of α-amylase, ISAI, GBSSI, GBSSII and SSIII as compared to the susceptible hybrid.

These results add credibility to previous experiments which were conducted in both controlled environment growth chambers (Prasad *et al.*, 2008; Narayanan *et al.*, 2015; Impa *et al.*, 2019, 2020) and small field-based enclosures (Lizana and Calderini, 2013; Garcia *et al.*, 2015, 2016). The reductions in yield, 200 kernel weight, and nutrient composition of experimental material exposed to high night-time temperature stress confirms that the current commercial populations of wheat and maize will not continue to produce at their current levels under future warmer scenarios. Food security throughout the world will reduce and the nutritional quality of grains produced will be severely deficient as compared to today. However, the study on the effects of high night-time temperature in maize did result in the identification of a single hybrid which could be classified as tolerant. This result stems the hypothesis that the physiological and genomic make up of high night-time temperature tolerant varieties do exist within current commercial populations and could be exploited with future research.

In order to elucidate different germplasm that maintain tolerance to high night-time temperature stress, experiments involving large diversity panels must be completed. For such experiments to be conducted, more resources must be committed to the production of purpose-built infrastructure which allows for these explorations. High night-time temperature stress is a difficult abiotic stress to evaluate in field-based settings. These experiments require electricity, a

source of heat, and irrigation. Using temporary infrastructure to accomplish this objective can be costly and hinder reliable reproducibility of experiments. Stable, easily accessible infrastructure is paramount to reducing the cost and labor requirements for this research. To identify key varieties with resilience, engineers, computer scientists, physiologists, geneticists and molecular biologist must work together in order to quickly and accurately identify tolerance in order to relate these findings to breeding programs for future introgression of these traits. Utilizing these various disciplines will allow for further integration of traditional agronomics and advancements in technology based high-throughput plant phenotyping. These new technology-based methodologies will allow for the identification and standardization of sensor-based indices which will allow for easier and highly temporal measurements of complex physiological processes such as night respiration. Future climate warming scenarios do not look promising, but high night-time temperature resilient cereals can be identified, integrated, and distributed worldwide in order to prevent significant nutritional and yield losses due to increased stress from high night-time temperatures.

References

García, G., Dreccer, M.F., Miralles, D.J., Serrago, R.A., 2015. High night temperatures during grain number determination reduce wheat and barley grain yield: a field study. Global Change Biology 21, 4153-4164. https://www.doi.org/10.1111/gcb.13009

García, G., Serrago, R.A., Dreccer, F., Miralles, D.J., 2016. Post-anthesis warm nights reduce grain weight in field-grown wheat and barley. Field Crops Research 195, 50-59. https://www.doi.org/10.1016/j.fcr.2016.06.002

Hein, N.T., Wagner, D., Bheemanahalli, R., Šebela, D., Bustamante, C., Chiluwal, A., Neilsen, M.L., Jagadish, S.V.K., 2019. Integrating field-based heat tents and cyber-physical system technology to phenotype high night-time temperature impact on winter wheat. Plant Methods 15, 41. https://www.doi.org/10.1186/s13007-019-0424-x

Hein, N.T., Bheemanahalli, R., Wagner, D., et al., 2020. Improved cyber-physical system captured post-flowering high night temperature impact on yield and quality of field grown wheat. Scientific Reports 10, 22213. https://www.doi.org/10.1038/s41598-020-79179-0

Impa, S.M., Sunoj, V.S.J., Krassovskaya, I., Bheemanahalli, R., Obata, T., Jagadish, S.V.K., 2019. Carbon balance and source-sink metabolic changes in winter wheat exposed to high night-time temperature. Plant, Cell & Environment 42, 1233-1246. https://www.doi.org/10.1111/pce.13488

Impa, S.M., Vennapusa, A.R., Bheemanahalli, R., Šebela, D., Boyle, D., Walia, H., Jagadish, S.V.K., 2020. High night temperature induced changes in grain starch metabolism alters starch, protein, and lipid accumulation in winter wheat. Plant, Cell & Environment 43, 431-447. https://www.doi.org/10.1111/pce.13671

Lizana, X.C., Calderini, D.F., 2013. Yield and grain quality of wheat in response to increased temperatures at key periods for grain number and grain weight determination: considerations for the climatic change scenarios of Chile. The Journal of Agricultural Science 151, 209-221. https://www.doi.org/10.1017/S0021859612000639

Narayanan, S., Tamura, P.J., Roth, M.R., Prasad, P.V., Welti, R., 2016. Wheat leaf lipids during heat stress: I. High day and night temperatures result in major lipid alterations. Plant, Cell & Environment 39, 787-803. https://www.doi.org/10.1111/pce.12649

Peng, S., Huang, J., Sheehy, J.E., Laza, R.C., Visperas, R.M., Zhong, X., Centeno, G.S., Khush, G.S., Cassman, K.G., 2004. Rice yields decline with higher night temperature from global warming. Proceedings of the National Academy of Sciences 101, 9971-9975. https://www.doi.org/10.1073/pnas.0403720101

Prasad, P.V.V., Pisipati, S.R., Bukovnik, U., Fritz, A.K., 2008. Impact of nighttime temperature on physiology and growth of spring wheat. Crop Science 48, 2372–2380. https://www.doi.org/10.2135/cropsci2007.12.0717

Wang, Y., Tao, H., Zhang, P., Hou, X., Sheng, D., Tian, B., Wang, P., Huang, S., 2020. Reduction in seed set upon exposure to high night temperature during flowering in maize. Physiologia Plantarum 169, 73-82. https://www.doi.org/10.1111/ppl.13049

Appendix A - Chapter 2

Figures

Appendix A Figure - 1 Heat tent before and after end wall plastic application

Appendix A Figure - 2 Caterpillar XQ35 Generator and 3,785-liter diesel tank

Appendix A Figure - 3 Raspberry Pi touch screen display with interior and exterior temperature.

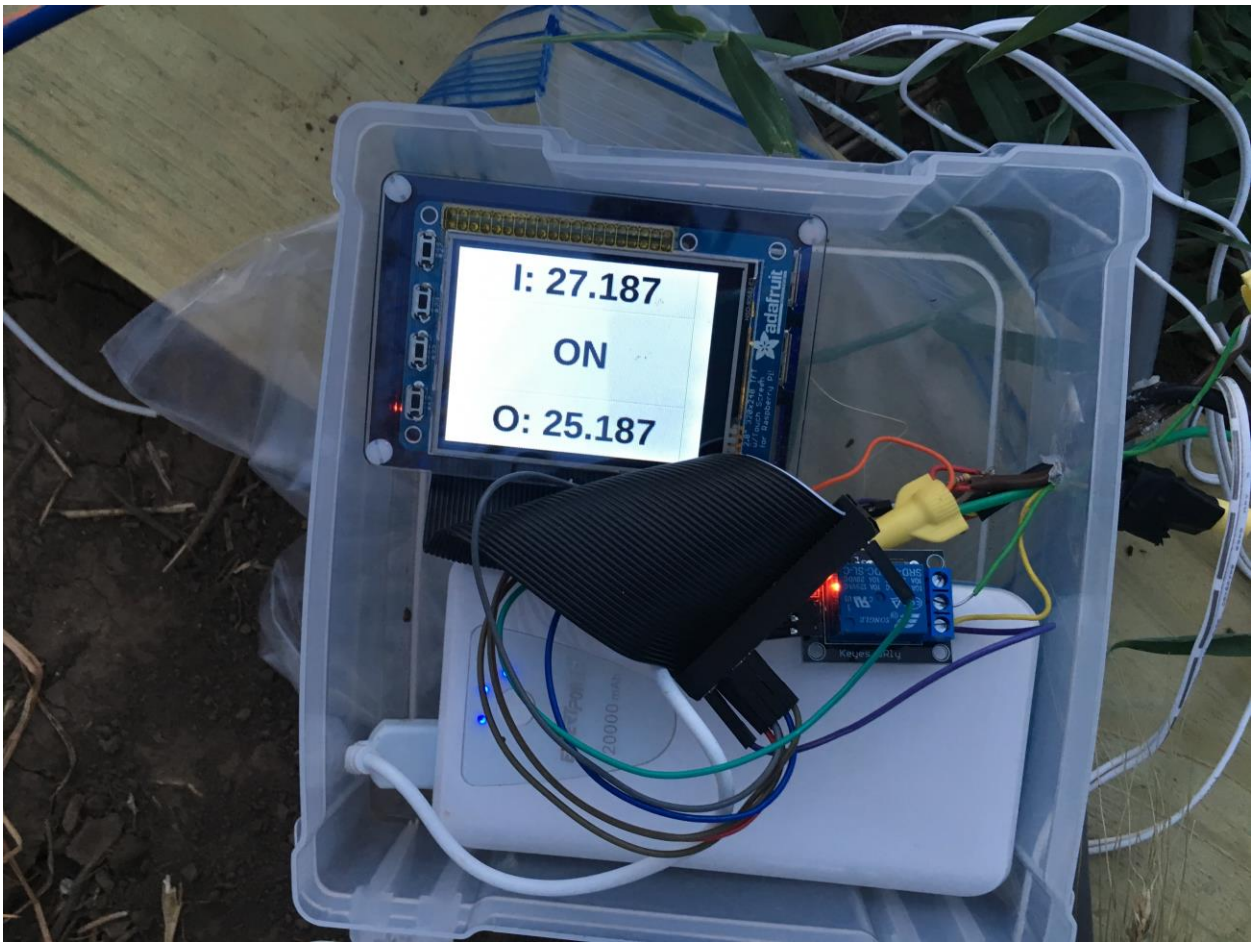

Tables

Appendix A Table - 1 Parts List and Cost per Tent

Pi System Components	Company	Description	Quantity	Unit Price	Total:
Raspberry Pi Model 3B	Adafuit	Central computer system for controllers	1	$ 35.00	$35.00
32GB MicroSD Card	Sandisk	Storage for system for logs, code	1	$9.99	$9.99
5V Solid State Relay	Keyes	Intermediate relay to power system	1	$2.69	$ 2.69
240V Relay	Funct.Devices	Connection from thermostat system to heater	1	$16.21	$16.21
24VAC Power Adapter	Lockstate	Power supply for 240V relay to allow switching	1	$16.00	$16.00
PiTFT Pibow+ Kit	Adafuit	Case for Pi systems (electrical components)	1	$19.95	$19.95
18/5 wiring, 500ft roll	Southwire	Sensor connections to Pi (5 leads)	1	$159.12	$159.12
DS18B20 sensor	Adafuit	Waterproof temperature sensor, two per tent	2	$9.95	$19.90
PiTFT touchscreen	Adafuit	Touchscreen display for Pi controllers	1	$34.95	$34.95
Essentials art box	ArtBin	6" x 6" storage box for waterproofing controllers	1	$4.99	$4.99
20k mAh Power Bank	ExpertPower	Power supply for Tent Systems for 24/7 runtime	1	$17.84	$17.84
Solder	Bernzomatic	Connects components together	1	$10.47	$10.47
Jumper wires	Alleu	Connects internal components	1	$6.49	$6.49
DS3231 RTC Breakout	Adafuit	Realtime clock for Pi system	1	$13.95	$13.95
CD1220 12mm battery	Adafruit	Power supply for DS3231 modules	1	$0.95	$0.95
Caulking	Hercules	Covers drilled hole in box for waterproof sealing	1	$4.19	$4.19

Heat Tent Components	Company	Description	Quantity	Unit Price	Total
Polyethylene Film	Sun Master	Greenhouse Film (Price per foot)	60	$3.98	$238.80
Wiggle Wire	Farmtek	Attaches plastic into lock channel (sold in 8' lengths)	32	$2.35	$75.20
Linear Actuator Motor	Venture Mfg	Open and closes top vent	2	$60.00	$120.00
12v VLRA Battery	MK Powered	Power storage for solar panel and motors	1	$27.99	$27.99
Temperature Control 4LZ95A	Dayton	Open and closes top vent	1	$165.00	$165.00
10' Treated 2"x6" Boards	Lumber Yard	Top and bottom of side roll up	10	$9.88	$98.80
10' 6'" Galvanized Poles	Home Depot	Bar plastic rolls up on for side roll up	5	$8.29	$41.45

#14 2-3/4 in. Phillips Flat-Head Self-Drilling Screw	Everbilt	Attaching wood to metal frame	1	$21.74	$21.74
#9 x 3 in. Star Flat-Head Wood Deck Screws	Deckmate	Attaching wood board to next wood board	1	$23.58	$23.58
#12 1 in. Hex-Head Self-Drilling Screws	Teks	Attaching lock channel and roll up bars together	2	$6.71	$13.42
#206 x 1-3/8 in. Zinc-Plated Steel Screw Eye	Everbilt	Attached Polypropylene Rope	24	$0.49	$11.76
1000' Polypropylene Rope	Farmtek	Keeps sideroll against building	1	$35.43	$35.43
1 3/8" Galvanized Elbows	TrueValue	Used to make right angle for handle	4	$2.99	$11.96
Ceiling-Mount Garage Heater	Thermosphere	Provided electrical Heat	1	$150.00	$150.00
18" Box Fan	Lasko	Moved air throughout the tent	1	$16.96	$16.96
16/3 Outdoor Extension Cord	HDX	Attached box fan to generator	1	$12.97	$12.97
10/2 UFB Wiring - 50'	Southwire	Attached heater to generator	1	$77.94	$77.94
Tank Top Portable Heater	Mr. Heater	Propane tank attachable heater	1	$39.99	$39.99
Concrete Blocks	Oldcastle	Raise propane tank above vegetation	6	$1.55	$9.30

*Cost of Generator, Diesel, and Propane will vary depending on number of systems. Cost: $1,564.98

**Must be sized according to total electrical load based on the number of systems.

Documents

Appendix A Document - 1 Python Script

Python code is available for download here.

Appendix B - Chapter 3

Figures

Appendix B Figure - 1 An illustration detailing individual components of the mobile field-based infrastructure.

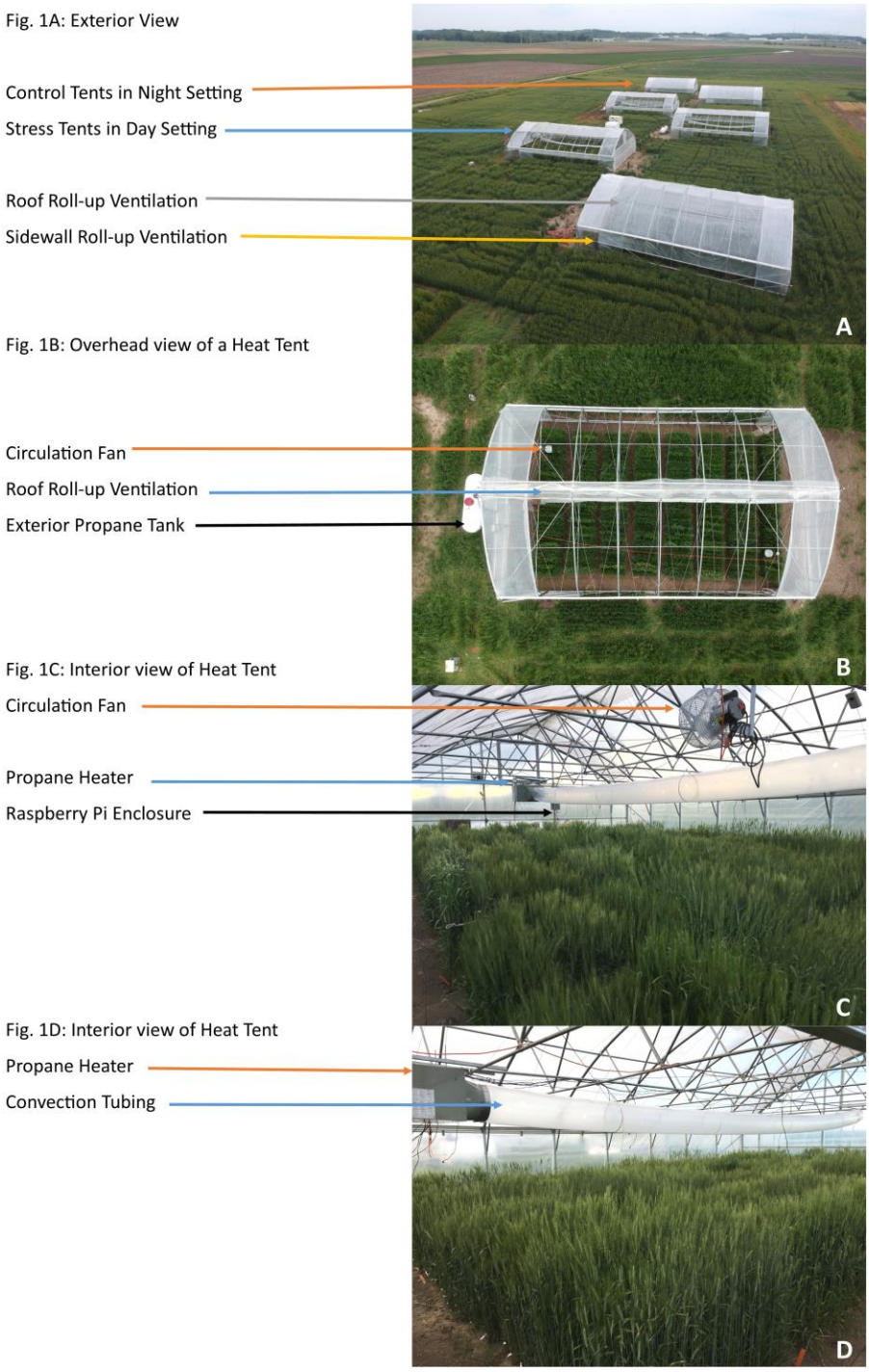

(A). Overhead view of field layout depicting the control tents in their night setting and the stress tents in day setting. Also visible is the roof roll-up ventilation and the sidewall roll-up ventilation systems. (B). Overhead view of stress tent with circulation fan, roof roll-up ventilation system and exterior propane tank. (C). Interior view of stress tent in its night setting looking towards the propane heater. Circulation fan, propane heater, and Raspberry Pi enclosure are visible. (D). Interior view of stress tent in its night setting looking opposite of the propane heater with the propane heater and convection tubing visible centrally located running the entire length of the stress tent.

Appendix B Figure - 2 The Raspberry Pi system for a control tent, stress tent, and its enclosure.

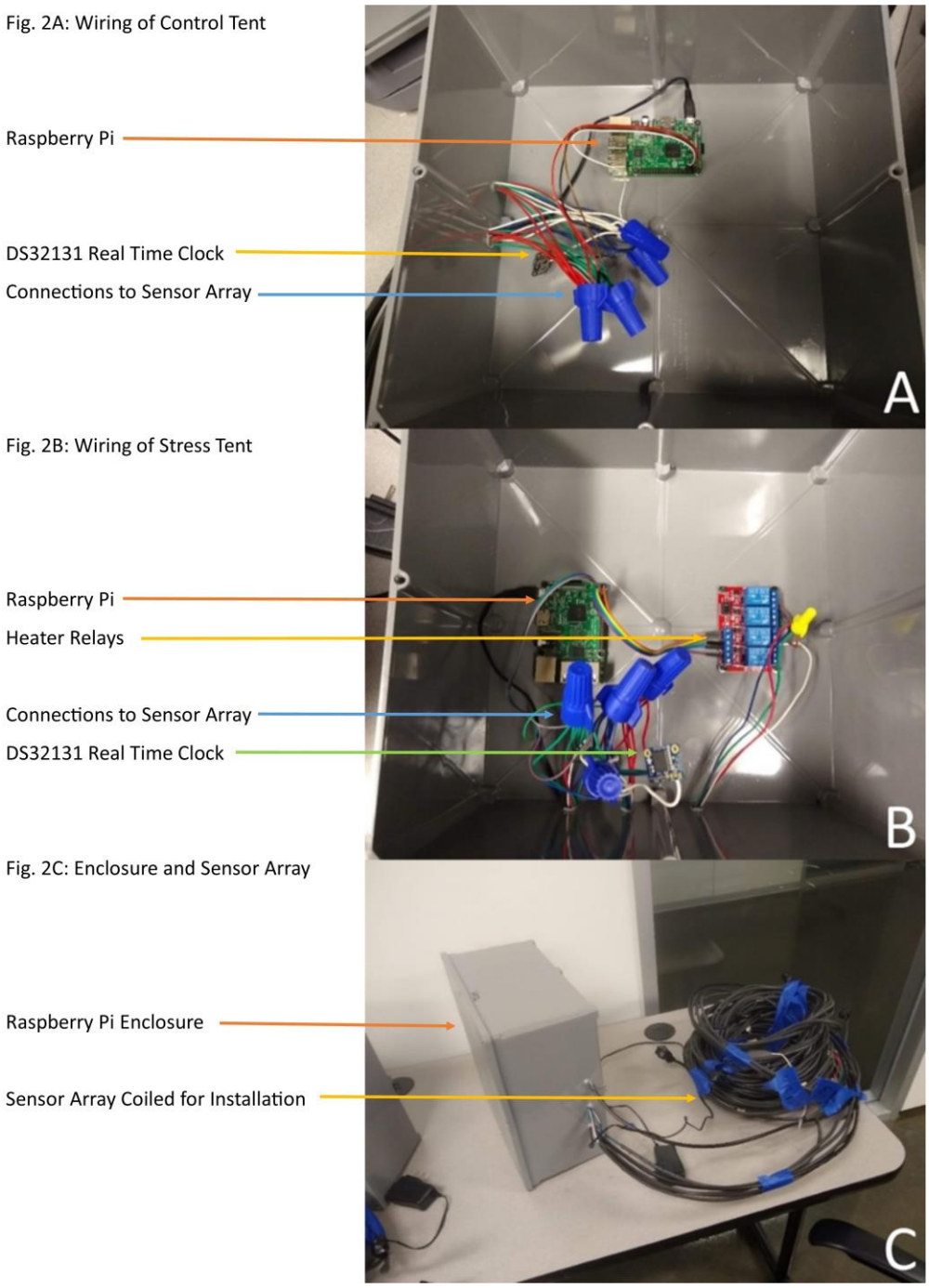

(A). A visual display of the enclosure for a Raspberry Pi system for a control tent. Enclosed is the Raspberry Pi itself, a DS32131 Real Time Clock and the connections between the Raspberry Pi and the six temperature sensor array. (B). The interior of an enclosure for a stress tent

consisted of a Raspberry Pi, the four relays used to control the propane heater, the connections to the six temperature sensor array, and a DS32131 Real Time Clock. (C). Exterior view of a Raspberry Pi enclosure with the six temperature sensor array coiled in preparation for installation. The enclosure and array were installed as seen and then the sensors uncoiled along the roof trusses into their predetermined positions (see Figure 3-2).

Appendix B Figure - 3 The set of four relays which were used to control the propane heater.

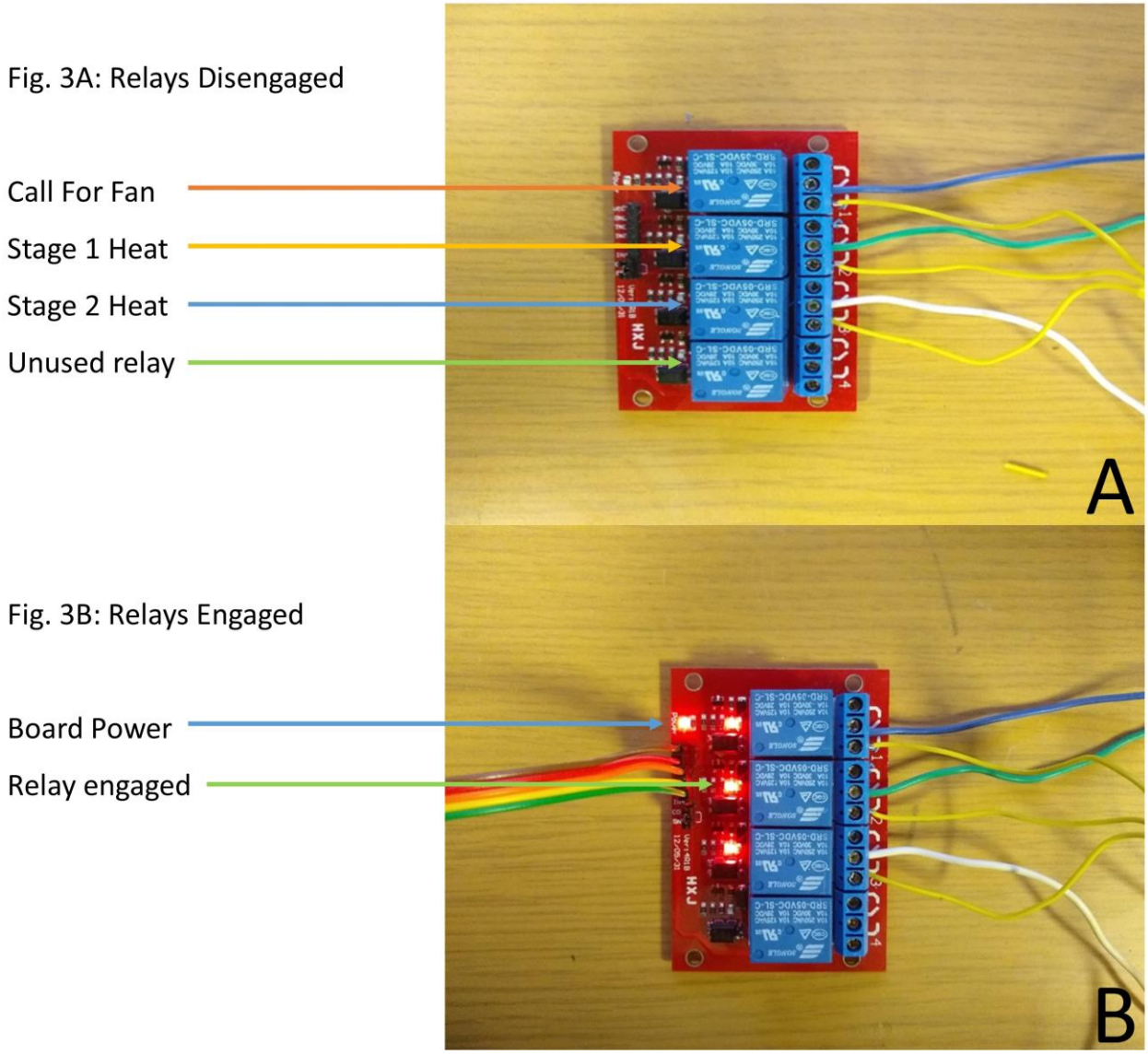

(A). Description of each of the three relays used and the unused relay indicated. The relays' NO ports were coalesced and connected to the 24VAC line off the heater, and the COM ports were connected to the G, W1, and W2 ports of the heater. (B). The relay board supplied with power as indicated by the Board Power light and the relays engaged indicated by the light next to each relay. This is the state of the relays to turn on stage 2 heating when the temperature differential was below the desired value for heat stress. The propane heater was able to function on three -

different settings; fan only (no heat), stage 1 heating (50%), and stage 2 heating (100%). After initial attempts to utilize both stage 1 heating and stage 2 heating, stage 1 heating was found to be insufficient to make a significant change within the tent and only stage 2 was used.

Appendix B Figure - 4 A system wiring diagram

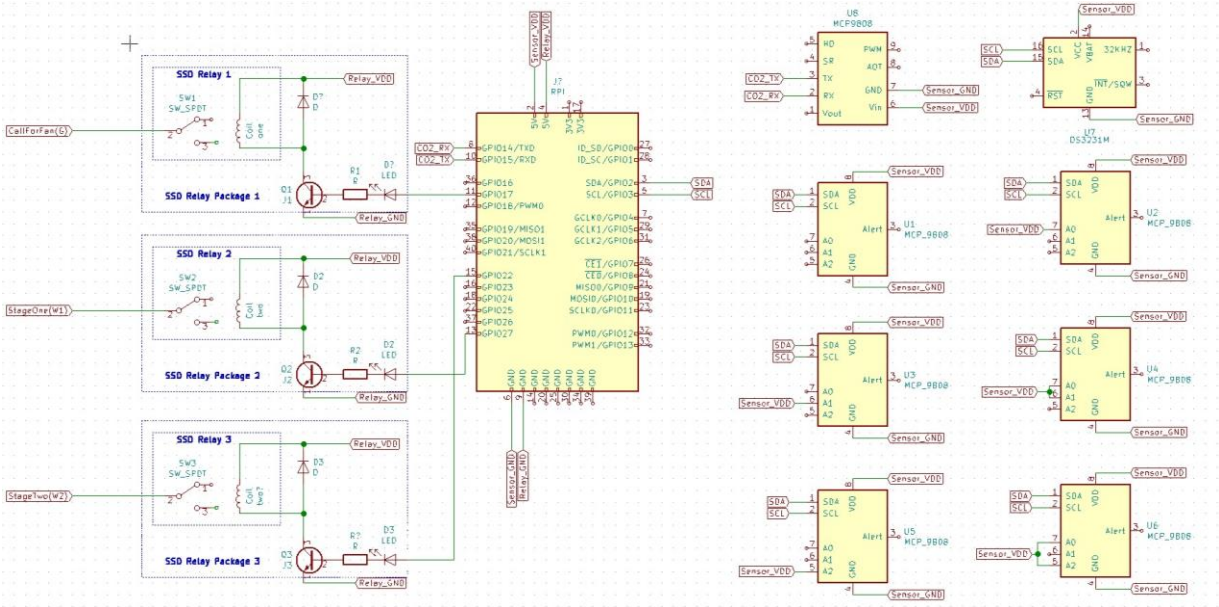

A system wiring diagram that connected the Raspberry Pi to the relays for the stress tents and to the temperature sensors, RTC module, and CO2 sensor for all tents. The Raspberry Pi can be seen in Appendix B Figure - 2 and the relays are seen in Appendix B Figure - 2 and 3. The Raspberry Pis were placed in both the control and stress tents and a diagram of their interactions can be seen in Figure 3-2.

Appendix B Figure - 5 Two classification methodologies compared

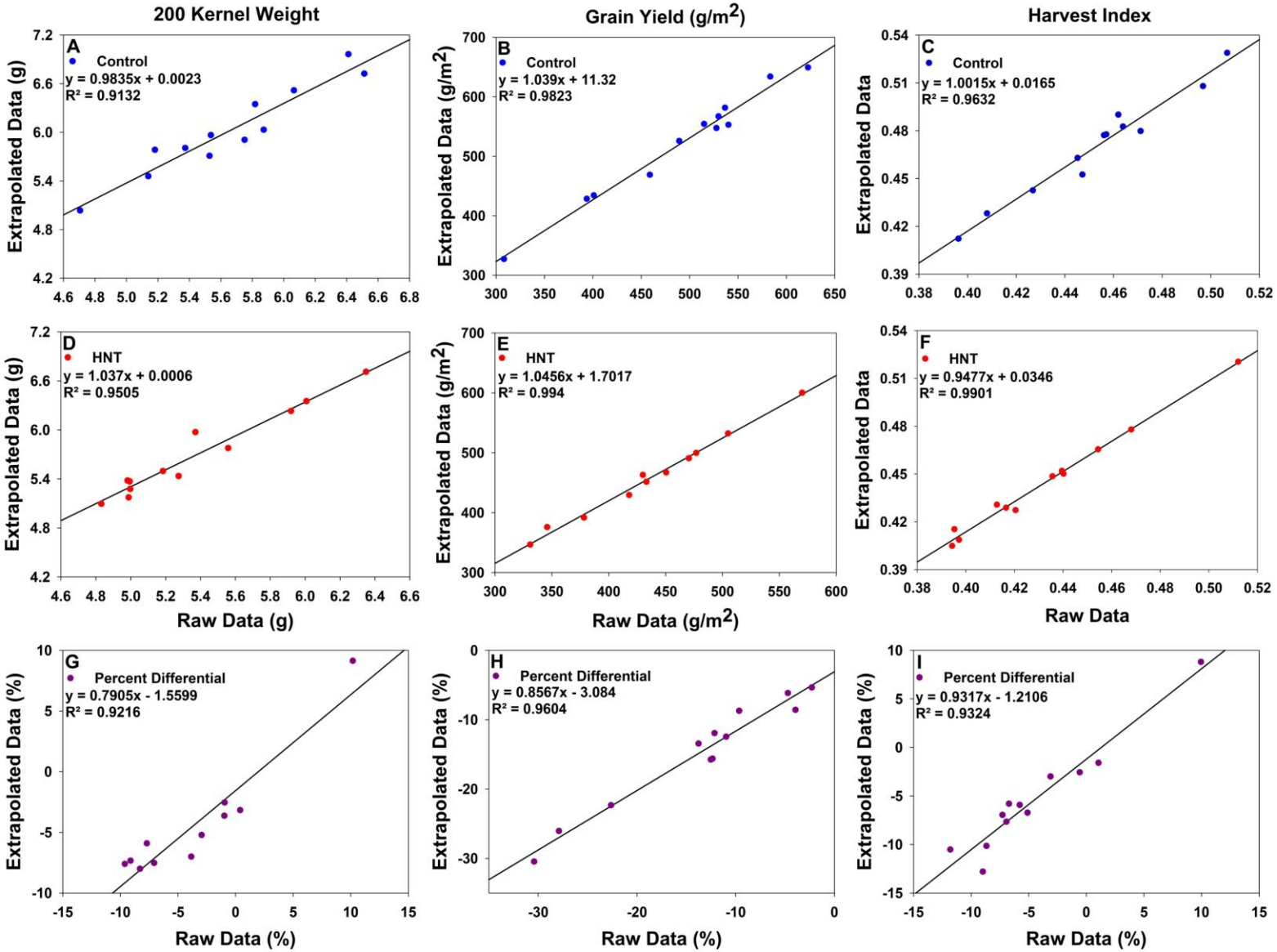

Two methods were compared to quantify the yield and yield components to ascertain the impact of Fusarium Head Blight. The seeds were separated into infected and non-infected categories and the agronomic parameters were extrapolated from the non-infected seed category. These results were then compared to the raw data results, which showed extremely high correlation between both methods and the non-categorized whole sample results were considered for all further analysis. Graphs A, B and C show the control data comparison for 200 kernel weight, grain yield and harvest index, respectively. Graphs D, E, and F show the HNT comparison for the 200 kernel weight, grain yield, and harvest index. While graphs G, H and I show the percent differential comparison for 200 kernel weight, grain yield, and harvest index, which compared the change in percentage between control and HNT.

Appendix B Figure - 6 Field Layout Diagram

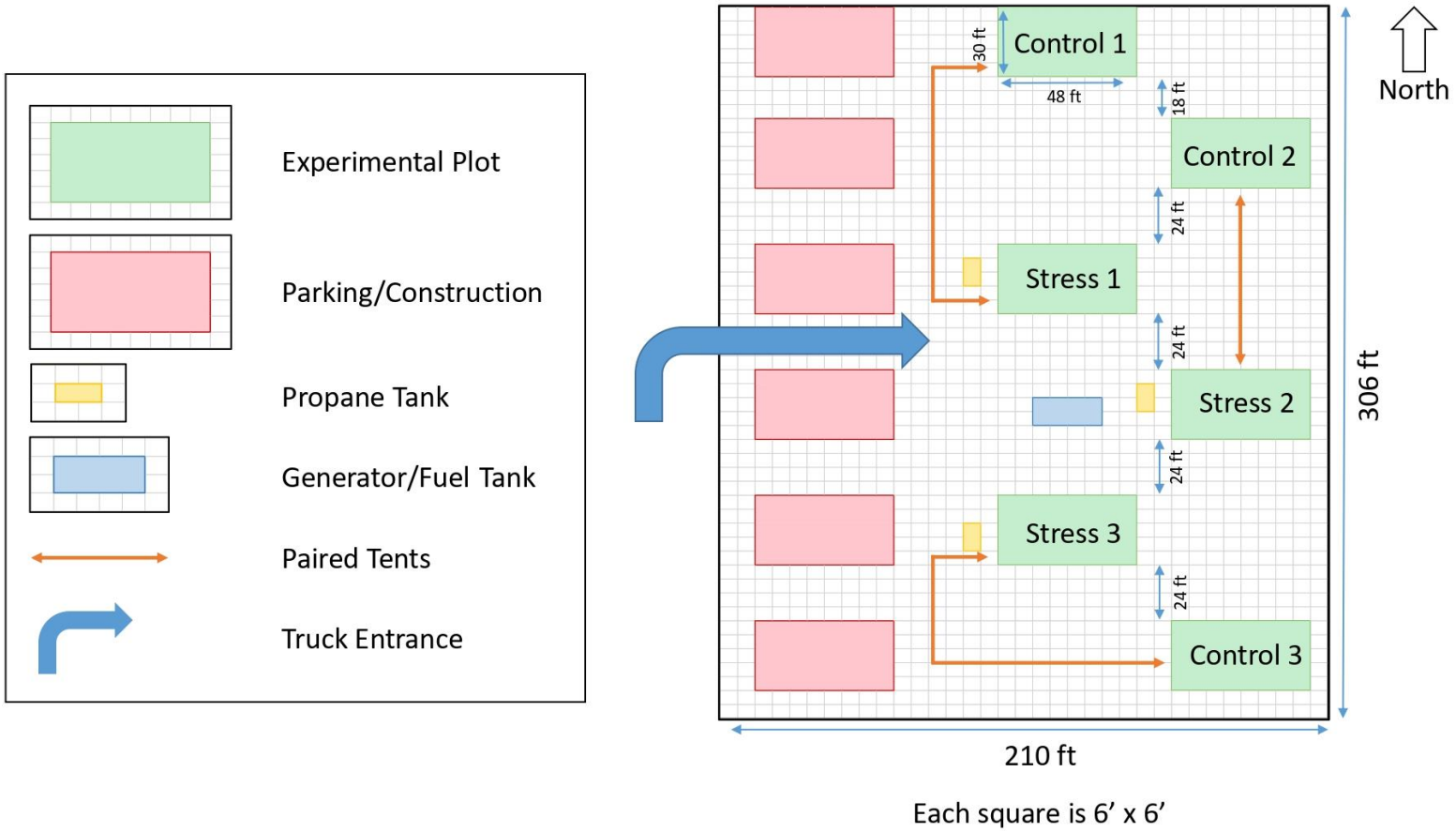

Diagram of field layout showing tents designated as control and stress tents. The field layout also shows the pairing of control and stress tents for the purposes of communication between the Raspberry Pi's between tents.

Appendix B Figure - 7 Seed number, biomass and harvest index.

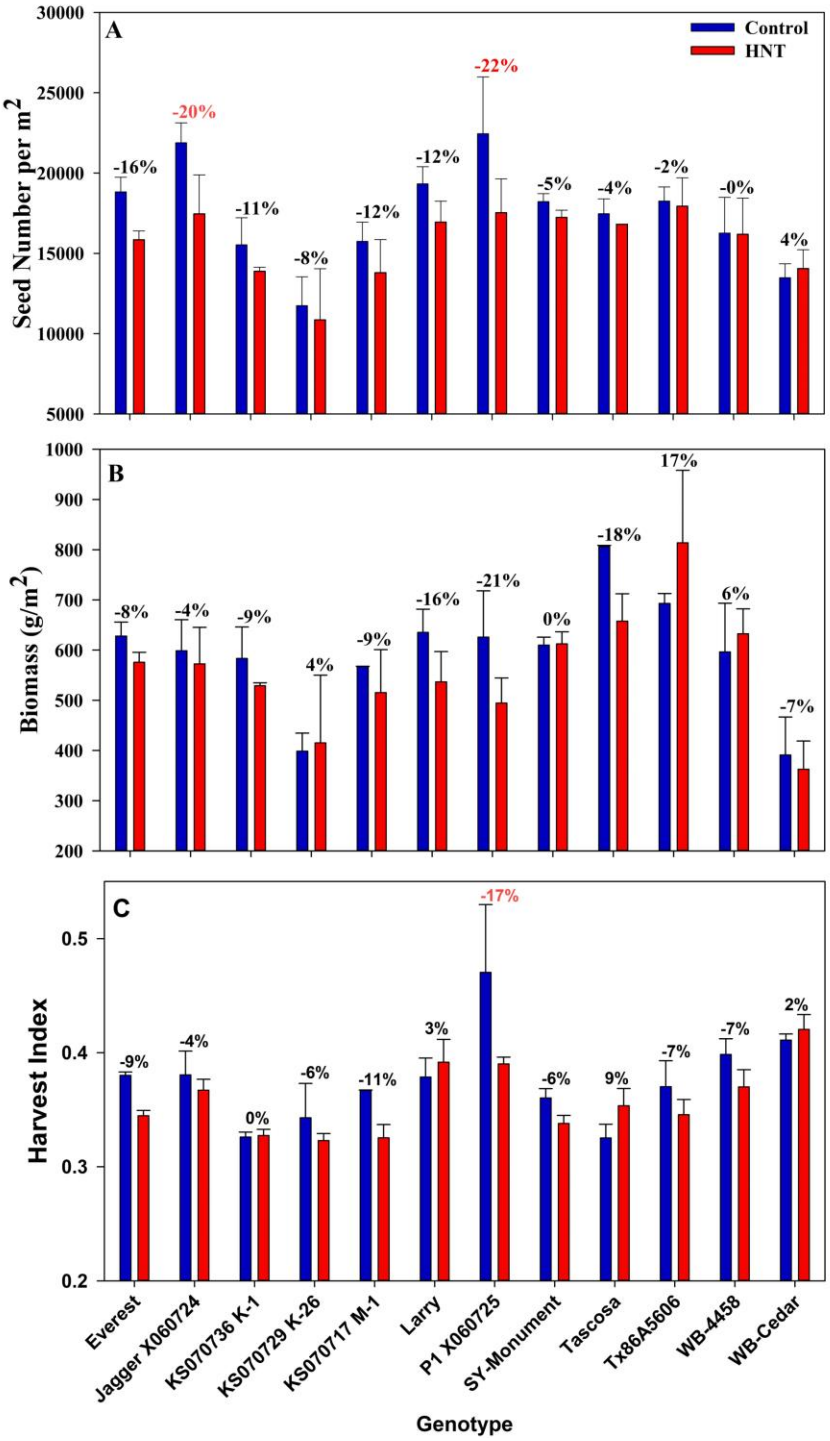

Seed number (A), biomass (B) and harvest index (C) in 12 winter wheat genotypes exposed to HNT stress and control conditions during the entire grain-filling period. Reductions in red signify a statistically significant reduction ($p < 0.05$).

Tables

Appendix B Table - 1 Part list for field-based HNT phenotyping infrastructure

Tents:

Qty.	Item	Link	Description
6	**30x48 Customizable Greenhouse**	https://www.smallfarmtools.com/	Our specific heat tents were custom designed. The company is very knowledgable with our project and their product and will help design heat tents to meet your needs.

Inside:

For One Control Tent:			
Qty.	**Item**	**Link**	**Description**
2	Circulation Fan	www.greenhousemegastore.com	12 inch. Use extra small pipe straps to hang under first truss in opposite corners of tent
4	Small Pipe Straps	Purchased from FST	Hangs Circulation fans from trusses
1	Power Tube Fan	www.greenhousemegastore.com	18 inch. Installed in front of and below the butterfly vent. Eyebolt comes out of top of fan (included) this eyebolt is placed just below the center purline.
2	Extra Square Steel	Extra square steel left over from build	installed standing vertically 24 inches apart underneath butterfly vent. Centered on the eyebolt of the fan's future placement
2	24 in Square Steel	www.homedepot.com	installed horizontally between the left over steel below butterfuly vent. Height is determined by fan placement so the fan can attach to end wall
8	Right angle Bracket	Purchased from FST	Used to install square steel to hang PTF
2 ft	14 gauge thnn wire	www.homedepot.com	Used to wire plug into PTF.
1	Female Plug	www.homedepot.com	Used to be able to connect PTF to electricity
3	Wire Connectors	www.homedepot.com	Used to connect wires to 14 ga thnn. A little bigger then the ones on the heat tent list. (30 pack)

45 ft	Convection Tubing	https://www.agriculturesolutions.com/	Call this company before you order to specify the fan size and length of run so they can punch the holes appropriately. Holes punched at 3 and 9 o'clock
6	Convection Tube Hangars	https://www.agriculturesolutions.com/	Must be trimmed down. Hang on wire rope strung just under the center purline
1	50' extension cord	www.homedepot.com	Connects the far circulation fan to the 3 outlet power hub for power to circulation fan
2	25' extension cord	www.homedepot.com	connects the Pi system and the other one connects the closer circulation fan.
1	3 Outlet Power Hub	www.homedepot.com	Takes power from outside and distributes it to circulation fans and Pi
10 ft	Wire Rope	Extra from FST build	Used to hang PTF from roof purlin. I just used excess leftover from our cross bracing.
50 ft	Wire Rope	www.homedepot.com	Hung underneath the center purline starting just after the PTF and ending at the other endwall
3	Turnbuckles	www.homedepot.com	Used to hang wire rope. 2 for the convection tubing and one for hanging the PTF.
12	Wire Clamp	www.homedepot.com	To tighten wire rope. 3 on each end. (purchase four of these packs to have enough clamps and thimbles for one tent.
4	Wire Thimble	www.homedepot.com	(FST Wire Clamps are better cause you can use a drill to tighten them, but these work too just have to use a wrench.)
3	Small Brace Bands	Extra from FST build	Used to connect Turnbuckles to purlins.
3	Carriage Bolts and Lock Nuts	Extra from FST build	Used to connect Turnbuckles to purlins.
Lots	Zip Ties of Various Length	www.homedepot.com	Very useful to control electrical cords and keep them in safe positions.
For One Heat Tent:			
Qty.	**Item**	**Link**	**Description**

2	Circulation Fan	www.greenhousemegastore.com	12 inch. Use extra small pipe straps to hang under first truss in opposite corners of tent
1	HDB100 Modine Propane Heater	www.greenhousemegastore.com	This is just a link to show the heater. I purchased the heater directly through Modine sales rep and a local provider. Definitely suggest finding a reliable HVAC guy locally that you can trust to ask questions if something goes wrong.
2	3/8 in Threaded Rod	www.homedepot.com	Used to hang the heaters
12	3/8 in nut	www.homedepot.com	Need 12 for the tent. Link is for a bag of 25. Enough to do two tents.
12	3/8 in lock washer	www.homedepot.com	Need 12 for the tent. Link is for a 3 pack. Would need 4 of 3 packs for a single tent.
12	5/16 in flat washer	www.homedepot.com	Need 12 for the tent. Link is for a bag of 25. Enough to do two tents.
2	7 ft square steel	Purchased from FST	Spans the endwall and first truss to hang heater from
2	Small Pipe Straps	Purchased from FST	Attaches square steel to first truss. Square steel lays on top of truss cross bar
1	54191 Discharge Transition	Purchased from Modine.	Purchased from Modine. No website for it. Transitions the square heater to round for tubing.
2	Right angle Bracket	Purchased from FST	Used to install square steel to end wall to hang heaters from. Underneat the butterfly vent
2 ft	14 gauge thnn wire	www.homedepot.com	Used to wire plug into PTF.
1	Female Plug	www.homedepot.com	Used to be able to connect Heater to electricity
3	Wire Connectors	www.homedepot.com	Bag of 30. Only need three per tent to connect 14 ga thnn to heater to run the plug outside the heater.
45 ft	Convection Tubing	www.agriculturesolutions.com	Call this company before you order to specify the heater size and length of run so they can punch the holes appropriately. Holes punched at 3 and 9 o'clock
6	Convection Tube Hangars	www.agriculturesolutions.com	Must be trimmed down. Hang on wire rope strung just under the center purline

50 ft	Wire Rope	www.homedepot.com	Hung underneath the center purline starting at the end of the duct transition and ending at the other endwall
2	Turnbuckles	www.homedepot.com	Used to hang wire rope. 2 for the convection tubing and one for hanging the PTF.
6	Wire Clamp	www.homedepot.com	To tighten wire rope. 3 on each end. (purchase two of these packs to have enough clamps and thimbles for one tent.
2	Wire Thimble	www.homedepot.com	(FST Wire Clamps are better cause you can use a drill to tighten them, but these work too just have to use a wrench.)
2	Small Brace Bands	Extra from FST build	Used to connect Turnbuckles to purlins.
2	Carriage Bolts and Lock Nuts	Extra from FST build	Used to connect Turnbuckles to purlins.
3	4" Type B Vent Pipe 12" Length	https://www.mtlfab.com/	Pipe used to exhaust the heaters out of the tent.
3	4" Type B Vent 90 Deg Elbow	https://www.mtlfab.com/	Pipe used to exhaust the heaters out of the tent.
1	4" Type B Vent Pipe 24" Length	https://www.mtlfab.com/	Pipe used to exhaust the heaters out of the tent.
1	4" Type B Vent Pipe 36" Length	https://www.mtlfab.com/	Pipe used to exhaust the heaters out of the tent.
2	4" Type B Vent Firestop	https://www.mtlfab.com/	Pipe used to exhaust the heaters out of the tent.
1	4" High Perform Vent Cap	https://www.mtlfab.com/	Pipe used to exhaust the heaters out of the tent.
1	3 Outlet Power Hub	www.homedepot.com	Takes power from outside and distributes it to circulation fans and Pi
1	50' extension cord	www.homedepot.com	Connects the far circulation fan to the 3 outlet power hub for power to circulation fan
2	25' extension cord	www.homedepot.com	connects the Pi system and the other one connects the closer circulation fan.
1	6' x 8' Tarp	www.homedepot.com	Used to cover heater during the day in case of rain. (extra precaution to protect electrical. Not necessary except for when chance of rains and must be removed before operation of heater
6 ft	Rope	Left over from side wall rope walls	Used to tie four corners together under the heater so tarp doesn't blow off during the day.

Misc. Items			
Qty.	**Item**	**Link**	**Description**
1	Wire strippers	www.homedepot.com	Strip Wires to install plugs and electrical
1	Tek #12 1 inch screws	www.homedepot.com	Only needed if you run out of screws from building the structures
1	1/4 in and 3/8 in drill bit	www.homedepot.com	For drilling through square steel to push the threaded rods through and hang heaters
1	Tape	www.homedepot.com	Used around the duct transition on the heater and the PTF.
1	Electrical Tape	www.homedepot.com	Nice to have when doing electrical however its not specifically used. Is used in the pi system though so good to have.
1	Aluminum Tape	Extra from FST build	Used for heater exhaust duct work
Outside Items			
Qty.	**Item**	**Link**	**Description**
1	XQ30 Caterpillar Generator	http://www.foleyeq.com/	Should be a local Cat rental place that can get their hands on the generator. Doesn't have to be exact model but has to be able to cover the power needs and have enough outlets of various kinds to run electricity.
2	50 Amp Spider Boxes	www.homedepot.com	Rented these boxes as well from the Cat rental
2	50 Amp generator cords	www.homedepot.com	Also rented these cords from the Cat dealer. They run from the back of the generator to the spider box. Number of cords will vary depending on field layout.

1	1000 Gallon Diesel Tank		Rented from local diesel supply company. Amount of diesel you fill the tank with will be determined by the total number of hours the generator will be running for your stress period times the amount of fuel required at 100% load per hour and then add on some extra fuel on top to make sure you have enough. We did it this way because our diesel guys are very nice and willing to come back out at the end of stress and suck out the left over diesel and give us a refund on it (minus a very small fee).
1	12 volt battery	www.homedepot.com	Our diesel tank has a battery powered motor to run the pump to move the diesel into the generator. Normal conditions I would pull my truck up and attach to that, but if its wet and I can't get the truck in, I use one of these.
3	Propane Tanks		Rented from local propane provider for a very small fee.
	Propane		Calculated by heater use per hour of propane times number of hours stress will be occuring to get over consumption need. Added extra on top just to make sure we don't run out.
	Propane Connections		My propane guys ran the copper to the heaters for me and pressure tested the heaters. They dropped the tanks, ran the lines to the heater, filled the tanks, and tested to make sure the propane was flowing.
Electrical Cords:			**Max Amps for Extension cords by size and length:**

	25/50 ft	100 ft	150 ft	200 ft
16 ga	13	10	X	X
14 ga	15	13	7	X
12 ga	20	15	10	8
10 ga	20	20	15	10

Electrical cords are hard for me to tell you exactly what to purchase because it comes down to a few factors that have to line up properly. First, the outlets on the spider boxes are gfci outlets with a 20 amp breaker which means the total amperage plugged into the top and bottom positions on the outlet can not exceed 20 amps. There are 4 or 5 gfci outlets on the spider boxes I use, so there are plenty of spots to plug into without going over the 20 amps. Also the box itself is a 50 amp box which means that the total of all inputs into the box can not exceed 50 amps. With the right layout this is more than enough to cover 2 tents and then some.

The size of the cord you need to run depends on the amount of amperage and distance of the cord.

The way our tents are set up is that the pi system and both fans run to the three prong power hub and that hub is plugged into an extension cord which runs to the spider box. The heaters and PTFs are ran on their own extension cord so each tent has two cords running to the spider boxes.

Heated Tent:	
	Amps:
HDB100:	12.1
VBG12 Fan:	1.5
VBG12 Fan:	1.5
Pi System	2
Total:	17.1
Control Tent:	
	Amps:
Power Tube Fan	7.2
VBG12 Fan:	1.5
VBG12 Fan:	1.5
Pi System	2
Total:	12.2

Technically the control tents can all be run on the same line to the spider box. At 12.2 amps normal draw you would need to use a minimium 14 ga extension cord for a 50 ft run (I would probably do 12 ga to be extra protected) and then a minimum 12 ga for the 100 ft run (again, though, thats close in amps so I'd go up to 10 ga to be protected). Once you get to that level of cords it can be extremely pricey. The other option is to split the load up. The PTF ran by itself is only 7.2 amps so it can be covered up to 100 ft with a 16 ga extension cord. The rest of the system can also be run off another 100 ft 16 ga extension cord. (100 ft 16 ga extension cord is 16 dollars at home depot. So having two of them would only cost 32 while a 12 ga 100 ft run costs 84 dollars. Thats a savings of 50 bucks by just splitting the power up.

For the heated tents I absolutely and completely suggest seperating the power. This will allow you to use a much cheaper 16 ga cord for the fans and pi system, and then allow you to use the smallest size extension cord that's safe for the heater. For the heater at 12.1 amps for a 50 ft run you can get by with a 14 ga cord but if you have to go to 100 then you have to upgrade to 12 ga.

This all is most easily done by just drawing out the layout of the field and start connecting the dots while ensuring the extension cords can handle the amperages from the load, the outlets on the spider boxes don't exceed 20 amps, and the spider boxes themselves do not exceed 50 amps. The generator itself will have at least 2 more 20 amp outlets on it as well so if the generator is well positioned it can handle most of two tents as well.

16 ga	25	www.homedepot.com
	50	www.homedepot.com
	100	www.homedepot.com
14 ga	25	www.homedepot.com
	50	www.homedepot.com
	100	www.homedepot.com
12 ga	25	www.homedepot.com
	50	www.homedepot.com
	100	www.homedepot.com
10 ga	25	www.homedepot.com
	50	www.homedepot.com
	100	www.homedepot.com

	25/50 ft	100 ft	150 ft	200 ft
16 ga	13	10	X	X
14 ga	15	13	7	X
12 ga	20	15	10	8
10 ga	20	20	15	10

Appendix B Table - 2 Components of the Raspberry Pi system, cost and links to their availability

Component	Description	Unit Price	Quantity	Total Cost	URL
Raspberry Pi Model 3B	Central computer system for controllers	$35.00	1	$35.00	https://www.adafruit.com/
32GB MicroSD Card	Storage for system for logs, code	$9.99	1	$9.99	https://www.amazon.com/
5V Solid State Relay	Intermediate relay to power system	$2.69	1	$2.69	https://www.amazon.com/
5V, 2.5A Power Adapter	Power supply for Pi	$7.95	1	$7.95	https://www.sparkfun.com/
12" Junction Box	Protective enclosure for whole controller system	$34.61	1	$34.61	https://www.menards.com/
18/5 wiring, 500ft roll	Sensor connections to Pi (6 leads)	$159.12	1	$159.12	https://www.homedepot.com/
MCP9809 Temp Sensor	High accuracy sensor to read temperature of tents	$4.95	6	$29.70	https://www.adafruit.com/
MH-Z19 Carbon Dixoide Sensor	Records carbon dioxide at +/- 50 ppm	$19.99	1	$19.99	https://www.winsen-sensor.com/
Solder	Connects components together	$10.47	1	$10.47	https://www.homedepot.com/
Jumper wires	Connects internal components	$6.49	2	$12.98	https://www.amazon.com/
DS3231 RTC breakout	Real-time clock for accurate Pi timing	$13.95	1	$13.95	https://www.adafruit.com/
Silicon caulking	Highly water resistant seal for MCP9809s	$3.98	1	$3.98	https://www.menards.com/
Electrical tape	Used to help with sensor water resistance	$1.97	1	$1.97	https://www.homedepot.com/
CR1220 battery	Power supply for DS3231	$0.95	1	$0.95	https://www.adafruit.com/
M3-0.5 x 20mm screw (3pk)	Secures Pi to the enclosure	$0.70	2	$1.40	https://www.homedepot.com/
Flat washer (5pk)	Secures Pi to the enclosure	$0.62	1	$0.62	https://www.homedepot.com/
Hex nut (5pk)	Secures Pi to the enclosure	$0.98	1	$0.98	https://www.homedepot.com/
				$346.35	

Appendix B Table - 3 Experiment Environmental Conditions

Hour	Heat	STDev Heat	Control	STDev Cont	Temp N	Diff	Diff N	STD Sens	STD Sens N	Stress CO2	Stress CO2 N	Control CO2	Control CO2 N
0	21.91	3.71	18.15	3.90	25440	3.77	5460	0.58	5460	541.13	2220	545.21	8866
1	21.50	3.90	17.73	4.07	25440	3.77	5460	0.63	5460	557.10	2220	552.37	8781
2	21.22	3.94	17.40	4.14	25440	3.84	5460	0.60	5460	564.54	2220	554.62	8676
3	20.78	3.95	16.96	4.07	25080	3.83	5400	0.60	5400	559.26	2220	559.31	8507
4	20.34	3.87	16.54	4.05	24720	3.81	5340	0.60	5340	565.45	2220	569.70	8435
5	20.10	3.66	16.27	3.84	24960	3.83	5400	0.59	5400	563.01	2220	576.65	8253
20	26.21	3.41	22.77	3.59	25080	3.50	5400	0.65	5400	457.12	2160	480.26	9373
21	23.82	3.44	20.08	3.57	25680	3.75	5460	0.59	5460	509.76	2220	527.64	9146
22	22.95	3.52	19.14	3.66	25680	3.82	5460	0.57	5460	525.94	2220	538.97	8786
23	22.41	3.58	18.59	3.77	25680	3.82	5400	0.55	5400	538.08	2220	542.68	8852
AVG:	22.13	3.70	18.37	3.87	253200	3.77	54240	0.60	54240	538.36	22140	543.89	87675

Appendix B Table - 4 ANOVA results in groupings based on the least significant difference at a 95% confidence interval for all tents and Everest check line divided into two groups within each tent for 200 kernel weight, grain yield, and harvest index.

	200 Kernel Weight	Grain Yield (g/m^2)	Harvest Index
Control 1.1	ab	abc	ab
Control 1.2	a	cd	ab
Control 2.1	ab	ab	ab
Control 2.2	abc	a	ab
Control 3.1	abc	ab	abc
Control 3.2	abc	a	ab
Stress 1.1	bcd	cd	abcd
Stress 1.2	bcde	d	d
Stress 2.1	de	cd	d
Stress 2.2	e	cd	cd
Stress 3.1	de	abc	d
Stress 3.2	cde	bc	bcd
LSD	0.418	108.58	0.027
Groupings based on LSD at a 95% Confidence Interval			

Appendix B Table - 5 Seedling emergence and vigor post-HNT stress. Different alphabets indicate significant differences between control and HNT at P<0.05.

	Emergence Index			Emergence (%)			Total Biomass (g)		
Genotype	CNT	HNT	% Difference	CNT	HNT	% Difference	CNT	HNT	% Difference
Everest	3.80	4.16	9.46	87.50	83.33	-4.76	62.63	56.16	-10.33
Jagger X060724	4.18	4.86	16.17	91.67	87.50	-4.55	58.37[a]	45.07[b]	-22.79
KS 070736 K-1	3.94	4.21	6.71	79.17	79.17	0.00	59.43	54.25	-8.72
KS 070729 K-26	4.25	4.98	17.09	95.83	81.25	-15.22	53.67	58.46	8.92
KS 070717 M-1	4.56	4.69	2.77	95.83	79.17	-17.39	54.56	52.87	-3.10
Larry	4.29	5.31	23.81	91.67	70.83	-22.73	56.79	45.11	-20.56
P1 X060725	4.65	5.33	14.54	91.67	87.50	-4.55	56.75[a]	44.05[b]	-22.38
SY-Monument	4.48	4.77	6.65	87.50	95.83	9.52	53.81	53.32	-0.91
Tascosa	5.15	4.51	-12.43	81.25	91.67	12.82	50.06	56.38	12.62
Tx86A5606	4.71	4.33	-7.96	87.50	100.00	14.29	52.90	64.60	22.12
WB 4458	4.61	4.89	6.07	75.00	79.17	5.56	58.57	52.49	-10.38
WB-Cedar	4.61	4.19	-9.23	95.83	68.75	-28.26	57.63	45.53	-20.99
Overall Average	4.44	4.69	5.61	88.37	83.68	-5.30	56.26[a]	52.36[b]	-6.94

Documents

Appendix B Document – 1 Cyber-physical System Review

Hardware Components and Connections

The relays required five wires to run: 5V power, ground, and an input signal for each relay; when raised high high, this signal completed the heater circuit on the control board and facilitated the heater's operation. These wires were connected to the Pi on the following pins using the board's physical numbering scheme:

- Pin 4 provided 5V power.
- Pin 9 provided ground.
- Pin 11 provided the first relay's input signal.
- Pin 15 provided the second relay's input signal.
- Pin 13 provided the third relay's input signal.

Each of the MCP9808s and the RTC required four lines: 5V power, ground, data (SDA), and clock (SCL). All six MCP9808 and the RTC were wired in parallel; the MCP9808s were interfaced with individually by connecting a combination of three address pins to 5V power. The MCP9808s were placed throughout each tent by using 18-gauge, 4 conductor sprinkler wire for waterproofing. Each sensor's wires were consolidated, and then connected to the physical pins on the Pi:

- Pin 2 provided 5V power.
- Pin 6 provided ground.
- Pin 3 provided the SDA signal.
- Pin 5 provided the SCL signal.

The relays were connected to the heater's internal control board via the normally open (NO) and common (COM) ports. Each NO port was connected to the heater's 24VAC line as the

COM ports were grounded in the relays. The COM ports were used for each of the signal lines: call for fan (G), stage one heat (W1), and stage two heat (W2); first stage heat required both G and W1 to be connected to 24VAC while second stage heat required all three signal lines to be connected to 24VAC.

The MH-Z19 sensor also required four lines: 5V power, ground, transmit (TX), and receive (RX). The sensor ran on the Universal Asynchronous Receiver/Transmitter (UART) protocol and connected to the physical pins on the Pi like below:

- Pin 2 provided 5V power.
- Pin 6 provided ground.
- Pin 8 provided the RX signal.
- Pin 10 provided the TX signal.

Software Description

The code was written in Python version 2.7 due to its simplicity, familiarity, and availability of software libraries for the system's sensors. The software exists as four scripts: main.py, sensor.py, heatcontroller.py, and controlcontroller.py; the latter two are for heat or control tents, respectively. When the Pi received power, it booted up and immediately began initializing the system. First, the system detected the type of sensor connected *via* the constructor passed into the controller; this is a user-defined interface to the sensor that is employed in their thermostat controller system. Next, it started up the associated controller depending on whether it is located inside a heat or control tent. Finally, the controller initialized the sensor data, system heath logging, reboot counter, and input/output error files for use in the code: these correlate to logging and debugging information used to collect data and handle system faults.

After all system initialization was performed, the main loop was entered. This loop calibrated the CO_2 sensor by zeroing out the scale. After calibration, it detected all MCP9808s that were connected to the system by polling the I2C bus and recording each unique address; all I2C addresses were, by design, assumed to be for the temperature sensors and must be specified via a list if they are reserved and should not be used for sensor readings. Then, the system attempted to connect to each detected MCP9808 for its temperature reading; if a read error occurred, then the error counter was incremented and compared against the maximum allowable number of errors to determine if a reboot was necessary. If a reboot was required, then the error counter was reset, and the system rebooted to fix the sensor error. However, if the maximum allowable reboots were reached, then the system remained on to maintain the stress period: for control tents, this kept them online for the heat tents to retrieve their outdoor temperature from; for heat tents, this allowed the tent to continue exhibiting heat stress onto the wheat. The number of allowable errors and reboots were recorded to file as a state-saving mechanism to ensure that the system remained in a consistent, controllable state: these were read upon system startup and after reboot. After errors were handled, the connected temperature sensors' readings were recorded to the sensor data CSV file on the Pi's storage medium. In the heat tents, the readings were averaged and compared to a 4 °C threshold to determine if the heater should be enabled; it wirelessly retrieved the outdoor temperature from its assigned control tent. If the difference between the indoor and the retrieved outdoor temperatures fell below this threshold, then the system engaged the heater in stage two heat ; stage one heat proved ineffective in maintaining the desired temperature. Meanwhile, the control tents logged their detected temperatures as the outdoor temperature for the heat tents to wirelessly retrieve. Finally, the system slept in a low-power state until the next read interval; by default, this value was set to one minute.

Each step was logged to the system health file for troubleshooting and archival purposes. Any errors that occurred were recorded, as well as the average indoor temperatures for the heat tent and the outdoor retrieved temperature. The main use of this file was to ensure that the system was functioning as intended; if a malfunction occurred, then the file helped isolate and reduce the time required for a technician to solve the problem.

Python code is available for download here.

Appendix C - Chapter 4

Figures

Appendix C Figure - 1 Heating system layout.

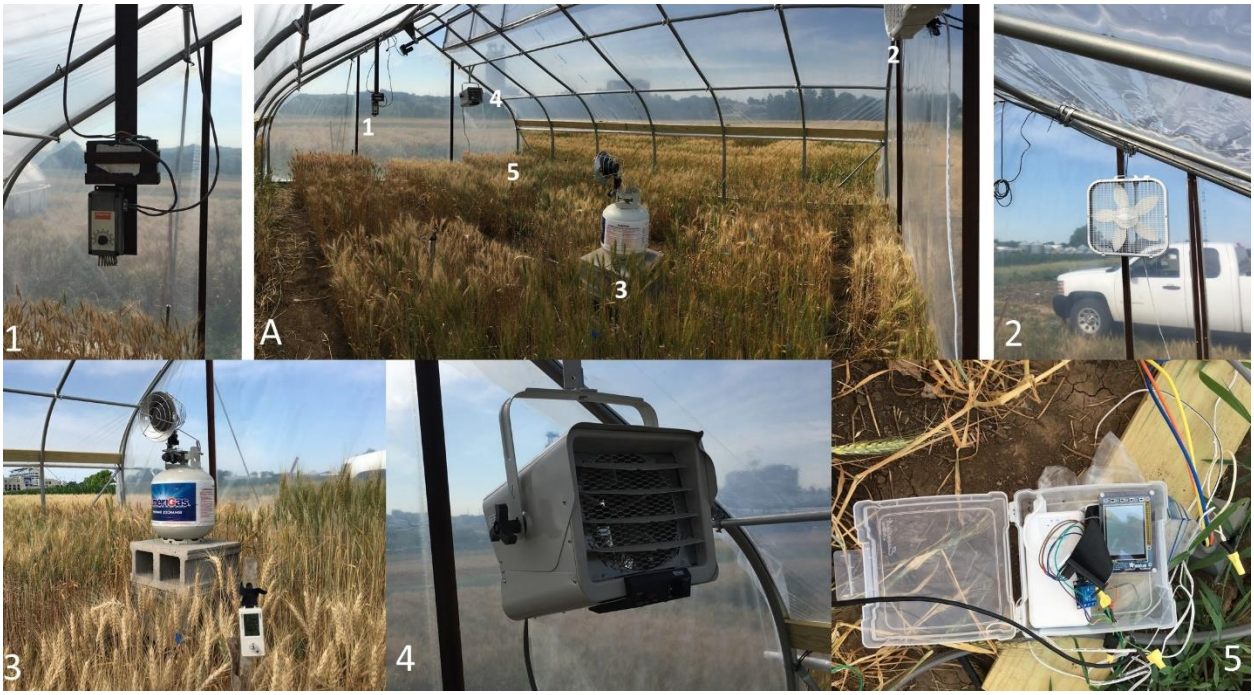

A: layout of heating system within the tent. 1: Dayton thermostat controller used to raise and lower the top vent. 2: Lasko 20-inch box fan. 3: Hobo temperature/relative humidity sensor and propane tank with the Sunrite™ by Mr. Heater® 15,000 BTU tank top portable propane heater. 4: Thermosphere 5000-watt ceiling-mount garage heater. 5: Thermostat controller system built using a Raspberry Pi. Obtained from Hein *et al*. (2019).

Tables

Appendix C Table - 1 Percent change in agronomic parameters.

Genotype	Biomass	Spike number	Spike weight	Grain yield	Grain number	Total biomass	200 grain weight	HI
Everest	-12.2	-16.3	-18.0	-17.9	-11.1	-14.4	-7.5	-2.5
Jagger X060724	7.0	11.8	2.3	1.4	8.9	6.1	-6.7	-2.5
KS070717 M-1	-10.8	-4.3	-14.9	-16.0	-12.8	-11.4	-5.9	-5.6
KS070729 K-26	-12.8	11.5	-9.2	-6.2	6.9	-9.6	-13.8	-3.2
KS070736 K-1	7.8	-7.4	6.6	12.1	9.0	3.4	9.1	4.0
Larry	-15.6	-6.9	-20.1	-21.7	-14.4	-15.7	-7.7	-3.1
P1 X060725	-7.0	4.5	-9.7	-14.7	-6.5	-10.3	-9.7	-4.9
SY-Monument	-13.1	-6.9	-13.4	-13.7	-8.5	-12.9	-5.3	-0.8
Tascosa	-3.9	-3.5	0.0	-3.7	2.3	-0.3	-6.8	-3.7
Tx86A5606	-0.5	7.1	-8.8	-11.9	-2.2	-0.8	-8.8	-5.1
WB-4458	-17.3	-11.4	-17.4	-14.9	-16.0	-19.6	0.8	3.2
WB-Cedar	-10.9	-10.1	-11.5	-11.2	-0.5	-11.4	-10.4	0.3
Average % Diff	**-7.4**	**-2.7**	**-9.5**	**-9.9**	**-3.7**	**-8.1**	**-6.1**	**-2.0**
Average % per °C	**-2.3**	**-0.8**	**-3.0**	**-3.1**	**-1.2**	**-2.5**	**-1.9**	**-0.6**

Percent change in agronomic parameters including biomass (g) (stem + leaves), spike number, spike weight (g), grain yield (g plant^{-1}), grain number, total biomass (g) (stem + leaves + spike), 200 grain weight (g), and harvest index (HI) among genotypes under HNT compared to control.

Appendix C Table - 2 Percent change in seed composition.

Genotype	Starch	Total N	Protein	Total C	P	K	Ca	Mg	SO_4-S	Cu	Fe	Mn	Zn
Everest	-14.4	-19.1	-19.1	-17.9	-22.6	-12.3	-11.7	-23.1	-20.2	-23.5	6.4	-18.1	-21.5
Jagger X060724	4.2	-3.7	-3.7	1.0	-5.3	1.2	20.8	-1.4	-0.6	-5.9	18.8	-5.3	-5.0
KS070717 M-1	-4.6	-18.4	-18.4	-16.4	-10.2	-4.1	-20.3	-5.4	-17.8	-14.1	-7.9	-10.6	-9.2
KS070729 K-26	-15.1	-10.3	-10.3	-6.0	-10.7	5.9	-1.5	-10.8	-12.7	-8.4	-34.0	-3.9	-8.8
KS070736 K-1	19.1	11.2	11.2	12.4	14.2	15.9	6.8	8.8	7.2	10.3	8.3	7.9	11.2
Larry	-22.3	-19.8	-19.8	-21.8	-22.9	-16.8	-20.2	-21.8	-19.8	-17.3	-14.3	-25.1	-17.3
P1 X060725	-14.4	-16.2	-16.2	-15.5	-14.8	-14.0	-18.7	-21.2	-18.3	-22.7	-23.6	-23.1	-23.2
SY-Monument	-11.7	-16.6	-16.6	-13.2	-2.9	1.1	-22.8	-3.8	-13.5	-13.7	-8.4	-13.2	-18.2
Tascosa	-2.6	-5.1	-5.1	-3.9	-4.5	-2.7	-10.7	-8.2	-9.0	-8.2	5.5	5.1	-6.7
Tx86A5606	-9.2	-9.0	-9.0	-11.9	-3.5	-0.3	-20.8	-11.0	-12.5	-17.3	-17.1	-19.6	-6.0
WB-4458	-13.9	-20.8	-20.8	-15.0	-11.7	-15.6	-31.1	-16.1	-15.1	-19.2	-2.2	-19.7	-11.4
WB-Cedar	-6.6	-12.3	-12.3	-11.1	4.9	-0.8	-20.4	-2.4	-13.7	-3.4	-6.3	-13.5	-10.2
Average % Diff	**-8.1**	**-12**	**-12**	**-10.2**	**-7.9**	**-4.1**	**-12.6**	**-9.9**	**-12.2**	**-11.9**	**-7.2**	**-12.1**	**-10.5**
Average % per °C	**-2.5**	**-3.7**	**-3.7**	**-3.2**	**-2.5**	**-1.3**	**-3.9**	**-3.1**	**-3.8**	**-3.7**	**-2.3**	**-3.8**	**-3.3**

Percent change in grain starch, total nitrogen (N), protein, total carbon (C), phosphorous (P), potassium (K), calcium (Ca), magnesium (Mg), sulfate sulfur (SO_4-S), copper (Cu), iron (Fe), manganese (Mn), and zinc (Zn) content.

Appendix C Table - 3 Grain concentration changes.

Genotype	Treat	Starch (%)	Total N (%)	Protein (%)	Total C (%)	P (%)	K (%)	Ca (%)	Mg (%)	SO_4-S (%)	Cu (ppm)	Fe (ppm)	Mn (ppm)	Zn (ppm)
Everest	CNT	61.43	2.6	14.6	41.6	0.3	0.33	0.05	0.15	0.16	5.3	61.8	48.9	40.5
	HNT	64.25	2.5	14.4	41.6	0.28	0.35	0.05	0.14	0.15	4.9	79.0	48.7	38.8
Jagger X060724	CNT	60.90	2.8	15.9	41.8	0.28	0.35	0.05	0.15	0.17	6.0	55.1	46.3	42.4
	HNT	62.42	2.7	15.2	41.6	0.26	0.35	0.06	0.14	0.16	5.6	63.0	43.7	39.7
KS 070729 K-26	CNT	58.62	2.8	15.9	42.0	0.29	0.32	0.05	0.14	0.16	5.5	83.1	51.0	49.5
	HNT	59.41	2.7	15.4	42.1	0.27	0.36	0.05	0.13	0.15	5.5	57.1	52.2	47.7
KS070717 M-1	CNT	61.52	3.1	17.8	42.0	0.32	0.35	0.05	0.16	0.19	6.8	53.6	47.9	49.9
	HNT	62.29	3.1	17.4	41.8	0.34	0.4	0.05	0.18	0.18	7.0	58.6	50.7	53.8
KS070736 K-1	CNT	57.74	2.9	16.6	41.8	0.29	0.32	0.06	0.16	0.18	6.7	69.6	55.0	52.6
	HNT	61.21	2.9	16.5	41.9	0.29	0.33	0.06	0.15	0.17	6.6	67.5	53.0	52.3
Larry	CNT	64.15	2.5	14.3	41.6	0.28	0.34	0.05	0.14	0.15	4.6	50.7	48.6	41.2
	HNT	63.95	2.6	14.6	41.6	0.28	0.36	0.05	0.14	0.15	4.8	54.5	46.1	43.1
P1 X060725	CNT	61.02	2.9	16.4	42.0	0.28	0.36	0.05	0.16	0.17	6.3	57.5	52.8	46.0
	HNT	61.66	2.8	16.1	41.6	0.28	0.37	0.04	0.14	0.16	5.7	52.1	47.2	41.4
SY-Monument	CNT	63.31	2.6	14.7	41.8	0.25	0.31	0.05	0.13	0.15	5.2	56.9	41.1	41.8
	HNT	65.39	2.5	14.1	41.9	0.28	0.36	0.05	0.15	0.15	5.1	58.4	40.7	38.5
Tascosa	CNT	63.37	2.6	15.1	41.8	0.28	0.28	0.06	0.14	0.17	5.1	51.7	42.9	42.1
	HNT	63.92	2.6	15.0	41.8	0.28	0.28	0.05	0.14	0.16	4.8	57.5	46.6	42.1
Tx86A5606	CNT	64.50	2.4	13.6	41.7	0.28	0.28	0.05	0.14	0.15	4.6	46.8	42.3	35.4
	HNT	65.99	2.5	14.0	41.6	0.31	0.32	0.04	0.14	0.15	4.3	43.6	38.3	38.3
WB 4458	CNT	60.24	2.9	16.5	42.2	0.28	0.34	0.05	0.15	0.17	6.1	55.5	60.4	45.5
	HNT	61.71	2.7	15.3	42.1	0.29	0.34	0.04	0.15	0.17	5.8	63.3	57.5	47.0
WB-Cedar	CNT	61.56	2.5	14.0	41.6	0.24	0.33	0.05	0.13	0.15	5.0	50.4	35.8	39.4
	HNT	64.21	2.5	14.0	41.6	0.28	0.38	0.04	0.14	0.15	5.6	53.4	34.9	40.1
Average	**CNT**	**61.50**	**2.71**	**15.44**	**41.81**	**0.28**	**0.33**	**0.05**	**0.15**	**0.16**	**5.58**	**57.73**	**47.75**	**43.86**
	HNT	**63.03**	**2.66**	**15.16**	**41.77**	**0.29**	**0.35**	**0.05**	**0.15**	**0.16**	**5.47**	**59.01**	**46.63**	**43.57**
	% Diff	**1.50**	**-1.72**	**-1.72**	**-0.09**	**2.54**	**7.2**	**-3.92**	**0.27**	**-2.32**	**-1.78**	**3.54**	**-2.2**	**-0.57**

Grain concentration changes in starch, total nitrogen (N), protein, total carbon (C), phosphorous (P), potassium (K), calcium (Ca), Magnesium (Mg), Sulfate Sulfur (SO_4-S), copper (Cu), iron (Fe), manganese (Mn), and zinc (Zn).

Appendix D - Chapter 5

Figures

Appendix D Figure - 1 Plant health and greenness at flowering

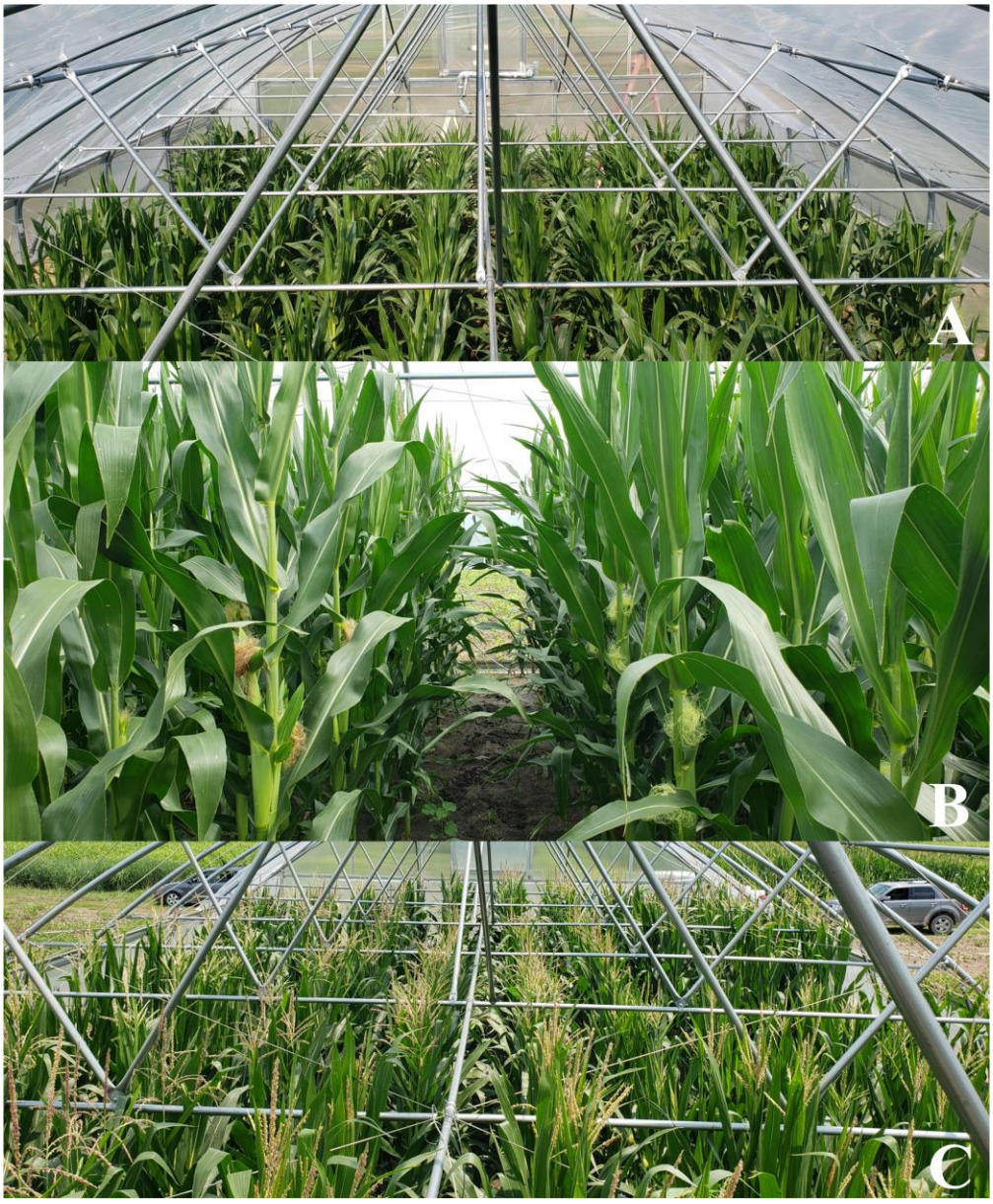

Figure illustrating plant health and greenness before and at flowering. A. Top view image of corn within a tent during plastic application approximately 1 week before flowering. B. View between corn hybrids during flowering. C. View from above of a repetition of hybrids during flowering.

Appendix D Figure - 2 Plant health during treatment

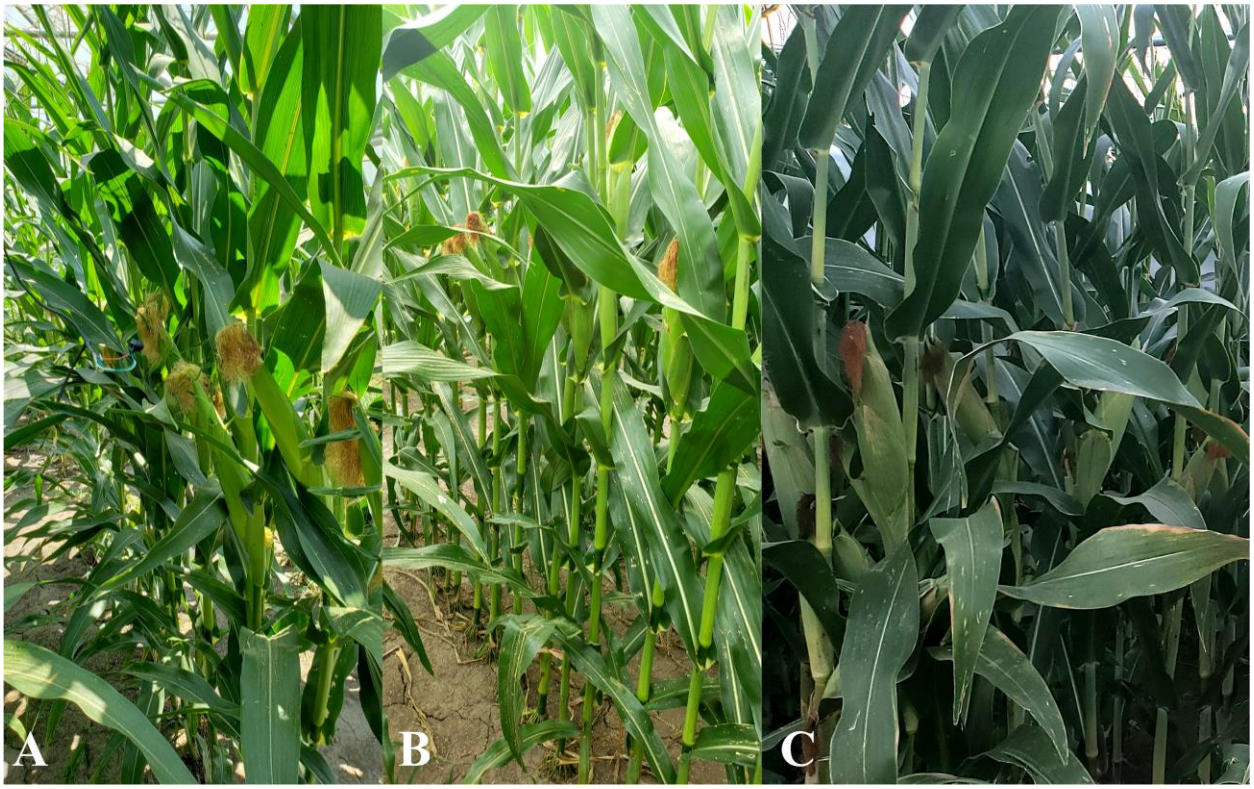

Figure illustrating plant health and greenness during treatment. A. Interior row view of a hybrid of corn 5 days after treatment. B. Interior row view of a hybrid of corn 13 days after treatment. C. View of a row of a hybrid 36 days after treatment.

Appendix D Figure - 3 Temperature differential within tents

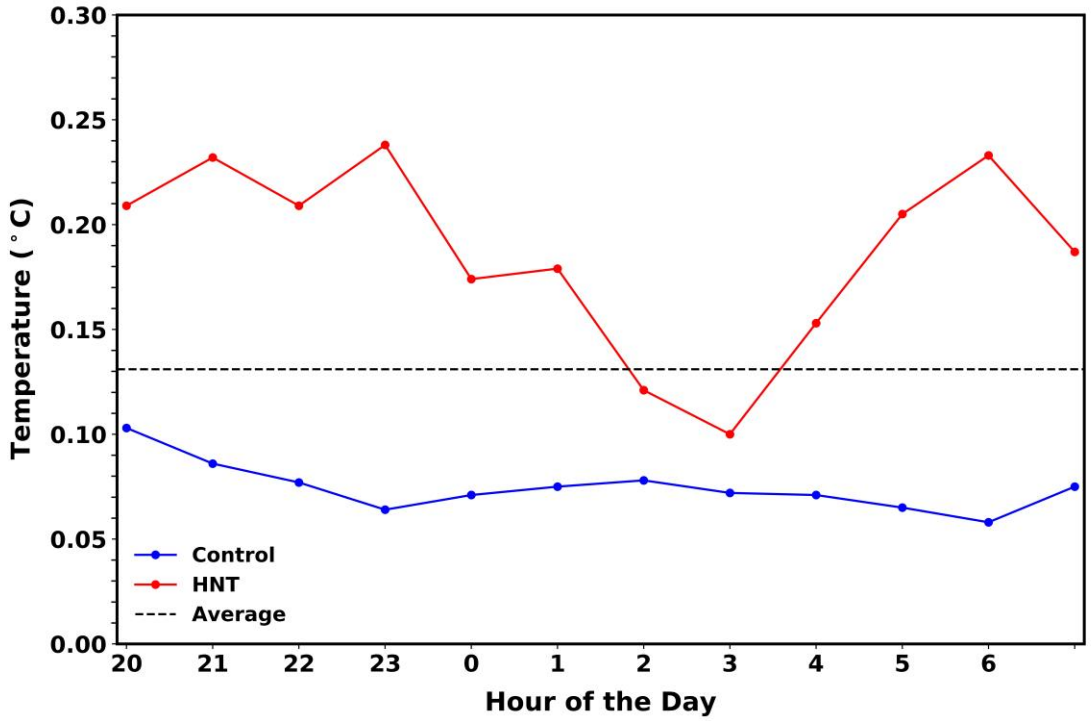

Temperature differential between sensors within the HNT and control tents during the stress period

Appendix D Figure - 4 Yield and 200 kernel weight results

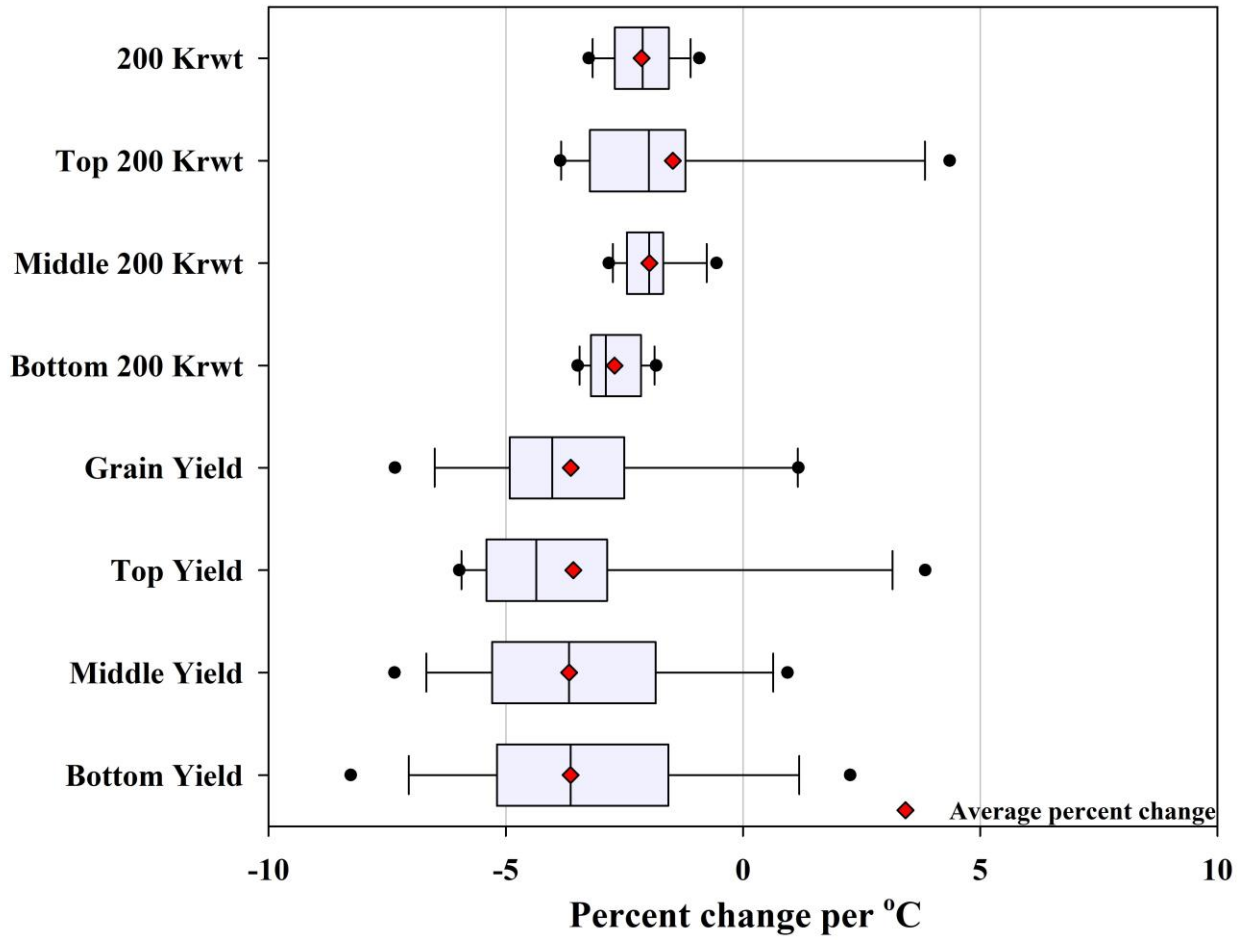

Total and spatially dependent results for 200 kernel weight and grain yield.

Appendix D Figure - 5 Starch metabolism and associated enzyme expression

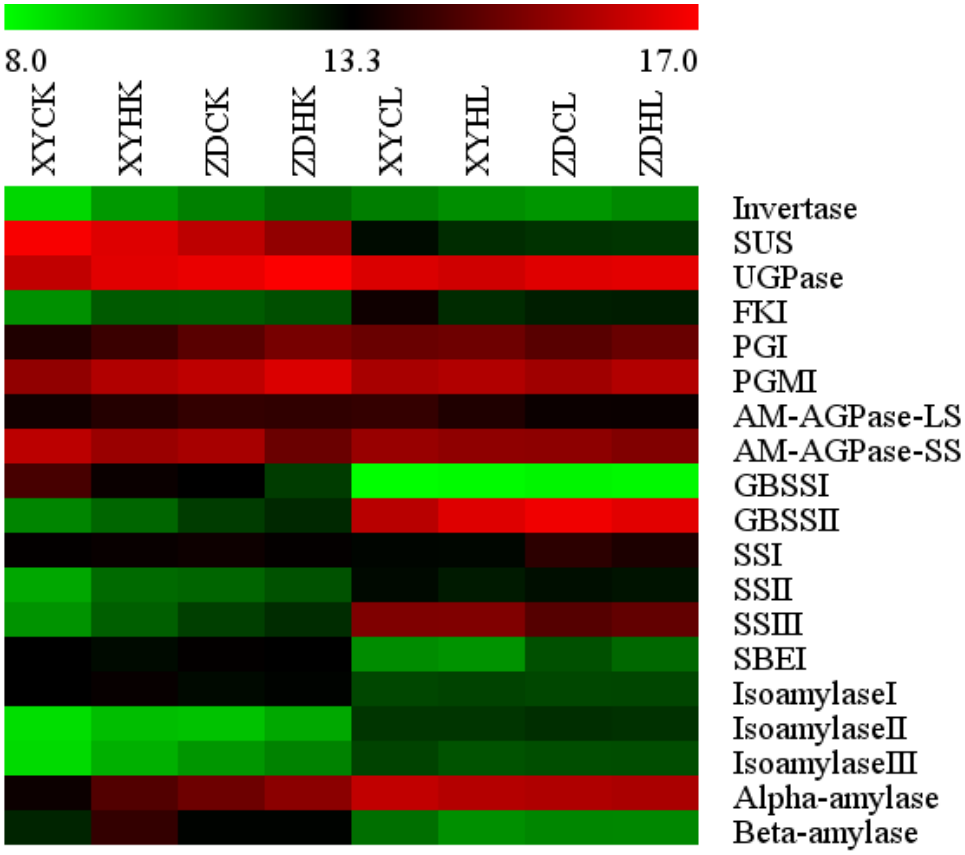

Expression of starch metabolism and associated enzymes. XYCK- Xianyu 335, control, kernel tissue; XYHK- Xianyu 335, heat, kernel tissue; ZDCK- Zhengdan 958, control, kernel tissue; ZDHK- Zhengdan 958, heat, kernel tissue; XYCL- Xianyu 335, control, leaf tissue; XYHL- Xianyu 335, heat, leaf tissue; ZDCL- Zhengdan 958, control, leaf tissue; ZDHL- Zhengdan 958, heat, leaf tissue.

Tables

Appendix D Table - 1 Starch metabolism and associated enzyme's primers

Gene	Primer
SUS_FP	GAGCTGGCGAACCTCGTGAT
SUS_RP	CACCGGATATGGCCCTTCAA
UGPase_FP	ACGCTCAAGGGCAAGGTGAC
UGPase_RP	CCTCAGGGCCATTGACATCC
PGMI_FP	TTCACAGGAGGCCCTTGCTC
PGMI_RP	GTGATAACGGTGGGGGCAGA
AM-AGPase-SS_FP	CGGTACCATTGCGGCATTTT
AM-AGPase-SS_RP	TGAAGGTGGCAGGTGTCGAG
GBSS1_FP	GCCACCCGGCTACTACATGC
GBSS1_RP	CATGAGCATGCGCTCGAACT
GBSS2_FP	TGCCTGTGGACTCGAGCATC
GBSS2_RP	GCCCACGAACTCTGGAATGG
SS3_FP	GGTCAAGTGCTCCCGTTGCT
SSIII_RP	CCATTGCCTTGCCAATGTGA
ISOAMYLASE1_FP	GGTGGTTGTTGGGCTTCCAG
ISOAMYLASEI_RP	CAGGCCATCGGTGAGGAAGT
a-AMYLASE_FP	CCACCAAGGGCATCCTCAAC
a-AMYLASE_RP	GACAAAGGTGACGGCCTTGG
ß-AMYLASE_FP	CCAAATGTCGATCCAGTTGCAC
ß-AMYLASE_RP	TCGAAGGGAAATGGCTCCAA

Appendix D Table - 2 SPAD and Fluorpen results

	Variables			Mean	
SPAD	**Treatment**	**Genotype**	**TxG**	**Control**	**HNT**
21 DAA / 12 DATrt					
3rd Leaf	0.913	0.532	0.187	59.19	59.28
6th Leaf	0.869	0.488	0.989	59.51	59.65
9th Leaf	0.910	0.195	0.995	57.69	57.80
Plant	0.883	0.306	0.984	58.79	58.91
32 DAA / 23 DATrt					
3rd Leaf	0.913	0.532	0.187	59.19	59.28
6th Leaf	0.869	0.488	0.989	59.51	59.65
9th Leaf	0.910	0.195	0.995	57.69	57.80
Plant	0.883	0.306	0.984	58.79	58.91
39 DAA / 30 DATrt					
3rd Leaf	0.732	**0.002**	0.6752	34.43	35.54
6th Leaf	0.360	**0.038**	0.6704	52.87	51.62
9th Leaf	0.072*	**0.0006**	0.0873*	52.42*	46.79*
Plant	0.183	**<0.0001**	0.5324	46.57	44.65
	Variables			**Mean**	
Fluorpen	**Treatment**	**Genotype**	**TxG**	**Control**	**HNT**
21 DAA / 12 DATrt					
3rd Leaf	0.330	**0.008**	0.348	0.729	0.722
6th Leaf	0.922	**0.042**	0.106	0.732	0.734
9th Leaf	0.345	0.209	0.881	0.724	0.710
Plant	0.572	**0.001**	0.543	0.729	0.722
32 DAA / 23 DATrt					
3rd Leaf	0.845	0.394	0.524	0.685	0.690
6th Leaf	0.497	0.244	0.473	0.707	0.693
9th Leaf	0.078*	**0.011**	0.416	0.694*	0.655*
Plant	0.476	0.063*	0.646	0.695	0.680
39 DAA / 30 DATrt					
3rd Leaf	0.578	**0.004**	0.789	0.653	0.646
6th Leaf	0.148	**0.05**	0.419	0.657	0.624
9th Leaf	0.562	0.6201	0.1507	0.635	0.628
Plant	0.211	**0.012**	0.099*	0.648	0.633

SPAD and Fluorpen results for the 3rd, 6th, and 9th leaves from 12 days after treatment (DATrt) to 30 DATrt.

Appendix D Table - 3 Nutrient adjustments due to HNT

Hybrid	Starch	Protein	Carbon	Phosphorous	Potassium	Calcium	Magnesium	Sulfate Sulfur	Copper	Iron	Manganese	Zinc
H1	-12.14	-18.01	-17.21	-16.00	-12.29	31.01	-20.17	-12.27	43.67	-26.49	-7.88	5.14
H2	-15.30	-13.36	-14.06	-10.26	-16.66	28.29	-12.28	-16.80	41.21	-9.43	-14.65	-15.36
H3	-12.57	-15.33	-15.61	-9.00	-14.00	-60.01	-15.37	-17.89	-8.25	-14.40	-20.62	-18.72
H4	2.53	12.65	6.88	7.35	9.47	5.48	4.70	10.40	26.00	-13.07	25.02	1.34
H5	-3.16	-9.21	-9.68	-6.85	-5.99	53.40	-6.87	-7.68	28.49	-4.89	13.07	-10.09
H6	-11.06	-3.87	-6.46	1.44	-0.07	14.50	0.34	-8.99	40.21	0.09	12.20	-12.29
H7	-15.17	-18.35	-18.74	-9.29	-12.38	14.19	-15.04	-11.84	56.02	-34.13	2.79	-12.49
H8	-11.11	-18.97	-18.70	-13.36	-18.74	-10.34	-18.42	-12.45	11.66	-2.60	-17.04	-4.88
H9	-7.69	-11.11	-13.01	-12.81	-9.44	47.83	-15.24	-6.15	15.04	-17.80	9.67	-7.00
H10	2.86	17.55	6.32	24.05	9.62	67.25	20.87	23.32	86.45	21.13	66.22	26.90
H11	-15.88	-15.26	-15.74	-13.96	-11.99	61.88	-12.10	-12.71	40.71	-21.23	-5.55	-12.33
H12	-20.97	-29.85	-26.79	-24.73	-26.64	-33.22	-28.00	-12.52	4.81	-34.05	-12.48	-29.15
All 12	-10.28	-11.42	-12.47	-7.79	-9.97	8.27	-10.97	-8.00	30.95	-15.66	2.45	-8.70
Avg Per °C	-2.68	-2.98	-3.26	-2.03	-2.60	2.16	-2.86	-2.09	8.08	-4.09	0.64	-2.27

Nutrient content adjustments due to HNT for each hybrid displayed as a percent change (%).